TECHNISCHE UNIVERSITÄT MÜNCHEN

Lehrstuhl für Erneuerbare und Nachhaltige Energiesysteme

Multi-modal on-site energy systems

Development and application of a superstructure-based optimization method for energy system design under consideration of part-load efficiencies

Sebastian M. Thiem

Vollständiger Abdruck der von der Fakultät für Elektrotechnik und Informationstechnik der Technischen Universität München zur Erlangung des akademischen Grades eines

Doktor-Ingenieurs

genehmigten Dissertation.

Vorsitzender:	Prof. Dr.-Ing. Wolfgang Kellerer
Prüfende der Dissertation:	1. Prof. Dr. rer. nat. Thomas Hamacher
	2. Prof. Dr.-Ing. Thomas Schulenberg

Die Dissertation wurde am 18.01.2017 bei der Technischen Universität München eingereicht und durch die Fakultät für Elektrotechnik und Informationstechnik am 24.10.2017 angenommen.

Chair of Renewable and Sustainable Energy Systems
Chair: Prof. Dr. rer. nat. Thomas Hamacher

Abstract

Finite fossil fuel resources, geopolitical worries and concerns about the environmental impact have raised questions about the sustainability of the existing energy system, not only at national level but also at smaller scale, e.g., at airports. Mathematical optimization methods offer the opportunity to optimize the design of energy systems with respect to costs or primary energy usage by identifying the optimal set of technologies to use for a particular application.

This Thesis deals with the development of an energy system design (ESD) method for multi-modal on-site energy systems, i.e., energy systems that use synergies between different energy forms. Part-load characteristics of energy converters and a variety of state-of-the-art technologies including turbine inlet air cooling were considered. In addition to this, a novel technology, ice-storage-integrated desalination, was developed and investigated in this Thesis. The optimization model was formulated as mixed-integer linear programming problem based on a superstructure approach. The objective of the ESD method was to minimize the total expenditures for a representative year.

The method was successfully benchmarked against a state-of-the-art ESD tool. The consideration of part-load efficiencies, however, was shown to considerably change the design of the energy system. The ESD method was demonstrated for an airport and campus case study. Combined heat and power plants with absorption chillers, compression chillers and thermal energy storages were key technologies. Furthermore, photovoltaic and desalination systems were economically attractive in a multitude of cases. Optimized on-site generation reduced total expenditures by 14% - 61% compared to cases with no on-site generation and by 8% - 47% compared to cases with conventional on-site energy systems using only gas boilers and compression chillers.

The presented ESD method can be used for optimizing multi-modal energy systems at project-level scale. Significant reductions of total expenditures are possible. The method could also be modified for optimizing primary energy usage. The described ESD method offers the opportunity for automating the energy system design process and may allow performance guarantees due to the detailed modeling of energy technologies.

Keywords
Energy system design
Multi-modal energy systems
Technical superstructure
Part-load efficiencies
Mixed-integer linear programming
Turbine inlet air cooling
Ice-storage-integrated desalination
Techno-economic assessment
Sensitivity analysis
Airports

Zusammenfassung

Begrenzte fossile Brennstoffreserven, geopolitische Bedenken und Sorgen um die Umweltauswirkungen haben zu Skepsis über die Nachhaltigkeit des aktuellen Energiesystems geführt, nicht nur auf nationaler Ebene sondern z.B. auch bei Flughäfen. Mathematische Optimierungsverfahren ermöglichen die optimierte Auslegung eines solchen Energiesystems.

Diese Arbeit beschäftigt sich mit der Entwicklung einer Methode für das Design (ESD) von multimodalen Energiesystemen, d.h. Energiesystemen, die die Synergien verschiedener Energieformen nutzen. Dabei wurden Teillastwirkungsgrade und verschiedene kommerziell erhältliche Technologien inkl. der Turbineneinlassluft-kühlung berücksichtigt. Zusätzlich wurde für diese Arbeit ein neuartiges in einem Eisspeicher integriertes Entsalzungssystem entwickelt und untersucht. Die ESD-Methode wurde als gemischt-ganzzahliges Opti-mierungsproblem basierend auf einem Superstrukturansatz formuliert. Ziel der Methode ist die Minimierung der Gesamt-ausgaben für ein repräsentatives Jahr.

Die Methode wurde erfolgreich gegen ein dem Stand der Technik entsprechendes ESD-Tool gebenchmarkt. Durch die Berücksichtigung von Teillastwirkungsgraden in der hier vorgestellten Methode kann das optimale Design eines Energiesystems sich signifikant verändern. Die ESD-Methode wurde anhand einer Studie für Flughäfen und Campus demonstriert. Hier zeigte sich, dass Blockheizkraftwerke mit Absorptions-kältemaschinen, Kompressionskältemaschinen (CC) und thermische Energiespeicher Schlüsseltechnologien sind. Zudem lohnten sich Photovoltaik und Entsalzungsanlagen in einer Vielzahl an Fällen. Die optimierte Eigenerzeugung konnte die Gesamtausgaben um 14-61% gegenüber Fällen ohne Eigenerzeugung und um 8-47% gegenüber Fällen, bei denen die Eigenerzeugung nur aus Gasboilern und CC bestand, verbessern.

Die vorgestellte ESD-Methode ermöglicht eine signifikante Einsparung der Gesamtausgaben. Die Zielsetzung der Methode kann auch an eine Minimierung des Primärenergiebedarfs angepasst werden. Mit der entwickelten ESD-Methode kann der Auslegungsprozess eines Energiesystems automatisiert werden und zusätzlich könnten auch Vergaben von Leistungsgarantien erprobt werden.

Schlüsselwörter
Energiesystemdesign
Multimodale Energiesysteme
Technische Superstruktur
Teillastwirkungsgrade
Gemischt-ganzzahlige Programmierung
Turbineneinlassluftkühlung
Eisspeicher-integrierte Entsalzung
Technisch-wirtschaftliche Betrachtung
Sensitivitätsanalyse
Flughäfen

Acknowledgements

I would like to thank my supervisor *Professor Thomas Hamacher* for his continuous support, valuable comments and his encouragement during the last three years. I'd like to extend my thanks to everyone from the *Chair of Renewable and Sustainable Energy Systems* at the Technische Universität München for their feedback and comments regarding my research. I also want to express my gratitude to *Professor Thomas Schulenberg* not only for acting as second reviewer of this Thesis but also his valuable feedback. I'd also like to thank *Professor Wolfgang Kellerer* for taking over the chair at my dissertation defense.

The work for this Thesis was financed by *Siemens AG*, for which I am very thankful. Furthermore, I would like to thank everyone at *Siemens Corporate Technology* who helped making this research project a success. In particular I'd like to thank my advisor *Dr. Vladimir Danov* and my manager and mentor *Dr. Jochen Schäfer* for their helpful feedback, their suggestions and the given freedom for exploring solutions to tackle research challenges. My acknowledgements belong also to the two Master students *Alexander Born* and *Marco Prenzel* who I was allowed to supervise during their theses.

I would like to extend my thanks also to the European Commission for the two Horizon 2020 projects, SENSIBLE (Storage enabled sustainable energy for buildings and communities) and MODER (Mobilization of innovative design tools for refurbishing buildings at district level), which I was allowed to contribute to with my research.

Last but not least, I would like to thank my family, in particular my wife *Chan* and my *parents*, for their love, warm support and faith in me. Especially I am grateful to my parents for giving me the chance to explore the world and for my wife to always being by my side and exploring the world together with me.

Contents

List of Figures

List of Tables

Abbreviations

AC	Absorption chiller
AC0	Absorption chiller (8 °C cooling supply temperature)
ACi	Absorption chiller (-5 °C cooling supply temperature)
ARE	United Arab Emirates
ASEAN	Association of Southeast Asian Nations
ASHRAE	American Society of Heating, Refrigerating and Air-Conditioning Engineers
ASUE	Arbeitsgemeinschaft für sparsamen und umweltfreundlichen Energieverbrauch e.V.
AUS	Australia
avg	Average
BOM	Mumbai (Bombay)
CAPEX	Capital expenditures
CC	Centralized compression chiller
CC0	Centralized compression chiller (8 °C cooling supply temperature)
CCi	Centralized compression chiller (-5 °C cooling supply temperature)
CDD	Cooling degree days
CHC	Combined heating and cooling technology (heat pump)
CHCP	Combined heat, cold and power
CHN	China
CHP	Combined heat and power
CM	Condition monitoring
Comm	Commodity

COP	Coefficient of performance
CPT	Cape Town
CWS	Chilled water storage
DER-CAM	Distributed energy resources customer adoption model
DEU	Germany
DewPoint	Active turbine inlet air cooling to dew-point temperature (see **Section 3.5.3**)
DG	Energy downgrading
DM	Decomposition method
DM-Month	Decomposition strategy with higher accuracy (see **Section 3.4.8**)
DM-Day	Decomposition strategy with lower accuracy (see **Section 3.4.8**)
DSM	Demand-side management
DZA	Algeria
EB	Electric boiler
EC	Energy converter
ECES	Electrochemical energy storage
ED	Energy demand
EER	Energy efficiency ratio
EF	Energy form
EIA	U.S. Energy Information Administration
EM	Energy management
EPA	U.S. Environmental Protection Agency
EPRI	Electric Power Research Institute
ES	Energy storage
ESD	Energy system design
ESP	Spain

Evap	Evaporative turbine inlet air cooling (see **Section 3.5.3**)
ewi	Energiewirtschaftliches Institut an der Universität zu Köln
FD	Freeze desalination
FPL	Florida Power & Light
FullProb	Full optimization problem spanning an entire year (see **Section 3.4.8**)
GB	Gas boiler
GB+CC	All energy demands but heating, hot water and cooling are drawn from external grids. Heating and hot water are supplied by a gas boiler, cooling by a compression chiller (see **Section 4.2.6**)
GC	Grid connection
GridOnly	All energy demands are drawn from external grids (see **Section 4.2.6**)
GT	Gas turbine
Gurobi	Commercial optimization solver for LP, MILP, … (Developed by Zhonghao **Gu**, Edward **Ro**thberg, Robert **Bi**xby)
GWS	Gesellschaft für Wirtschaftliche Strukturforschung mbH
HDD	Heating degree days
HEX	Heat exchanger
HKG	Hong Kong
HNL	Honolulu
HOMER	Hybrid optimization model for multiple energy resources
HOU	Houston
HP	(Electric) heat pump
HRSG	Heat recovery steam generator
HTF	Heat transfer fluid (brine)
HVAC	Heating, ventilation and air conditioning (equipment)
HWS	Hot water storage
ICE	Internal combustion engine

IEA	International Energy Agency
isiD	Ice-storage integrated desalination
ISO	Default gas turbine inlet conditions
	International organization for standardization
	Active turbine inlet air cooling to ISO temperature (see **Section 3.5.3**)
ISR	Israel
ITES	Ice thermal energy storage
LBY	Libya
LCOE	Levelized costs of electricity generation
LeadAcid	Lead-acid battery
LiIon	Lithium-ion battery
LoadC	Cooling load
LoadEl	Electric load
LoadH	Heating load
LoadHW	Hot water load
LoadW	Water load
LP	Linear programming
LPG	Load profile generation
MAD	Madrid
MAP	Mean annual precipitation
MAT	Mean annual temperature
MATLAB®	Matrix laboratory (mathematical software)
MED	Multiple-effect distillation
MEX	Mexico City
MGEOS	Modular general energetic optimization system

MIA	Miami
MILP	Mixed-integer linear programming
MINLP	Mixed-integer nonlinear programming
MinPLR	Minimum part-load ratio (≠ 0)
MMES	Multi-modal energy systems
MSFD	Multi-stage flash distillation
N/A	Not available
NonlinEta	Non-constant part-load efficiencies
NoTIAC	No turbine inlet air cooling method installed (see **Section 3.5.3**)
O&M	Operation and maintenance (costs)
OC	Optimal control
OPEX	Operating expenditures
Optim	Optimized on-site generation (see **Section 4.2.6**)
P2X	Power-to-X converters
PCM	Phase change material
PHX	Phoenix
PV	Photovoltaic
QAT	Qatar
RAM	Random-access memory
RE	Renewable energy (converter)
Ref	Reference
REFPROP	Reference Fluid Thermodynamic and Transport Properties Database
rHP	Reversible heat pump
RIO	Rio de Janeiro
RO	Reverse osmosis

RUBA	Rule-based (design method)
RYD	Riyadh
SAU	Saudi Arabia
SGT	Siemens medium-scale gas turbine
SIN	Singapore
SOTA	State-of-the-art (optimization model)
SQP	Sequential quadratic programming
ST	Steam turbine including heat recovery steam generator, condenser and feedwater pump (entire steam cycle)
SYD	Sydney
TES	Thermal energy storage
TIAC	(Gas) turbine inlet air cooling
TMY	Typical meteorological year
TOTEX	Total expenditures
TRNSYS	Transient system simulation tool
US, U.S.	United States
VDI	Verein Deutscher Ingenieure
W	Waste
WACC	Weighted average costs of capital
WS	Water storage
WT	Wind turbine

Symbols

Latin letters

a	[1/a]	Annuity factor
C	[$]	Costs, expenditures
c	[-]	Concentration
	[-]	Parameter
c_p	[J/kg/K]	Specific heat at constant pressure
c_v	[J/kg/K]	Specific heat at constant volume
CDD	[°C]	Cooling degree days
COP	[-]	Coefficient of performance
DG	*N/A*	Set of energy downgrading (e.g., converting heat from higher to lower temperature)
E	[J]; [m³]	Energy storage level
	[J]; [m³]	Energy; Volume
$\dot{E}$	[W]	Exergy flow rate
EC	*N/A*	Set of energy converters
ED	*N/A*	Set of energy demands
EER	[-]	Energy efficiency ratio
$empl$	[-]	Number of employees (working in the business park)
ES	*N/A*	Set of energy storages
f	*specific;* [$/a]	Objective function
g	[-]	Dimensionless factor (for the decomposition

		method)
	specific	Inequality constraint function
GC	*N/A*	Set of grid connections
GHI	[W/m²]	Global horizontal irradiance
gr_1	[$]	Fixed government grants
gr_2	[$/W]; [$/J]; [$/(m³/s)]; [$/m³]	(Variable) specific government grants
GT	*N/A*	Set of gas turbines
h	*specific*	Equality constraint function
	[J/kg]	Specific enthalpy
HDD	[°C]	Heating degree days
I	[-]	Installation of equipment
I_{TIAC}	[-]	Installation of turbine inlet air cooling equipment
i	[-]	Generic counter variable
i_1	[$]	Fixed capital costs
i, i_2	[$/W]; [$/J]; [$/(m³/s)]; [$/m³]	(Variable) specific capital costs
IN_j	*N/A*	Set of input connections for an energy converter (j)
ins	[-]	Building insulation quality factor
l	[(% of Q)/(100 h)]	Self-discharge rate (of an energy storage)
M	*specific*	Helper variable (for rewriting equations with products of Boolean and continuous variables to linear equations; in particular the maximum limit)
$\dot{m}$	[kg/s]	Mass flow rate
MAP	[mm]	Mean annual precipitation

MAT	[°C]	Mean annual temperature
N	[-]	Number of days
n	[a]	Economic lifetime, depreciation time
n_s	[-]	Number of stages
n_x	[-]	Number/Quantity of x
O	[-]	Online status of energy converters
O_{TIAC}	[-]	Online status of turbine inlet air cooling method
o_1	[$/a]	Fixed operation and maintenance costs
o_2	[$/W/a]; [$/J/a]; [$/(m³/s)/a]; [$/m³/a]	(Variable) specific operation and maintenance costs
$OUT_{\text{def},j}$	*N/A*	Set of output connections for an energy converter (j) including the defining output power flow (with index m=1)
OUT_j	*N/A*	Set of output connections for an energy converter (j) excluding the defining output power flow (with index m=1)
P	[W]; [m³/s]	Power flow; Volumetric flow rate
	[mm]	Precipitation
p	[Pa]	Pressure
	[$/J]; [$/m³]	Specific commodity price
pax	[-]	Annual number of passengers (in the airport)
PER	*N/A*	Set of time periods
Q	[W]; [J]; [m³/s]; [m³]	Nominal capacity
$\dot{Q}$	[W]	Heat flow rate

q	[J/kg]	Specific heat
R	[J/kg/K]	Individual gas constant
	[$/a]	Revenue
r	[-]	Interest rate
	[(% of Q)/(100 h)]	Specific ramping limits
RE	*N/A*	Set of renewable energy converters
s	[J/kg/K]	Specific entropy
	[$/(W Q)]; [$/(m³/s Q)]	Specific start-up costs
SOC	[-]	State-of-charge
SP	*N/A*	Set of subproblems
$staff$	[-]	Number of campus staff
$stud$	[-]	Number of students at the university
T	[K]	Temperature
t	[°C]	Temperature
	[s]	Time
TM	*N/A*	Set of time steps
u	[-]	Part-load ratio
$\dot{V}$	[m³/s]	Volumetric flow rate
v	[m/s]	Speed
W	*N/A*	Set of energy waste
w	[J/kg]	Specific work
	[-]	Weighting factor (for the decomposition method)
X	[-]	Humidity ratio
X, Y	*N/A*	Generic sets for the optimization variables
x, y	*specific*	Optimization variable

Y	[-]	Helper variable (for rewriting a nonlinear storage constraint to a linear equation)
Z	[-]	Helper variable (for determining start-up costs)

Greek letters

α	[-]	Description of the energy system superstructure (definition whether a certain power flow is relevant/connected for a certain form of energy)
α	[-]	Factor for the amount of cooling supplied by the ice storage
β	[kg/kg]	Ratio of ice to storage material
	[1/K]	Temperature coefficient (for PV model)
ζ	[-]	Heat ratio
η	[-]	Efficiency
κ	[-]	Heat capacity ratio
ν	[-]	Grade
ξ	[-]	Ammonia-water concentration
π	[-]	Pressure ratio
ρ	[kg/m³]	Density
φ	[-]	Relative humidity
χ	[-]	Water vapor content

Indices (Subscripts and superscripts)

-	Lower boundary
*	Optimum
	Redefinition
	Specific quantity related to the mass of dry air
+	Upper boundary

0	Default
	Initial
1, 2, 3,…	Specific counter (e.g., number or state)
a	(Dry) air
a	Year
abs	Absorber
amb	Ambient
avg	Average
c	Compressor
	Cooling
	Cut-in (wind speed)
C/O	CAPEX to OPEX ratio
CAPEX	Capital expenditures
Carnot	Carnot cycle
ch	Charge (of an energy storage)
CHC	Combined heating and cooling technology (heat pump)
cold	Coldest month (in the year)
comb	Combustor
Comm	Commodity (e.g., electricity)
cond	Condenser, condensation
d	Dew-point state
dch	Discharge (of an energy storage)
dem	Demand-related charges
dry	Driest month
e	Energy-related charges

e	Counter variable for a specific energy form
el	Electric
eq	Equality constraints
evap	Evaporator, evaporation
f	Fuel
	Furling (wind speed)
fix	Fixed charges
fw	Fresh water
gen	Generator
h	Heating
hot	Hottest month (in the year)
i	Freezing (liquid water to ice)
i	Counter variable for a specific turbine inlet air cooling method
ICE	Internal combustion engine
in	Inlet
ineq	Inequality constraints
init	Initial
isiD	Ice-storage-integrated desalination
ITES	Ice storage
j	Counter variable for a specific technology (e.g., a specific power plant)
k	Counter variable for a specific (discrete) time step
l	Counter variable for a specific subproblem
m	Counter variable for a specific input or output connection
	Month
max	Maximum

min	Minimum
mon,10	Number of months (per year), where the temperature was greater than 10 °C
net	Net
O&M	Operation and maintenance (O&M), in particular O&M costs
OPEX	Operating expenditures
out	Outlet
p	Counter variable for a specific time period
	Pressure
$p1, p2$	Reference points
pump	Pump
PV	Photovoltaic
r	Rated (wind speed)
	Rich (concentration)
ref	Reference
s	Saturation
	Stages
	Summer
s	Isentropic
SU	Start-up, in particular start-up costs
sw	Salt water
T	End of the optimization horizon
t	Technical
	Turbine
th	Thermal
threshold	Threshold value

TIAC	Turbine inlet air cooling
tot	Total
TOTEX	Total expenditures
tr	Triple point (of water)
v	Vaporization (liquid water to vapor)
v	Specific volume
w	Water
	Weak (concentration)
	Wet-bulb state
	Wind
	Winter
wet	Wettest month
WT	Wind turbine

1 Introduction

1.1 Motivation

Concerns about finite resources of fossil fuels and their environmental impact as well as geopolitical worries have raised questions about the sustainability of current energy systems (Crastan, 2010). As a consequence, governments have promoted the expansion of renewable energies and research in the development of new technologies, such as nuclear fusion reactors (Aichele, 2012). The intermittency of power generation from renewable energy sources requires measures for balancing supply and demand. Energy storages, demand-side management and sector coupling may be economically attractive options for augmenting the flexibility of the energy system (Lund, 2014; Sterner & Stadler, 2014). Other measures include improved part-load efficiencies, lower part-load ratios, better start-up capabilities and less stringent ramping constraints of conventional power plants, as well as enhanced interconnection of the power grid for averaging regional fluctuations of wind power generation (Hamacher, 2015). For all of these measures, digitization is a key enabler (Brynjolfsson & McAfee, 2014): Improvements of conventional power plants require detailed modeling, simulation and optimization of the design of the power plant. Forecasting and optimal control methods enable the largest feasible exploitation of energy drawn from renewable sources (Claessen & Poutré, 2014). Furthermore, the optimal design of the energy system can also be computed beforehand by the use of optimization models (Aboumahboub, Schaber, Tzscheutschler, & Hamacher, 2010a).

Due to the German energy transition and its promotion of renewable energies through feed-in tariffs, technologies such as photovoltaic achieved significant cost reductions through economies of scale (Cengiz & Mamiş, 2015). In addition to this, renewable energies have a different economic structure. They have rather high fixed costs, but can generate power with very low marginal costs in those instances in time, when renewable energy sources are available. Hence, wholesale and end-customer electricity prices are affected accordingly (Ballester & Furió, 2015).

The availability of new and cheaper energy technologies and altered commodity prices raise the question for the reassessment of the optimal design of the energy system: Which energy conversion and storage technologies should be used? In which combination and where should they be installed? How large should their capacity be? And how should they be operated? Legal constraints, individual preferences, subsidies and many other factors may influence the result of this assessment. However, optimization models offer the possibility to determine the optimal system design from a strictly mathematical point of view. As opposed to engineering rules of thump, optimization methods can guarantee an optimum with respect to a defined objective (Papageorgiou, Leibold, & Buss, 2012). Furthermore, they can easily be automated and applied to other cases, and, most importantly, they can consider energy systems in a holistic framework.

When considering energy systems in a holistic framework, synergies between different forms of energy can be exploited (see **Table 1.1**). For example, electricity could be converted into heat by highly-efficient heat pumps and used in the heating sector or stored in thermal energy storages (TES) if needed (Lund, 2014). Furthermore, cogeneration (combined heat and power, CHP) or trigeneration (combined heat, cold and power) can be more attractive than individual generation (Mancarella, 2014). For this Thesis, such energy systems incorporating all relevant forms of energy in a holistic framework were defined as multi-modal energy systems (MMES).

Table 1.1: Characteristics of various forms of energy (see, e.g., Sterner & Stadler (2014)).

	Electricity	Heat	Cold	Fuel	Potable water
Transportation	Very good	Poor	Poor	Good	Good
Storage	Difficult or expensive	Easy	Easy	Easy	Very easy
Conversion	Very good	Good (temperature-dependent)	Poor	Good	None

The energy transition, in particular the investment in renewable energies and the assessment of energy systems, takes place on a local level (e.g., in rural areas or city districts). Due to the involvement of many different stakeholders, the holistic implementation of MMES in rural areas or cities proves to be very difficult (Guinot, 2016). Therefore, the first to actively consider and implement MMES (in a holistic framework) will most likely be defined sites with one operator firm (e.g., airports). Airports are particularly interesting. Global air transport (passengers carried) has increased at compound growth rates of 5.5% annually since the 1970s, in China even at 17% (The World Bank, 2016). Other similar on-site energy systems could be implemented at business parks[1] or university campuses (see **Figure 1.1**).

All of these sites have the following in common:

- They demand different forms of energy (e.g., electricity, heating and cooling) (Cardona, Piacentino, & Cardona, 2006; Cardona, Sannino, Piacentino, & Cardona, 2006; Powell et al., 2016);
- They may utilize different conversion technologies (e.g., heat pumps);
- They have the possibility to store energy in different forms (e.g., thermal energy);
- And they exhibit large demands in a confined area, making them particularly interesting for a holistic energy system design assessment. Due to their large loads, on-site generation can also be economically attractive (Williams, 2013).

[1] In this Thesis, business parks are commercial but not industrial areas.

Figure 1.1: The three use case sites.

Many of the megacities built in the last years and that will be built in the upcoming years are located in cooling-dominated climates, such as the ASEAN countries, Brazil, China, India, Saudi Arabia or the United Arab Emirates. Air conditioning of buildings (in the following referred to as *cooling*) stresses the power grid tremendously. Intelligent management of these cooling loads utilizing active (e.g., TES) or passive thermal energy storage (e.g., building thermal mass) may help to reduce stress on the power grid and thus increase economics of the energy supply system (Y. Zhang & Lu, 2013). Furthermore, due to climate change and increased prosperity, use of air conditioning is likely to increase even more (Wang & Chen, 2014).

To date, the process of designing and managing on-site MMES in a holistic and optimal framework is not well established. Therefore, this Thesis deals with a process-oriented view on the design and management of on-site MMES in particular for cooling-dominated climates.

1.2 Objective and scope of work

The overall objective of this Thesis was threefold:

1. Development of a method for the optimal design of complex on-site MMES while considering detailed component models;
2. Demonstration of this method for an airport and campus case study to answer some practical questions regarding the optimal set of technologies;
3. Development and experimental validation of optimal control for an example small-scale multi-modal energy system.

1. Development of an energy system design (ESD) method

Voll (2013) summarized the limitations of current energy system design methods. According to him, future research should investigate:

- Optimal design of *complex* systems;
- Decomposition methods to achieve reasonable computation times;
- Consideration of different forms of energy that may be of different quality (e.g., thermal energy at different temperature levels);
- Good modeling practice and modeling frameworks;
- Modeling of further and practical technologies;

- Integration of energy storages.

Accordingly, in this Thesis, a comprehensive superstructure including a multitude of energy conversion and storage technologies shall be proposed. Thermal energy shall be considered at different temperature levels representing its quality. As opposed to other tools, such as urbs (TUM ENS, 2014), this Thesis focuses on complex, local technical systems integrating several cutting-edge technologies described by detailed component models. The main questions to be answered were:

- Is it possible to optimize the design of such complex systems at all?
- With which decomposition method can reasonable computation times be achieved?
- How can energy storages, in particular also long-term storage options, be included within the optimization method?
- How can part-load efficiencies, as well as other part-load constraints, be integrated in the method?
- How can gas turbine inlet air cooling be incorporated and investigated?
- What should a good modeling framework for energy conversion and storage technologies look like?

2. Answer to practical questions by demonstration of the ESD method

This Thesis shall determine energy demands (load profiles) of the presented use case sites (see Figure 1.1) based on a similarity analysis. The developed method shall then be applied to these sites to answer the following practical questions:

- Which technologies are economically most attractive?
- Can we identify trends between the optimal generation share and the prevalent price structure?
- Is there *one* optimal energy system design for the whole world?
- How sensitive is the design to changes of commodity prices and capital costs of technologies?
- Can ice-storage-integrated desalination challenge existing and proven desalination technologies?
- Which gas turbine inlet air cooling methods should be used and where?

3. Development and experimental validation of optimal control for a MMES

The last part of this doctorate study dealt with an experimental cooling system with ice storage. A model-based predictive controller for the operational optimization of the system was developed, implemented and tested. This part is not presented in this Thesis but was thoroughly published at conferences (Thiem, Born, Danov, Schäfer, Hamacher, et al., 2016; Thiem, Born, Danov, Vandersickel, et al., 2016; Thiem, Born, Danov, Schäfer, & Hamacher, 2016; Thiem, Danov, Schaefer, & Hamacher, 2015; Thiem, Danov, Schäfer, & Hamacher, 2015) and also in a journal paper (Thiem, Born, et al., 2017).

1.3 Structure of this Thesis

This Thesis is divided into five chapters (see **Figure 1.2**). **Chapter 1** put the topic of this Thesis into current global perspective and outlined the focus of this research. In **Chapter 2**, mathematical optimization is briefly introduced and existing tools and previous research are reviewed. **Chapter 3** develops and benchmarks a superstructure-based optimization method for the optimal design and operation of multi-modal on-site energy systems. The optimization problem is formulated; furthermore selected models are introduced. In **Chapter 4**, the method is used to determine the optimal energy system design of airports, business parks, and university campuses located in cooling-dominated climates across the world. Also the background of **Figure 1.2** illustrates the global focus of this Thesis. Finally, **Chapter 5** concludes the Thesis and outlines consequences for future research.

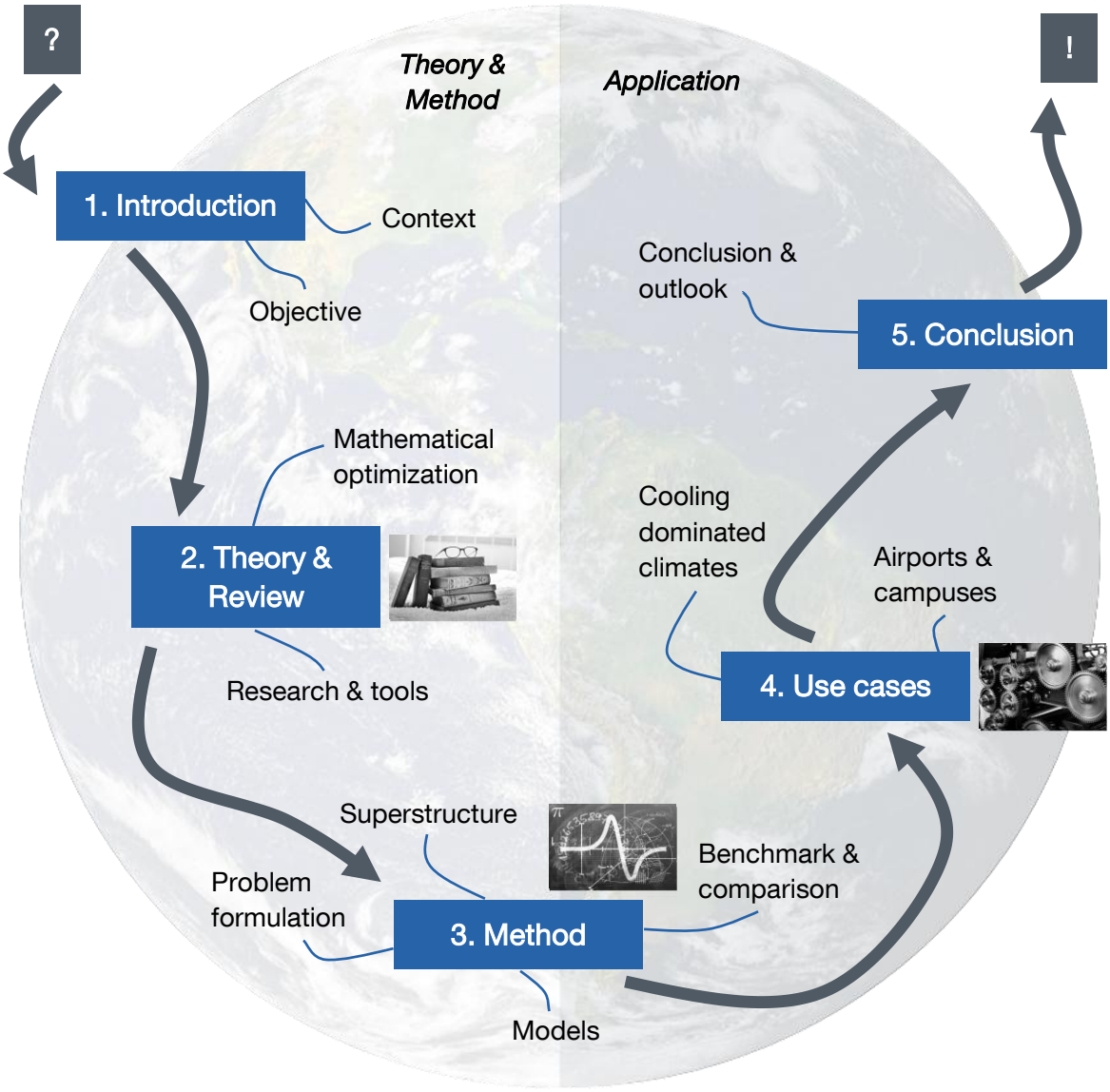

Figure 1.2: Structure of this Thesis.

2 Basic theory and concise review

2.1 Overview

Due to the long lifetime of energy conversion and storage technologies, purchase and installation of new energy systems (Greenfield approach) or expansion of existing systems (Brownfield approach) are long-term investments. Therefore, a detailed technical and economical analysis considering also future constraints is required.

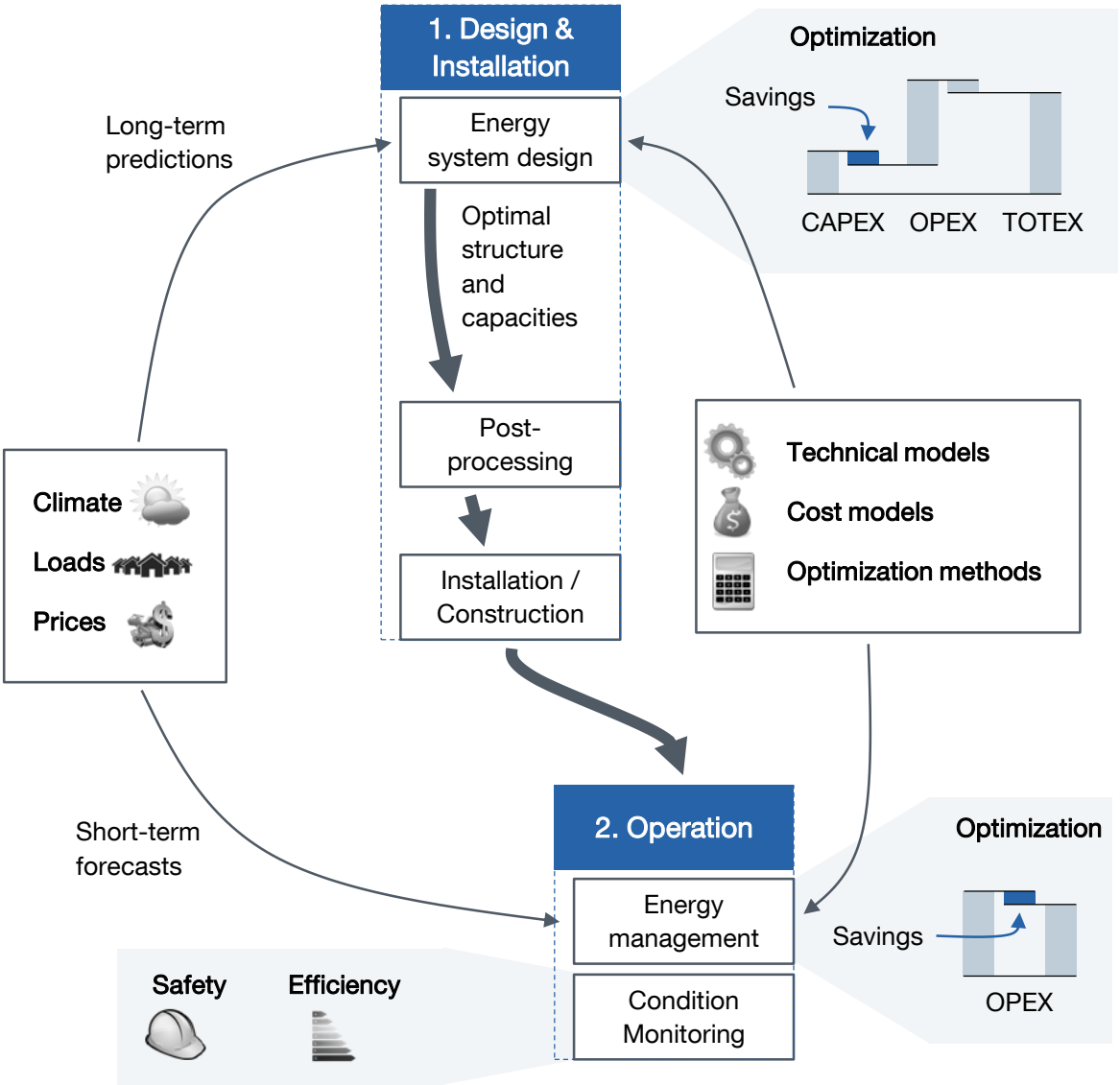

Figure 2.1: Optimal design, installation and operation of energy systems: A schematic process flow diagram depicting required inputs and objectives (adapted from Thiem, Danov, et al. (2017)).

Figure 2.1 schematically shows the two-stage process of optimal design and operation of energy systems. The two essential methods were defined as *energy system design* (ESD) and *energy management* (EM) in this Thesis.

The objective of ESD is to determine the optimal set of technologies and their capacities for a given use case considering all relevant constraints. Many parameters, such as the particular location and site, commodity prices, loads, climatic conditions, existing infrastructure and technology, individual preferences, acceptance, legal, political, economical and many other constraints influence the optimal design. Therefore, in a first step, information about the use case must be acquired. Since ESD is a planning and decision method for *future* installations, *actual* load profiles are not available. Therefore, adequate methods need to estimate the future energy demand. Such methods can be building simulation tools, as well as similarity assessments taking into account past experience from similar sites. The latter will be introduced for three sites in **Section 4.1.2**. In this Thesis, the design of the energy system is optimized with respect to total expenditures (TOTEX), i.e., the sum of capital expenditures (CAPEX) and operating expenditures (OPEX) (see also **Figure 2.1**). By considering emission prices, the environmental dimension can be included in the economical objective. Furthermore, high primary energy utilization is encouraged, if it is economically feasible. Alternative methods, such as multi-objective optimization could also be adopted (Fazlollahi, Mandel, Becker, & Maréchal, 2012). In one way or another, the trade-off between the three pillars of sustainability – economy, society and environment – must be solved (United Nations General Assembly, 2005). ESD provides a preliminary design of the energy system, which is optimal with respect to the chosen objective function. Further constraints (for example, quotes for components, backup, reliability and legal issues, as well as individual preferences) must be taken into account before purchase of equipment and installation of the energy system (Konstantin, 2013).

Although optimizing TOTEX, ESD only allows for cost savings in CAPEX. For an *overall* optimal energy system project, OPEX savings can be achieved by optimal control of the system once it was installed and is operated. Here, rather short-term forecasts of climatic conditions, loads and prices are indispensable. EM methods are distinguished in model-free and model-based control strategies (Thiem, Born, Danov, Schäfer, Hamacher, et al., 2016; Thiem, Born, Danov, Vandersickel, et al., 2016; Thiem, Danov, Schaefer, et al., 2015). Methods for automated model parameter identification were developed and implemented together with a model-predictive controller for an experimental cooling system with ice storage (Thiem, Born, et al., 2017; Thiem, Born, Danov, Schäfer, & Hamacher, 2016; Thiem, Danov, Schäfer, et al., 2015).

The models, sensors and data acquisition and processing system used for EM can also be used for *condition monitoring* (CM). For the experimental cooling system, measured input-output parameters were compared to the plant model. Depending on the deviation, model parameters were adapted (rather small drift), or could be used for fault detection and diagnosis (sudden or significant deviation) (Blanke, Kinnaert, Lunze, & Staroswiecki, 2006).

The focus of this Thesis is the development of an ESD method for multi-modal on-site energy systems. Therefore, in the following sections, mathematical optimization is briefly described and thereafter existing ESD tools and previous research are reviewed.

2.2 Brief description of mathematical optimization

A mathematical optimization problem can be formally written as

$$\min\left\{f(\mathbf{x},\mathbf{y}) \mid \begin{matrix}\mathbf{g}(\mathbf{x},\mathbf{y}) \le \mathbf{0} \\ \mathbf{h}(\mathbf{x},\mathbf{y}) = \mathbf{0}\end{matrix}, \begin{matrix}\mathbf{g}: X \times Y \to \mathbb{R}^{n_{\text{ineq}}} \\ \mathbf{h}: X \times Y \to \mathbb{R}^{n_{\text{eq}}}\end{matrix}, \begin{matrix}\mathbf{x} \in X \subseteq \mathbb{R}^{n_x} \\ \mathbf{y} \in Y \subseteq \mathbb{Z}^{n_y}\end{matrix}\right\}. \tag{2.1}$$

The optimal values for the continuous variables ($\mathbf{x}$) and integer variables ($\mathbf{y}$) are determined according to the objective function (f), subject to inequality constraints ($\mathbf{g} \le \mathbf{0}$) and equality constraints ($\mathbf{h} = \mathbf{0}$) (Kallrath, 2013).

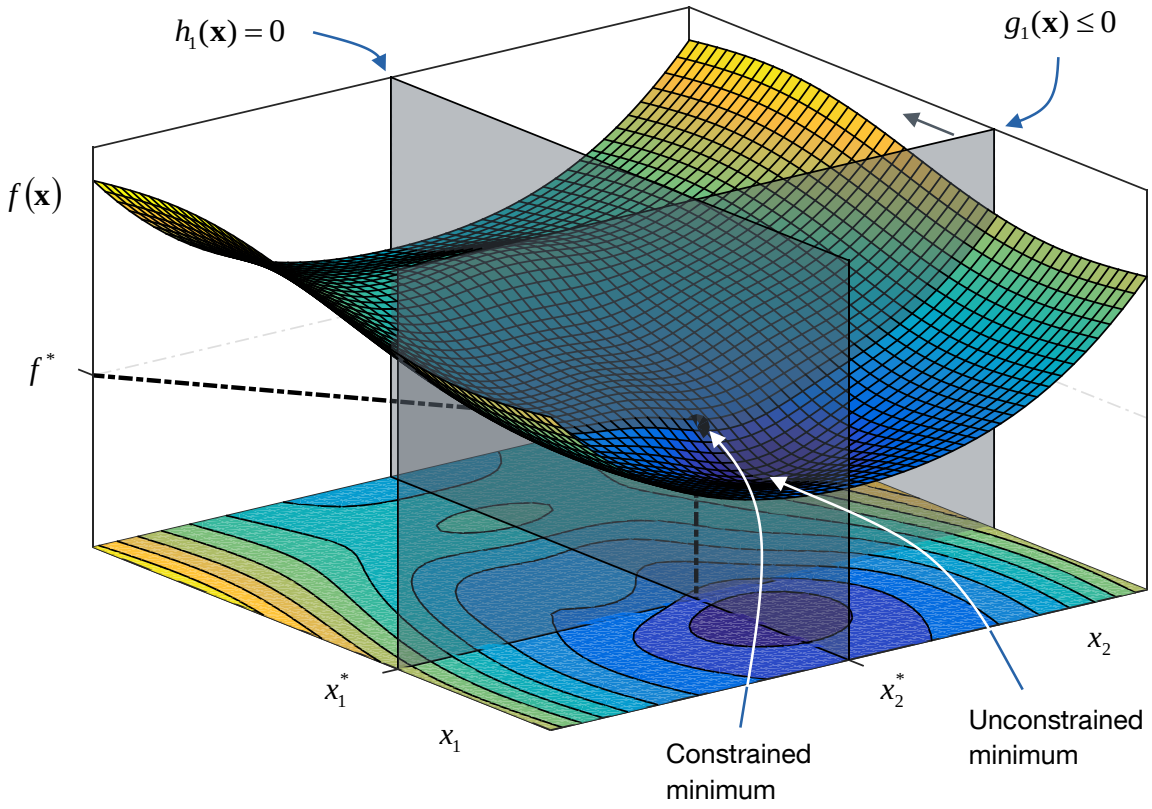

Figure 2.2: Constrained nonlinear optimization problem with two variables and one objective.

A constrained, nonlinear, continuous optimization example is illustrated in **Figure 2.2**. Both an inequality constraint ($g_1 \le 0$) and an equality constraint ($h_1 = 0$) confine the feasible region for $\mathbf{x}$. Accordingly, the constrained minimum differs from the unconstrained minimum.

Optimization is an entire field of mathematics. Tremendous amount of research has focused on the development of computationally-efficient and reliable solving strategies (Biegler & Grossmann, 2004). The solvers are designed for specific optimization problems. These can be distinguished as follows (Papageorgiou et al., 2012):

- Continuous, discrete or mixed variables;
- Unconstrained or constrained;
- None, one or more objectives;

- Deterministic or stochastic;
- Linear or nonlinear;
- And in case of nonlinear, convex or non-convex (minimization).

This Thesis employed Gurobi, a state of the art solver for linear and mixed-integer linear optimization problems (Gurobi Optimization Inc., 2015). Model equations were reformulated into the form specified by the solver (compare **Equation (2.1)**). The solver returned those variables $(\mathbf{x}^*,\mathbf{y}^*)$ that optimally solved the objective function subject to the given constraints.

Current solvers for mixed integer linear programming (MILP), the class of the optimization problem introduced in **Section 3.4**, rely on the Simplex or interior-point method for the linear programming problem, and combinations of cutting planes and branch and bound for solving the integer part of the problem (Gurobi Optimization Inc., 2015). Detailed description of the optimization methods would exceed the scope of this Thesis. For further information on optimization techniques, see, for example, Biegler & Grossmann (2004), Papageorgiou et al. (2012) or Kallrath (2013).

2.3 Existing tools

Based on numerous review papers and own research, 57 tools were reviewed regarding their applicability for the optimal design and operation of on-site MMES (Bhattacharyya & Timilsina, 2010; Connolly, Lund, Mathiesen, & Leahy, 2010; Keirstead, Jennings, & Sivakumar, 2012; Lam, Klemeš, Kravanja, & Varbanov, 2011; Mendes, Ioakimidis, & Ferrão, 2011; Jordi Ortiga, 2010). From these 57 tools, the eleven most suited tools were selected and were further evaluated. **Table 2.1** classifies the ESD tools according to:

- Forms of energy: Essential for the multi-modal context of this Thesis; which forms of energy can be considered and analyzed;
- Operation optimization: Mathematical optimization of the dispatch (control) of energy conversion and storage devices;
- Design optimization: Optimal selection and sizing of energy system technologies;
- Time step: Simulation or optimization time interval.

Table 2.1 shows that only two tools consider potable water as a form of energy. *EnergyPLAN* incorporates seawater desalination technologies; *urbs* could be extended for it. Moreover, some tools only focus on the power and heating sector, such as *Balmorel*, *HOMER Pro®* and *MARKAL & TIMES*. Notice that only three tools (*Balmorel*, *DER-CAM*, and *urbs*) enable the combined mathematical optimization of design and operation. The check mark is placed in brackets, if some other method attempts to identify good solutions. *HOMER Pro®*, for example, uses a scenario-based technique for the design optimization (Lambert, Gilman, & Lilienthal, 2006). The tools were also categorized into groups (see last column of the table). The groups are explained further in the following section and in **Figure 2.3**.

Table 2.1: Classification of the eleven most promising energy system design tools.[2]

Tool	Forms of energy					Optimization		Time step					Group (see Figure 2.3)
	Power	Heat	Cold	Fuel	Water	Operation	Design	Seconds	Minutes	Hours	Months	Years	
Balmorel	✓	✓		✓		✓	✓			✓	✓		I)
DER-CAM	✓	✓	✓	✓		✓	✓		✓	✓			III)
EnergyPLAN	✓	✓	✓	✓	✓	(✓)	(✓)			✓			I)
energyPRO	✓	✓	✓	✓		(✓)			✓	✓			II)
HOMER Pro®	✓	✓		✓		(✓)	(✓)		✓	✓			II)
MARKAL & TIMES	✓	✓		✓		(✓)	✓			✓	✓	✓	I)
MGEOS	✓	✓	✓	✓		✓				✓			VI)
RETScreen	✓	✓	✓	✓							✓	✓	I)
TOP-Energy®	✓	✓	✓	✓		✓	(✓)			✓			III)
TRNSYS	✓	✓	✓	✓		✓	(✓)	✓	✓	✓			VI)
urbs	✓	✓	✓	✓	✓	✓	✓			✓			I)

The selected tools are briefly introduced in the following. *Balmorel* is a model for analyzing the electricity and combined heat and power sectors in international markets, thus not applicable for this Thesis (Münster & Lund, 2009). *DER-CAM* optimizes the design and operation of energy systems simultaneously; however, only for representative days. Furthermore, potable water is not considered and the source code was not available for commercial use (M. Stadler, 2016). Although *EnergyPLAN* considers all five forms of energy (power, heat, cold, fuel and potable water), the tool is based on analytical calculations (Lund, 2014) and therefore the model structure was fixed and its complexity limited. *energyPRO*, on the other hand, was designed for techno-economic single-project assessments (EMD International A/S, 2014). An example case[3], however, revealed that *energyPRO* did not satisfy all constraints (e.g., minimum and maximum storage capacities). *HOMER Pro*® was originally designed for the electricity sector.

[2] (Balmorel, 2014; Department of Development and Planning at Aalborg University, 2014; EMD International A/S, 2014; Energy Technology Systems Analysis Program, 2014; gfai tech GmbH, 2014; HOMER Energy, 2014; Microgrids at Berkeley Lab, 2016; Natural Resources Canada, 2014; Jordi Ortiga, 2010; M. Stadler, 2016; TRNSYS, 2014; TUM ENS, 2014); see also Connolly et al. (2010), Keirstead, Jennings, & Sivakumar (2012), Mendes, Ioakimidis, & Ferrão (2011).

[3] Results for an example case with cold storage computed with *energyPRO* showed that storage constraints were not fulfilled.

Therefore, only a limited number of technologies for thermal energy were available (Lambert et al., 2006). *MARKAL & TIMES* are two model generators and focus on the national grid level similar to *Balmorel*, but could also be adapted to municipality level. However, the operation of the system is not optimized (Mendes et al., 2011). *MGEOS* (Modular general energetic optimization system) is a very interesting tool developed by Ortiga (2010) for polygeneration systems. Besides that desalination technologies and sizing of components are not included, the tool was simply not available for usage or further modification. On a larger time scale (monthly time steps), *RETScreen* screens alternative energy system designs based on user-defined scenarios (compared to a reference case). Both operation and design are not optimized in *RETScreen (Mendes et al., 2011)*. *TOP-Energy*® is a tool for the analysis and optimization of industrial energy systems. However, to the best of the author's knowledge, also *TOP-Energy*® did not include desalination technologies and was not modifiable due to its commercial license. Building and other small-scale energy systems could be evaluated in the transient system simulation tool (*TRNSYS*). *TRNSYS* includes an interface to the derivative-free optimization tool GenOpt (Kummert, 2007). However, derivative-free optimization can be very time-consuming. Finally, *urbs* is an open-source tool allowing the design and operational optimization of distributed energy systems including all forms of energies. However, as outlined also in **Figure 2.3**, the model level of detail was limited (e.g., constant efficiencies for energy conversion technologies) (Schaber, 2013).

The survey showed that none of the tools fulfilled all of the requirements for the energy system design of complex energy systems described by detailed component models. Hence, a new ESD model was required to be developed for this research study.

2.4 Previous research

The preceding section reviewed existing energy system design *tools*. However, previous academic research has also investigated other aspects of energy system design without developing tools for other researchers or practitioners to use. This section examines in which extend existing methods could contribute to the development of the ESD method for this Thesis. **Figure 2.3** classifies previous research according to two dimensions:

- Application: Spatial dimension of analysis (building, city or national level);
- Model level of detail: Very simple models with constant efficiencies, consideration of part-load efficiencies or complex nonlinear models;

Typical types of the optimization problem are also indicated in the figure. The most common optimization class is mixed-integer linear programming (MILP). Neglecting start-up and shut-down of power plants, strongly simplified models can also be based on linear programming (LP). On the other side, for detailed nonlinear models mixed-integer nonlinear programming (MINLP) is required. **Figure 2.3** also *qualitatively* indicates the computation time. The computational effort strongly increases from LP to MILP and from MILP to MINLP. As indicated in the figure, past research and tools - with particular attention to both multi-modal context and energy system design - have been categorized into six groups (I through VI). The following review introduces previous research according to these groups.

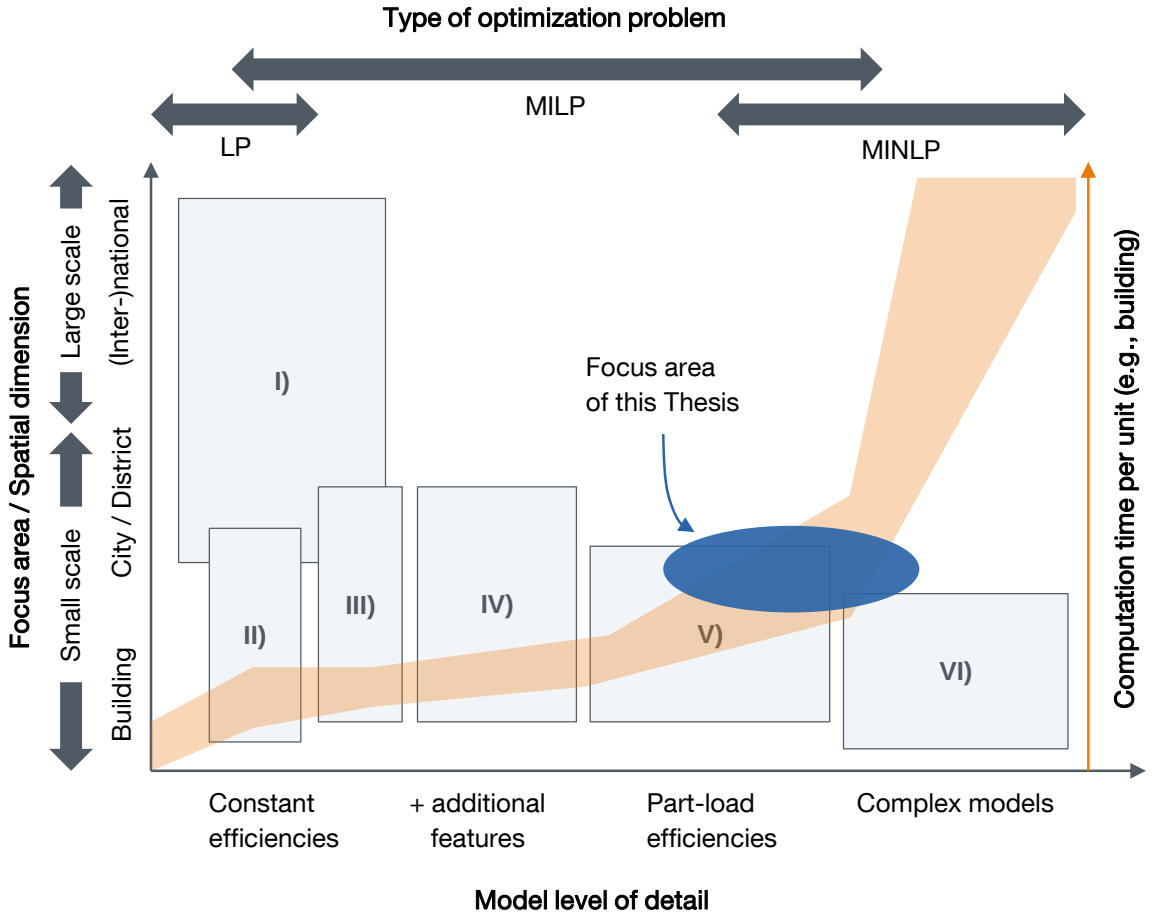

Figure 2.3: Classification of previous research and focus area of this Thesis.

Group I): Large-scale grid studies relying on simplified models

Focusing particularly on the large-scale integration of renewable energy sources, Lund, Mathiessen, Connolly et al. investigated MMES on national and international levels. Tools for analyzing the integration of renewable energy were reviewed by Connolly et al. (2010). Lund's book gives a summary of their research (Lund, 2014):

- In 1997, Lund analyzed and proposed alternatives to centralized conventional power plants (Lund, 1997).
- In further research, Lund et al. investigated the flexibility of CHP plants combined with heat pumps for balancing of fluctuating wind power (Lund & Münster, 2006).
- They proposed the integration of transport into energy system assessments (Mathiesen, Lund, & Nørgaard, 2008).
- In this way, they strongly suggested considering MMES by integrating more sectors in energy planning (Lund, Andersen, Østergaard, Mathiesen, & Connolly, 2012; Mathiesen et al., 2015).
- Storage technologies, e.g., compressed air energy storage (Lund & Salgi, 2009) and pumped hydroelectric energy storage (Connolly, Lund, Finn, Mathiesen, &

Leahy, 2011; Connolly, Lund, Mathiesen, Pican, & Leahy, 2012), were also analyzed by them.

- They also assessed the use of waste (Münster & Lund, 2009).
- And they investigated energy systems with large shares of renewable energy sources in other countries, e.g., Ireland (Connolly, Lund, Mathiesen, & Leahy, 2011) and China (W. Liu, Lund, & Mathiesen, 2011).
- Last but not least, they showed that extended use of district heating is economically very attractive, in particular in urban areas (Connolly et al., 2014; Lund et al., 2014; Möller & Lund, 2010; Østergaard & Lund, 2011).

Aboumahboub et al. determined the optimal configuration of a renewable-based electricity supply sector on a global and European level (Aboumahboub et al., 2010a; Aboumahboub, Schaber, Tzscheutschler, & Hamacher, 2010b; Aboumahboub, Schaber, Wagner, & Hamacher, 2012). Schaber, Hamacher et al. compared transmission grid extensions, energy storage options and sector coupling with one another, particularly on a European level (Schaber, Steinke, & Hamacher, 2012; Schaber, Steinke, Mühlich, & Hamacher, 2012; Steinke, Wolfrum, & Hoffmann, 2013). Furthermore, Hamacher et al. investigated the feasibility of nuclear fusion in renewable energy systems (Hamacher, Huber, Dorfner, Schaber, & Bradshaw, 2013).

Henning and Palzer (2013) analyzed the German energy system, including in particular also the heat and mobility demand.

Tools, which were introduced in the previous section belonging to this group, are *Balmorel*, *EnergyPLAN*, *MARKAL & TIMES*, *RETScreen* and *urbs*.

Group II): Simple tools for quick assessments of small scale energy systems

energyPRO and *HOMER Pro®* can be categorized in this group. Both tools do not use an actual mathematical optimization. In *energyPRO*, a semi-heuristic strategy called "Minimizing Net Production Cost" determines the operating strategy (EMD International A/S, 2013). *HOMER Pro®*, on the other hand, uses a scenario-based optimization technique for computing a fairly *good* design of the energy system.

Group III): Building and city district energy system design studies with simplified models

One of the first to evaluate several cogeneration and solar technologies for the power and heating sector of a municipal energy system were Bruckner et al. (1997).

Geidl, Andersson et al. formalized the concept of multi-carrier energy systems by proposing the *energy hub* concept. An energy hub represents an interface between different forms of energy. Within the hub, energy can be converted, conditioned or stored (M. Geidl et al., 2007). The conversion process, as well as storage, is mathematically described by a coupling matrix linking an output to an input power vector (Martin Geidl, 2007; Martin Geidl & Andersson, 2005; Krause, Andersson, Fröhlich, & Vaccaro, 2011). Energy hubs provide a formal academic framework for modeling and optimizing multi-modal energy systems. Other researchers used this framework for examining the cost-optimal multi-energy supply of buildings (Adamek, Arnold, & Andersson, 2014), developing a MINLP-based operational optimization of building energy supply (Moghaddam, Saniei, & Mashour, 2016), and implementing a robust optimization

approach for energy management under uncertainties (Parisio, Del Vecchio, & Vaccaro, 2012).

The tools *DER-CAM* and *TOP-Energy*® belong to this group; however, they did not use the energy hub concept.

Group IV): On-site energy system studies with additional features

The research studies were grouped according to their additional features:

- Experimental evaluation: The University of Genoa smart polygeneration microgrid was an experimental test bed integrating several technologies, such as photovoltaic, micro CHP gas turbine, micro wind turbine, absorption chillers, electrochemical energy storage and electric vehicles (Bracco, Delfino, Pampararo, Robba, & Rossi, 2013b). Bracco et al. investigated optimal control strategies for this microgrid (Bonfiglio et al., 2013; Bracco, Delfino, Pampararo, Robba, & Rossi, 2012, 2013a).
- Legal constraints: Lozano et al. developed a MILP model for optimal design and operation of a CHCP system considering legal constraints (M. A. Lozano, Ramos, Carvalho, & Serra, 2009; M. A. Lozano, Ramos, & Serra, 2010).
- Superstructure: Lozano et al. proposed a superstructure defining all feasible technologies. According to this superstructure, the optimal set of technologies was selected, and their capacity and operation determined (Lozano Serrano & Saravia, 2010).
- Environmental constraints: In other research, Lozano et al. also evaluated the influence of environmental constraints on the design of the trigeneration system (Carvalho, Serra, & Lozano, 2011), and allocated economic costs for CHCP at variable load conditions (M. a. Lozano, Carvalho, & Serra, 2011). An overview of their research can be found in M. Carvalho et al. (2013).
- Desalination: Likewise, Rubio-Maya et al. used a superstructure-based approach to determine the optimal design for an energy supply system for a tourist resort. Specifically, they included water as form of energy and also included desalination technologies (Rubio-Maya, Uche-Marcuello, Martínez-Gracia, & Bayod-Rújula, 2011; Rubio-Maya, Uche, & Martínez, 2011).
- Multi-objective optimization: In a tripartite paper, Fazlollahi et al. assessed the multi-objective optimization of district energy systems. Here, they studied the selection of typical operating periods (Fazlollahi, Bungener, Mandel, Becker, & Maréchal, 2014), daily thermal storage (Fazlollahi, Becker, & Maréchal, 2014a), and distribution networks (Fazlollahi, Becker, & Maréchal, 2014b). Further aspects of multi-objective optimization were assessed in Fazlollahi et al. (2012).
- Multi-node microgrids: Menon et al. also studied the optimal design of multi-node microgrids (Menon, Paolone, & Maréchal, 2013).
- Others: Stadler et al. developed a novel sizing method that included an indicator for self-consumption (P. Stadler, Ashouri, & Maréchal, 2016). Criteria for the design of micro CHCP systems were proposed by A. Piacentino & Cardona (2008). In further research, Piacentino et al. developed a method for the optimal design and operation of microgrids that were connected to CHCP systems on the

one side and a cluster of buildings on the other side (Antonio Piacentino & Barbaro, 2013; Antonio Piacentino, Barbaro, Cardona, Gallea, & Cardona, 2013). Heat was considered on two different temperature levels, namely high-grade and low-grade heat. Another mixed-integer linear programming model for the optimal design of district-scale distributed energy systems considering simplified component models was recently developed by Y. Yang, Zhang, & Xiao (2015a, 2015b).

Above-mentioned research focused mostly on the optimization of energy systems described as one-node model, as is also the focus of this Thesis. Other scientists, however, also studied the layout optimization of grid infrastructure, in particular in city districts. Niemi et al. explored the spatial distribution of electricity, heating and cooling demands in a Northern town and an Asian megacity (Niemi, Mikkola, & Lund, 2012). District heating networks were optimized by J. Söderman & Pettersson (2006) and J. Dorfner & Hamacher (2014). The latter also extended their concept to electricity and natural gas grids (Dorfner, 2015, 2016)

Group V): Mixed-integer linear programming with part-load efficiencies

To the best of the author's knowledge, research that was introduced above did not consider detailed component models. In particular, full-load efficiencies were also assumed for part-load operation (constant efficiency approach), when optimizing the system. However, Yokoyama et al. developed a method for considering non-constant part-load efficiencies in the optimization, while – and that is the key point – preserving the linearity of the model (Yokoyama, Hasegawa, & Ito, 2002). The mathematical formulation of this method is explained in Section 3.4. However, the following example shall briefly explain the idea. When considering economic dispatch (optimal control) problems, installation and capacity of technologies are known a priori. In this case, the only optimization variables are on/off status of energy conversion technologies and their power output. Efficiencies can be linear or piecewise-linearized functions of the part-load ratio (ratio of output power over capacity). When optimizing the design of the system, on the other hand, the capacity is also an optimization variable and the part-load ratio cannot be defined by a linear equation (ratio of two variables). Therefore, the problem could be decoupled by considering input and output power separately and defining input power as linear function of the output power of the conversion technology or vice versa. Efficiency is defined as the ratio of output power over input power. Choosing these linear functions properly, nonlinear part-load efficiencies (rational functions) for conversion technologies can be implemented. Notice that the optimization problem remains linear. Yokoyama et al. employed their method in several research studies:

- Gamou, Yokoyama et al. used this method to determine the optimal technologies of an energy supply system for an office building (Gamou, Ito, Yokoyama, & Yoshida, 2004).
- Furthermore, they also evaluated gas turbine inlet air cooling (TIAC) in combination with an ice storage (Yokoyama & Ito, 2004). Here, they only considered active TIAC by the use of the ice storage, cooling the inlet air to a fixed temperature. In addition to this, their study was limited to six representative days with two-hourly time steps.

- Yokoyama and Ito also developed a tool for energy system design studies called *OPS-Design* (Yokoyama & Ito, 2006). As in other papers, the tool only considered representative days per year for reducing the problem complexity. However, in this case, storages were not properly described and actual annual costs would differ. Further information regarding the tool, as well as the tool itself, was not available.
- In advancing research, they investigated the optimal design of energy supply systems driven by both gas turbines (Yokoyama, 2007) and gas engines (Wakui & Yokoyama, 2011).
- They also proposed a framework for the operational optimization of a cogeneration-based residential energy supply network (Wakui, Kinoshita, & Yokoyama, 2014) and assessed the optimal design of a residential cogeneration system including fuel cells for minimizing primary energy consumption (Wakui, Kawayoshi, & Yokoyama, 2016; Wakui & Yokoyama, 2014), as well as with battery (Wakui & Yokoyama, 2015).
- In another study, Yokoyama et al. developed a method for robust optimal design of energy systems under uncertainty based on the minimax regret criterion (Yokoyama, Fujiwara, Ohkura, & Wakui, 2014); here, however, with very simple component models (i.e., constant part-load efficiencies).

A summary of their energy system design method was published by Yokoyama, Shinano, Taniguchi, Ohkura, & Wakui (2014). During their entire research, Yokoyama et al. formulated their energy system design problem as MILP and selected the optimal technologies from a predefined superstructure.

Voll et al. also made use of Yokoyama's method:

- In particular, they developed an approach for automated generation of superstructures based on the P-graph maximal structure generation algorithm, which was used prior to solving the optimal design problem (Voll, 2013; Voll, Klaffke, Hennen, & Bardow, 2013).
- Furthermore, they developed a method for superstructure-free synthesis, in which an evolutionary algorithm as part of the optimal design combined a predefined set of technologies in a way that an optimal structure is achieved (Voll, Lampe, Wrobel, & Bardow, 2012). **Figure 2.4** schematically illustrates these two approaches.
- Schneider investigated branch-and-price for the optimization of distributed energy supply systems (Schneider, 2014).
- Voll et al. also showed that it is important to evaluate near-optimal solutions instead of focusing on a single global optimum (Voll, Jennings, Hennen, Shah, & Bardow, 2015).

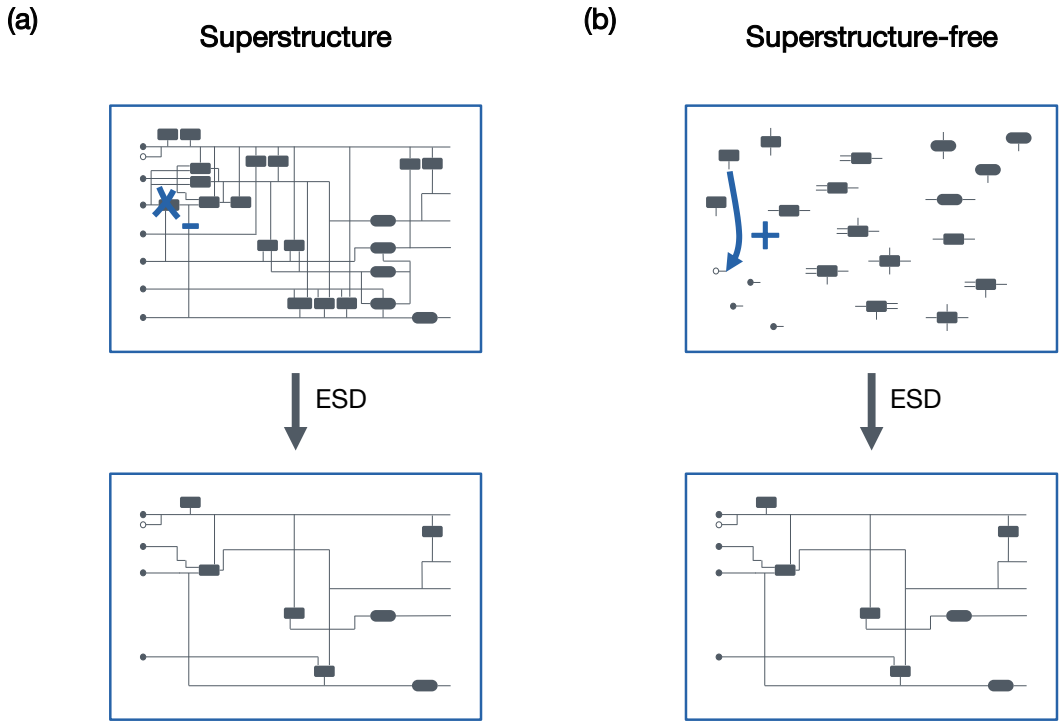

Figure 2.4: (a) Superstructure-based and (b) superstructure-free synthesis approaches for energy system design.

Last but not least, Yokoyama's part-load efficiency approach was also used by Capuder & Mancarella (2014) and Bracco, Dentici, & Siri (2016, 2013).

Group VI): Mixed-integer nonlinear programming with complex models

For increasing the model level of detail, previous research also developed optimization models based on mixed-integer nonlinear programming (MINLP). Depending on the formulation of the nonlinear models, the complexity of the problem can increase manifold compared to the linear formulation. Moreover, problems can be unsolvable or require nondeterministic, meta-heuristic evolutionary or Monte-Carlo-based algorithms. With these, the solution process is difficult to predict, optimality difficult to determine, and the computational efforts can be tremendous (Kallrath, 2013; Kallrath, Rebennack, Pardalos, & Scheidt, 2009; Russell & Norvig, 2012). The following summary briefly reviews research within this group:

- Liu et al. investigated MINLP models for polygeneration energy systems that included synthesis of chemical fuels (P. Liu, 2009; P. Liu, Gerogiorgis, & Pistikopoulos, 2007). For these systems, they also considered multiple objectives, namely economical and environmental (P. Liu & Pistikopoulos, 2010). Furthermore, they evaluated a stochastic programming approach for ESD under uncertainty (P. Liu, Pistikopoulos, & Li, 2010). An overview of their research was published in Liu, Georgiadis, & Pistikopoulos (2011). Liu et al. also employed a superstructure-based optimization method, while only considering selected periods of a year.

- Weber (2008) developed a method for the multi-objective ESD of district energy systems without energy storages. She formulated the overall problem as MINLP, which was then divided into two parts, a MINLP subproblem solved with an evolutionary algorithm and a MILP subproblem. In a later paper, Weber & Shah (2011) reformulated a similar problem as MILP optimization model, here also including thermal energy storages.
- After a review of optimization models for the design of polygeneration energy systems (Jordi Ortiga, Bruno, Coronas, & Grossman, 2007), Ortiga et al. developed a modeling environment for the design and optimization of such energy systems (Coronas & Bruno, 2007; Jordi Ortiga, 2010; Jordi Ortiga, Bruno, & Coronas, 2008). Their model was formulated as MINLP optimization problem and was employed for the operational optimization of the PolyCity project's polygeneration energy system (J Ortiga, Bruno, & Coronas, 2012; Jordi Ortiga, Bruno, & Coronas, 2013). Ortiga's tool *MGEOS*, as well as the tool *TRNSYS* previously introduced, were built upon nonlinear models.
- Fuentes-Cortés et al. also developed a MINLP-based model for the optimal design of multigeneration systems for building complexes (Fuentes-Cortés, Dowling, Rubio-Maya, Zavala, & Ponce-Ortega, 2016).
- Destro, Benato, Stoppato, & Mirandola (2016) implemented a particle swarm optimization algorithm for the optimal design of trigeneration systems with energy storages.
- The expansion planning of cogeneration of (desalinated) water and power in the United Arab Emirates was investigated by Saif & Almansoori (2016). Kim, Chen, & Garcia (2016) developed a dynamic model for a reverse osmosis desalination system and evaluated its performance as flexible load resource.
- Target-oriented robust optimization for handling uncertainties in the energy system design was analyzed by Aviso, Sy, Ubando, & Tan (2015).

Forms of energy considered in previous research

The previous review highlighted the evolution of *multi-modal energy systems*, as well as main research in the field of energy system design, regarding both the focus area and complexity of the modeling, respectively. Some core concepts of ESD, such as superstructures and Yokoyama's part-load efficiency approach, were explained briefly.

In previous research, MMES were also referred to as:

- Multi-energy systems (Mancarella, 2014);
- Smart energy systems (Lund, 2014; Lund et al., 2014, 2012);
- Multicarrier energy systems (Adamek et al., 2014; M. Geidl et al., 2007);
- Integrated energy systems (Fuentes-Cortés et al., 2016; Orecchini & Santiangeli, 2011; Wu et al., 2016);
- Or hybrid energy systems (Basrawi, Yamada, & Obara, 2014).

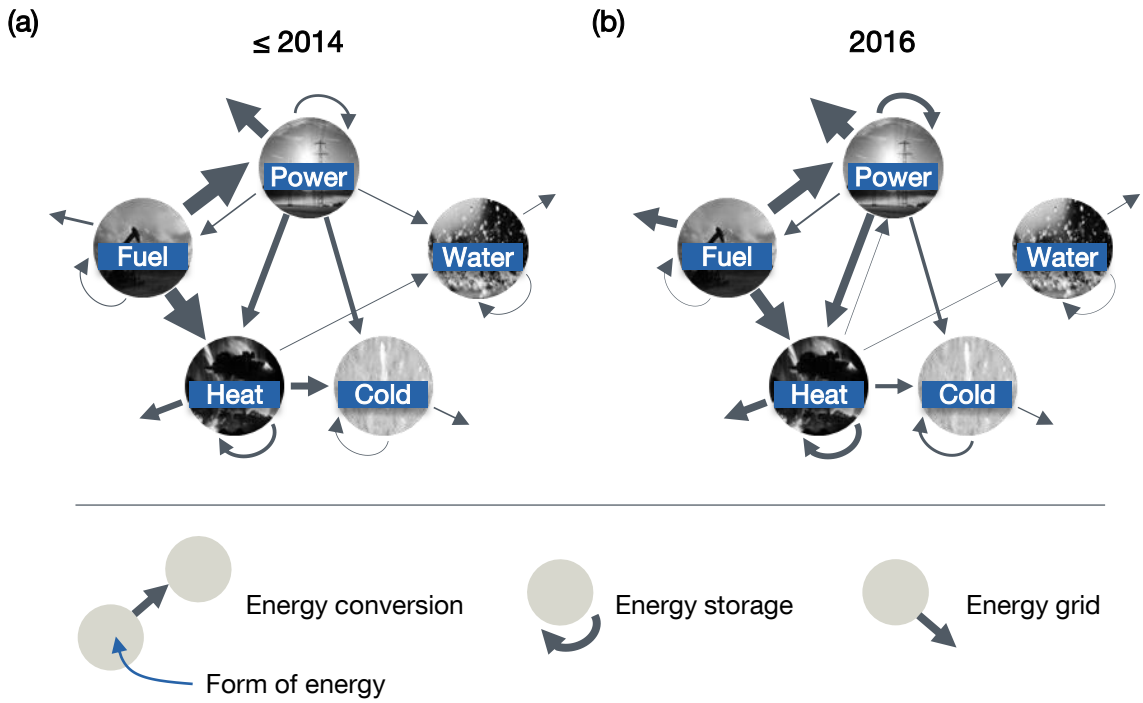

Figure 2.5: Forms of energy considered in previous research: Analysis of (a) Mancarella (2014), (b) Wu et al. (2016).

Figure 2.5 quantifies previous research regarding the forms of energy that were actively examined. MMES, here with five different forms of energy (power, fuel, heat, cold and potable water), can be depicted in the shown way, with energy conversion, storage and transport as indicated. 147 references from a review paper (Mancarella, 2014) and 27 references from a recently published editorial of the journal *Applied Energy* concerning integrated energy systems (Wu et al., 2016) were analyzed regarding their focus area of research in terms of forms of energy. Without doubt, the sampling size of the second group is rather small. However, both papers published prior or in 2014 and papers published in 2016 focused mainly on cogeneration technologies, spanning mostly the energy sectors fuel, power and heat. Heat pumps and chillers, both absorption and compression chillers, were also evaluated in a number of studies. Integration of desalination technology and potable water, on the other hand, was only sparsely examined. From 2014 to 2016, the focus (which may also be subject to the selection of references) shifted to more studies concerning the integration of gas grids and power grids, as well as to the consideration of energy storages. Another review of trigeneration system optimization was published by Ünal, Ercan, & Kayakutlu (2015).

2.5 Concluding remarks

The review of existing tools and previous research revealed that the field of energy system design and multi-modal energy systems has grown significantly over the course of the last two decades. Due to the same underlying physics, mathematical formulations of the optimization models were similar and could be grouped according to their problem classes (e.g., LP, MILP and MINLP) and focus area (e.g., national, district and building

level). However, as in other engineering topics, there is no single solution for all problems. Optimization models were applied to different cases, use different solution strategies, different assumptions, simplifications, components, models, and differentiate in many other aspects. Furthermore, many research questions, such as the integration of long-term energy storage options, different gas turbine inlet air cooling methods, decomposition strategies and many others are still unanswered.

This Thesis makes an attempt to answer the most relevant of these questions (see the objectives in **Section 1.2** for details). The mathematical formulation of the superstructure-based energy system design method is explained in the following chapter. The focus area of this Thesis was illustrated in **Figure 2.3**. Last but not least, the development of an own ESD algorithm and solution method supported the understanding of its limitations and thus helped in drawing better conclusions. To conclude, the practical questions posed in **Section 1.2** necessitated the development of a new ESD method, because the existing tools and previous research were not able to give an answer.

Parts of this Thesis were published after submission of this Thesis (but before publication of it) in a journal paper (Thiem, Danov, et al., 2017). The paper was adapted from this Thesis. However, due to the later publication of this Thesis, the paper is cited in this Thesis only where it is absolutely essential.

3 Superstructure-based optimization method

3.1 Introduction

In this chapter, the new energy system design (ESD) method developed during this research project is formulated as mathematical optimization problem. The method was on the one hand intended for further usage, but on the other hand the results from the use case studies may also contribute to future ESD projects. The requirements and assumptions for the developed method are outlined in this section. In the following section (Section 3.2), the algorithm is schematically illustrated. Section 3.3 introduces the technical superstructure, which was used for the investigations in this Thesis. The actual mathematical formulation of the ESD method is outlined in Section 3.4. Thereafter, models of some selected components are explained. Finally, the method is benchmarked against a state of the art method in Section 3.6. The implementation in a tool with graphical user interface is shown in Section 3.7.

3.1.1 Requirements

The core requirements for the ESD method were derived from the practical questions that this Thesis shall answer (see Section 1.2). Specifically, these requirements extended state of the art ESD tools as outlined in the previous chapter. The requirements were derived as follows:

- Optimal selection and sizing of technologies defined by a technical superstructure;
- Optimal operation of the energy system;
- Consideration of electricity, heating, hot water, cooling and potable water demands;
- Taking into account grid connections, such as the power grid, district heating and district cooling;
- Development and implementation of a modeling framework for energy conversion and storage technologies;
- Detailed modeling, in particular considering dependency of part-load and ambient conditions;
- Consideration of short- and long-term energy storages and their optimization;
- Integration of turbine inlet air cooling and climatic conditions;
- Achieving reasonable computation times.

3.1.2 General assumptions and restrictions

The following list summarizes the general assumptions and restrictions made for the development of the ESD method:

- Quasi-steady state: The energy system was described with quasi-steady state models. However, due to energy storages, time steps were coupled with one another (algebraic equations resulting from discretization of ordinary differential equations).
- Representative year: For this Thesis, a time horizon spanning one year was considered and capital costs were discounted accordingly and considered as equivalent annual costs.
- Ageing: Technology ageing was ignored. Nonetheless, the method could be easily extended to include both multiple years and technology ageing. The optimization problem, however, would become immensely more complicated to solve.
- Integrated planner: The system was *not* described as multi-agent system with distributed intelligence. Instead, this study assumed that an integrated planner operating the multi-modal on-site energy system was the only person in charge for the design and operation of the system (centralized approach).
- One-node energy system: Furthermore, because of the centralized approach, the energy system was also described as single node system. Hence, this study assumed that energy transport losses at the particular site are negligibly small. The description of multiple forms of energy, however, necessitated multiple power balances (multiple nodes from a technical but not necessarily spatial point of view).
- Determinism and inelasticity: Climatic conditions, commodity prices and loads were assumed deterministic and to be known a priori. In particular, the energy system was considered as price taker unable to change the market prices. Furthermore, the demands were assumed inelastic.

3.2 Schematic illustration of the method

Figure 3.1 schematically illustrates the ESD method. The method consists of four nested layers. In the first layer, the optimization problem was solved with constant part-load efficiencies (**Figure 3.1: 1.1**). While doing so, turbine inlet air cooling (TIAC) was ignored in order to reduce the computational effort. A good value for a parameter, the CAPEX-OPEX weight ($w_{\mathrm{C/O}}$), which will be explained in more detail in **Section 3.4**, was determined in multiple iterations. Thereafter, the determined set of technologies was fixed but their capacity loosened in order to optimize the energy system with non-constant part-load efficiencies, also including TIAC (**Figure 3.1**: **1.2**). Furthermore, the capacity of a generic gas turbine with continuously-variable capacity from (**Figure 3.1**: **1.1**) was translated to a combination of actual gas turbines with discrete capacities (**Figure 3.1**: **1.2**). This was automated by the formulation of a small optimization problem, which is not of further relevance here. For each of the iterations in **Layer (1)**, in **Layer (2)**, the design of the system and the operation was optimized (**Figure 3.1**: **2.1**). Subsequently, capacities were fixed and only the operation of dispatchable conversion

technologies and energy storages was optimized (**Figure 3.1**: **2.2**). The latter was required due to the problem decomposition in **Layer (3)**. Energy storages directly couple time steps with one another. To elaborate more on this, consider the following example. An energy storage could be charged in the morning and discharged in the evening of a particular day or vice versa. The optimal strategy depends on many factors, such as price levels and hourly loads. The coupling of the time steps increases the complexity of the optimization problem and magnifies the effort for solving. Two strategies were proposed by other researchers for simplifying the problem:

- Only take representative days/periods into account instead of an entire year (see, e.g., J. Ortiga, Bruno, & Coronas (2011) or Schaber, Steinke, & Hamacher (2012));
- Enforce a periodic storage constraint, i.e., the state of charge of a storage at the end of a day equals the state of charge at the beginning of the day (see, e.g., Y. Yang et al. (2015b)).

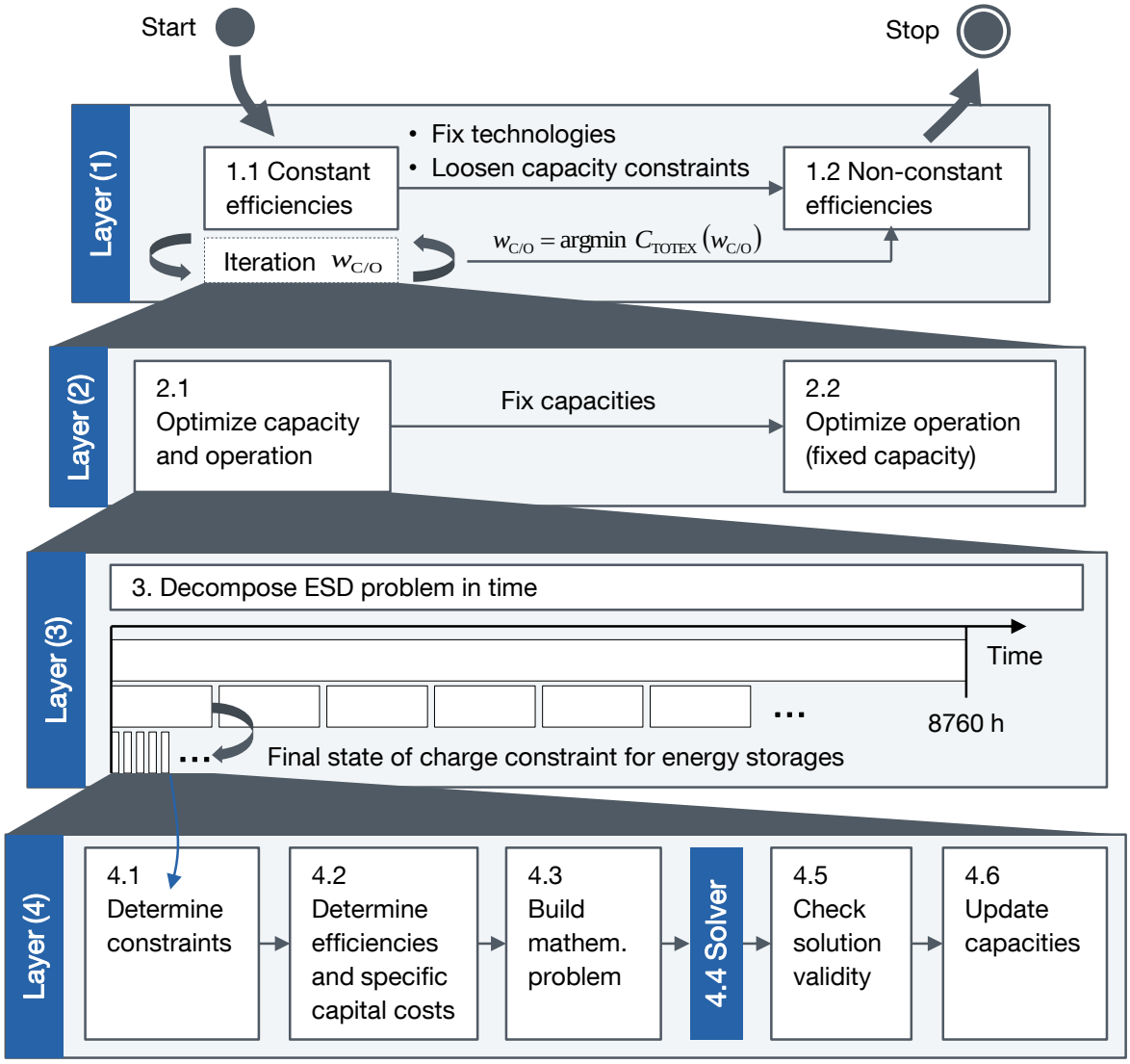

Figure 3.1: Schematic illustration of the ESD method (adapted from Thiem, Danov, et al. (2017)).

Both of these strategies had obvious disadvantages. When considering only representative days of the year, other periods were completely neglected. Hence, the result strongly depended on how these *representative* periods were selected. Furthermore, long-term storage options could not be analyzed. Enforcing periodic storage constraints had similar drawbacks. Long-term storage, which extend the daily constraint, were neglected. This Thesis proposes a novel decomposition strategy based on a time-scale separation for solving the optimal design and operation problem, in particular when considering also long-term storage opportunities. The method in **Layer (3)** is schematically depicted in **Figure 3.1**. Details of the approach are explained in **Section 3.4.8**.

Finally, in **Layer (4)**, first, the constraints (e.g., ambient climatic conditions, loads and prices) for each subproblem were determined (**Figure 3.1**: **4.1**). Thereafter, the efficiencies (see **Section 3.4.2**) and specific capital cost functions (see **Section 3.4.5**) of energy conversion and storage technologies were derived (**Figure 3.1: 4.2**). Based on this information, the mathematical optimization problem could be built (**Figure 3.1: 4.3**) and solved (**Figure 3.1: 4.4**). The validity of the solution was checked (**Figure 3.1: 4.5**) and the determined optimal capacities for the subproblem were treated as minimum capacities for the subsequent subproblem (**Figure 3.1: 4.6**).

3.3 Technical superstructure

Opposed to the *superstructure-free* design approach, which was proposed by Voll et al. (2012) (see also **Figure 2.4**), this Thesis developed a *superstructure-based* energy system design method (Mussati, Barttfeld, Aguirre, & Scenna, 2008; Voll et al., 2013; Yeomans & Grossmann, 1999; Zhou, Liu, Li, & Ni, 2013). The former is based on a list of technologies that the ESD method could combine in any way to meet demands. However, due to many theoretically possible interconnections of energy conversion and storage technologies, this problem is very tedious to solve. Moreover, technically and economically feasible connections are limited and known a priori. The latter, superstructure-based ESD, was computationally more efficient and results were by definition physically feasible. Based on a predefined superstructure of energy conversion and storage technologies that were connected in all physically possible ways, the optimization problem was set up to determine the economically most attractive technologies.

The technical superstructure was designed to be most comprehensive including a vast amount of different state-of-the-art technologies (see **Figure 3.2**). All system inputs are shown on the left hand side of the figure. The energy system could purchase electricity, hot, chilled and potable water from the overlying power, district heating, cooling and water grid, respectively, when the required grid infrastructure was available at a particular location. Furthermore, the energy system could draw in ambient air, as well as salt water, assumed free of charge in this Thesis. The sites demanded different forms of energy. These are shown on the right hand side of the figure. Electricity, hot water, heating, cooling and potable water were considered in this Thesis. In addition to this, electricity could be sold at the wholesale electricity market, when such a market was established in the country under investigation. Energy conversion and storage technologies were plotted in the middle of **Figure 3.2**.

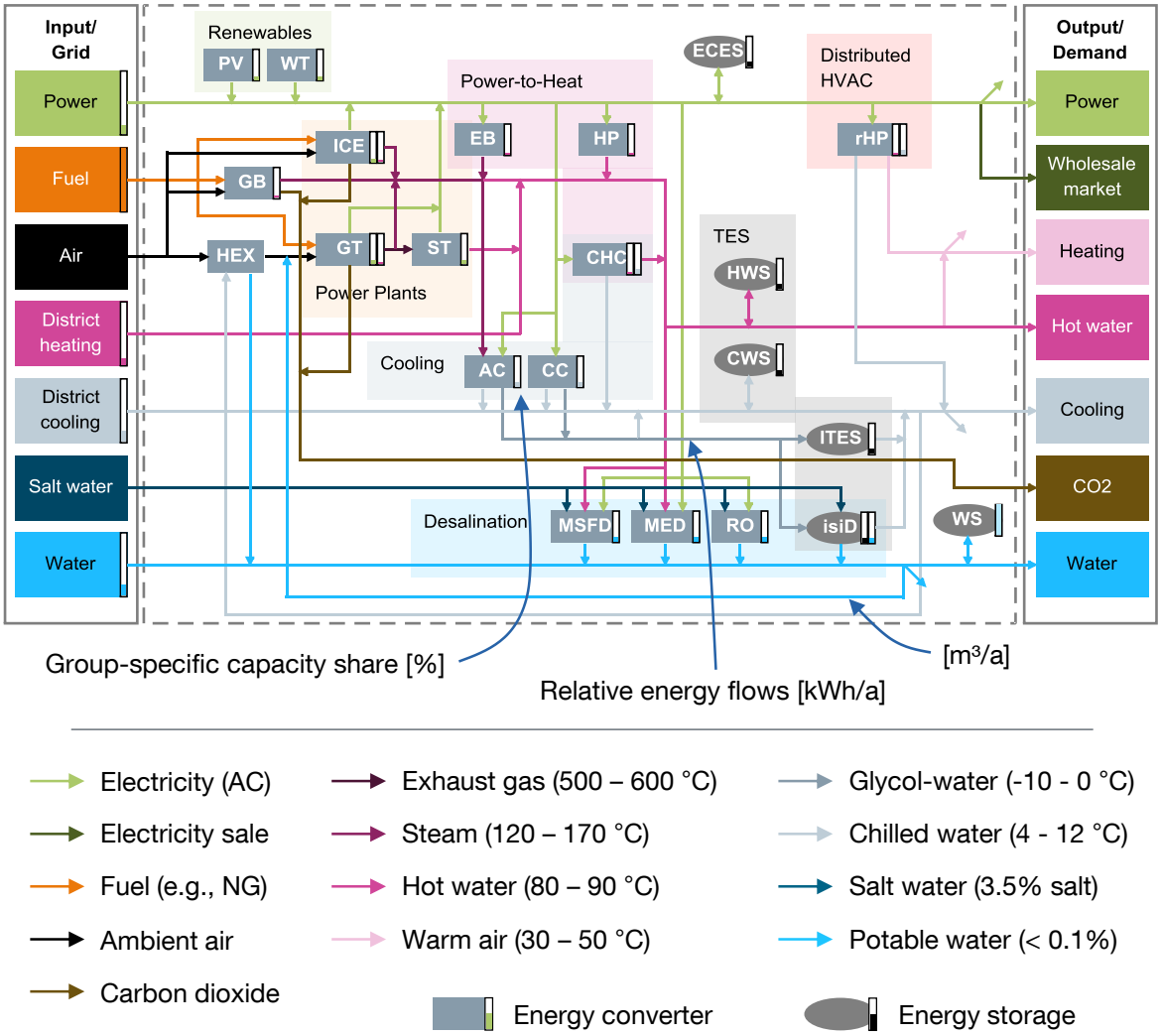

Figure 3.2: Technical superstructure (adapted from Thiem, Danov, et al. (2017)).

These technologies were categorized in the following way:

- Renewables: Solar photovoltaic (PV), and wind turbines (WT);
- Thermal power plants: Gas turbine (GT), steam turbine including heat recovery steam generator, condenser and feedwater pump (ST; entire steam cycle), and internal combustion engine (ICE);
- Gas boiler (GB) and evaporative or active (with heat exchanger, HEX) turbine inlet air cooling (TIAC);
- Power-to-Heat: Electric boiler (EB) and electric heat pump (HP);
- Chillers (cooling): Single-effect lithium bromide/water absorption chiller (AC0) for cooling supply temperatures greater than 0 °C, single-effect ammonia-water absorption chiller (ACi) for cooling supply temperatures less than 0 °C, and compression chillers (CC0 and CCi);

- Distributed heating, ventilation and air-conditioning (HVAC): Reversible heat pump (rHP), which can supply either heating or cooling depending on the direction of the refrigerant flow. Usually, rHP are small-scale to medium-scale units and therefore distributed across the site;
- Combined heating and cooling (CHC), which is a heat pump that supplies both heating and cooling simultaneously;
- Desalination plants: Multi-stage flash distillation (MSFD), multiple-effect distillation (MED), and reverse osmosis (RO);
- Thermal energy storage (TES): Hot water storage (HWS), chilled water storage (CWS), and ice thermal energy storage (ITES);
- Ice-storage integrated desalinated (isiD): The isiD system was developed and experimentally validated during this study and is the only non-commercially available technology investigated in this Thesis (see **Section 3.5.4**). It uses the phase change within an ice storage for *freeze desalination* of salt water;
- Other storages, such as electrochemical energy storages (ECES, specifically lead-acid (LeadAcid) and lithium-ion (LiIon) batteries), and a water storage (WS).

Thermal energy was considered at six different temperature levels, thereof heat at four and cooling at two different levels. With a heat recovery steam generator (HRSG), high temperature (500 °C to 600 °C) exhaust gases from gas turbines could be used for generating steam, which could drive a steam cycle (combined cycle power plant). For ammonia-water absorption chillers (AC), a physical model based on the *Reference Fluid Thermodynamic and Transport Properties Database (REFPROP)*[4] was developed. At cooling supply temperatures less than 0 °C and very high ambient temperatures (e.g., 40 °C), AC required high driving temperatures (up to 150 °C). Additionally, hot water (80 °C to 95 °C) and warm air (30 °C to 50 °C) were distinguished. Both glycol-water mixtures (-10 to -2 °C) and chilled water (4 °C to 12 °C) could carry 'cold', an exergetic potential to extract heat (cooling) from something. Salt water was assumed to be either seawater or brackish water and unlimitedly available without any payment due. The average salt content was assumed to 35 g salt per kg water (3.5%, compare Fritsch et al. (2010)). Salt contents within fresh water must not exceed 0.1%. The extraction or generation (e.g., by desalination) of potable water, as well as the distribution to the end-customer, requires energy. Hence, in this Thesis, potable water was considered as a form of energy. Carbon dioxide (CO_2) emissions were also taken into consideration.

As shown in **Figure 3.2**, the introduced system allowed the analysis of multi-modal on-site energy systems. In particular, the economically most efficient technologies could be determined depending on a number of parameters, such as the location, climate and price structure. Specifically, the following groups could be compared with each other:

- On-site generation vs. energy supply from external sources;
- Renewables vs. thermal power plants;

[4] REFPROP was developed by the National Institute of Standards and Technology and is available at: http://www.nist.gov/srd/nist23.cfm

- Heating using high-grade electricity vs. fossil fuels vs. district heating;
- Cooling of buildings by utilizing district cooling vs. electricity- vs. heat-based cooling;
- Distributed (e.g., rHP) vs. centralized heating (e.g., HP) and cooling (e.g., CC0);
- On-site integrated desalination vs. water supply from external water infrastructure;
- Thermal vs. electrochemical vs. no energy storages.

In **Figure 3.2** and in the illustrations of the ESD study results that are shown in **Chapter 4**, the bars next to the energy conversion and storage technologies indicate group-specific capacity shares. The different groups are depicted with different colors (e.g., black for energy storages). The lines, on the other hand, embody relative annual energy flows (*Sankey diagram*).

The presented superstructure is much more comprehensive than those of previous research studies (compare **Section 2.4**) due to the following criteria:

- It contains many more energy technologies including a variety of heating, cooling and desalination plants;
- A multitude of different energy forms are considered; in particular also thermal energy at different temperature levels representing its quality;
- The superstructure extensively uses energy storage options.

3.4 Mathematical formulation

This Thesis proposes a mixed-integer linear programming (MILP) formulation of the ESD method (Thiem, Danov, et al., 2017). The basic governing equations, such as the power balance, ramp-up and ramp-down constraints, were well known in literature (see **Chapter 2**). The fundamental equations, however, were, first, applied to a novel energy system, and second, extended for including new models (e.g., TIAC), more modeling details as well as other features such as long-term energy storages.

Figure 3.3 depicts the outline of the following mathematical formulation. First, the variables and mathematical sets are introduced (**Section 3.4.1**). Based on these, energy converters (**Section 3.4.2**), storages (**Section 3.4.3**) and grid connections (**Section 3.4.4**) are modeled. Constraints for the installation of these technologies (**Section 3.4.5**) as well as a power balance for the overall energy system (**Section 3.4.6**) are developed. Finally, the objective function is derived (**Section 3.4.7**) and the decomposition strategy introduced (**Section 3.4.8**).

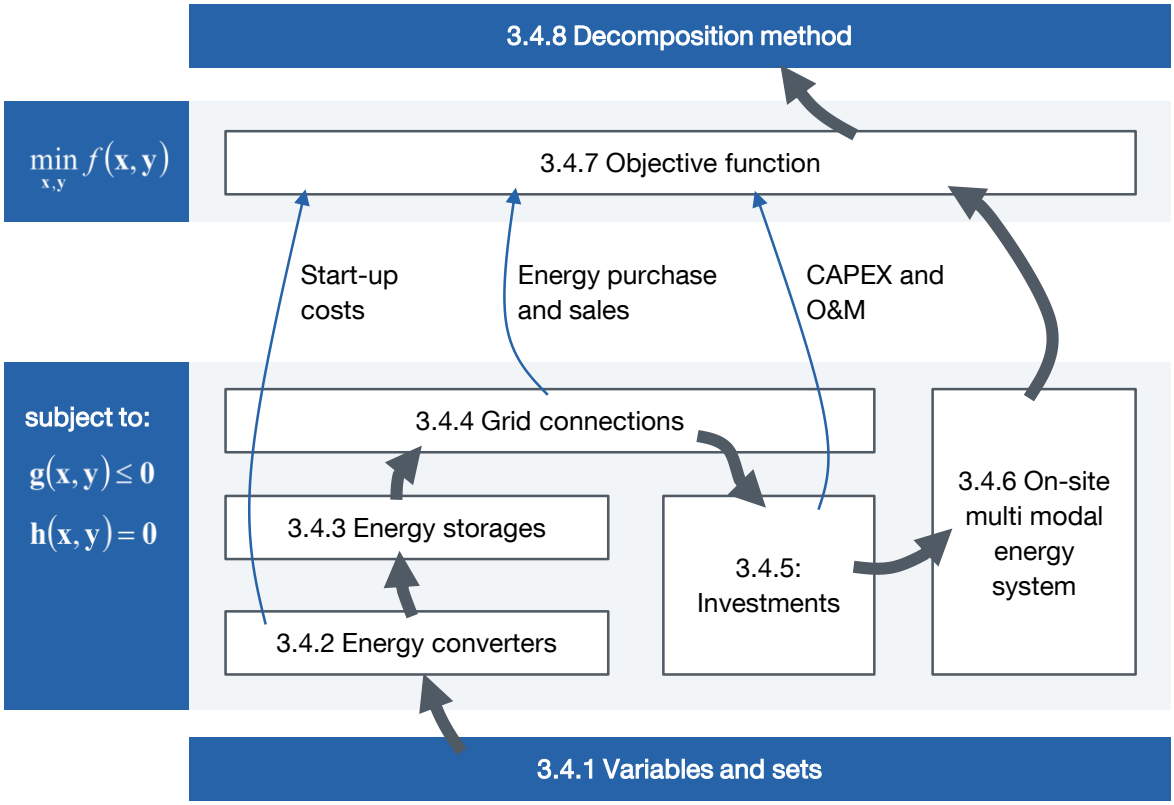

Figure 3.3: Outline of the mathematical formulation.

3.4.1 Variables and sets

The ESD problem was designed to optimize the installation of energy conversion and storage technologies, as well as the usage of grid connections, ($\mathbf{I} \in \{0,1\}^{n_I}$), their nominal capacities ($\mathbf{Q} \in \mathbb{R}_{\geq 0}^{n_Q}$), and at the same time to solve an economic dispatch problem finding optimal power flows ($\mathbf{P} \in \mathbb{R}_{\geq 0}^{n_P \times n_T}$) and storage levels ($\mathbf{E} \in \mathbb{R}_{\geq 0}^{n_E \times n_T}$) at each instance in time ($\mathbf{t} \in \mathbb{R}_{\geq 0}^{n_T}$). The number of technologies that could be installed (n_I), the number of capacities to be optimized (n_Q) and the number of power flows (n_P) and storage levels (n_E) were defined beforehand. In addition to this, the optimization time (one year) was discretized (n_T). Furthermore, for each instance in time, energy converters could be online or offline ($\mathbf{O} \in \{0,1\}^{n_{EC} \times n_T}$), given the number of energy converters (n_{EC}).

The climatic conditions at a particular location were characterized by their ambient temperature ($\mathbf{T}_{amb} \in \mathbb{R}_{\geq 0}^{n_T}$), pressure ($\mathbf{p}_{amb} \in \mathbb{R}_{\geq 0}^{n_T}$), relative humidity ($\boldsymbol{\varphi}_{amb} \in \mathbb{R}_{\geq 0}^{n_T}$), global horizontal irradiance ($\mathbf{GHI} \in \mathbb{R}_{\geq 0}^{n_T}$) and wind speed ($\mathbf{v}_w \in \mathbb{R}_{\geq 0}^{n_T}$).

The technical superstructure was a combination of several components. The components were categorized into groups; and mathematical sets were defined for these groups:

- Energy converters[5]: EC;

[5] In this Thesis, *energy converters (EC)* denote energy conversion technologies.

- Renewable energy converters: RE;
- Energy storages: ES;
- Inlet and outlet grid connections: GC_{in} and GC_{out};
- Energy demands: ED;
- Energy downgrading, e.g., converting high-temperature heat to medium-temperature heat: DG;
- Energy that is not put to any use but wasted: W.

For the following formulations, note the following example of an expression:

$$h(Q_j) = 0, \quad \forall j \in EC, \quad h: \mathbb{R}_{\geq 0} \rightarrow \mathbb{R}. \tag{3.1}$$

The expression means that the function (h) evaluated for the capacities ($\mathbf{Q}$) of all energy converters defined by their set (EC) must be equal to 0.

3.4.2 Energy converters

In their basic functionality, energy converters (EC) convert one or multiple input energies into one or multiple output energies. The capacity of the EC was related to its defining output power, e.g., the electric power output for gas turbines.

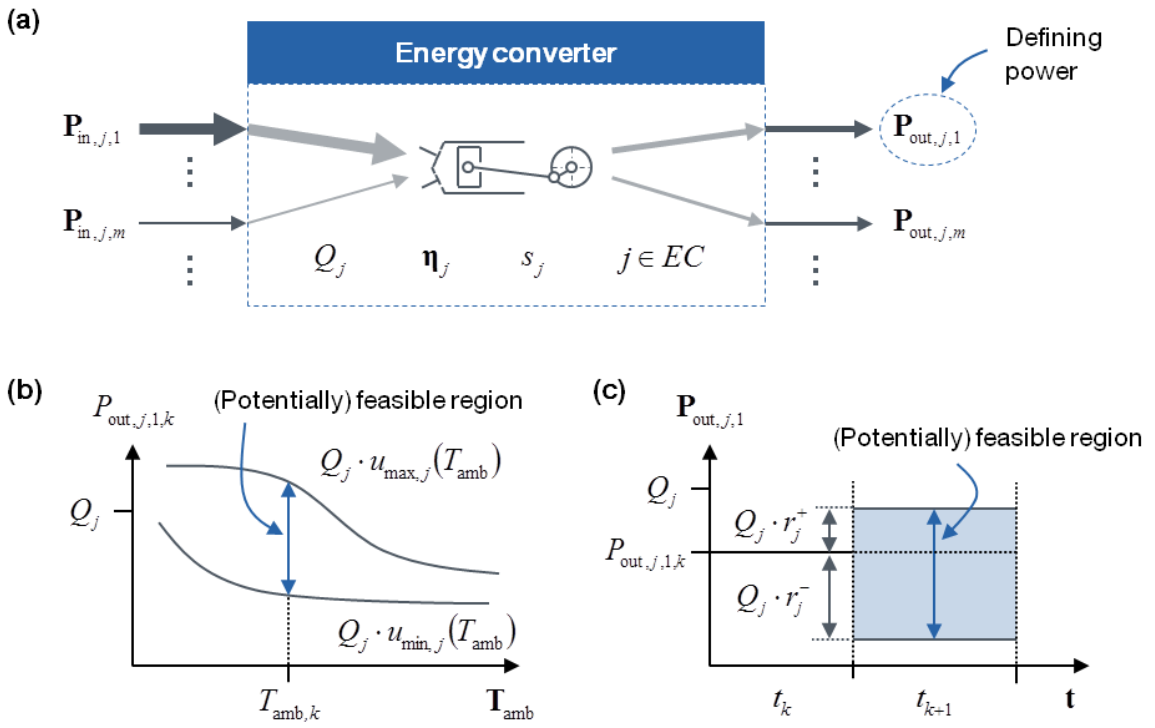

Figure 3.4: Energy converters: (a) Multiple input-output scheme and variables, (b) Minimum and maximum part-load ratio constraint, (c) Ramp-up and ramp-down constraints.

Figure 3.4 (a) schematically illustrates an example of an EC. The shown EC converts multiple input power flows ($\mathbf{P}_{\text{in},j}$) to multiple output power flows ($\mathbf{P}_{\text{out},j}$), both subsets of

the power flow matrix ($\mathbf{P}$) introduced above. The basic model parameters of EC are listed in **Table 3.1**. The table also outlines the units of the particular parameters, as well as on which other variables (e.g., ambient temperature) these could depend on. For the latter, parameters were defined as functions.

Table 3.1: Energy converter model parameters.

Parameter	Variable	Units		Function of
Specific ramp-up and ramp-down limits	r^+, r^-	[(% of Q)/(100 h)]		-
Specific start-up costs	s	[$/(W Q)]	[$/(m³/s Q)]	-
Minimum and maximum part-load ratios	$\mathbf{u}_{\min}$, $\mathbf{u}_{\max}$	[-]		$\mathbf{T}_{amb}$, $\mathbf{p}_{amb}$, $\boldsymbol{\varphi}_{amb}$, Q
Efficiencies (electrical, thermal, ...)	$\boldsymbol{\eta}$	[-]		$\mathbf{T}_{amb}$, $\mathbf{p}_{amb}$, $\boldsymbol{\varphi}_{amb}$, Q, $\mathbf{u}$

An energy conversion technology (j) could only go online ($O_{j,k}$) and convert energy, if it was installed (I_j),

$$O_{j,k} \leq I_j, \quad \forall j \in EC, \forall k \in TM \tag{3.2}$$

with the set (TM) defining all feasible time steps (k). As illustrated in **Figure 3.4 (b)**, the energy converter might only operate within a certain minimum ($\mathbf{u}_{\min}$) and maximum ($\mathbf{u}_{\max}$) part-load ratio, which could be defined as functions of the ambient temperature or other climatic conditions. The condition was implemented as

$$Q_j u_{\min,j,k} O_{j,k} \leq P_{\text{out},j,1,k} \leq Q_j u_{\max,j,k} O_{j,k}, \quad \forall j \in EC, \forall k \in TM. \tag{3.3}$$

The part-load ratio ($\mathbf{u}_j$) of an EC was defined as the defining power output ($\mathbf{P}_{\text{out},j,1}$), relative to its capacity (Q_j),

$$\mathbf{u}_j = \frac{\mathbf{P}_{\text{out},j,1}}{Q_j}, \quad \forall j \in EC. \tag{3.4}$$

The flexibility of energy converters is limited due to the inertia of the underlying physical components. For example, in conventional power plants, large temperature differences across components with thick walls cause thermal stress. Due to their heat capacity and the need for thermal conduction, these components have a non-negligible thermal inertia. Hence, the thick-wall components require time in order to not exceed acceptable temperature differences across their walls (Schröder, Kunz, Meiss, Mendelevitch, & von Hirschhausen, 2013). The maximum ramp-up ($Q_j r_j^+$) and ramp-down ($Q_j r_j^-$) of the power output ($\mathbf{P}_{\text{out},j,1}$) were restricted by the following expression (see also **Figure 3.4 (c)**):

$$Q_j r_j^- \leq \frac{P_{\text{out},j,1,k+1} - P_{\text{out},j,1,k}}{t_{k+1} - t_k} \leq Q_j r_j^+, \quad \forall j \in EC, \forall k \in TM. \tag{3.5}$$

Equation (3.3) and **Equation (3.5)** define potentially feasible regions for the power flow control space. The intersection of these two regions defines the feasible space. Note that time steps were coupled by **Equation (3.5)**.

In addition to the ramp-up and ramp-down constraints (**Equation (3.5)**), the number of start-ups of an energy conversion technology could be restricted. This could be modeled by defining minimum uptimes and downtimes of EC (further constraints). In this Thesis, however, costs were introduced for the start-ups of energy converters. The start-up costs were included in the objective function. With the overall goal of minimizing total expenditures, the optimizer could reduce start-ups as far as economically feasible. Start-ups cause costs due to two reasons (Kumar, Besuner, Lefton, Agan, & Hilleman, 2012; Schröder et al., 2013):

- Requirement of start-up fuels, auxiliary energy, chemicals or personnel;
- Wear and tear of the components causing higher maintenance and shorter life times.

The two portions of costs depend on each other. When starting an energy converter faster, costs for start-up fuels and auxiliary energy are reduced, but wear and tear increase. For reducing wear and tear, the EC must generally be started slower and may need more start-up fuel. Further, hot, warm and cold starts could be distinguished (Schröder et al., 2013). However, this study did not focus on the economic dispatch of the energy system; instead, the optimal design was the core focus. Therefore, for example, deterministic load profiles and perfect foresight were assumed (see, e.g., **Section 3.1.2**). Hence, this study used average start-up costs and assumed that the EC could be started on time due to the perfect foresight. In energy system design, the capacity ($\mathbf{Q}$) is an optimization variable. Starting a small EC causes different costs than starting a large EC of the same type. Therefore, specific start-up costs ($s = \mathrm{const.}$) were proposed for modeling start-ups. Hot, warm and cold starts were difficult to distinguish within the MILP optimization model and were therefore not taken into account (as this is also not the focus area of this Thesis).

For coupling time steps and determining when a start-up has happened, a new helper variable ($\mathbf{Z} \in \{0,1\}^{n_{\mathrm{EC}} \times n_T}$) was introduced. With the following two equations,

$$O_{j,k+1} - O_{j,k} \leq Z_{j,k+1}, \quad \forall j \in EC, \forall k \in TM, \tag{3.6}$$

$$C_{\mathrm{SU},j,k} = Z_{j,k} s_j Q_j, \quad \forall j \in EC, \forall k \in TM, \tag{3.7}$$

the start-up costs ($C_{\mathrm{SU},j,k}$) for the EC (j) and time step (k) could be determined. Note that $C_{\mathrm{SU},j,k} \sim Z_{j,k}$ and the cost term ($C_{\mathrm{SU},j,k}$) was part of the objective function (see **Section 3.4.7**). Hence, the solver chose $Z_{j,k+1} = 0$, if $O_{j,k+1} = O_{j,k}$, and $Z_{j,k+1} = 1$, if $O_{j,k+1} = 1 > O_{j,k} = 0$. The total start-up costs over the entire optimization horizon and all energy conversion technologies were derived as follows:

$$C_{\mathrm{SU}} = \sum_{j \in EC} \left[\sum_{k \in TM} \left(C_{\mathrm{SU},j,k} \right) \right]. \tag{3.8}$$

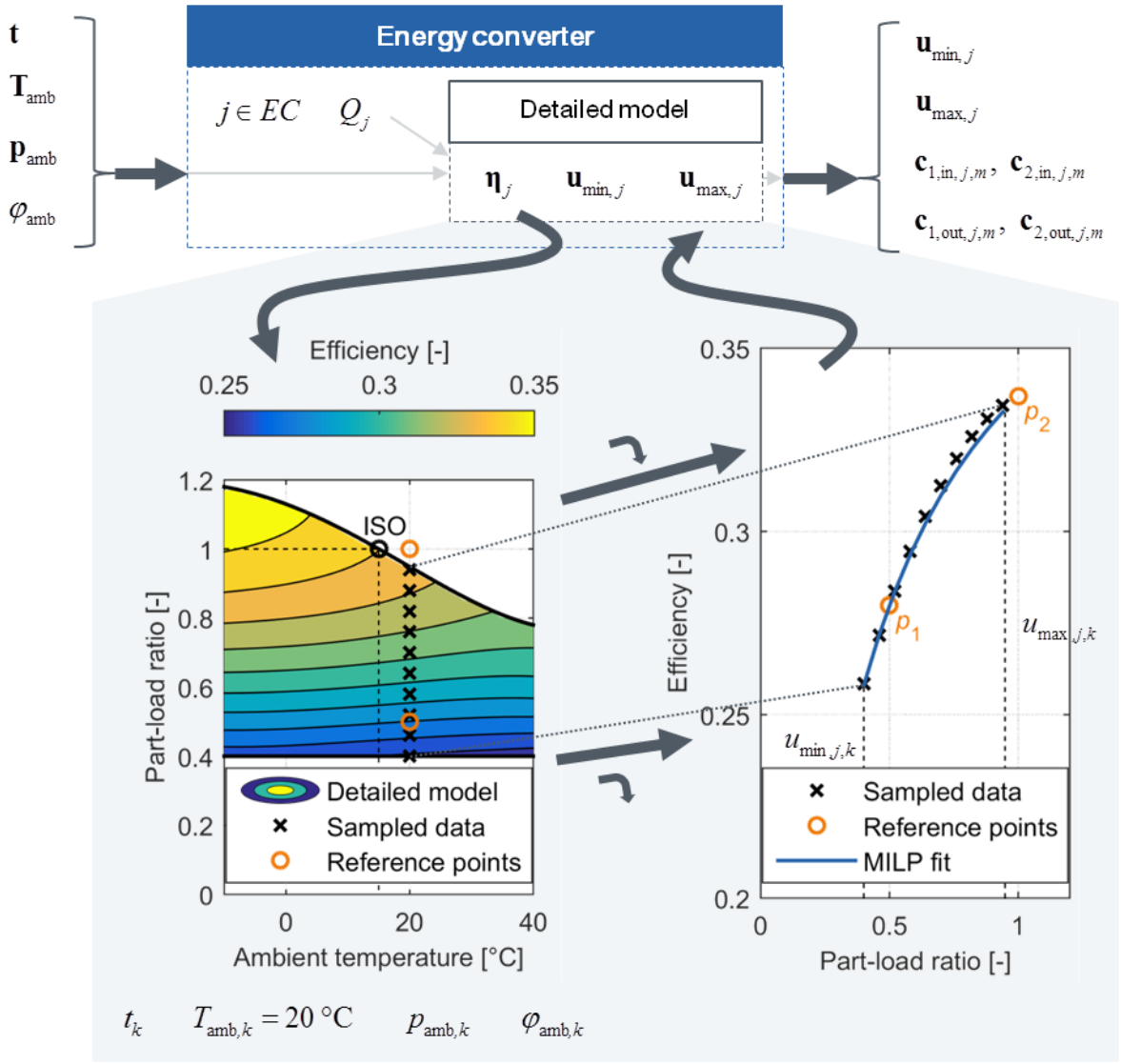

Figure 3.5: Energy conversion technology[6] modeling framework: Integration of detailed models and climatic conditions (adapted from Thiem, Danov, et al. (2017)).

Finally, output power flows of energy converters were related to input power flows by their respective efficiencies. Yokoyama's (2002) approach for integrating non-constant part-load efficiencies in the MILP optimization model was outlined in **Section 2.4**. On the contrary to Yokoyama's approach, input power flows ($\mathbf{P}_{\text{in},j,m}$) were related to the defining output power flow ($\mathbf{P}_{\text{out},j,1}$), instead of the opposite,

$$P_{\text{in},j,m,k} = \left[c_{1,\text{in},j,m,k} P_{\text{out},j,1,k} + c_{2,\text{in},j,m,k} Q_j\right] O_{j,k}, \quad \forall j \in EC, \forall m \in IN_j, \forall k \in TM. \tag{3.9}$$

IN_j is the set defining the input connections to the energy converter (j). By formulating the relation in this way, the defining output power could be described without an offset (as independent power). The input power, on the other hand, had an offset, which could

[6] Example technology: Siemens gas turbine SGT-400 (Siemens AG, 2009b).

also be physically motivated. The input power, therefore, was the sum of a fixed part that was independent of the part-load ratio, and a variable part that depended on the part-load ratio. Further advantages of formulating the input-to-output power relation in this way are outlined below. In this Thesis, to the best of the author's knowledge, the first time multiple input and multiple output energy converters were considered. Therefore, also other output power flows were related to the defining output power flow,

$$P_{\mathrm{out},j,m,k} = \left[c_{1,\mathrm{out},j,m,k} P_{\mathrm{out},j,1,k} + c_{2,\mathrm{out},j,m,k} Q_j\right] O_{j,k}, \quad \forall j \in EC, \forall m \in OUT_j, \forall k \in TM, \tag{3.10}$$

with the set (OUT_j) defining all output connections but the defining connection (compare **Figure 3.4 (a)**) for the energy conversion technology (j).

The parameters ($c_{1,\mathrm{in},j,m,k}$, $c_{2,\mathrm{in},j,m,k}$, $c_{1,\mathrm{out},j,m,k}$ and $c_{2,\mathrm{out},j,m,k}$) were constant for a particular EC (j), time step (k) and input or output (m). They were determined according to the modeling framework illustrated in **Figure 3.5**. The framework is part of Step (**Figure 3.1: 4.2**) depicted in the schematic illustration of the algorithm in **Figure 3.1**. Based on time ($\mathbf{t}$), climatic conditions ($\mathbf{T}_{\mathrm{amb}}$, $\mathbf{p}_{\mathrm{amb}}$ and $\boldsymbol{\varphi}_{\mathrm{amb}}$) and an average capacity (Q_j), a detailed model determined the minimum and maximum part-load ratios, as well as the parameters ($\mathbf{c}_{1,\mathrm{in},j,m}$, $\mathbf{c}_{2,\mathrm{in},j,m}$, $\mathbf{c}_{1,\mathrm{out},j,m}$ and $\mathbf{c}_{2,\mathrm{out},j,m}$). In **Figure 3.5**, results for the efficiency of a particular input (m) to defining output were plotted on the left hand side. At a particular time step, the ambient temperature ($T_{\mathrm{amb},k}$) was assumed to 20 °C. As shown in the figure, the efficiency results obtained with the detailed models were sampled at this temperature. The detailed model was executed outside of the solver (**Figure 3.1: 4.4**). Therefore, the detailed model could be very complex. The framework further suggests deriving the MILP fit plotted in **Figure 3.5**, which is essentially an approximation to the detailed model at particular conditions.

When deriving the MILP fit plotted in **Figure 3.5**, the following equations shall be considered. For input power flows (**Equation (3.9)**), the efficiency could be defined as a ratio of defining output power flow and considered input power flow,

$$\eta_{j,m,1,k} = \frac{P_{\mathrm{out},j,1,k}}{P_{\mathrm{in},j,m,k}} = \frac{P_{\mathrm{out},j,1,k}}{\left[c_{1,\mathrm{in},j,m,k} P_{\mathrm{out},j,1,k} + c_{2,\mathrm{in},j,m,k} Q_j\right] O_{j,k}}. \tag{3.11}$$

With $P_{\mathrm{out},j,1,k} = u_{j,k} Q_j$, **Equation (3.11)** could be rewritten as follows:

$$\eta_{j,m,1,k} = \frac{u_{j,k} Q_j}{\left[c_{1,\mathrm{in},j,m,k} u_{j,k} Q_j + c_{2,\mathrm{in},j,m,k} Q_j\right] O_{j,k}} = \frac{u_{j,k}}{\left[c_{1,\mathrm{in},j,m,k} u_{j,k} + c_{2,\mathrm{in},j,m,k}\right] O_{j,k}}. \tag{3.12}$$

Hence, when the energy converter was online, the efficiency ($\eta_{j,m,1,k}$) of an energy converter (j) input (m) to the defining output (1) at time step (k) was a rational function of the part-load ratio ($u_{j,k}$). The two parameters ($c_{1,\mathrm{in},j,m,k}$ and $c_{2,\mathrm{in},j,m,k}$) could be chosen to optimally fit the efficiency determined with the detailed model. Instead of performing a regression analysis, choosing two reference points ($u_{p1} = 0.5$ and $u_{p2} = 1$), the coefficients could be determined to

$$c_{1,\mathrm{in},j,m,k} = \frac{2}{\eta_{p2,j,m,1,k}} - \frac{1}{\eta_{p1,j,m,1,k}}, \tag{3.13}$$

$$c_{2,\mathrm{in},j,m,k} = \frac{1}{\eta_{p1,j,m,1,k}} - \frac{1}{\eta_{p2,j,m,1,k}}, \tag{3.14}$$

which is shown in **Figure 3.5**. The rational function for the efficiency could be adjusted to fit many energy converter efficiencies very well. For example, the part-load electric efficiency of the gas turbine in **Figure 3.5** was fitted sufficiently well. Advantages of using the approach with two reference points were:

- There was no regression analysis required;
- Only two parameters (η_{p1} and η_{p2}) needed to be transmitted; the detailed model could be encapsulated and hidden for confidentiality;
- Furthermore, the model framework enabled the use of models with different levels of details for different converters. Additionally, the models could be implemented without the need to understand or change the optimization model formulation.

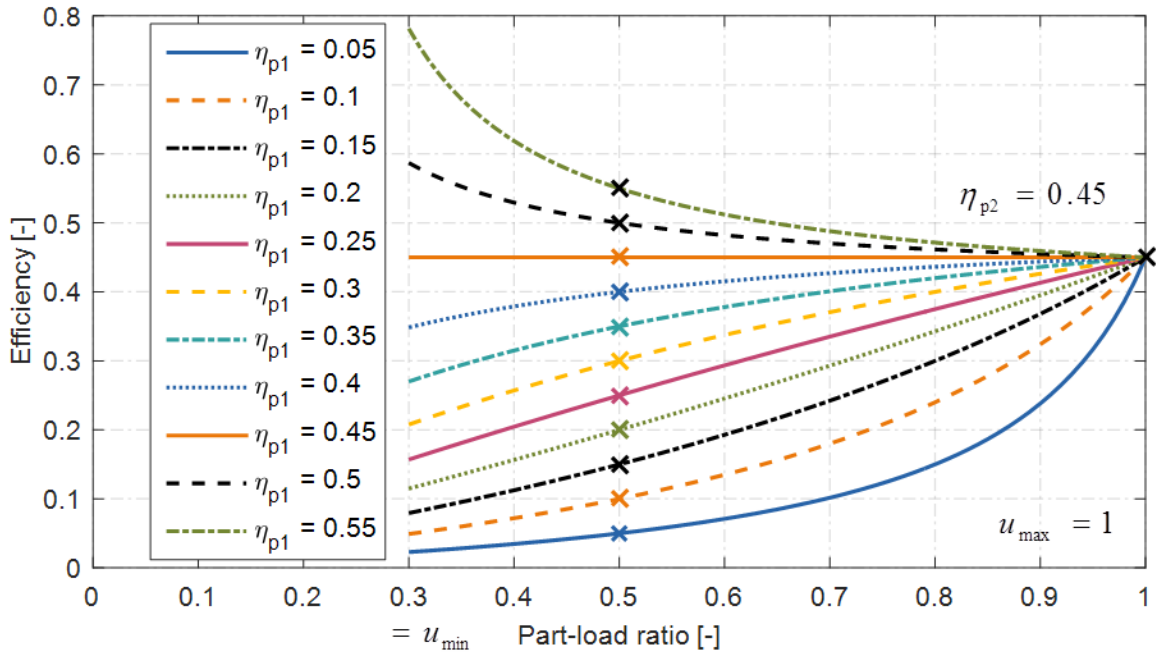

Figure 3.6: Example family of efficiency curves that could be obtained with the described MILP fit.

Figure 3.6 illustrates the family of efficiency curves using the described MILP fit for an example ($\eta_{p2} = 0.45$, $u_{min} = 0.3$, $u_{max} = 1$). The curves with parameters ($\eta_{p1} \in \{0.2, 0.3, 0.35, 0.4\}$) could be adequate for the electrical efficiency of a particular gas turbine type. The curves with parameters ($\eta_{p1} \in \{0.5, 0.55\}$), on the other hand, could be good fits for the thermal efficiency of a gas turbine in part load.

For output power flows (**Equation (3.10)**), when only the efficiency from input to output is known (e.g., thermal efficiency for a gas turbine), **Equations (3.13) and (3.14)** must be modified to

$$c_{1,\mathrm{out},j,m,k} = \frac{2}{\frac{\eta_{p2,j,1,m,k}}{\eta_{p2,j,1,1,k}}} - \frac{1}{\frac{\eta_{p1,j,1,m,k}}{\eta_{p1,j,1,1,k}}}, \tag{3.15}$$

$$c_{2,\mathrm{out},j,m,k} = \frac{1}{\frac{\eta_{p1,j,1,m,k}}{\eta_{p1,j,1,1,k}}} - \frac{1}{\frac{\eta_{p2,j,1,m,k}}{\eta_{p2,j,1,1,k}}}. \tag{3.16}$$

For example, $\eta_{p1,j,1,1,k}$ and $\eta_{p2,j,1,1,k}$ could denote the electric efficiencies, $\eta_{p1,j,1,m,k}$ and $\eta_{p2,j,1,m,k}$ could denote the thermal efficiencies at the reference points $p1$ and $p2$, respectively.

According to this framework, the detailed models were stored in a model library in external files and were accessed through the standardized interface with defined input and output variables illustrated in **Figure 3.5**.

Equations (3.3), **(3.7)**, **(3.9)** and **(3.10)** were nonlinear equations, because they contained products of a continuous and a binary variable. These could be rewritten to mixed integer linear formulations (see, e.g., Glover (1975)). For example, consider **Equation (3.7)**. Given $s_j Q_j < M_j = s_j Q_{\max,j} = \mathrm{const.}$, the nonlinear equality constraint was rewritten to the following four mixed integer linear inequality constraints:

$$C_{\mathrm{SU},j,k} \leq Z_{j,k} M_j, \quad \forall j \in EC, \forall k \in TM, \tag{3.17}$$

$$C_{\mathrm{SU},j,k} \geq 0, \quad \forall j \in EC, \forall k \in TM, \tag{3.18}$$

$$C_{\mathrm{SU},j,k} \leq s_j Q_j, \quad \forall j \in EC, \forall k \in TM, \tag{3.19}$$

$$C_{\mathrm{SU},j,k} \geq M_j \cdot \left(Z_{j,k} - 1\right) + s_j Q_j, \quad \forall j \in EC, \forall k \in TM. \tag{3.20}$$

3.4.3 Energy storages

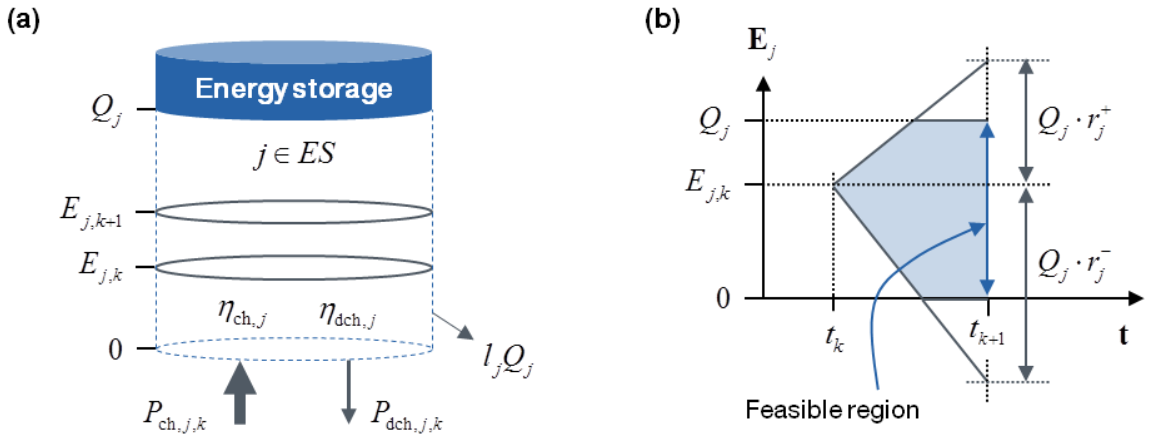

Figure 3.7: Energy storages: (a) Schematic illustration, (b) Maximum charge and discharge constraints.

Energy storages offer the possibility to transport energy in time, charging them at some point in time and discharging them some time later. **Figure 3.7 (a)** shows the basic variables for the modeling of energy storages.

In this figure, the energy storage is net charged between two time steps (t_k and t_{k+1}). The power flow into the energy storage ($P_{\mathrm{ch},j,k}$) is greater than the outgoing energy flow ($P_{\mathrm{dch},j,k}$) and its losses ($l_j Q_j$). Here, l_j denoted a specific self-discharge rate. Furthermore, constant charge (η_{ch}) and discharge efficiencies (η_{dch}) could reduce the power flow into and the usable flow out of the energy storage. The governing equation for the energy storage level was mathematically expressed as follows:

$$\frac{E_{j,k+1} - E_{j,k}}{t_{k+1} - t_k} = \eta_{\mathrm{ch}} P_{\mathrm{ch},j,k} - \frac{1}{\eta_{\mathrm{dch}}} P_{\mathrm{dch},j,k} - l_j Q_j, \quad \forall j \in ES, \forall k \in TM. \tag{3.21}$$

All basic parameters for the description of energy storages are summarized in **Table 3.2**.

Table 3.2: Energy storage model parameters.

Parameter	Variable	Units	Function of
Specific ramp-up and ramp-down limits	r^+, r^-	[(% of Q)/(100 h)]	-
Charge and discharge efficiency	η_{ch}, η_{dch}	[-]	-
Self-discharge rate	l	[(% of Q)/(100 h)]	-

The energy storage (level ($E_{j,k}$) might not exceed the installed storage capacity (Q_j), as well as the storage might not be more than fully depleted,

$$0 \leq E_{j,k} \leq Q_j, \quad \forall j \in ES, \forall k \in TM. \tag{3.22}$$

Furthermore, the rate of charging and discharging the storage could be constrained by

$$Q_j r_j^- \leq \frac{E_{j,k+1} - E_{j,k}}{t_{k+1} - t_k} \leq Q_j r_j^+, \quad \forall j \in ES, \forall k \in TM. \tag{3.23}$$

Finally, for achieving physically feasible solutions, when the charge and discharge efficiency of storages was chosen to 100%, the following condition ensured that the storages were not charged and discharged at the same time,

$$P_{\mathrm{ch},j,k} P_{\mathrm{dch},j,k} = 0, \quad \forall j \in ES, \forall k \in TM. \tag{3.24}$$

By introducing a new helper variable ($\mathbf{Y} \in \{0,1\}^{n_{\mathrm{ES}} \times n_T}$), and with $M_j = Q_{\mathrm{max},j} = \mathrm{const.}$, which is the maximum allowed capacity, the nonlinear equality constraint (**Equation (3.24)**) could be rewritten to

$$P_{\mathrm{ch},j,k} \leq Y_{j,k} M_j, \quad \forall j \in ES, \forall k \in TM, \tag{3.25}$$

$$P_{\mathrm{dch},j,k} \leq \left(1 - Y_{j,k}\right) \cdot M_j, \quad \forall j \in ES, \forall k \in TM. \tag{3.26}$$

3.4.4 Grid connections

In this Thesis, grid connections denote all connections from the investigated energy system to overlying grids, e.g., the power or district heating grid. Depending on the direction of the flow, input and output grid connections could be distinguished. The power flows ($P_{j,k}$) were constrained according to the capacity (Q_j) of the connection (j)

$$0 \leq P_{j,k} \leq Q_j, \quad \forall j \in \{GC_{\mathrm{in}}, GC_{\mathrm{out}}\}, \forall k \in TM. \tag{3.27}$$

In addition to this, the rate at which the power flow from or towards the grid was changed, could be limited,

$$Q_j r_j^- \leq \frac{P_{j,k+1} - P_{j,k}}{t_{k+1} - t_k} \leq Q_j r_j^+, \quad \forall j \in \{GC_{\mathrm{in}}, GC_{\mathrm{out}}\}, \forall k \in TM. \tag{3.28}$$

The supply of energy from overlying grids to the energy system is accompanied with a flow of money in the opposite direction. All considered grid connections offer (or demand) power flows that have no special feature across the market of the particular grid. Hence, they could be called *commodities*. The purchase and sale of commodities (C_{Comm}) could be billed as a combination of fixed charges ($C_{\mathrm{Comm,fix}}$) for the availability of the grid connection, demand charges ($C_{\mathrm{Comm,dem}}$) depending on the monthly peak demand, and energy charges ($C_{\mathrm{Comm,e}}$) for the actual amount of energy consumed within a certain period,

$$\begin{aligned} C_{\mathrm{Comm}} &= C_{\mathrm{Comm,fix}} + C_{\mathrm{Comm,dem}} + C_{\mathrm{Comm,e}} \\ &= \sum_{j \in \{GC_{\mathrm{in}}, GC_{\mathrm{out}}\}} \left(C_{\mathrm{Comm,fix},j} + C_{\mathrm{Comm,dem},j} + C_{\mathrm{Comm,e},j}\right). \end{aligned} \tag{3.29}$$

For a particular commodity, these three portions of cost were computed by

$$C_{\mathrm{Comm,fix},j} = I_j \cdot p_{\mathrm{fix},j}, \quad \forall j \in \{GC_{\mathrm{in}}, GC_{\mathrm{out}}\}, \tag{3.30}$$

$$C_{\mathrm{Comm,dem},j} = 12 \cdot Q_j \cdot p_{\mathrm{dem},j}, \quad \forall j \in \{GC_{\mathrm{in}}, GC_{\mathrm{out}}\}, \tag{3.31}$$

$$C_{\mathrm{Comm,e},j} = \sum_{k \in TM} \left(\Delta t_k \cdot P_{j,k} \cdot p_{\mathrm{e},j,k}\right), \quad \forall j \in \{GC_{\mathrm{in}}, GC_{\mathrm{out}}\}, \tag{3.32}$$

In **Equations (3.30) to (3.32)**, $p_{\mathrm{fix},j}$ was a fixed annual price for the grid connection (j), $p_{\mathrm{dem},j}$ the monthly demand price and $p_{\mathrm{e},j,k}$ the energy price. Multiplying the capacity (Q_j) with the demand price ($p_{\mathrm{dem},j}$) and including the total commodity costs in the objective function, demand charges could be approximated (billed based on the annual peak demand) and considered in the optimization problem. Carbon dioxide emissions were handled analogously and also treated as a type of grid connection.

3.4.5 Investments

The overall goal of the ESD method was to determine the economically most attractive technologies and their capacities. The installation of energy conversion and storage technologies on site are *investments*. These require fixed one-time expenses (the actual investment, capital costs) at the beginning and operation and maintenance (O&M) costs every year. For making both portions of cost comparable, equivalent annual costs of the capital costs were computed. Equivalent annual costs are equal payments throughout the economical life time of the asset (component). These are further denoted as capital expenditures (CAPEX). **Table 3.3** gives an overview of the cost model parameters.

Table 3.3: Cost model parameters.

Parameter	Variable	Units		Function of
Minimum and maximum allowed capacities	$Q_{\min}$, $Q_{\max}$	[W]	[m³/s]	-
		[J]	[m³]	
Fixed and (variable) specific capital costs (including transportation and installation)	i_1, i_2	[$]; [$/J]	[$]; [$/m³]	Q
		[$]; [$/J]	[$]; [$/m³]	
Fixed and (variable) specific government grants	gr_1, gr_2	[$]; [$/J]	[$]; [$/m³]	Q
		[$]; [$/J]	[$]; [$/m³]	
Fixed and (variable) specific operation and maintenance (O&M) costs	o_1, o_2	[$/a]; [$/W/a]	[$/a]; [$/(m³/s)/a]	-
		[$/a]; [$/J/a]	[$/a]; [$/m³/a]	
Asset depreciation range (economical life time)	n	[a]		-

When a specific energy conversion or storage device (j) was installed ($I_j = 1$), the capacity was constrained by its minimum ($Q_{\min}$) and maximum allowed capacities ($Q_{\max}$). Some technologies might only be available within a certain range, or it might be practical to specify this range beforehand due to other reasons (e.g., reducing the feasible region). The investments in renewable energy technologies and grid connections could also be constrained in the same manner. The constraint was written as follows:

$$I_j Q_{\min,j} \leq Q_j \leq I_j Q_{\max,j}, \quad \forall j \in \{EC, RE, ES, GC_{\text{in}}, GC_{\text{out}}\}. \tag{3.33}$$

The annuity factor for computing equivalent annual costs depends on both the prevalent interest rate (r) for the particular site and the depreciation range (n_j, economical

life time) of the particular technology (j). The annuity factor (a_j) is defined as (Konstantin, 2013),

$$a_j = \frac{r \cdot (1+r)^{n_j}}{(1+r)^{n_j} - 1}, \quad \forall j \in \{EC, RE, ES\}. \tag{3.34}$$

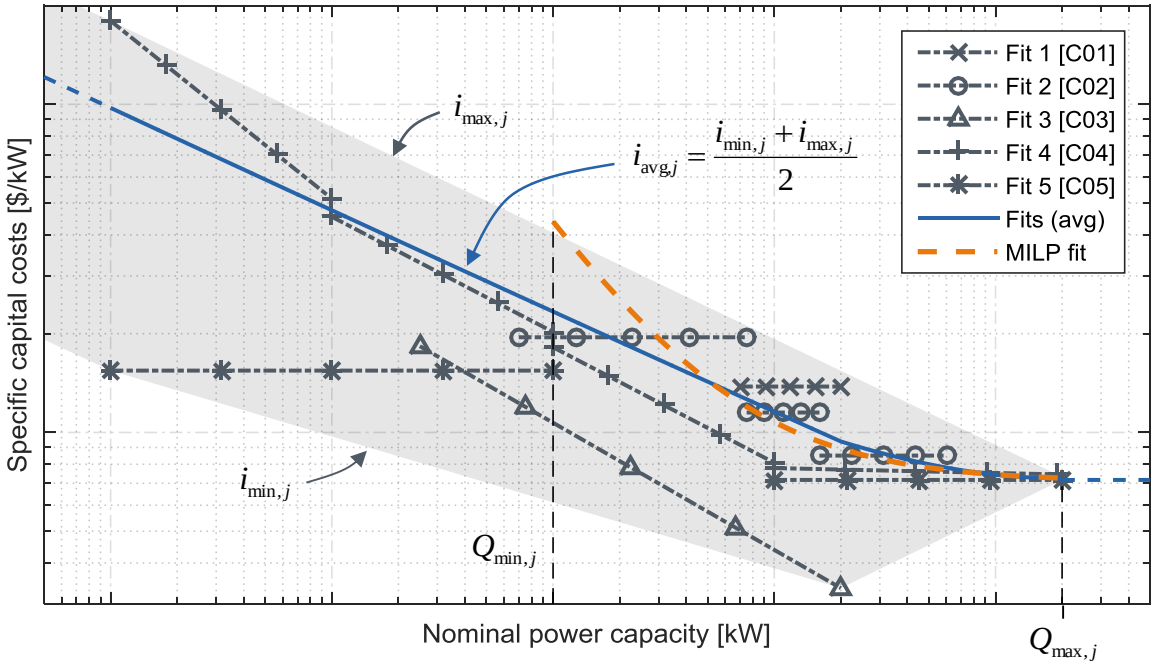

Figure 3.8: Specific capital cost approach (exemplarily for an internal combustion engine) (adapted from Thiem, Danov, et al. (2017)).[7]

The capital expenditures (C_{CAPEX}) for the entire energy system were computed as follows:

$$C_{\mathrm{CAPEX}} = \sum_{j \in \{EC,RE,ES\}} \left[a_j \cdot \left(i_{1,j} I_j + i_{2,j} Q_j \right) \right]; \tag{3.35}$$

and the operation and maintenance costs ($C_{\mathrm{O\&M}}$) as follows:

$$C_{\mathrm{O\&M}} = \sum_{j \in \{EC,RE,ES\}} \left(o_{1,j} I_j + o_{2,j} Q_j \right). \tag{3.36}$$

The specific capital costs strongly depend on the capacity of the component. From datasheets and literature, different fits could be obtained for specific technologies. These

[7] The fits for internal combustion engine were derived from C01 (Energinet.dk & Energistyrelsen, 2012), C02 (Lako, 2010), C03 (Gebhardt et al., 2002), C04 (ASUE, 2014) and C05 (Henning & Palzer, 2013).

fits were plotted for an example in the log-log plot in **Figure 3.8**. The fits do not lie on top of each other; instead, they span an area in the log-log space. Computing the convex hull of these fits in the log-log space for a specific technology (j), piecewise-defined linear functions for the lower ($i_{\min,j}$) and upper ($i_{\max,j}$) boundaries could be determined. Further, the average ($i_{\text{avg},j}$) was defined as

$$i_{\text{avg},j} = \frac{i_{\min,j} + i_{\max,j}}{2}, \quad \forall j \in \{EC, RE, ES\}. \tag{3.37}$$

The average line was always fitted in the feasible capacity range ($Q_{\min,j} \leq Q_j \leq Q_{\max,j}$) by a fit that was suitable for the MILP optimization model. The fit along with the average specific capital costs was also plotted for the example in **Figure 3.8**. The MILP fit was in fairly good agreement with the average line. However, at capacities close to the lower boundary, the fit slightly deviated from the average, but was still within the convex hull. However, the MILP fit was a much better approximation of the specific capital costs than a constant value could be. The capital costs ($C_{0,j}$ in \$) of investing in a certain technology (j) could be derived to

$$C_{0,j} = \frac{C_{\text{CAPEX}}}{a_j} = i_{1,j} I_j + i_{2,j} Q_j = I_j \cdot \left(i_{1,j} + i_{2,j} Q_j\right), \quad \forall j \in \{EC, RE, ES\}. \tag{3.38}$$

The specific capital costs (i_j in \$/capacity unit) could be written as follows:

$$i_j = \frac{C_{0,j}}{Q_j} = \frac{I_j \cdot \left(i_{1,j} + i_{2,j} Q_j\right)}{Q_j} = I_j \cdot \left(\frac{i_{1,j}}{Q_j} + i_{2,j}\right), \quad \forall j \in \{EC, RE, ES\}. \tag{3.39}$$

Equation (3.39) is a hyperbolic function for the specific capital costs and dependent on the capacity of the technology (Q_j) (see **Figure 3.8**). The two coefficients ($i_{1,j}$ and $i_{2,j}$) could be determined from a linear fit of **Equation (3.38)**. Government grants (gr_1 and gr_2) could also be included in this investment model by defining new coefficients ($i^*_{1,j} = i_{1,j} - gr_{1,j}$ and $i^*_{2,j} = i_{2,j} - gr_{2,j}$).

3.4.6 Multi-modal on-site energy system

The multi-modal on-site energy system was introduced in **Section 3.3**, where the technical superstructure was developed. The individual generic components, such as energy converters, renewable energy technologies and energy storages, were described in the previous sections. The energy system could be described by interconnecting the power flows from these components according to the technical superstructure flow chart (see **Figure 3.2**). According to the first law of thermodynamics, energy within an isolated system is conserved (Baehr & Kabelac, 2009). In terms of power, power balances for all considered forms of energy were derived,

$$\begin{aligned}
&\sum_{j\in GC_{\text{in}}}\left(\alpha_{j,e}P_{j,k}\right)-\sum_{j\in GC_{\text{out}}}\left(\alpha_{j,e}P_{j,k}\right)+\sum_{j\in RE}\left(\alpha_{j,e}P_{j,k}\right)\\
&+\sum_{j\in EC}\left[\sum_{m\in OUT_{\text{def},j}}\left(\alpha_{\text{out},j,m,e}P_{\text{out},j,m,k}\right)-\sum_{m\in IN_j}\left(\alpha_{\text{in},j,m,e}P_{\text{in},j,m,k}\right)\right]\\
&+\sum_{j\in ES}\left(\alpha_{\text{dch},j,e}P_{\text{dch},j,k}-\alpha_{\text{ch},j,e}P_{\text{ch},j,k}\right)\\
&+\sum_{j\in DG}\left(\alpha_{\text{DG,in},j,e}P_{j,k}-\alpha_{\text{DG,out},j,e}P_{j,k}\right)\\
&=\sum_{j\in ED}\left(\alpha_{j,e}P_{j,k}\right)+\sum_{j\in W}\left(\alpha_{j,e}P_{j,k}\right),\qquad \forall e\in EF,\forall k\in TM,
\end{aligned} \tag{3.40}$$

with the constraint to satisfy the instantaneous demands of all forms of energy. $OUT_{\text{def},j}$ defined a set of output connections for an energy converter (j) including the defining output power flow. The new variable ($\boldsymbol{\alpha}\in\{0,1\}^{n_{\text{P}}\times n_{EF}}$) is a matrix that indicated whether a certain power flow ($\mathbf{P}_j$) is relevant for a certain form of energy (e). $\boldsymbol{\alpha}$ could be determined directly from the superstructure. EF was a set defining all forms of energy. According to the technical superstructure, the power balance was formulated for in total eleven different forms of energy ($n_{EF}=11$).

3.4.7 Objective function

The selection, sizing and operation of the energy system were optimized to achieve minimum total costs. For simplifying the optimization problem, these total costs were considered on an annual basis. Hence, the objective function (f) was the minimization of total expenditures (C_{TOTEX}),

$$f=C_{\text{TOTEX}}=\underbrace{C_{\text{CAPEX}}}_{\text{Equation (3.35)}}+\overbrace{\underbrace{C_{\text{O\&M}}}_{\text{Equation (3.36)}}+\underbrace{C_{\text{Comm}}}_{\text{Equation (3.29)}}+\underbrace{C_{\text{SU}}}_{\text{Equation (3.8)}}}^{C_{\text{OPEX}}}. \tag{3.41}$$

By introducing the objective function (previous equation) and power balance (**Equation (3.40)**) in the outlined way, the two concepts of levelized costs of 'generating' a certain form of energy (e.g., LCOE for electricity) and marginal costs were automatically included. For the operational optimization, eleven markets for all considered forms of energy were implicitly implemented. At these markets, marginal costs for 'generating' a certain type of energy were compared for an inelastic demand of electricity, hot water, heating, cooling and potable water. Furthermore, the on-site energy system was assumed to act as a price taker unable to influence the price of energy drawn from the overlying grid infrastructure. This assumption was fairly good. For the use cases introduced in **Chapter 4**, actual industrial customer tariffs were considered. Additionally, the wholesale electricity market usually spans over an entire country (or through power grid interconnections even further than that). An impact from the rather small on-site energy system on the wholesale market price could be neglected. However, with elastic (price sensitive) demands, the system could achieve even lower total costs by means of implementing demand-side management strategies.

3.4.8 Decomposition method

The previous equations (**Equations (3.2) to (3.41)**) were to some extend state of the art. For example, the power balance was based on the first law of thermodynamics. The overall formulation of the method, as well as the framework for the integration of detailed energy converter models was newly developed for this Thesis. The optimization horizon of the *full* problem spanned over an entire year. The installation, capacities and operation of the energy technologies were optimized simultaneously. Hence, the problem became so complex that a solution for such a complex system (compare the superstructure) was not possible on the computer hardware available for this study. Other researchers encountered similar problems before. To cope with the problem complexity they either neglected most parts of the year by considering only a couple of representative periods (e.g., 5 days), or strongly simplified the system and the technology models. Both options were not suitable for this research, which dealt with the optimization of a complex energy system described by detailed technology models over the span of an *entire* year. The problem, however, could not just be split into several subproblems. Ramp-up and ramp-down constraints, start-up costs and particularly energy storages coupled the time steps. Furthermore, the power output constraints were functions of the respective capacities, variables that comprise the entire optimization horizon. The result of the ESD method should be *one* optimal design for the entire year and not different designs for every month. Therefore, a novel decomposition method (DM) based on a time-scale separation was developed and implemented.

Strategies

Before explaining how the decomposition method actually works, three different strategies are introduced: The optimization of the original full problem (FullProb), and further two DM strategies (DM-Month and DM-Day). Properties of the three strategies are summarized in **Table 3.4** (compare also **Layer (3)** in **Figure 3.1**).

Table 3.4: Solving strategies.

Subproblem	Number of periods	Period size [h]	Time step [h]		
			FullProb	DM-Month	DM-Day
1	1	8760	1	8760	8760
2	1	8760	-	720	720
3	12 (13)	720	-	1	24
4	365 (366)	24	-	-	1

What is the advantage of decomposing the optimization problem?

For the three strategies introduced above, **Figure 3.9 (a)** shows the number of optimization variables for the subproblem periods. The problem complexity grew approximately quadratically with the number of optimization variables. As **Figure 3.9 (b)** for an example depicts, the computation time (including both setting up of the optimization problem and solving it) tremendously decreased by applying the DM proposed below. The computation time for the sum of the individual period optimization problems was much smaller than for the full problem.

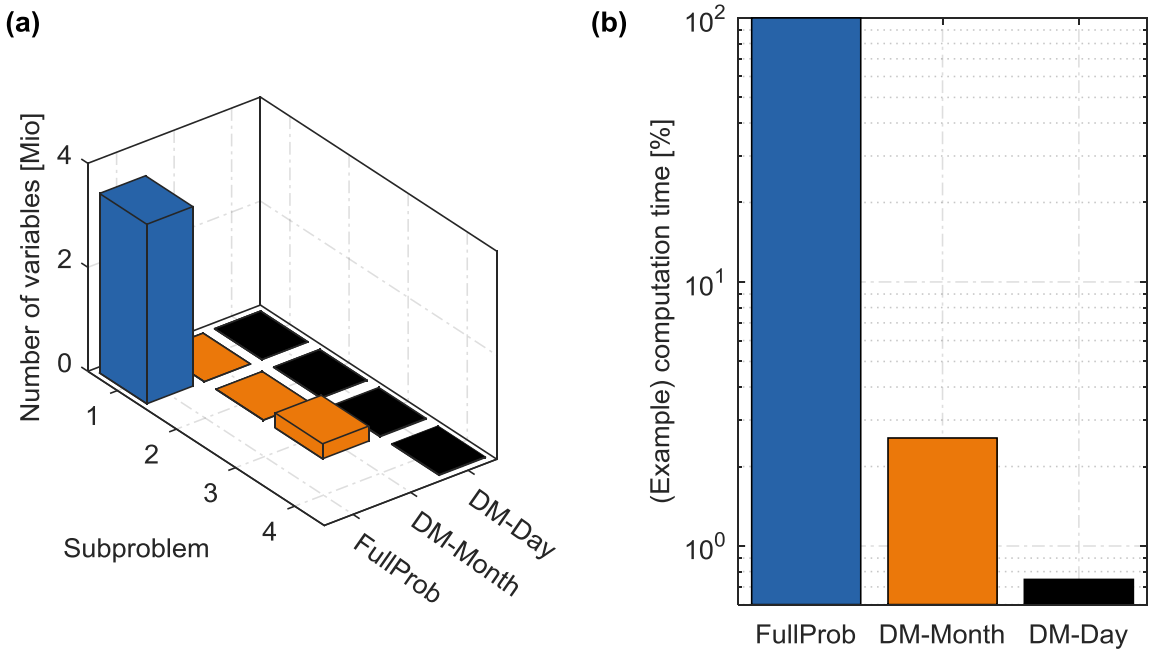

Figure 3.9: Three different solution strategies: (a) Problem complexity (number of variables per period), (b) Computation time for an example (relative to FullProb).

Mathematical formulation of the decomposition method

The idea of the DM was to split the entire year into several suproblems with *increasing granularity*. Essentially, the ESD problem was considered from different distances, starting from far with low granularity to very close moving along the optimization horizon with fine granularity. For each subproblem, one or more periods were considered. A new time variable ($\mathbf{t}_p$, time of a particular period) was defined for each of these periods. All constraints, such as climatic conditions, commodity prices and load profiles, were transformed into the new problem space defined by $\mathbf{t}_p$ (compare **Figure 3.1: 4.1**). Let t_{p,k_p} be a certain point in time in the decomposed period. t_{p,k_p} can be mapped to a number of time points in the original problem space ($\mathbf{t}_{k\in[n_k,m_k]}$), defined by its lower (n_k) and upper boundary (m_k). Hence, new values of all constraints, e.g., a particular (j) load ($\mathbf{L}_j$), can be expressed as:

$$L_{j,k_p} = \overline{L_{j,k\in[n_k,m_k]}}, \quad \forall k_p \in TM_p. \tag{3.42}$$

The entire optimization problem was then transformed by substituting k_p for k in **Equations (3.2) to (3.41)**.

For each period, the initial and final boundary conditions for the energy storages were expressed as follows:

$$E_{j,k_p=0} = \begin{cases} Q_j SOC_0, & t_{p,k_p} = t_0 \\ E_{j,k_{p-1}=n_{T,p-1}} = E_{j,k_p,0}, & \text{otherwise} \end{cases}, \quad \forall j \in ES, \forall k_p \in TM_p, \tag{3.43}$$

$$E_{j,k_p=n_{T,p}} = \begin{cases} Q_j SOC_T, & t_{p,k_p} = t_T \\ E_{j,k_p,T}, & \text{otherwise} \end{cases}, \quad \forall j \in ES, \forall k_p \in TM_p. \tag{3.44}$$

The two parameters (SOC_0 and SOC_T) were defined beforehand and in this Thesis they were both constants (with the value 0.5). $E_{j,k_p,0}$ and $E_{j,k_p,T}$ were determined from the previous subproblem. The example case study below explains this approach in more detail. Besides substituting k_p for k in **Equations (3.2) to (3.41)**, also the objective function must be modified. For that, time spans of a year ($\Delta t_a = t_T - t_0 = 8760\,\mathrm{h}$), a month ($\Delta t_m = 720\,\mathrm{h}$) and the current period ($\Delta t_p = t_{p,k_p=n_{T,p}} - t_{p,k_p=0}$) were defined. With these, the following dimensionless factors could be defined,

$$g_{\mathrm{fix},p} = \frac{\Delta t_p}{\Delta t_a}, \quad \forall p \in PER_l, \forall l \in SP, \tag{3.45}$$

$$g_{\mathrm{dem},p} = \left\lceil \frac{\Delta t_p}{\Delta t_m} \right\rceil, \quad \forall p \in PER_l, \forall l \in SP, \tag{3.46}$$

Furthermore, when considering multiple periods per subproblem (moving along the optimization horizon), decisions on installation and capacities within the individual periods must be aligned with one another to achieve one design for the entire year. Therefore, capacities of preceding periods were treated as minimum capacities for following periods. This, on the other hand, required to overweight CAPEX-related costs, because otherwise overall suboptimal technologies were installed (that were only feasible in a particular period). A CAPEX-OPEX weighting factor ($w_{\mathrm{C/O}} \in \mathbb{R}, 0 \leq w_{\mathrm{C/O}} \leq 1$) was introduced. Given $w_{\mathrm{C/O}}$, further dimensionless factors for CAPEX and O&M were computed by

$$g_{\mathrm{CAPEX},p} = g_{\mathrm{O\&M},p} = \frac{\Delta t_p}{\Delta t_a} + w_{\mathrm{C/O}} \cdot \left(1 - \frac{\Delta t_p}{\Delta t_a}\right), \quad \forall p \in PER_l, \forall l \in SP, \tag{3.47}$$

Good values for $w_{\mathrm{C/O}}$ could be determined in an iterative approach (compare **Figure 3.1: 1.1**). The benchmark and comparison in **Section 3.6.5** elaborates more on this subject. The objective function was accordingly modified to f_p expressed as follows:

$$\begin{aligned} f_p = {} & g_{\mathrm{CAPEX},p} \cdot C_{\mathrm{CAPEX},p} + g_{\mathrm{O\&M},p} \cdot C_{\mathrm{O\&M},p} + g_{\mathrm{fix},p} \cdot C_{\mathrm{Comm,fix},p} + g_{\mathrm{dem},p} \cdot C_{\mathrm{Comm,dem},p} \\ & + C_{\mathrm{Comm,e},p} + C_{\mathrm{SU},p}, \quad \forall p \in PER_l, \forall l \in SP, \end{aligned} \tag{3.48}$$

The index (p) indicates that the cost terms were evaluated for a particular period (p). PER_l defined the set of periods for subproblem (l), which were element of the set (SP).

Example case study

The objective of the DM was to achieve a good, near-optimal solution, which was an upper bound to the ESD problem. The decomposition method is explained with reference to an example of a simple heating system. The heating system consisted of a heat pump (HP) and a hot water storage (HWS). The system had to supply hot water to a building according to a heat demand profile. The heat pump therefore could draw electricity from the power grid. The key parameters are summarized in **Table 3.5**. The objective was to determine the optimal capacities and operation of the heating system for the entire year.

Table 3.5: Motivational example: Parameters.

Parameter	Variable	Value
Power grid		
Electricity price	$p_{\mathrm{el,e}}$	16.6 ct/kWh
Heat pump (HP)		
Specific capital costs	i_{HP}	400 \$/kW$_{\mathrm{th}}$
Specific O&M costs	o_{HP}	30 \$/kW$_{\mathrm{th}}$/a
Economic lifetime	n_{HP}	20 a
Coefficient of performance (COP)	COP_{HP}	4
Hot water storage (HWS)		
Specific capital costs	i_{HWS}	25 \$/kWh$_{\mathrm{th}}$
Economic lifetime	n_{HWS}	20 a
Thermal load (inelastic demand)		
Peak load	$\dot{Q}_{\mathrm{h,max}}$	223.1 kW
Other parameters		
Interest rate	r	7%

Instead of considering the full optimization problem spanning over 8760 h with 1 h time steps (FullProb, see **Figure 3.10 (a)**), the problem was split into several subproblems (see **Figure 3.10 (b) – (d)**). For the first subproblem, the entire year was considered as one time step only (i.e., 8760 h, see **Figure 3.10 (b)**). Self-evidently, no HWS was installed and the HP was sized to meet the average annual heating demand. Monthly time steps were considered for the second subproblem (**Figure 3.10 (c)**). Here, too, only one period was considered for this subproblem. As the figure shows, a seasonal hot water storage was not feasible. The heat pump was once again sized to the maximum average monthly heating demand. However, if a seasonal hot water storage was feasible, the storage level at the end of each month could be determined ($E_{j,k_p,0}$ and $E_{j,k_p,T}$). This information was passed on to the next subproblem (**Figure 3.10 (d)**). Here, every month was considered separately as single period and optimized. Constraints for the final storage level of the hot water storage ($E_{j,k_p,0}$ and $E_{j,k_p,T}$) were taken from the previous subproblem. Furthermore, optimal capacities determined at each period were treated as minimum capacities for subsequent periods and subproblems, respectively. As **Figure 3.10 (a)** and **Figure 3.10 (d)** reveal, optimizing the full problem and the decomposed problem led to the same optimal capacities for both HP and HWS, although the operation of the system slightly differed. Because the electricity price and all efficiencies were constant (time-independent) and no further restrictions (e.g., minimum part-load ratios) were assumed, indeed, no single optimal solution for the operation of the heating system existed. As long as the heat demand was met and the heat pump and the storage were within their constraints, the heat pump could generate heat an hour earlier or later without influencing the operating expenditures.

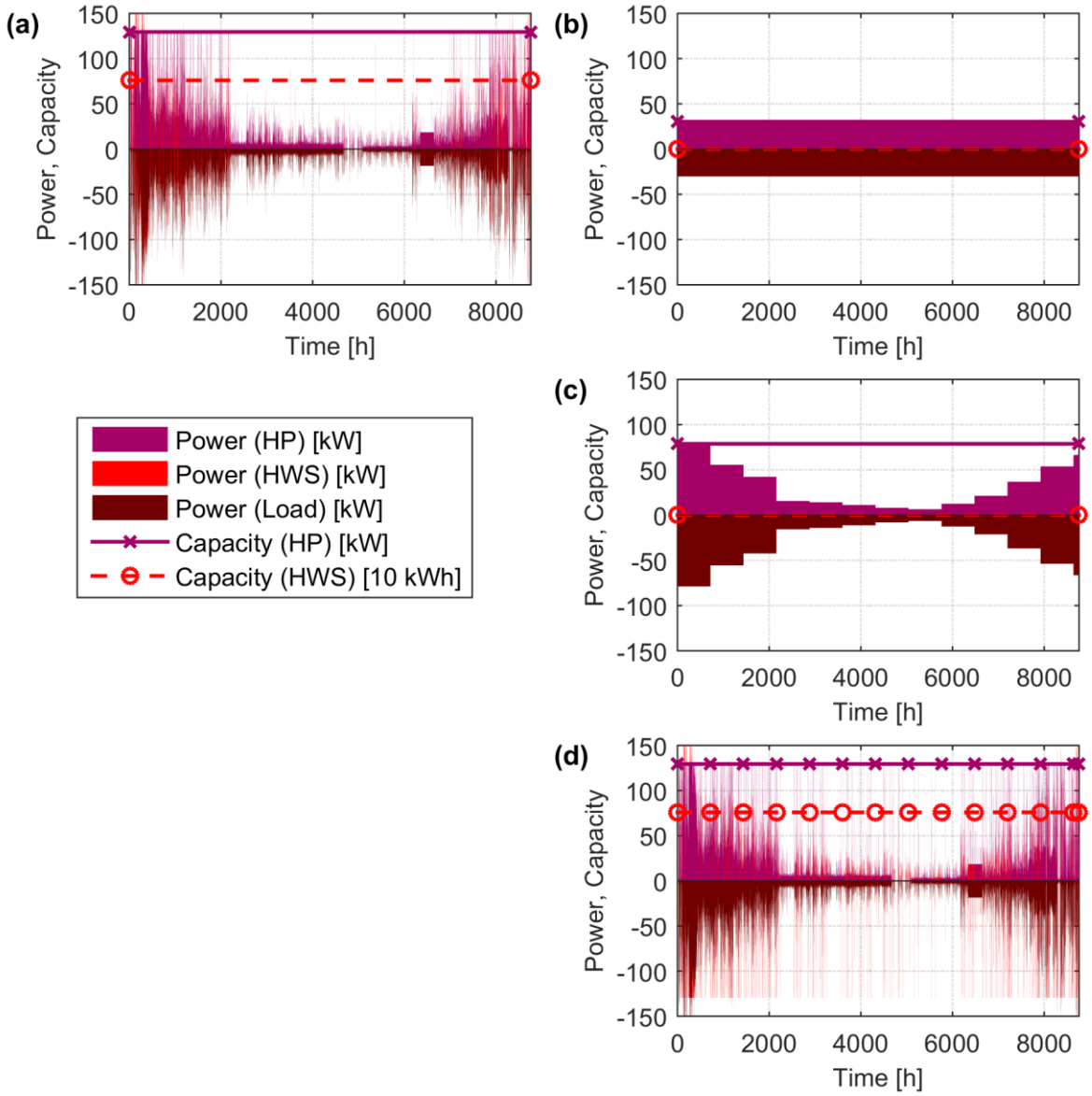

Figure 3.10: Example heating system: Optimal power flows and capacities as result of (a) FullProb, and (b) - (d) DM-Month.

Figure 3.11 (a) shows the total expenditures (TOTEX) that could be achieved by optimizing the example heating system using the three strategies. As the figure shows, for the example, the same TOTEX could be achieved using FullProb and DM-Month. With DM-Day, however, the global optimum could not be reached. The optimized capacities of the HP and the HWS are illustrated in **Figure 3.11 (b)**. With DM-Day, the HP was slightly oversized. The daily storage operation was suboptimal compared to the other two strategies, requiring a larger HP capacity.

The idea of the DM is further elaborated in **Figure 3.12**. Here, the storage level of the HWS was plotted for the Subproblems 2 to 4 of DM-Day. The figure clearly shows the increasing granularity of the subproblems. For example, Subproblem 4 was able to identify and to optimize the fluctuations of the storage level around a coarser curve determined by Subproblem 3. The figure shows the time-scale separation idea of the

decomposition method. In Subproblem 2, seasonal time scales are considered; in Subproblem 4, on the other hand, hourly time scales and respective fluctuations can be determined.

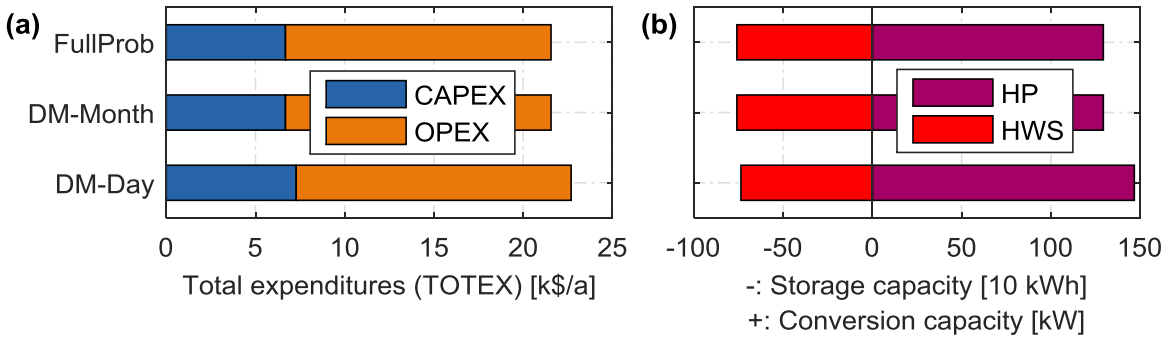

Figure 3.11: Example heating system: (a) Total expenditures, (b) Capacities of the heat pump (HP) and hot water storage (HWS).[8]

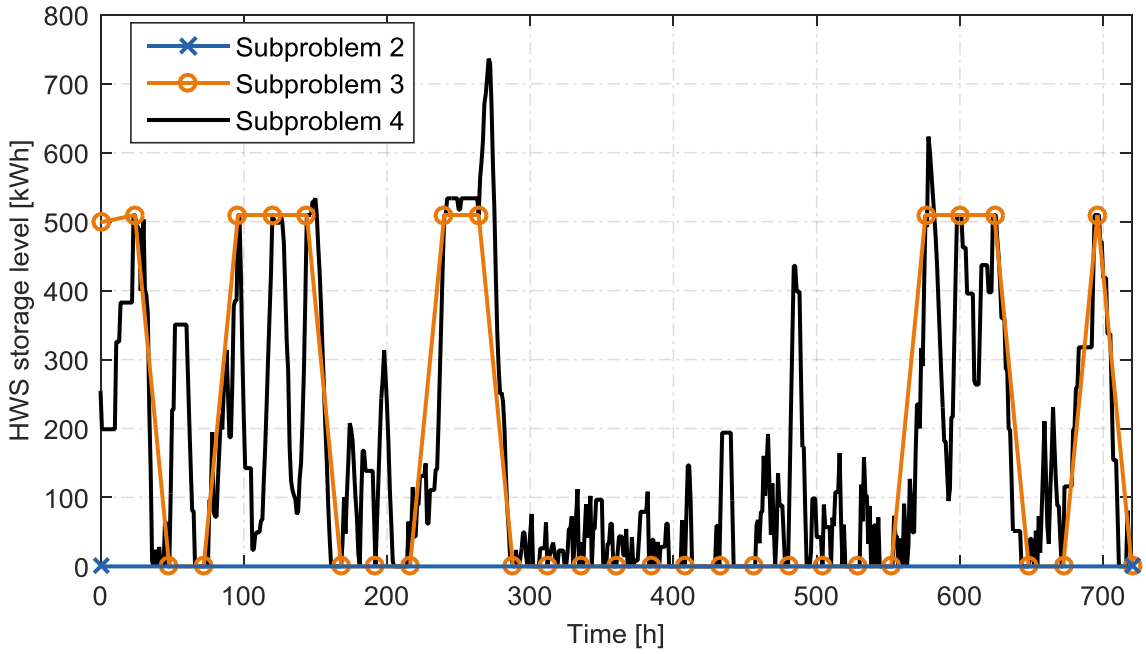

Figure 3.12: Example heating system: Hot water storage (HWS) storage level for the first month using the DM-Day strategy.

Concluding remarks

The decomposition method developed in this section enabled the energy system design of complex energy systems described by detailed models over the span of an entire year.

[8] Note that the storage capacities were accumulated in negative horizontal direction, converter capacities in positive horizontal direction.

By decomposing the ESD problem into several subproblems, the problem complexity could be reduced significantly. Accordingly, the problem could be computed on computer hardware with less random-access memory (RAM) and in a shorter amount of time. However, note that the optimal solution determined for the decomposed problem was only *near-optimal*. The presented DM is not a mathematically strict decomposition but *heuristic*. The necessity for the CAPEX-OPEX weighting factor and the suboptimal storage operation on a long-term timescale deteriorate the optimization result. Furthermore, note that for the complex energy system no solution could be determined without the described decomposition method. DM-Day gave quick insights into trends; DM-Month could be used for deriving very good near-optimal results.

3.5 Models of selected technologies

Modeling of technologies is always a trade-off between accuracy and simplicity. The former determines the reliability and quality of the results, the latter the computation time and solvability. The description of technology models is not the focus area of this document, although for this Thesis many technologies were modeled in detail using the methods that are introduced below. The presented modeling framework (see Section 3.4.2) provided a common interface for all energy conversion technology models. Furthermore, the model functions could be executed outside of the actual optimization solver. Therefore, both complex models and models with different levels of detail could be used. The models were obtained by employing one of the following three methods:

- Modeling according to information provided by manufacturer datasheets or literature and validation by cross-referencing (M1);
- Physical modeling and validation based on either experimental results or data from literature (M2);
- Development and validation of an empirical model based on experimental results (M3).

The three methods were sorted according to their required efforts. Self-evidently, the first method necessitated the least effort and was therefore employed for modeling most of the technologies. Physical models for gas turbines, turbine inlet air cooling, ammonia-water absorption chiller and ice storages were developed. In addition to this, an internal combustion engine CHP, a Lithium-bromide water absorption chiller, a two-stage compression chiller, a hot water storage, an ice storage of type ice-on-coil and an ice-storage integrated desalination system were experimentally investigated. To outline the different modeling approaches, models of the following energy technologies are introduced exemplarily below:

- M1: Photovoltaic modules (PV) and wind turbines (WT): Section 3.5.1.
- M1 and M2: Electric heat pumps (HP) and absorption chillers (AC): Section 3.5.2.
- M2: Turbine inlet air cooling (TIAC): Section 3.5.3.
- M3: Ice-storage integrated desalination (isiD): Section 3.5.4.

The main parameters of all technology models were summarized in Appendix A. Appendix B outlines the specific capital cost functions.

3.5.1 Intermittent renewable energy sources

The efficiency and power output of photovoltaic modules (PV) was described according to Skoplaki & Palyvos (2009). For standard test conditions, i.e., reference temperature ($T_{\text{ref}} = 25\ °\text{C}$) and global horizontal irradiance ($GHI_{\text{ref}} = 1000\ \text{W}/\text{m}^2$), the relative power output ($u_{\text{PV},k}$) for a particular time step (k) was modeled as

$$u_{\text{PV},k} = \left[1 - \beta_{\text{ref}} \cdot \left(T_{\text{amb},k} - T_{\text{ref}}\right)\right] \cdot \frac{GHI_k}{GHI_{\text{ref}}}, \quad \forall k \in TM, \tag{3.49}$$

with the temperature coefficient ($\beta_{\text{ref}} = 0.0045\ 1/\text{K}$). **Equation (3.49)** assumed a horizontal arrangement of the panels, which was a conservative approach for the potential of PV.

The relative power output of wind turbines ($\mathbf{u}_{\text{WT}}$) was formulated as piecewise-defined function (Lydia, Kumar, Selvakumar, & Prem Kumar, 2014; Rekioua, 2014),

$$u_{\text{WT},k} = \begin{cases} 0, & v_{\text{w},k} < v_{\text{w,c}} \\ c_1 \cdot \sin\left[c_2 \cdot \left(v_{\text{w},k} - c_3\right)\right] \cdot v_{\text{w},k}^3, & v_{\text{w,c}} \le v_{\text{w},k} < v_{\text{w,r}} \\ 1, & v_{\text{w,r}} \le v_{\text{w},k} \le v_{\text{w,f}} \\ 0, & v_{\text{w},k} > v_{\text{w,f}} \end{cases}, \quad \forall k \in TM. \tag{3.50}$$

The power output of wind turbines was 0 below their cut-in speed ($v_{\text{w,c}} = 2\ \text{m/s}$). The relative power output for wind speeds greater than the wind turbines' cut-in speed and lower than their rated speed ($v_{\text{w,r}} \approx 12\ \text{m/s}$) was determined according to a power curve fitted for a typical onshore wind turbine with 2 MW rated power output (ENERCON GmbH, 2015). The numeric values of the parameters (c_1, c_2 and c_3) are shown in **Table A.2** in the appendix. Until the furling wind speed was reached ($v_{\text{w,f}} = 25\ \text{m/s}$), the wind turbines delivered their rated power output, beyond that it was 0.

The actual power output ($\mathbf{P}_j$) of the renewable energy converter (j) was computed by multiplication of the relative power output ($\mathbf{u}_j$) with its capacity (Q_j),

$$\mathbf{P}_j = \mathbf{u}_j Q_j, \quad \forall j \in RE, \forall k \in TM. \tag{3.51}$$

3.5.2 Heat pumps and absorption chillers

Electric heat pumps (HP) use electricity to extract heat from a cold side and release it to a warmer side. **Figure 3.13 (a)** shows the basic process and instrumentation diagram of a heat pump. The thermodynamic cycle was plotted in **Figure 3.13 (b)**. Heat pumps operate at two pressure levels, condenser pressure (p_{cond}) and evaporator pressure (p_{evap}). These pressures (and corresponding temperatures) are determined in a way to meet the satisfied heating (T_{h}) and cooling (T_{c}) supply temperatures, respectively. The compressor sucks refrigerant vapor from the evaporator (1) and compresses it to a higher pressure level (2). The compressed vapor is cooled down and condensed (3). In the expansion valve the pressure of the liquid refrigerant is reduced to evaporation pressure (Baehr & Kabelac, 2009).

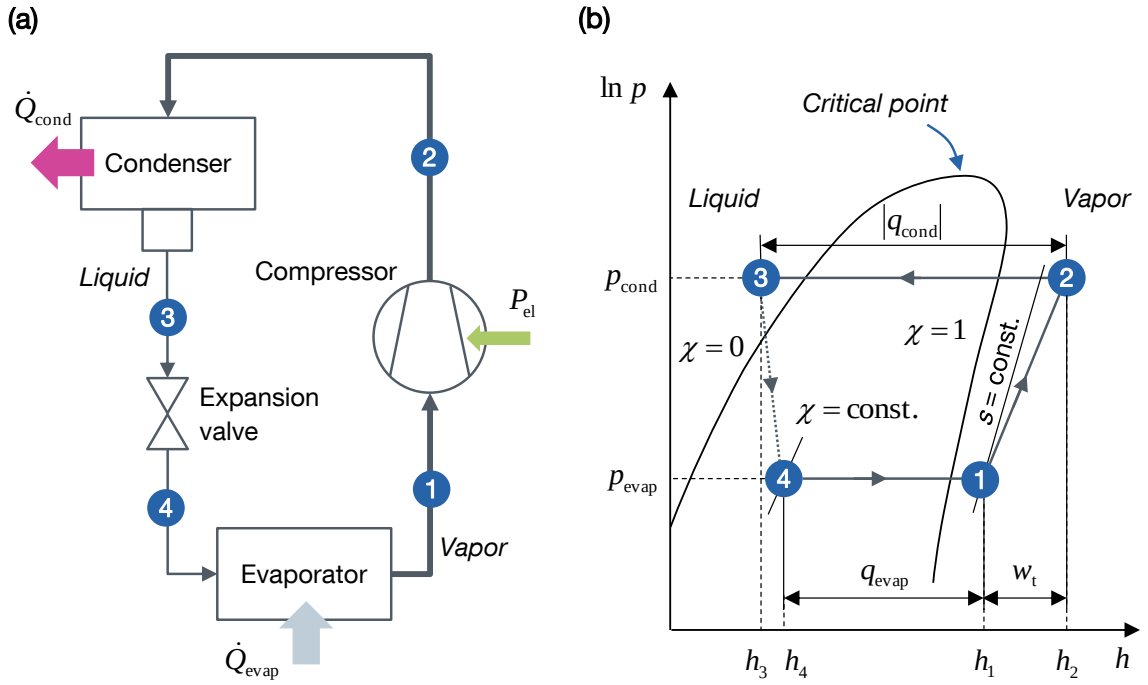

Figure 3.13: Electric heat pump: (a) Process and instrumentation diagram, (b) Thermodynamic cycle (adapted from Baehr & Kabelac (2009)).

Depending on the desired output, heat pumps (HP) and compression chillers (CC) can be distinguished. The former is used for heating, the latter for cooling. The efficiency of a HP is described by its coefficient of performance (COP),

$$COP = \frac{|\dot{Q}_{cond}|}{P_{el}} = \frac{|q_{cond}|}{w_t} = \frac{h_2 - h_3}{h_2 - h_1}, \tag{3.52}$$

the efficiency of a CC by its energy efficiency ratio (EER),

$$EER = \frac{\dot{Q}_{evap}}{P_{el}} = \frac{q_{evap}}{w_t} = \frac{h_1 - h_4}{h_2 - h_1}. \tag{3.53}$$

q_{cond} denotes the specific condenser heat, q_{evap} the specific heat transferred in the evaporator and w_t the specific technical work that is supplied to the system by the compressor (Baehr & Kabelac, 2009). The maximum thermodynamically feasible values for COP and EER can be derived for a Carnot cycle (v. Cube, 1981),

$$COP_{Carnot} = \frac{T_h}{T_h - T_c}, \tag{3.54}$$

$$EER_{Carnot} = \frac{T_c}{T_h - T_c} < COP_{Carnot}. \tag{3.55}$$

Equations (3.54) and **(3.55)** illustrate that both the maximum COP and the maximum EER increase with a decreasing lift (temperature lift between heat source and sink, $T_h -$

T_c). Gordon and Ng derived a semi-empirical steady-state chiller model from the first and second law of thermodynamics. The EER is implicitly determined by

$$\frac{T_{\text{evap,in}}}{T_{\text{cond,in}}}\left(1+\frac{1}{EER}\right)-1=c_1\frac{T_{\text{evap,in}}}{\dot{Q}_{\text{evap}}}+c_2\frac{T_{\text{cond,in}}-T_{\text{evap,in}}}{T_{\text{cond,in}}\dot{Q}_{\text{evap}}}+c_3\frac{\dot{Q}_{\text{evap}}}{T_{\text{cond,in}}}\left(1+\frac{1}{EER}\right), \tag{3.56}$$

with the condenser inlet temperature ($T_{\text{cond,in}}$) and the evaporator inlet temperature ($T_{\text{evap,in}}$) (Lee & Lu, 2010; Ng, Chua, Ong, Lee, & Gordon, 1997). According to Ng et al. (1997), the parameters (c_1, c_2 and c_3) have a physical meaning. c_1 is the total internal entropy production, c_2 is the equivalent heat leak and c_3 is the total heat exchanger thermal resistance. For a chiller with 70.4 kW cooling capacity, the parameters were determined to $c_1 = 0.0366\ \text{kW/K}$, $c_2 = 26.1\ \text{kW}$ and $c_3 = 0.127\ \text{K/kW}$ (Ng et al., 1997). The equation can be reformulated to consider part-load ratios (u) applicable to chillers with capacities, which are unknown beforehand, instead of evaporator heat flow rates ($\dot{Q}_{\text{evap}}$) for compression chillers with fixed capacities.

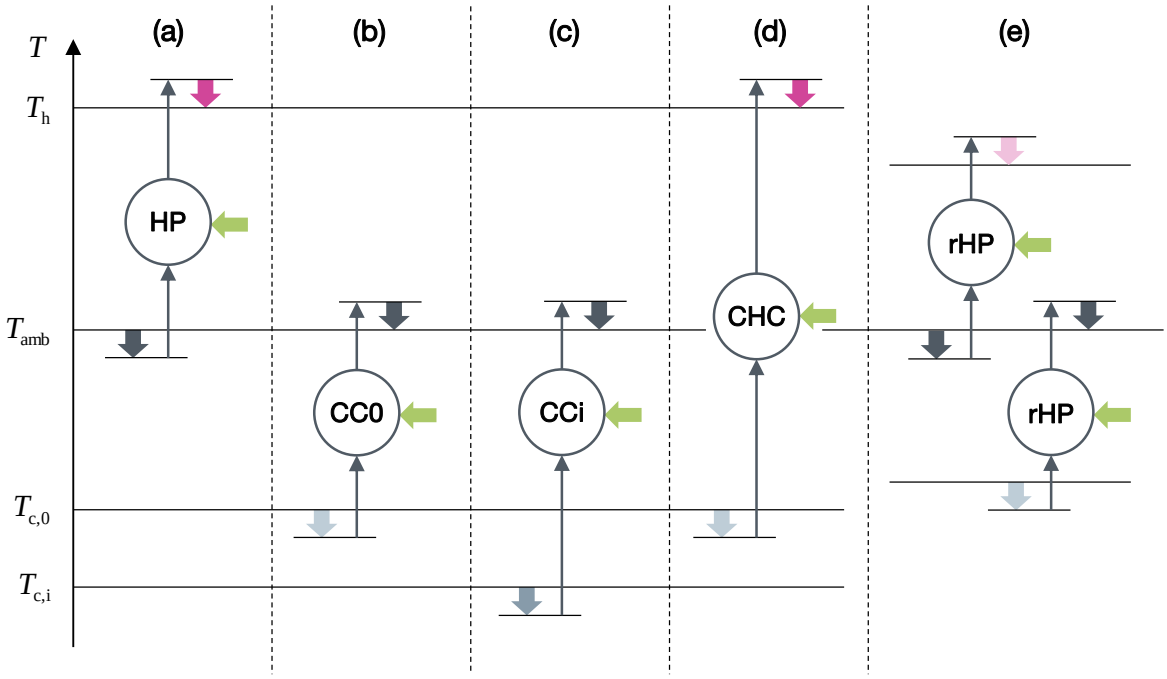

Figure 3.14: Electric heat pump technologies: (a) Heat pump, (b) Compression chiller, (c) Compression chiller with cooling supply temperatures below 0 °C, (d) Combined heating and cooling, (e) Reversible heat pump.

Figure 3.14 depicts possible heat pump technologies. First of all, a standard centralized heat pump could be used (a). Likewise, a standard centralized compression chiller could be used (b). For cooling supply temperatures below 0 °C to charge, for example, an ice storage, the evaporation temperature must be lowered (c). Instead of using separate technologies for heating and cooling (e.g., HP and CC0), alternatively, a combined heating and cooling (CHC) device could be implemented (d). The advantage of such a technology is that there is no energy wasted by releasing it to ambience. Depending on the particular conditions, the coefficient of performance (COP_{CHC}) can be improved to

$$COP_{\mathrm{CHC}} = \frac{|\dot{Q}_{\mathrm{cond}}| + \dot{Q}_{\mathrm{evap}}}{P_{\mathrm{el}}}. \tag{3.57}$$

Note that the two individual efficiencies for the heating (COP) and cooling (EER) side decrease due to the increased lift. Therefore, the COP of the CHC is not the sum of the COP and EER of the HP and the CC, respectively. Last but not least, a reversible heat pump (rHP) could be used (e). In winter, the rHP can run as heat pump, in summer as compression chiller. The reversible heat pump is commonly a small-size to medium-size decentralized heating ventilation and air conditioning (HVAC) solution.

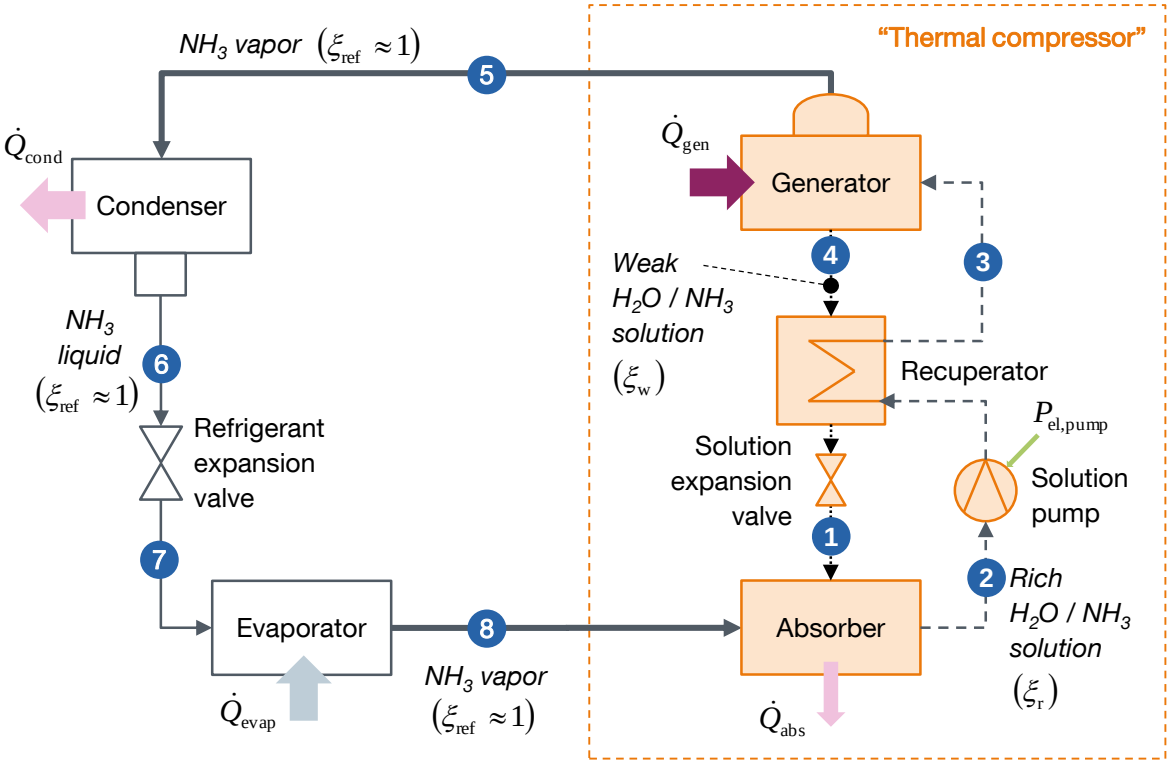

Figure 3.15: Process and instrumentation diagram of a single-effect ammonia-water absorption chiller (adapted from Baehr & Kabelac (2009)).

An alternative solution to the usage of compression chillers for cooling applications is the usage of absorption chillers. Absorption chillers (AC) replace the electrically-driven compressor (compare **Figure 3.13**) by a "thermal compressor". **Figure 3.15** shows the general process and instrumentation diagram of a single-effect ammonia-water AC. Similar to the CC, AC operate at two pressure levels, evaporator (p_{evap}) and condenser (p_{cond}) pressure, see also **Figure 3.16**. In the generator, rich (ξ_{r}) solution of ammonia (NH_3) in water (H_2O) (3) is evaporated driven by the generator heat input ($\dot{Q}_{\mathrm{gen}}$). A weak (ξ_{w}) solution (4) with less ammonia leaves the generator. Ideally, the vapor leaving the generator (5) is pure ammonia ($\xi_{\mathrm{ref}} = 1$). In reality, this case is only reached by rectification. Other ACs operating with water and lithium bromide (LiBr) achieve this state without rectification. However, since H_2O-LiBr absorption chillers use the refrigerant water, cooling supply temperatures below 0 °C are not feasible. Analogously to compression chillers, the refrigerant vapor is condensed (6) and afterwards expanded to

evaporator pressure levels (p_{evap}) (7). At evaporation temperature, heat is transferred to the refrigerant to evaporate it (8). The weak solution leaving the generator (4) flows through the recuperator transferring heat to the rich solution (3) before it enters the generator. In the solution expansion valve, the weak solution is expanded to evaporator pressure. The refrigerant vapor (8) is absorbed by the weak solution (1). A solution pump pumps the rich solution (2) from the absorber through the recuperator to the generator. The "thermal compressor" is able to increase the pressure of the refrigerant by exergy that is supplied to the absorption chiller along with $\dot{Q}_{\mathrm{gen}}$. Besides small amounts of electric power for the solution pump ($P_{\mathrm{el,pump}}$) and other auxiliary equipment, ACs are driven by thermal energy (Baehr & Kabelac, 2009). Thus, simplified, this technology converts heat to cold.

The efficiency of absorption chillers was defined in different ways. Efficiencies relate the useful output of a conversion unit to the desired input. The grade (ν) defines an exergy ratio,

$$\nu = \frac{\dot{E}_{\mathrm{evap}}}{\dot{E}_{\mathrm{gen}}} = \frac{\left(T_{\mathrm{amb}} - T_{\mathrm{evap}}\right)/T_{\mathrm{evap}}}{\left(T_{\mathrm{gen}} - T_{\mathrm{amb}}\right)/T_{\mathrm{gen}}} \cdot \frac{\dot{Q}_{\mathrm{evap}}}{\dot{Q}_{\mathrm{gen}}}, \tag{3.58}$$

with the evaporator temperature (T_{evap}), driving generator temperature (T_{gen}), evaporator exergy rate ($\dot{E}_{\mathrm{evap}}$) and generator exergy rate ($\dot{E}_{\mathrm{gen}}$) (Zetzsche, 2012). Another way of defining an efficiency for ACs is the heat ratio (ζ), defined as follows:

$$\zeta = \frac{\dot{Q}_{\mathrm{evap}}}{\dot{Q}_{\mathrm{gen}}}. \tag{3.59}$$

The maximum possible heat ratio (ζ_{max}), also called Carnot heat ratio (ζ_{Carnot}), is derived by setting $\nu = 1$,

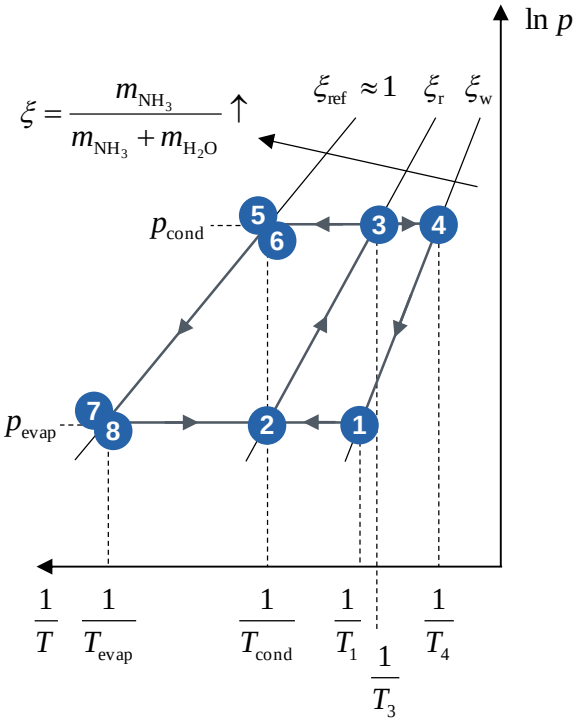

Figure 3.16: Thermodynamic cycle of a single-effect ammonia-water absorption chiller (adapted from v. Cube (1981)).

$$\zeta_{\mathrm{max}} = \zeta_{\mathrm{Carnot}} = \zeta(\nu = 1) = \frac{\left(T_{\mathrm{gen}} - T_{\mathrm{amb}}\right)/T_{\mathrm{gen}}}{\left(T_{\mathrm{amb}} - T_{\mathrm{evap}}\right)/T_{\mathrm{evap}}} = \frac{1/T_{\mathrm{amb}} - 1/T_{\mathrm{gen}}}{1/T_{\mathrm{evap}} - 1/T_{\mathrm{amb}}}, \tag{3.60}$$

which is less than 1 according to **Figure 3.16** (Baehr & Kabelac, 2009; v. Cube, 1981). Analogously to compression chillers, the energy efficiency ratio (EER) can be defined as

$$EER = \frac{\dot{Q}_{\mathrm{e}}}{\dot{Q}_{\mathrm{gen}} + P_{\mathrm{el,pump}}}. \tag{3.61}$$

The energy efficiency ratio considers both the generator heat flow rate ($\dot{Q}_{\mathrm{gen}}$) and the electric power drawn by the solution pump ($P_{\mathrm{el,pump}}$) as input (Zetzsche, 2012). Gordon and Ng also developed a semi-empirical steady-state model for absorption chillers (Gordon & Ng, 1995),

$$\frac{1}{\zeta} = \frac{T_{\mathrm{cond,in}} - T_{\mathrm{evap,out}}}{T_{\mathrm{evap,out}}} \cdot \frac{T_{\mathrm{gen,in}}}{T_{\mathrm{gen,in}} - T_{\mathrm{cond,in}}} + \frac{1}{\dot{Q}_{\mathrm{evap}}} \cdot \frac{T_{\mathrm{gen,in}}}{T_{\mathrm{gen,in}} - T_{\mathrm{cond,in}}} \cdot \left(c_1 - c_2 \frac{T_{\mathrm{cond,in}}}{T_{\mathrm{gen,in}}} \right). \tag{3.62}$$

$T_{\mathrm{gen,in}}$ denotes the generator inlet temperature, $T_{\mathrm{evap,out}}$ the evaporator outlet temperature. The equation can be reformulated to account for part-load ratios (u) instead of the evaporator heat flow rate ($\dot{Q}_{\mathrm{evap}}$), e.g., by replacing $\left(1/\dot{Q}_{\mathrm{evap}}\right) \cdot c_i$ with $(1/u) \cdot \tilde{c}_i$ for $i = \{1,2\}$. Hence, $\tilde{c}_i = \left(u/\dot{Q}_{\mathrm{evap}}\right) \cdot c_i = (1/Q) \cdot c_i$ with the capacity of the absorption chiller (Q). Based on a physical model developed according to v. Cube (1981) and benchmarked with experimental data and data published by Plank (1959), the parameters were determined to $\tilde{c}_1 = 2.494$ and $\tilde{c}_2 = 2.756$.

3.5.3 Turbine inlet air cooling

A gas turbine (GT) is a constant-flow, open cycle heat engine with internal combustion. As shown in **Figure 3.17 (a)**, air (1) is sucked by a compressor into the gas turbine. The inlet air is compressed by a certain pressure ratio (2) and enters the combustor at a higher pressure (and temperature). Fuel is injected into the compressed air and ignited. Due to the combustion, the temperature of the gas mixture increases. This gas (3) leaves the combustor and enters the turbine, where it is expanded to near-atmospheric pressures (4) producing work on the shaft that is used to power the compressor. The rest is available as net electrical power output of the GT (Lechner & Seume, 2010). The exhaust gas (4) leaves the GT at high temperatures and thus further heat can be extracted. Hence, simplified, gas turbines convert the chemical energy of fuel to electricity and heat. **Figure 3.17 (b)** shows the thermodynamic cycle of a GT in a specific enthalpy (h) – specific entropy (s) diagram. In reality, both the compressor and the turbine do not operate isentropically (index s) but polytropically. Hence, the required specific work by the compressor (w_{c}) is greater than in the ideal case ($w_{\mathrm{c},s}$) and the turbine produces less specific work ($w_{\mathrm{t}} < w_{\mathrm{t},s}$). Furthermore, a pressure drop across the combustor occurs (Boyce, 2012). The gas turbine is only able to generate excess electricity in the turbine due to the divergence of the isobaric curves in the h-s diagram.

The thermal efficiency ($\eta_{\mathrm{th},s}$) of the ideal thermodynamic cycle (Joule/Brayton cycle) could be derived to

$$\eta_{\mathrm{th},s} = 1 - \frac{T_1}{T_{2s}} = 1 - \frac{1}{\pi^{(\kappa-1)/\kappa}}, \tag{3.63}$$

with the pressure ratio (π) and heat capacity ratio ($\kappa = c_p/c_V$). The net specific work output ($w_{\mathrm{net},s}$) is

$$w_{\mathrm{net},s} = \left|w_{\mathrm{t},s}\right| - w_{\mathrm{c},s} = c_p T_1 \eta_{\mathrm{th},s} \cdot \left[\frac{T_3}{T_1} - \frac{1}{1 - \eta_{\mathrm{th},s}} \right], \tag{3.64}$$

with the average specific heat at constant pressure (c_p) (Lechner & Seume, 2010). For derivations of the thermal efficiency and the specific net work output for more realistic cycles, see, for example, Lechner & Seume (2010) or Razak (2007). The real cycle is described by several more parameters, such as the combustor pressure loss and the polytropic compressor and turbine efficiencies.

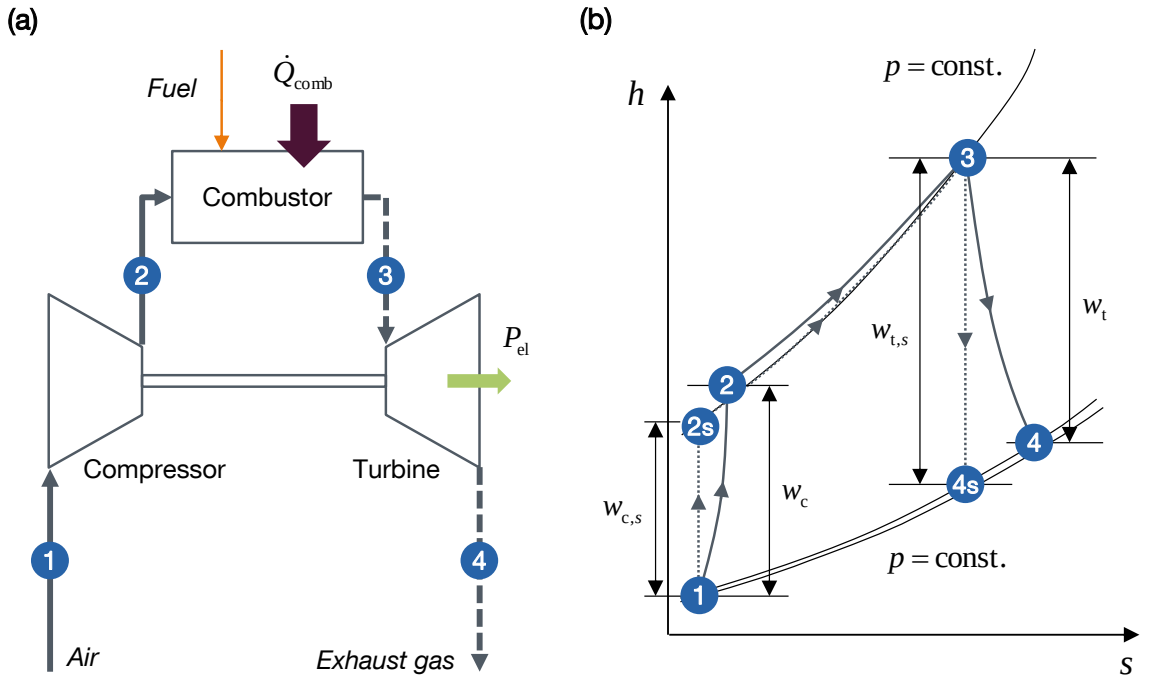

Figure 3.17: Gas turbine: (a) Process and instrumentation diagram, (b) Thermodynamic cycle (adapted from Baehr & Kabelac (2009) and Lechner & Seume (2010)).

The maximum efficiency of GTs are limited by the maximum allowable turbine inlet temperature (T_3), which is limited due to material constraints. Thus, when the temperature (T_{2s}) is accordingly limited, the thermal efficiency of the ideal cycle increases with lower air inlet temperatures (T_1). Furthermore, the power output of the gas turbine is increased with lower inlet air temperatures. Gas turbines are constant (volumetric) flow engines ($\dot{V} \approx \text{const.}$). The net power output (P_{net}) is determined to

$$P_{\text{net}} = \dot{m} w_{\text{net}} = \rho \dot{V} w_{\text{net}} = \left(\rho \dot{V}\right)_1 w_{\text{net}}, \tag{3.65}$$

with the mass flow rate ($\dot{m}$), volumetric flow rate ($\dot{V}$) and density (ρ). According to the ideal gas law, which is a fairly good approximation for air (Baehr & Kabelac, 2009), the density is proportional to the pressure (p) and inversely proportional to the temperature (T),

$$\rho \sim \frac{p}{T}, \rho_1 \sim \frac{p_1}{T_1}. \tag{3.66}$$

Therefore, this simple derivation shows that at lower inlet temperatures (T_1) and higher ambient pressures (p_1), the gas turbine net power output increases. This means that during day time, where the electrical demand (and ambient temperature) is generally

larger, the available power output from the GT is lower. Furthermore, at elevated sites the power output is reduced due to the lower ambient pressure. However, the compressor inlet temperature further influences the volumetric flow rate ($\dot{V}$) and the net specific work output (w_{net}). Therefore, in this Thesis, gas turbines were modeled according to datasheets published by the manufacturer (Siemens AG, 2005, 2009a, 2009b, 2014, 2015), see also **Table A.3** in the appendix.

Turbine inlet air cooling (TIAC) cools the inlet air prior to the compressor air intake to augment power output and efficiency (depending on the design and control strategy of the gas turbine). Several different technologies for TIAC exist, which can be classified according to Al-Ibrahim & Varnham (2010) and Ibrahim, Rahman, & Abdalla (2011) into (compare also **Figure 3.18**):

- Evaporative cooling: Evaporation of injected small water droplets, fog or snow draws energy from its surroundings and thus cools the inlet air. The cooling effect is limited by the maximum allowed humidity that the compressor can handle.
- Active cooling: Mechanically- (Compression chiller), thermally- (Absorption chiller) or TES-driven cooling coils extract heat from the inlet air. Dehumidification may be required for avoiding oversaturated moist air in the compressor.

Previous research proofed that TIAC could improve economical and environmental performance of gas turbine power generation (Alhazmy & Najjar, 2004; M. Ameri & Hejazi, 2004; Barigozzi, Perdichizzi, Gritti, & Guaiatelli, 2015; C. Yang, Yang, & Cai, 2009). The integration of thermal energy storages on the cold side (chilled water or ice storages) enabled shifting of cooling loads to night times (with lower ambient temperatures) and improved the performance and efficiency at peak times during the day (at higher ambient temperatures) (Mohammad Ameri, Hejazi, & Montaser, 2005; Dawoud, Zurigat, & Bortmany, 2005; Sanaye, Fardad, & Mostakhdemi, 2011; Zurigat, Dawoud, & Bortmany, 2006). Last but not least, Ehyaei et al. (2015) optimized the design and operation of an evaporative TIAC system. All of the mentioned research lacked in consideration of part-load characteristics. As mentioned in the literature review in **Chapter 2**, Yokoyama & Ito (2004) investigated active TIAC for gas turbines, also considering part-load efficiencies. However, to the best of the author's knowledge, all of the previous research did not describe the physics of moist air, a mixture of dry air and water, in detail. This Thesis analyzed TIAC methods in a holistic framework including both evaporative and active TIAC. Furthermore, the analysis was based on the fundamental physics of moist air, which are summarized below.

The humidity ratio (X) was defined as

$$X = \frac{m_{\mathrm{w}}}{\mathrm{m_a}}, \tag{3.67}$$

with the mass of water (m_{w}) and mass of dry air (m_{a}). The Antoine equation (Baehr & Kabelac, 2009) described the saturation partial pressure of water vapor ($p_{\mathrm{w}}^{\mathrm{s}}$) as function of the temperature (t in °C, T in K)

$$\ln\frac{p_{\mathrm{w}}^{\mathrm{s}}}{p_{\mathrm{tr}}}=\begin{cases}17.2799-\dfrac{4102.99}{\dfrac{t}{°\mathrm{C}}+273.431}; & 0.01\ °\mathrm{C}\le t\le 60\ °\mathrm{C}\\ 22.5129\cdot\left(1-273.16\dfrac{\mathrm{K}}{T}\right); & -50\ °\mathrm{C}\le t<0.01\ °\mathrm{C}\end{cases}. \tag{3.68}$$

For this and following equations, material properties of dry air and water were used. **Table 3.6** summarizes the parameters and their respective numeric values.

Table 3.6: Material properties of dry air and water (Baehr & Kabelac, 2009; VDI-Gesellschaft Verfahrenstechnik und Chemieingenieurwesen, 2010).

Parameter	Symbol	Value
Individual gas constants [J/kg/K]		
Dry air	R_{a}	287.05
Water	R_{w}	461.52
Specific heat capacities [J/kg/K]		
Dry air	$c_{p,\mathrm{a}}$	1004.6
Water vapor	$c_{p,\mathrm{w}}$	1863
Liquid water	c_{w}	4191
Ice	c_{i}	2070
Specific enthalpies of phase change [kJ/kg]		
Vaporization	Δh_{v}	2500.9
Freezing	Δh_{i}	333.1
Triple point of water		
Temperature [°C]	t_{tr}	0.01
Pressure [kPa]	p_{tr}	611.657

With Dalton's law, the humidity ratio (X) and relative humidity (φ) could be related to one another (Baehr & Kabelac, 2009),

$$\varphi=\frac{X}{\dfrac{R_{\mathrm{a}}}{R_{\mathrm{w}}}+X}\cdot\frac{p}{p_{\mathrm{w}}^{\mathrm{s}}(T)}, \tag{3.69}$$

$$X=\frac{R_{\mathrm{a}}}{R_{\mathrm{w}}}\cdot\frac{p_{\mathrm{w}}^{\mathrm{s}}(T)}{\dfrac{p}{\varphi}-p_{\mathrm{w}}^{\mathrm{s}}(T)}. \tag{3.70}$$

For $\varphi=1$, the humidity ratio at saturation (X_{s}) was derived to

$$X_{\mathrm{s}}=\frac{R_{\mathrm{a}}}{R_{\mathrm{w}}}\cdot\frac{p_{\mathrm{w}}^{\mathrm{s}}(T)}{p-p_{\mathrm{w}}^{\mathrm{s}}(T)}. \tag{3.71}$$

Below, quantities with asterisk (x^*) are specific values related only to the mass of dry air (m_a) (e.g., $h^* = H/m_a$, opposed to actual specific values related to the entire mass (m), e.g., $h = H/m$). Moist air can exist in several states, unsaturated (with water vapor), just saturated, or supersaturated with water or ice condensate. For each of these states, the specific enthalpy (h^*) was derived to (Baehr & Kabelac, 2009)

Unsaturated: $$h^*(T,X) = c_{p,a}(T - T_{tr}) + X\left[\Delta h_v + c_{p,w}(T - T_{tr})\right]; \quad (3.72)$$

Saturated: $$h_s^*(T) = h^*(T,X_s) = c_{p,a}(T - T_{tr}) + X_s\left[\Delta h_v + c_{p,w}(T - T_{tr})\right]; \quad (3.73)$$

Supersaturated, water condensate: $$h^*(T,X) = h_s^*(T) + (X - X_s)c_w(T - T_{tr}); \quad (3.74)$$

Supersaturated, ice condensate: $$h^*(T,X) = h_s^*(T) + (X - X_s)[-\Delta h_i + c_i(T - T_{tr})]. \quad (3.75)$$

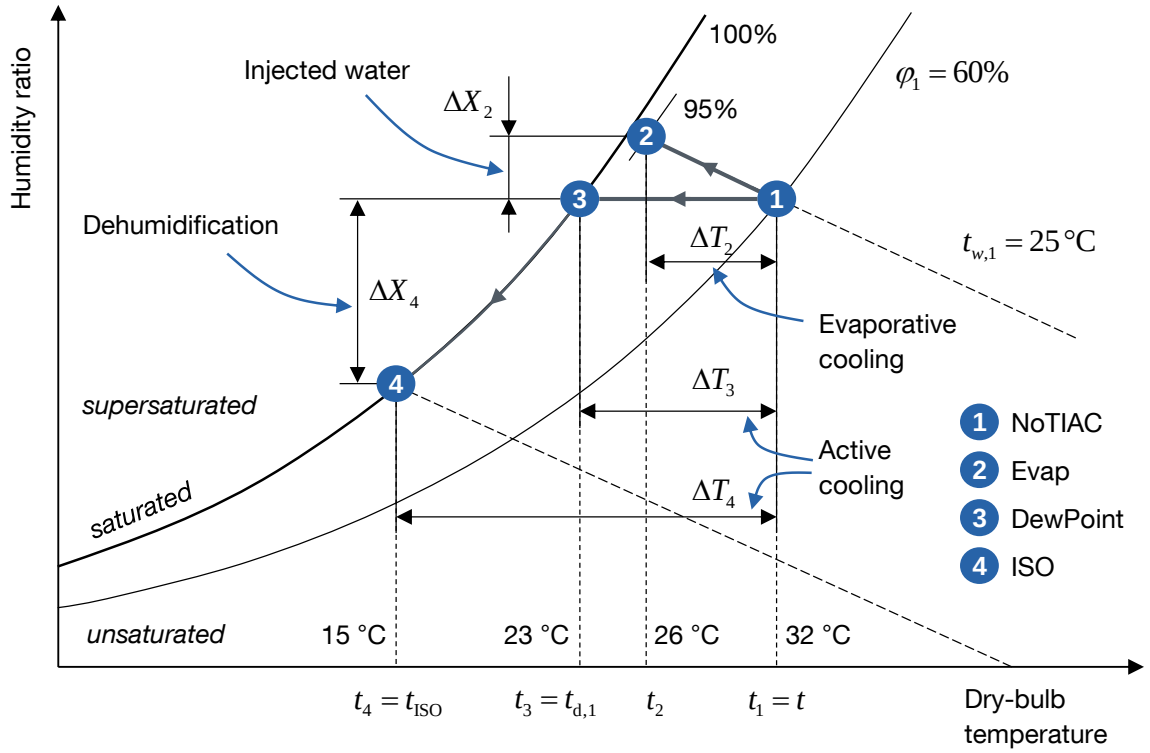

Figure 3.18: Turbine inlet air cooling methods: (1, NoTIAC) Example initial state; (2, Evap) Evaporative cooling with 95% relative humidity constraint; (3, DewPoint) Active cooling to the dew-point temperature; and (4, ISO) Active cooling to reach the ISO temperature (15 °C) (adapted from Thiem, Danov, et al. (2017)).

For moist air, three different temperatures could be defined:

- Dry-bulb temperature (T and t): Common temperature that is measured with thermometers;

- Wet-bulb temperature (T_w and t_w): Lowest temperature that can be reached with evaporative cooling;
- Dew-point temperature (T_d and t_d): Temperature to which moist air (at constant air pressure and humidity ratio) must be cooled to reach saturation.

Based on their definition, the following governing conditions for the latter two temperatures could be defined,

$$h_\mathrm{s}^*[T_\mathrm{w}, X_\mathrm{s}(T_\mathrm{w}, p)] = h^*(T, p), \tag{3.76}$$

$$X_\mathrm{s}(T_\mathrm{d}, p) = X(T, p), \tag{3.77}$$

which must be satisfied to calculate their respective temperature.

Figure 3.18 shows the change of state due to evaporative and due to active TIAC (and dehumidification). Furthermore, the dry-bulb (t), wet-bulb (t_w) and dew-point temperatures (t_d) were indicated for the initial state, State (1, NoTIAC). By injection of water droplets and evaporation, State (2, Evap) could be reached. This study considered a maximum relative humidity of 95% to avoid any water droplets in the compressor. When using evaporative TIAC, the temperature that could be reached was limited and strongly depended on the initial relative humidity (here $\varphi_1 = 60\%$). With active cooling, on the other hand, the dew-point temperature could be reached (3, DewPoint). Furthermore, the inlet air could be dehumidified with cooling coils and even lower temperatures (4, ISO) could be reached. The latter came at the cost of increased cooling energy requirements due to the required condensation of water vapor and removal of the condensate.

Turbine inlet air cooling was integrated in the technical superstructure (compare **Figure 3.2**). Water for evaporative cooling could either be drawn from the water grid or from one of the desalination plants (which might require further treatment for TIAC). Accordingly, the cooling energy could be supplied from a number of sources. The previously introduced ESD method was extended for TIAC. The gas turbine (set $GT \subseteq EC$) input and output power flows were computed by

$$P_{\mathrm{in},j,m,k} = \sum_{i=1}^{4} \left[\left(c_{1,\mathrm{in},j,m,i,k} P_{\mathrm{out},j,1,k} + c_{2,\mathrm{in},j,m,i,k} Q_j \right) O_{\mathrm{TIAC},j,i,k} \right], \quad \forall j \in GT, \forall m \in IN_j, \forall k \in TM, \tag{3.78}$$

$$P_{\mathrm{out},j,m,k} = \sum_{i=1}^{4} \left[\left(c_{1,\mathrm{out},j,m,i,k} P_{\mathrm{out},j,1,k} + c_{2,\mathrm{out},j,m,i,k} Q_j \right) O_{\mathrm{TIAC},j,i,k} \right], \quad \forall j \in GT, \forall m \in OUT_j, \forall k \in TM. \tag{3.79}$$

The online status ($\mathbf{O}_{\mathrm{TIAC},j,i} \subseteq \mathbf{O}$) of a particular TIAC method (i) was constrained as follows:

$$\sum_{i=1}^{4} \left(O_{\mathrm{TIAC},j,i,k} \right) = O_{j,k}, \quad \forall j \in GT, \forall k \in TM, \tag{3.80}$$

$$O_{\mathrm{TIAC},j,i,k} \leq I_{\mathrm{TIAC},j,i}, \quad \forall j \in GT, \forall i \in \{2,3,4\}, \forall k \in TM, \tag{3.81}$$

whereby $I_{\mathrm{TIAC},j,i}$ ($\mathbf{I}_{\mathrm{TIAC}} \subseteq \mathbf{I}$) described the installation of a particular turbine (j) inlet air cooling method (i).

For modeling the capital expenditures resulting from the investment in TIAC technologies, a new helper variable ($\mathbf{Z}_{\mathrm{TIAC}} \in \{0,1\}^{n_{\mathrm{GT}}}$) was introduced and defined as:

$$Z_{\mathrm{TIAC},j} = \sum_{i=2}^{4} I_{\mathrm{TIAC},j,i}, \quad \forall j \in GT. \tag{3.82}$$

Capital expenditures for investments in TIAC technologies were then computed by

$$C_{\mathrm{CAPEX,TIAC}} = \sum_{j \in GT} \left(\sum_{i=2}^{4} \left[a_j \cdot \left(i_{\mathrm{TIAC},1,j,i} I_{\mathrm{TIAC},j,i} + i_{\mathrm{TIAC},2,j,i} Q_{\mathrm{TIAC},j,i} \right) \right] \right). \tag{3.83}$$

For **Equation (3.83)**, TIAC-related capacities were defined as

$$Q_{\mathrm{TIAC},j,i} = \begin{cases} \left(1 - Z_{\mathrm{TIAC},j}\right), & i = 1 \\ I_{\mathrm{TIAC},j,i} Q_{\mathrm{TIAC},j,i}, & i \in \{2,3,4\} \end{cases}, \quad \forall j \in GT. \tag{3.84}$$

The objective function (see **Equations (3.41)** and **(3.48)**) was accordingly modified to account for TIAC related CAPEX:

$$f_{\mathrm{TIAC},p} = f_p + g_{\mathrm{CAPEX},p} \cdot C_{\mathrm{CAPEX,TIAC},p}, \quad \forall p \in PER_l, \forall l \in SP, \tag{3.85}$$

For this Thesis, the simultaneous installation of multiple TIAC technologies for a particular gas turbine (j) was neglected,

$$\sum_{i=2}^{4} \left(I_{\mathrm{TIAC},j,i} \right) \leq I_j, \quad \forall j \in GT. \tag{3.86}$$

The specific capital cost parameters ($\mathbf{i}_{\mathrm{TIAC},1}$ and $\mathbf{i}_{\mathrm{TIAC},2}$) were estimated based on price lists for water spray nozzles (EXAIR Corporation, 2016; Lechler, 2016) and information on air cooler heat exchangers (Sachan, 2012), respectively.

The different turbine inlet air cooling methods are compared and analyzed for different use cases in **Section 4.2.7**.

3.5.4 Ice-storage-integrated desalination

Using water in its solid state (ice) for refrigeration has been well known since the 16th century (Cummings, 1949). In the 19th century, utilization of ice for food preservation resulted into a global ice trade and a demand for ice storages. However, with the development of compression and absorption chillers the demand for ice as commodity strongly declined (Anderson, 1953; Blain, 2006; Ingels, 1991). In the 1980s, the Electric Power Research Institute (EPRI) introduced demand-side management (DSM) for avoiding imported and expensive fuels for peak power plants in the United States

(Balijepalli, Pradhan, Khaparde, & Shereef, 2011). With the introduction of DSM, interest in modern-style ice thermal energy storages (ITES) revived.

Ice storages belong to the group of latent thermal energy storages (TES). TES were categorized according to their underlying process of storing energy, see **Figure 3.19**. Most thermal energy storages store energy either by heating or cooling the storage medium (sensible heat) or by using its phase change (latent heat) (Dinçer & Rosen, 2011). For each of the three TES (Hot and chilled water storages and ice storages) shown in **Figure 3.19**, several subcategories might exist. For example, ice storages were commercially available as ice-on-coil, sheet ice harvester, encapsulated ice and ice slurry types (Urbaneck et al., 2005).

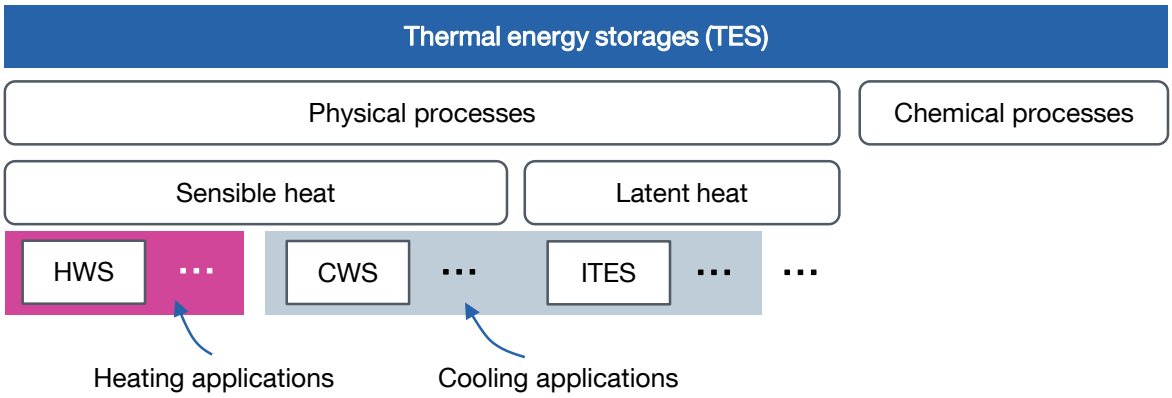

Figure 3.19: Classification of TES that were considered in this Thesis (adapted from Mehling & Cabeza (2008)).

The schematic sketch in **Figure 3.20 (a)** illustrates the working principle of the most common ice storage type, ice-on-coil internal melt. Ice-on-coil ice storages are charged by heat transfer fluid (HTF, water-glycol mixture) that enters the ice storage "coils" (heat exchanger) with a temperature of less than 0 °C (phase change temperature of water). The heat exchanger tubes are submerged in water, which is stored in an insulated tank. As illustrated in **Figure 3.20 (a)**, HTF entering with temperatures less than 0 °C into the ITES will extract heat from the water stored in the tank and increase the temperature of the HTF. The water inside the tank, however, will cool down to the phase change temperature of water, eventually supercool and crystallize to ice. During discharge of the ice storage, HTF with temperatures greater than 0 °C flows through the heat exchanger piping and releases heat to the storage medium melting the stored ice from the inside. Hence, this particular ice storage type is called internal melt. The ideal cycle is further elaborated in an temperature (T)-enthalpy (h) diagram in **Figure 3.20 (b)**. Due to the density difference of water (≈1000 kg/m³) and ice (≈920 kg/m³) (Chaplin, 2016; VDI-Gesellschaft Verfahrenstechnik und Chemieingenieurwesen, 2010), the liquid level of the water in the ice storage is a good indicator for the state of charge (Stovall & Tomlinson, 1990; West & Braun, 1999).

The required phase change within the ice storage could also be utilized for desalinating salt water based on the freeze desalination (FD) process. Such an ice-storage-integrated desalination (isiD) system is a new technology combining both an energy storage and a desalination system and was developed and investigated during this research project (Danov, Schäfer, & Thiem, 2016). The idea behind FD is shown in

the phase diagram of sodium chloride (NaCl) in water (H_2O) in **Figure 3.21 (b)**. Sea water with typical temperatures in the range 10 – 30 °C and average salt concentrations of 35 g/kg (3.5%) was fed into the isiD system (1).[9] In the ice storage, heat was extracted from the salt water and transferred to the heat transfer fluid. Eventually, the storage medium reached the phase change boundary (< 0 °C) and ice (H_2O) crystallized along the heat exchanger tubes. Finally, the storage was fully charged and reached state (2). Due to kinetic effects (rate of diffusion), the ice contained pockets of salt water, as indicated in **Figure 3.21 (a)**. After removing the remaining liquid water (with an increased salt concentration), the ice around the heat exchanger coils could be melted (discharge of the ice storage) and used as product water.

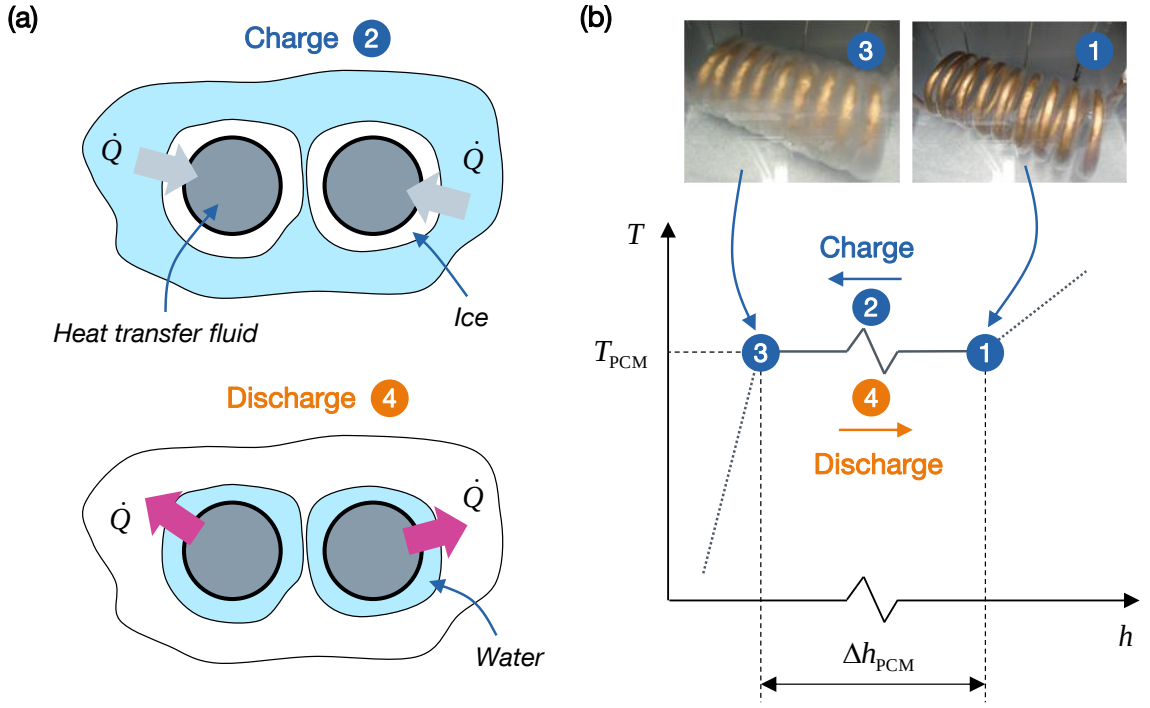

Figure 3.20: Ice storage: (a) Schematic sketch of an ice-on-coil internal melt storage, (b) Temperature-enthalpy diagram for the phase change material (PCM = water).

According to Rahman, Ahmed, & Chen (2006), freeze desalination had the following potential advantages compared to established desalination technologies:

- Use of inexpensive plastics and less corrosion problems due to low operating temperatures;
- No pre-treatment or any chemicals required;
- Insensitive to fouling.

On the other hand, freeze desalination also had drawbacks:

[9] The average concentration of salt within sea water is 35 g/kg. The salt consists mostly (86%) of sodium chloride (NaCl) (Fritsch et al., 2010).

- Retention of undesirable flavors and aromas that are initially present in the feed water;
- Multiple stages and/or crushing and re-crystallization of the ice required due to trapping of salt water in the ice during crystallization;
- Increasing concentrations of dissolved substances and non-condensable gases.

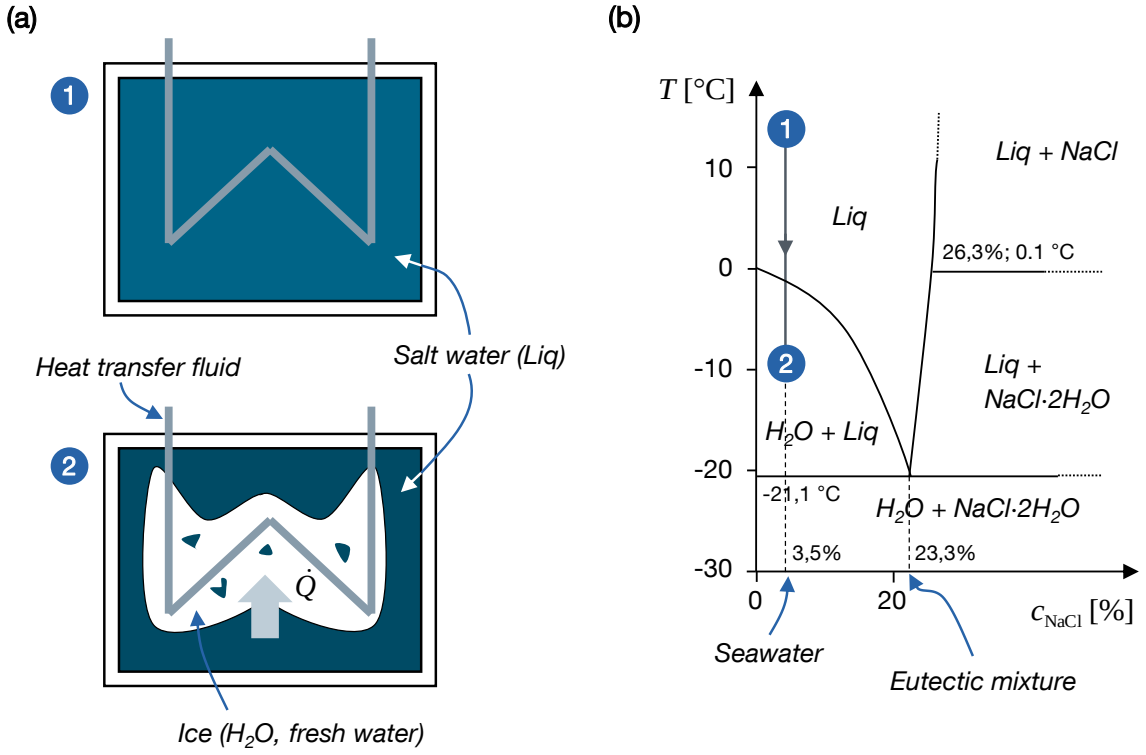

Figure 3.21: Ice-storage-integrated desalination: (a) Schematic sketch, (b) Temperature-Sodium chloride concentration diagram (adapted from Clark (2014)).

Because there was no isiD system ever built before, there was no past experience that could be used. Therefore, a new experimental setup was developed and built. The setup was well-equipped with multiple temperature, flow rate and conductivity sensors. Two types of ice storages, ice-on-coil and sheet ice harvester, as well as different heat exchanger geometries (i.e., smooth and twisted tubes) were investigated. In a number of experiments, the optimal operating strategy was determined. Since freeze desalination is a diffusion-controlled process, the cooling supply temperature setpoint was chosen in a way to keep the ice growth rate rather small. Furthermore, sweating (i.e., discarding a small proportion of the product water that was melted first) improved the desalination efficiency (Mandri et al., 2011; Rich et al., 2012). Further details of the experimental setup and procedure were summarized by Prenzel (2015).

For the modeling level of detail of this Thesis, the *overall efficiency* of the desalination process within the isiD system must be known. **Figure 3.22** shows that fresh water quality (< 1 g salt per kg water) could not be reached with a single ice storage desalination cycle (one stage). Instead, about four stages were required. The desalination efficiency per stage was in the range of 52% to 72%.

Accordingly, for the isiD model, four stages were assumed to be sufficient for reaching fresh water quality. However, the water in an ice storage is not completely frozen to avoid stress from changes in density and due to the solid state of ice. Experimental results obtained for another larger scale ice storage setup (Ice-on-coil internal melt ice storage manufactured by Fafco with 210 kWh latent storage capacity) showed that at a fully charged state about 50% of the storage was filled with water. Given the enthalpy of fusion of pure water (Δh_i = 333.1 kJ/kg = 92.53 kWh/m³) (VDI-Gesellschaft Verfahrenstechnik und Chemieingenieurwesen, 2010), the enthalpy of fusion for 50% of the stored water (PCM) related to the total water volume (tot) equaled to $0.5\ \mathrm{m^3_{PCM}/m^3_{tot}} \cdot 92.53\,\mathrm{kWh/m^3_{PCM}} = 46.26\,\mathrm{kWh/m^3_{tot}}$. Due to energy needed for the sensible cooling of water (and ice), the practical value that was required was higher. Indeed, experimental results showed that $55.56\,\mathrm{kWh/m^3_{tot}}$ were necessary. Hence, with four stages, the required energy for freeze desalination was approximately determined to $\sum_{i=1}^{4}(1/i) \cdot 55.56\,\mathrm{kWh/m^3_{tot,init}} \cdot 2^4\ \mathrm{m^3_{tot,init}/m^3_{fw}} = 1666.67\,\mathrm{kWh/m^3_{fw}}$, where fw denotes fresh water.

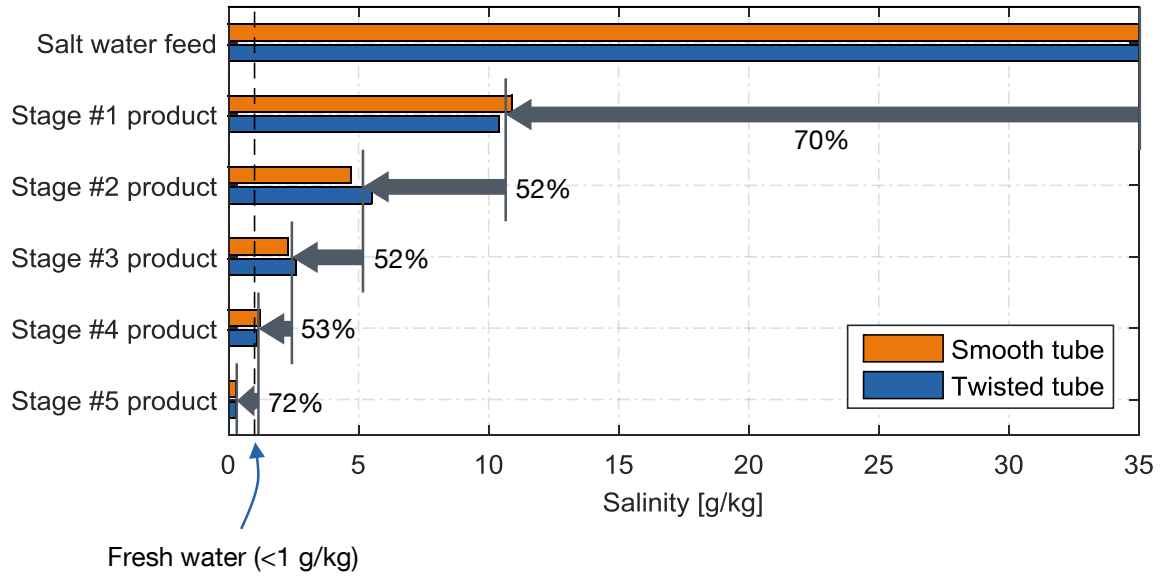

Figure 3.22: Experimental results for the isiD system (adapted from Prenzel (2015)).

A quick comparison of this value (1666.67 kWh_{th}/m^3) with state-of-the art desalination technologies (e.g., multi-stage flash distillation: ≈76.4 kWh_{th}/m^3, see **Table A.11** in the appendix) showed that the isiD system could only be energy-efficient and economically interesting if fresh water was available as a by-product of a by-itself economically attractive ice storage. Among others (such as electricity price spreads), large cooling loads are required to make ice storages economically feasible. **Figure 3.23** plots the specific desalination capacity of individual countries vs. specific cooling requirements. Countries with larger cooling requirements tend also to have larger desalination requirements, compare, e.g., Saudi Arabia, Qatar or the United Arab Emirates. Ice-storage-integrated desalination could be of great interest in particular for the aforementioned countries. In **Section 4.2.7**, isiD systems are analyzed in more detail.

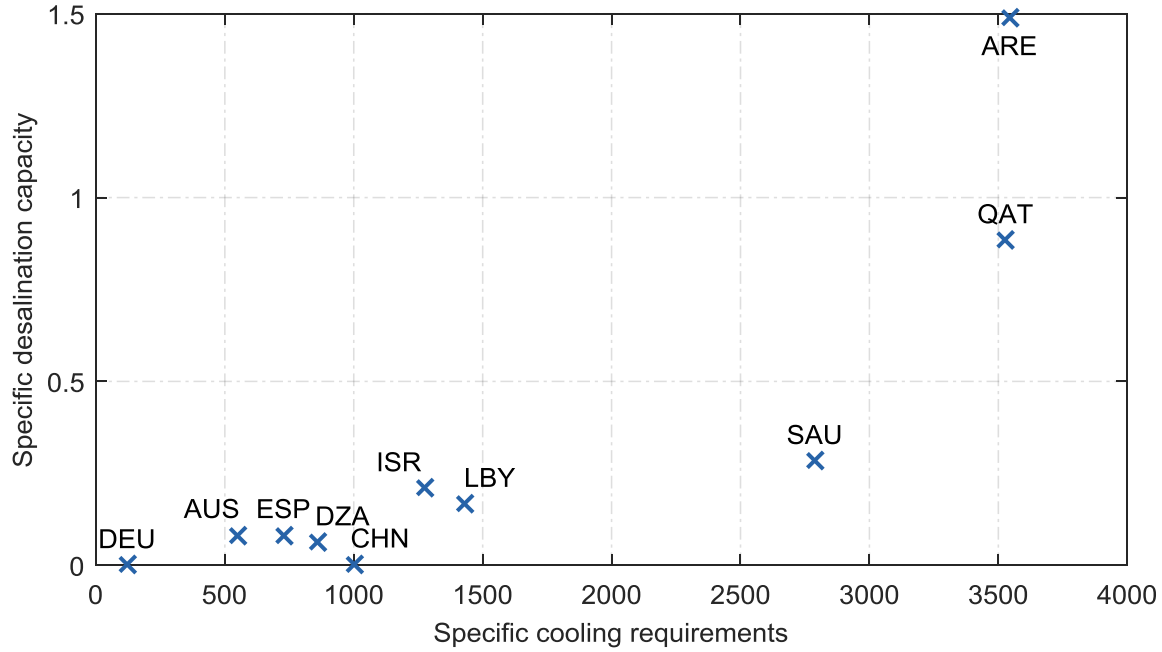

Figure 3.23: Specific desalination capacity (Specific capacity of commissioned desalination plants [m³/d/capita] (WaterWorld, 2013)) vs. specific cooling requirements (average cooling degree days (18.3 °C reference) [°C] (ASHRAE, 2009)) for different countries (adapted from Prenzel (2015)).[10]

3.6 Benchmark: Office building in Frankfurt

3.6.1 Example case description

Before the described method for the optimal design of multi-modal energy systems could be used for investigating any use case, the method had to be benchmarked. A state-of-the-art optimization model (in the following denoted SOTA[11]) served as reference. Furthermore, the method was compared to a rule-based design method (RUBA). The latter indicated the potential advantages that could be achieved by using optimization methods in comparison to heuristic methods. The rule-based design method was based on the following rules/steps:

1. Determine feasible technology packages (e.g., one package could be a combination of PV, internal combustion engine CHP, hot water storage and absorption chiller).

[10] Countries were abbreviated according to ISO 3166: ARE: United Arab Emirates, AUS: Australia, CHN: China, DEU: Germany, DZA: Algeria, ESP: Spain, ISR: Israel, LBY: Libya, QAT: Qatar, SAU: Saudi Arabia.

[11] The state-of-the-art optimization model is a Siemens-internal modification of *Energy System Development Plan (ESDP)*, which was originally developed in a collaboration of the RWTH Aachen and Siemens AG (Raths et al., 2015). At the time of the investigation, the tool's capabilities were very similar to those of *urbs* (see **Section 2.3** and, e.g., Schaber, Steinke, & Hamacher (2012)).

2. Determine (initial) capacities of the chosen technologies based on the peak load demands and the load duration curves.
3. Set (initial) minimum and maximum state of charge points for the energy storages to determine the times, when the corresponding energy conversion units should be turned on and when they should be off (e.g., when the state of charge of the hot water storage falls below 20%, the internal combustion engine CHP should turn on).
4. Based on visual inspection and consideration of the energy balances and costs, iteratively repeat Steps 2 and 3 until all constraints of the energy system are satisfied and a point is reached, where the total expenditures do not change anymore (i.e., the total expenditures are minimal from the point of view of the expert).
5. Repeat Steps 2 – 4 for each technology package determined in Step 1.
6. Among those solutions (technology packages) satisfying all constraints of the energy system, choose the solution (technology package) with the best fulfillment of the objective (i.e., minimum total expenditures).

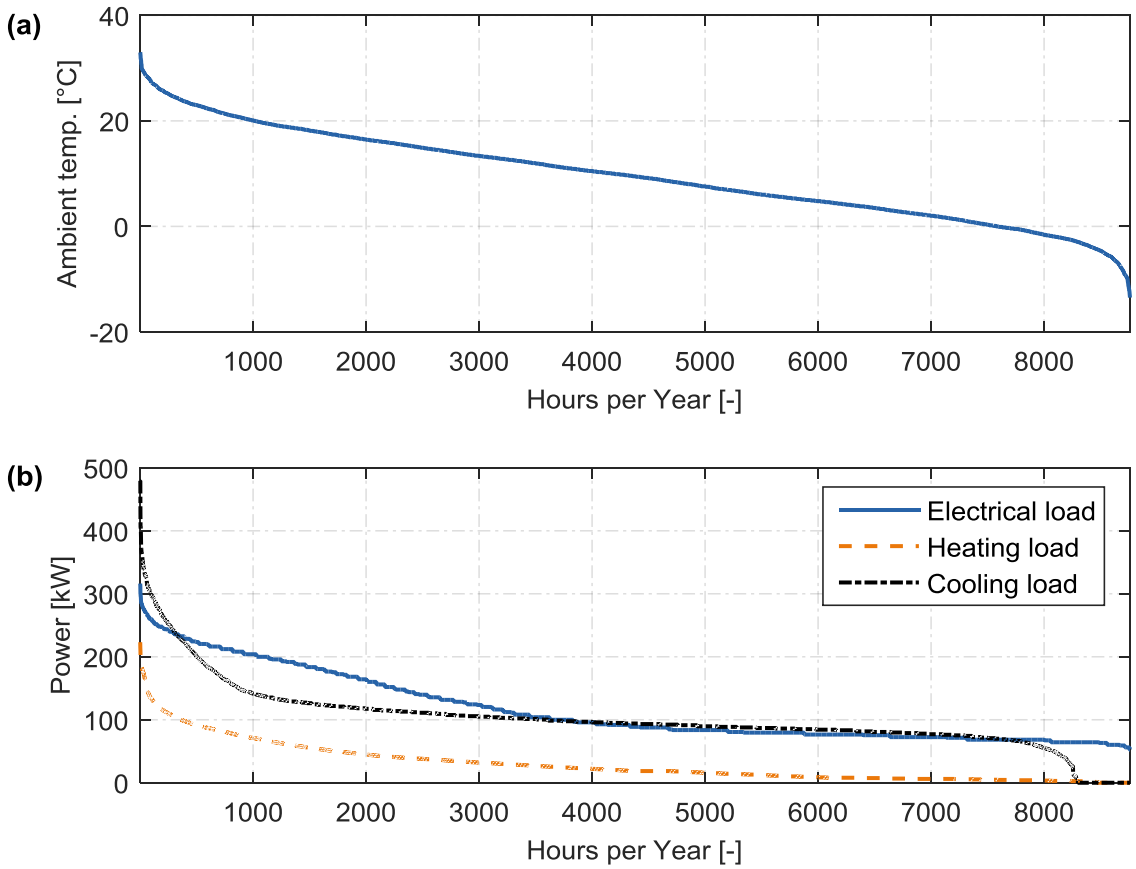

Figure 3.24: Frankfurt office building example case: (a) Temperature duration curve, (b) Load duration curves.

Because at the time of the investigation, both SOTA and RUBA were not able to model the energy system and its technologies in the same detail as the method of this Thesis, a simplified example case was considered.

The example was an office building in Frankfurt (Germany). For this building, the optimal design of the system (with respect to total expenditures) was supposed to be determined. The energy system had to meet given inelastic electricity, heating and cooling loads. The load duration curves along with the temperature duration curve were plotted in **Figure 3.24**. The load duration curves clearly indicate that energy system design based on peak load would run mostly in part-load operation. The design method could choose between a combination of the following technologies: Photovoltaic, internal combustion engine CHP, gas boiler, absorption chiller, compression chiller, hot water storage and chilled water storage. For all technologies, the economic life time was assumed to 20 a at weighted average costs of capital (WACC) of 7%. The assumed specific capital costs and O&M costs, the efficiencies and the commodity prices are summarized in **Table 3.7**.

Table 3.7: Frankfurt office building example case: Parameters.

Parameter	Value		Parameter	Value
Photovoltaic (PV)				
Specific capital costs	1380 €/kW		Specific O&M costs	0 €/kW/a
Efficiency	const.		Max. capacity	50.5 kW
Internal combustion engine (ICE)				
Specific capital costs	1172 €/kW_{el}		Specific O&M costs	81.6 €/kW_{el}/a
Electrical efficiency	0.33		Thermal efficiency	0.47
Gas boiler (GB)				
Specific capital costs	220 €/kW		Specific O&M costs	6.25 €/kW/a
Efficiency	1.0		Min. capacity	230 kW
Absorption chiller (AC0)				
Specific capital costs	745 €/kW		Specific O&M costs	40 €/kW/a
Energy efficiency ratio	0.75			
Compression chiller (CC0)				
Specific capital costs	365 €/kW		Specific O&M costs	29 €/kW/a
Energy efficiency ratio	4.0			
Hot water storage (HWS)				
Specific capital costs	25 €/kWh/a		Specific O&M costs	0 €/kWh/a
Charge efficiency	1.0		Discharge efficiency	1.0
Chilled water storage (CWS)				
Specific capital costs	25 €/kWh/a		Specific O&M costs	0 €/kWh/a
Charge efficiency	1.0		Discharge efficiency	1.0
Commodity prices				

Parameter	Value		Parameter	Value
Natural gas price	4.4 ct/kWh			
Electricity price (purchase)	16.6 ct/kWh		Electricity price (sale)	8.56 ct/kWh

3.6.2 Benchmark of the method

The multi-modal energy system of the office building located in Frankfurt was determined using different methods and strategies. First, the design and operation of the system was computed with a rule-based design method (RUBA) using if-then conditions. The energy system design result of RUBA was optimally controlled (operated) in another case (OC). The state-of-the-art optimization (SOTA) method computed the optimal design and operation of the energy system based on strategy FullProb (compare **Table 3.4**). Furthermore, the ESD method of this Thesis was evaluated using strategies FullProb, DM-Month and DM-Day.

The operation of the system (strategy FullProb) is illustrated in **Figure 3.25**. For a week in January (left side) and a week in July (right side) the accumulated power generation (> 0) and power consumption (< 0) flows for electricity, heating and cooling are shown. **Figure 3.25 (c) and (d)** show that the internal combustion engine was sized to satisfy a certain heat demand. For heating loads greater than the thermal capacity of the ICE, the gas boiler or hot water storage was used. The waste heat of the ICE can further be used in the absorption chiller to generate ‘cold’. The remaining cooling demand was supplied from the compression chiller and the intelligent usage of the chilled water storage (see **Figure 3.25 (e) and (f)**).

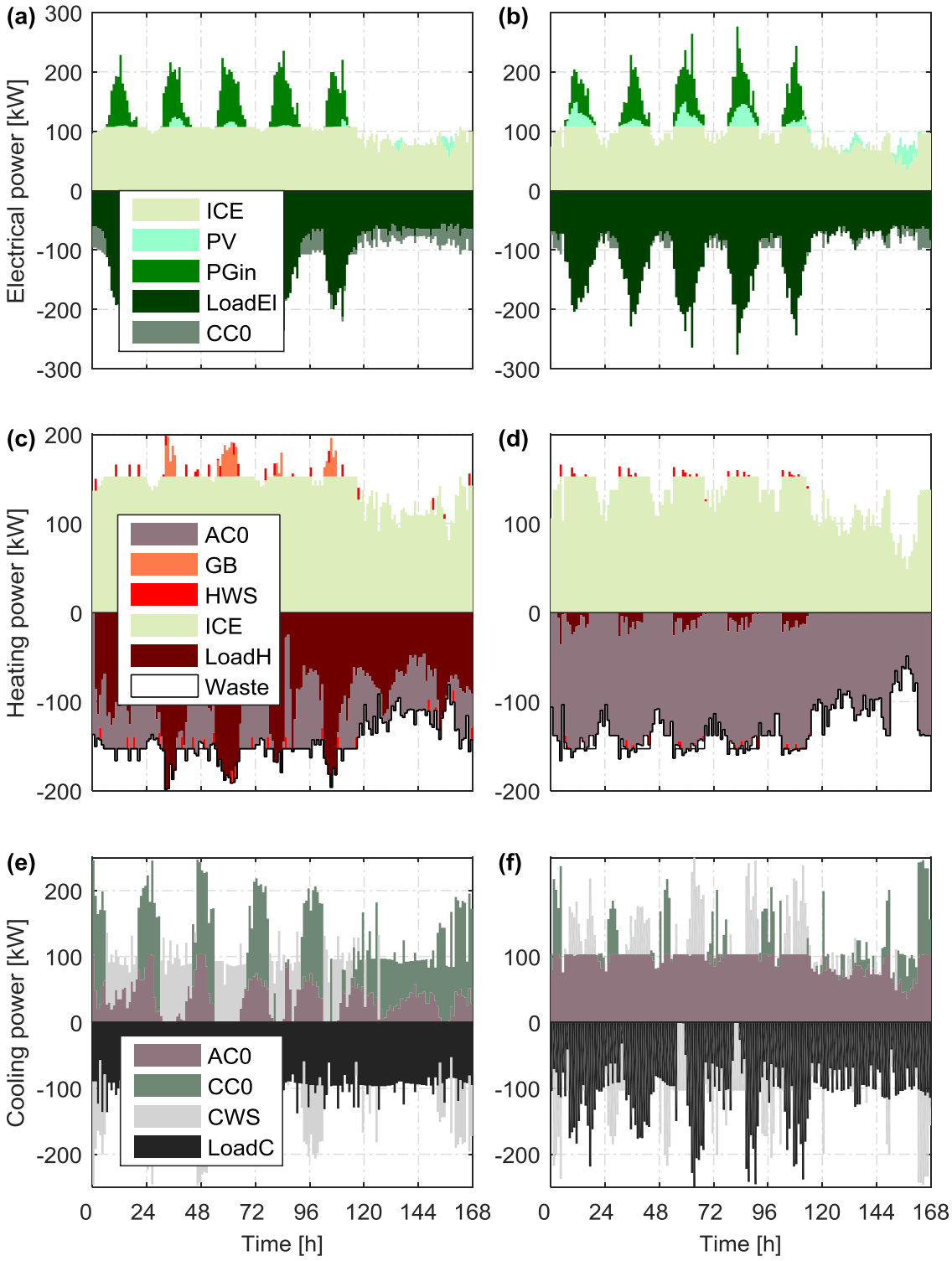

Figure 3.25: Optimal operation of the system: Electrical power, heating and cooling power for (a), (c), (e) week in January; (b), (d), (e) week in July.

The marginal costs for generating electricity using the internal combustion engine without making use of its waste heat ($MC_{\mathrm{ICE}} = p_{\mathrm{f}}/\eta_{\mathrm{ICE,el}} = 13.33\,\mathrm{ct/kWh}$) was lower than the electricity purchase price. Therefore, up to its capacity, the generation of electricity

using the ICE - even when making no use of its waste heat - was economically more attractive than the purchase of electricity from the power utility. The PV generation coincided with the peak power demand and reduced the amount of energy drawn from the power grid (compare **Figure 3.25 (a) and (b)**).

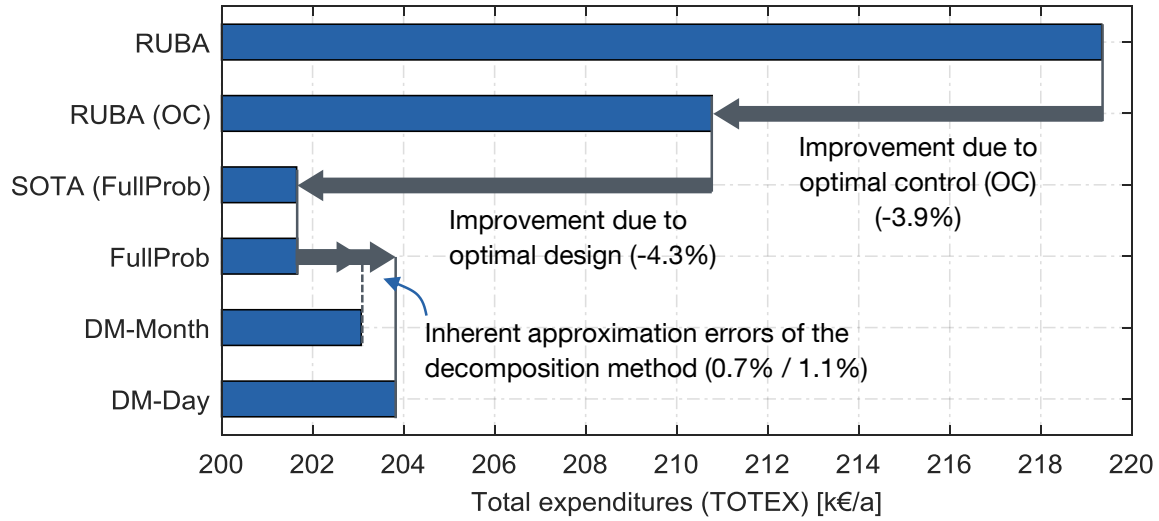

Figure 3.26: Total expenditures for the rule-based design method (RUBA), the state-of-the-art optimization model (SOTA) and the three strategies (FullProb, DM-Month and DM-Day).

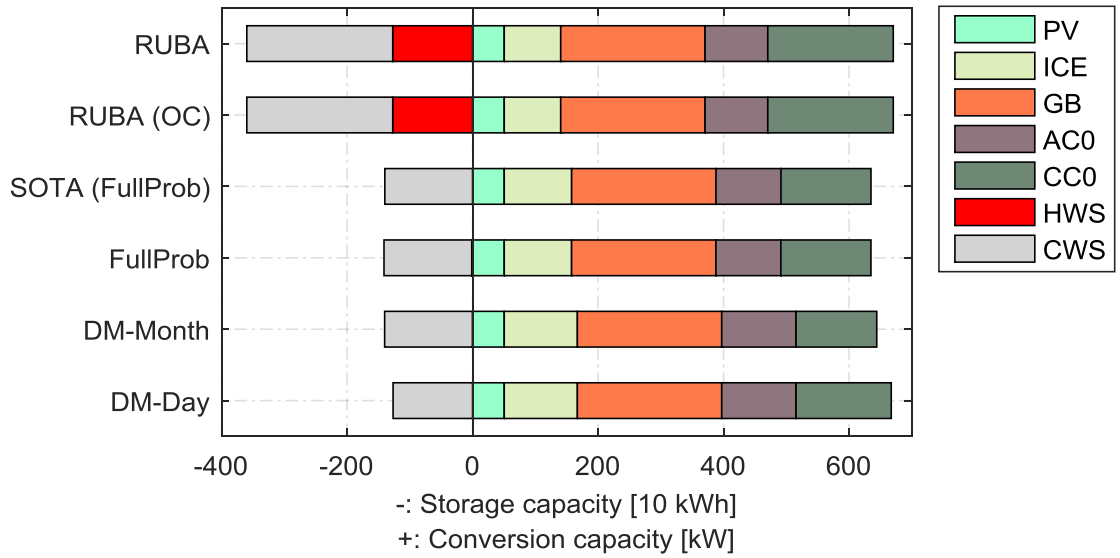

Figure 3.27: Conversion and storage capacities for the rule-based design method (RUBA), the state-of-the-art optimization model (SOTA) and the three strategies (FullProb, DM-Month and DM-Day).

The total expenditures (TOTEX) for the six strategies were plotted in **Figure 3.26**. As the figure shows, the optimization models (both the SOTA model and the ESD method (FullProb) presented here) outperformed the RUBA design by approximately 8%. For the

example system, both optimizing the operation and optimizing the design contributed about the same share to the cost improvement. When using strategies DM-Month and DM-Day, the TOTEX increased by 0.7% and 1% compared to FullProb, respectively. The reasons for these differences were inherent approximation errors of the latter two strategies. **Section 3.6.6** briefly discusses these approximation errors.

Finally, **Figure 3.27** shows the capacities of the energy system technologies determined with the six strategies. Note that in particular the storage capacities were difficult to determine using rule-based methods. Also, due to a suboptimal storage operation, other technologies (e.g., CC0) might have suboptimal capacities.

3.6.3 Impact of non-constant part-load efficiencies on the optimal design

The previous example assumed very simple technology models, i.e., constant part-load efficiencies and no part-load constraints, to make the ESD method of this Thesis comparable to the state-of-the-art optimization model. The ESD method presented in this Thesis, however, is capable of designing energy systems with much more complicated technology models. In reality, energy converters cannot be operated at all part-load ratios between off and full load. Moreover, for many converters, the efficiency of energy conversion decreases when lowering the part-load ratio. **Table 3.8** shows the assumed parameters.

Table 3.8: Frankfurt office building example case: Parameters for non-zero minimum part-load ratios and non-constant part-load efficiencies.

Parameter	Value		Parameter	Value
Internal combustion engine (ICE)				
Min. part-load ratio	0.5			
Full-load electrical efficiency	0.33		Electrical efficiency at 50% load	0.25
Full-load thermal efficiency	0.47		Thermal efficiency at 50% load	0.5
Gas boiler (GB)				
Min. part-load ratio	0.1			
Full-load efficiency	1		Efficiency at 50% load	0.98
Absorption chiller (AC0)				
Min. part-load ratio	0.15			
Full-load energy efficiency ratio	0.75		Energy efficiency ratio at 50% load	0.7
Compression chiller (CC0) – with variable-speed compressor				
Min. part-load ratio	0.2			
Full-load energy efficiency ratio	4		Energy efficiency ratio at 50% load	4

The optimal design of the energy system was investigated for the following three cases:

- Ref: The previous example case with constant part-load efficiencies and no part-load constraints;
- $u_{\min} > 0$: Minimum part-load ratios as indicated in the table;
- $u_{\min} > 0,\ \eta \neq \text{const.}$: Both minimum part-load ratios and non-constant part-load efficiencies.

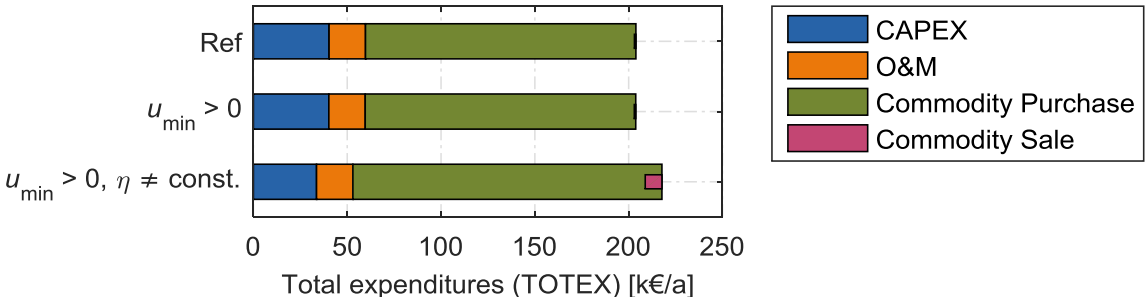

Figure 3.28: Total expenditures when considering non-zero minimum part-load ratios and non-constant efficiencies.

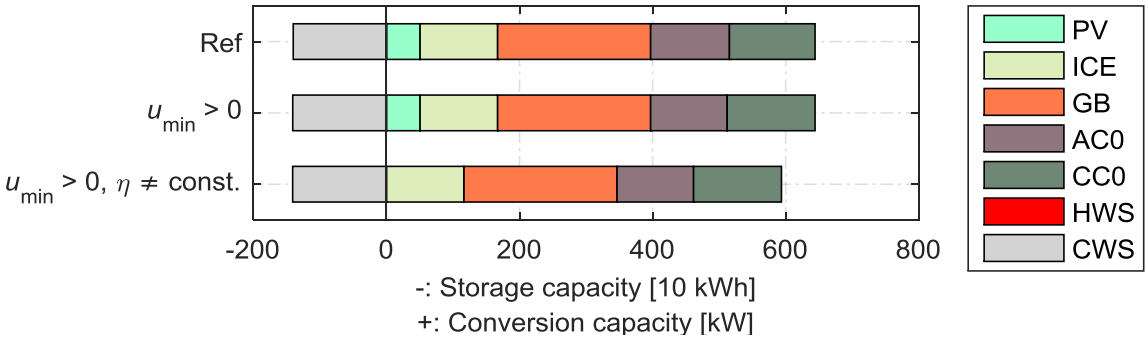

Figure 3.29: Conversion and storage capacities when considering non-zero minimum part-load ratios and non-constant efficiencies.

Figure 3.28 and **Figure 3.29** show the resulting optimized TOTEX and capacities of the energy systems, respectively. The two figures show that – for the particular example case - the introduction of *part-load constraints* (i.e., minimum part-load ratios) did not change the economical result and the design of the system significantly. By considering *part-load efficiencies*, however, the installation of photovoltaic panels became economically unattractive. Due to the decreased part-load efficiency of the internal combustion engine, it was operated more often at higher part-load ratios (compare **Figure 3.30**). Photovoltaic power generation, however, was phased out in this particular case, because the CHP plant also supplied the heating energy demand. Furthermore, **Figure 3.28** shows that – as a result of the marginal costs – the sale of electricity at the wholesale market became attractive to achieve greater part-load ratios and higher efficiencies.

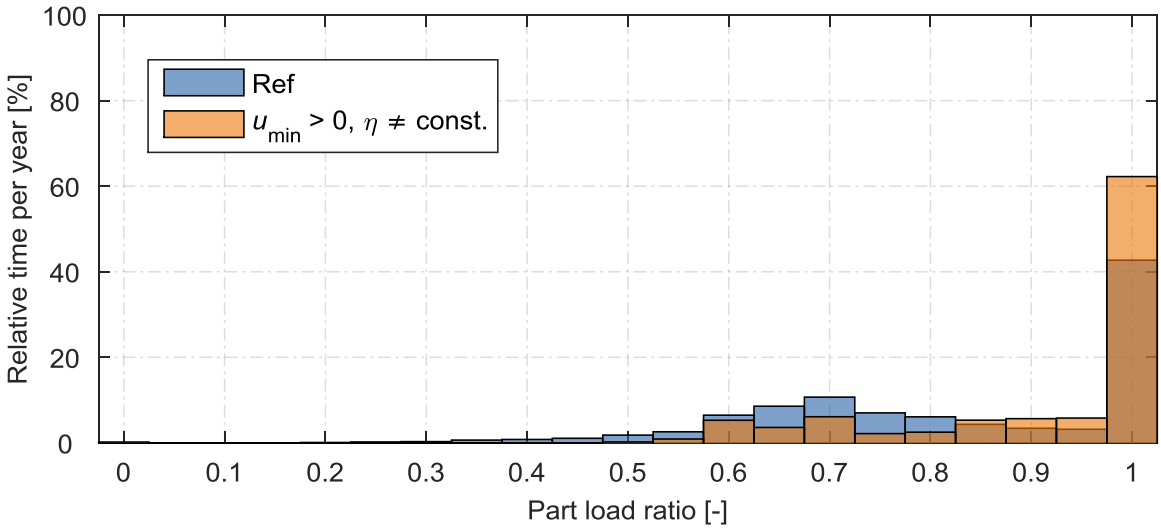

Figure 3.30: Optimal operation characteristics for the internal combustion engine CHP system when considering non-zero minimum part-load ratios and non-constant efficiencies.

This simple example illustrates the impact of non-constant part-load efficiencies very well. Assuming constant part-load efficiencies (as it was done in most of the previous research, compare the review in **Chapter 2**), could result in the installation and usage of suboptimal technologies.

3.6.4 Sensitivity of the design

The results for the benchmark of the ESD method (see **Figure 3.26** and **Figure 3.27**) showed that the optimization models could achieve roughly 8% lower total expenditures compared to rule-based heuristic methods, although the number of free optimization variables (approximately proportional to the number of technologies minus the number of inelastic demands that were considered) was small. For elaborating the sensitivity of the energy system design, the example case (Ref) was further simplified. Both thermal energy storages, HWS and CWS, were ignored. Additionally, the heat redundancy condition was dropped.

Figure 3.31 illustrates the result of this sensitivity analysis. The capacities of both the internal combustion engine (ICE) and the compression chiller (CC0) were systematically varied (scatter search). The capacities of the other technologies (GB and AC0) as well as the operation of the system were free optimization variables. **Figure 3.31 (a)** (in the lower left corner) shows a contour plot of total expenditures for different combinations of ICE and CC0 capacities. The adjacent plots (**Figure 3.31 (b) – (e)**) show the capacities of the technologies and the total expenditures for two distinct cross sections indicated by white arrows and black lines in **Figure 3.31 (a)**. First of all, see that the ESD method presented in this Thesis was able to identify the global optimum. Note that the global optimum could not be found on the discrete scatter. Furthermore, the scatter search method was very time-intense. The contour plot, however, enabled the discussion of the sensitivity of the design. The plot shows that the total expenditures (here in only two dimensions) quite smoothly increased around the global optimum. In a small area around the global optimum, the resulting TOTEX only increased insignificantly. Hence, for this particular

case, configurations with technologies with *near-optimal* capacities would achieve similar total expenditures. This also substantiates the importance of near-optimal solutions, if they can be computed in a fraction of the time required to determine global optima.

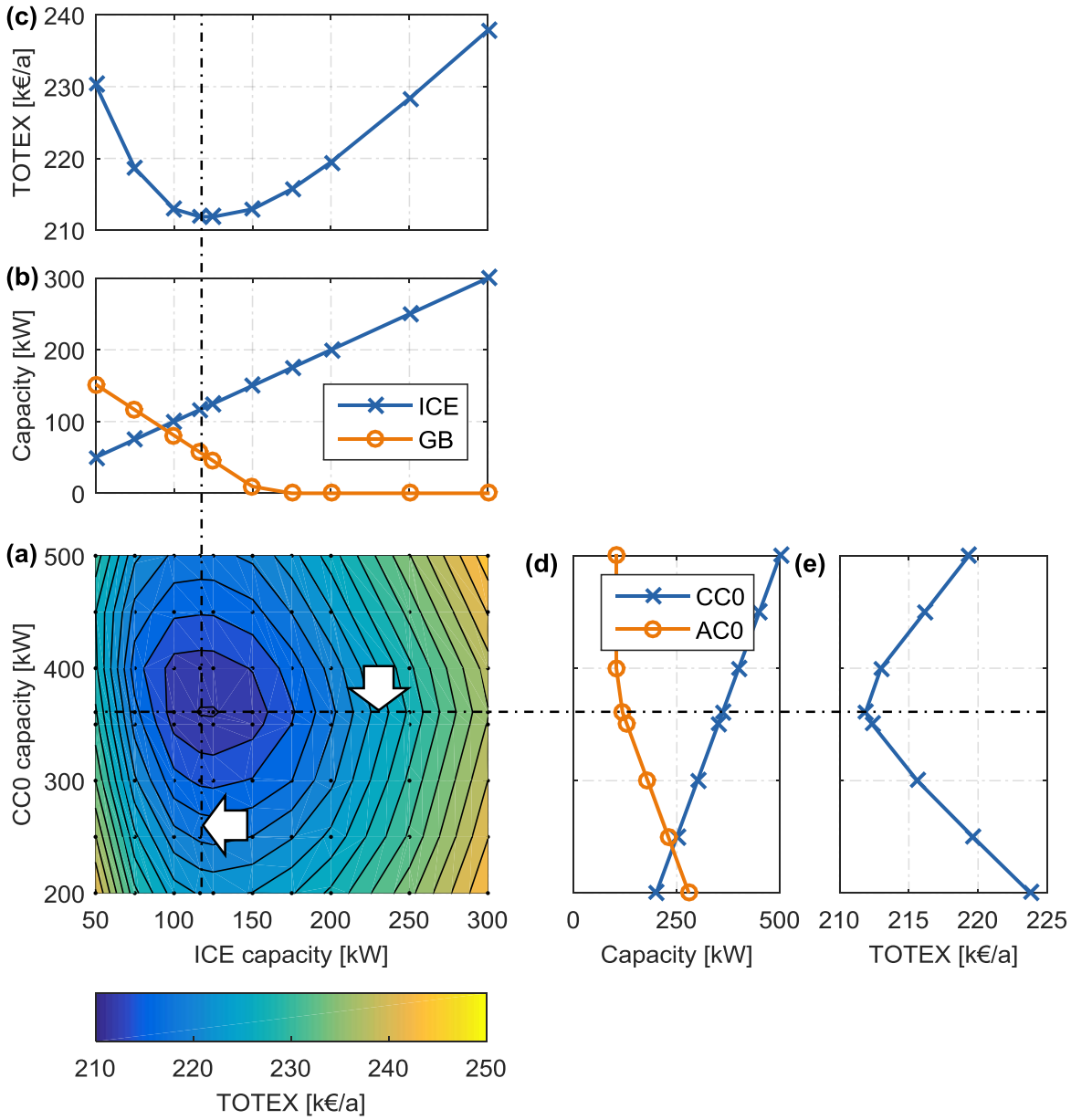

Figure 3.31: Sensitivity of the optimal design: Total expenditures (TOTEX)[12] for variations of the capacities of the internal combustion engine (ICE) and compression chiller (CC0).

[12] Filled contour plot in (a) was linearly interpolated based on indicated data points.

3.6.5 Comments on the CAPEX-OPEX weighting factor and interest rate

Along with the decomposition method, a CAPEX-OPEX weighting factor ($w_{C/O} \in \mathbb{R}, 0 \leq w_{C/O} \leq 1$) was introduced that overweighed CAPEX-related costs to avoid installation of technologies in *certain periods* that were economically unattractive when considering the entire year (compare **Section 3.4.8**).

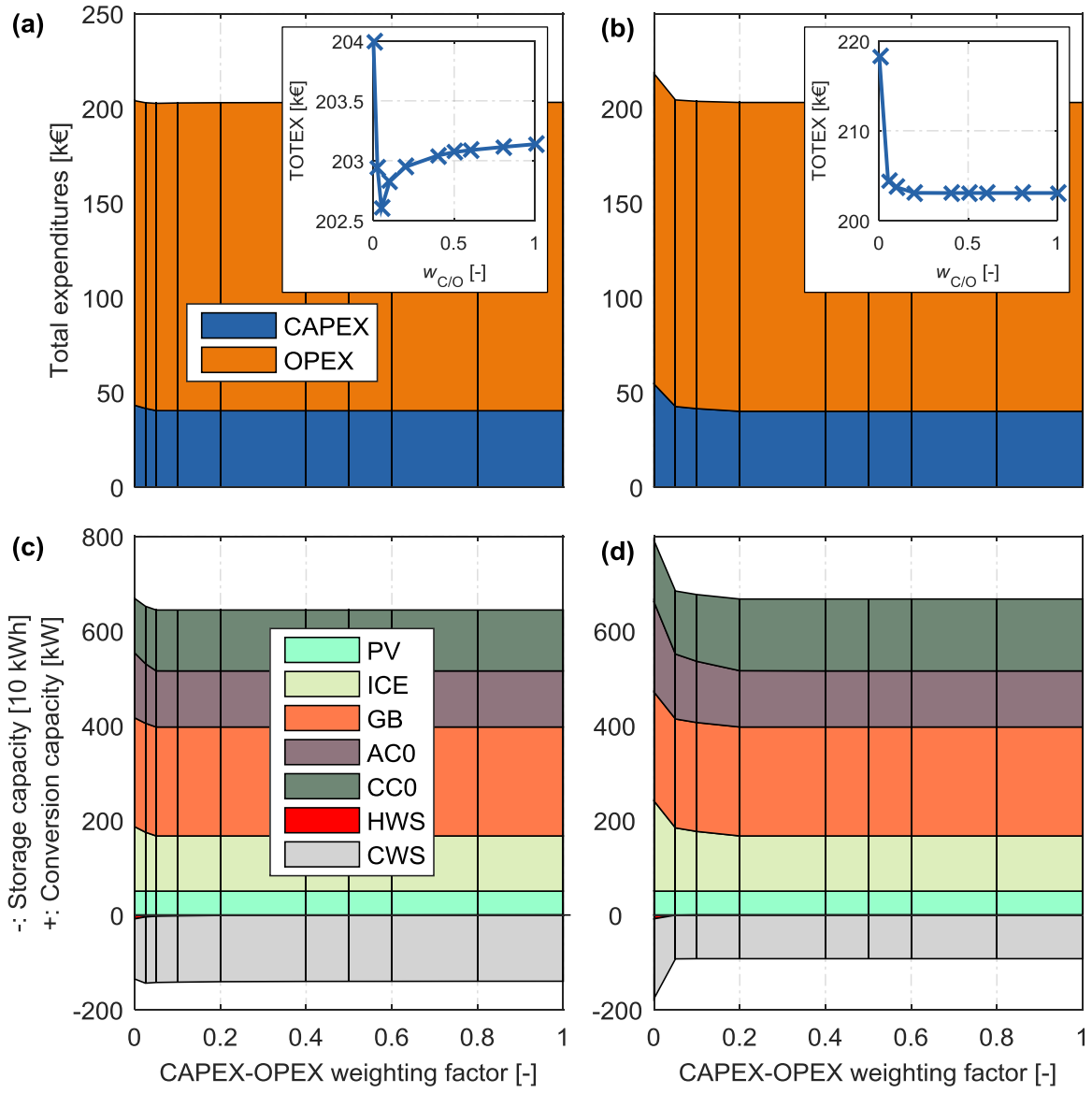

Figure 3.32: Effect of the CAPEX-OPEX weighting factor on the total expenditures and capacities: (a), (c) Strategy DM-Month; (b), (d) Strategy DM-Day.

Figure 3.32 shows the total expenditures and optimal capacities determined for different values of $w_{C/O}$ (indicated by vertical lines) and both strategies (DM-Month and DM-Day) for the reference case (Ref). **Figure 3.32 (a) and (b)** depict that, without the weighting factor (i.e., $w_{C/O} = 0$), technologies were installed that were suboptimal. For strategy DM-Month, a minimum of the total expenditures was found (at $w_{C/O} \approx 0.05$). For

other cases, this minimum was shifted towards larger weighting factors. For this particular case, the TOTEX for DM-Day decreased asymptotically with increasing $w_{C/O}$. An iterative procedure (compare **Layer (1)** in **Figure 3.1**) could identify the best $w_{C/O}$ value.

An indicator for the variability of certain periods compared to other periods was the mean value of a distinct load divided by its maximum value within a certain period. This ratio is, for example, a good indicator for the feasibility of energy storages. The ratio was plotted in **Figure 3.33** for (a) monthly periods (→ DM-Month) and (b) daily periods (→ DM-Day). The two plots clearly indicated that the spread of values in **Figure 3.33 (a)** was much smaller than in **Figure 3.33 (b)**. This means that the variability of periods with monthly time intervals was much smaller than those with daily time intervals. Hence, the optimal weighting factor was smaller ($w_{C/O} = 0.05$ for DM-Month). However, a clear correlation between the spread in **Figure 3.33** and the optimal value of $w_{C/O}$ was not found based only on this example. Furthermore, in the use cases analyzed in the next chapter, other constraints, such as commodity price profiles, influence the factor. Therefore, the following results in this Thesis were computed using a safe but conservative value for the weighting factor ($w_{C/O} = 0.5$).

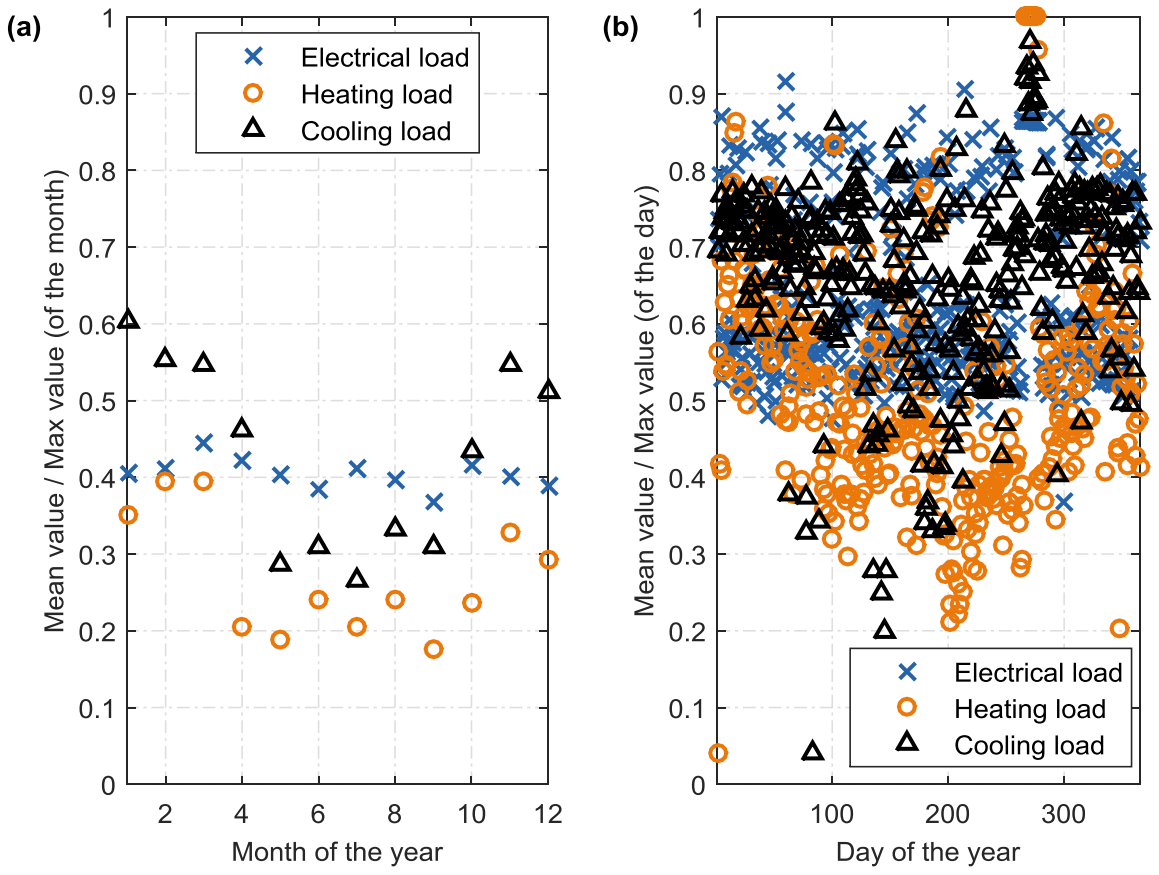

Figure 3.33: Variability of certain periods compared to other periods measured by the ratio of mean and maximum load: (a) Per monthly period, (b) per daily period.

Additionally, the prevalent interest rate (r) influences the optimal design of the energy system. For a wide range of interest rates ($0.01 \leq r \leq 0.25$), the optimal energy system designs for the office building reference case (Ref) were determined and plotted in **Figure**

3.34. For the particular case, the total expenditures increased almost linearly with the interest rate. The optimal capacity of most of the technologies (exception: photovoltaic) were the same for different interest rates, because the capacities were strongly constrained by the inelastic loads. Photovoltaic panels, however, became eventually economically unattractive ($r \geq 0.1$). Furthermore, with increasing interest rates, the capacities of less capital-intense technologies were gradually increasing (e.g., CC0 instead of AC0). The size of the CWS was reduced, too.

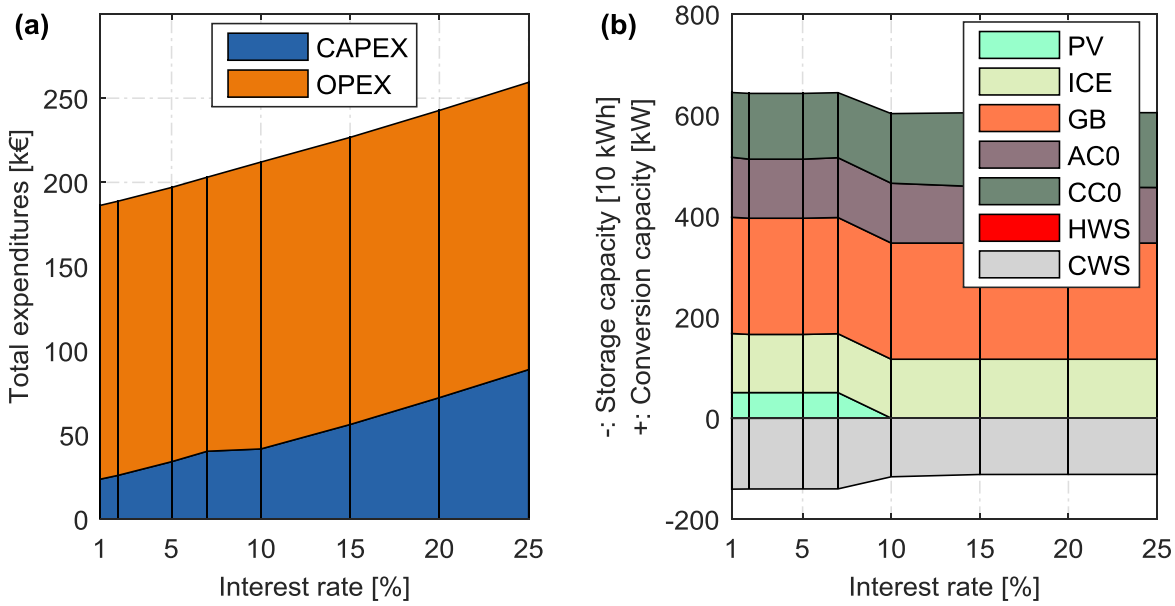

Figure 3.34: Impact of interest rate changes: (a) Total expenditures, (b) Capacities (DM-Month).

To some extent, all results presented in this Thesis depend on the assumed interest rates. The interest rates (or weighted average cost of capital, WACC) depend on the location (e.g., countries) of the sites and creditability of their owners. Unless stated otherwise, an interest rate of 7% was assumed in this Thesis. A sensitivity analysis of the interest rate is shown in **Section 4.2.5**. Results are presented in a similar way as shown in **Figure 3.32** and **Figure 3.34**. Note that vertical lines indicate the discrete scenarios (= sampling points).

3.6.6 Concluding discussion of near-optimality and approximation errors

The previous results showed that the energy system design could be optimized with reasonable effort. The decomposition strategy and its simplifications reduced the computation time and processing power. To put it all in a nutshell, the presented ESD method had two great advantages:

- The decomposition method enabled the optimization of the energy system design and its operation on computer systems that were not top-edge. Furthermore, the computation time could be reduced significantly;
- The ESD method could be automated and applied to many other cases. For complex cases with many free optimization variables (see **Chapter 4**), rule-based

design methods provide non-optimal results. Furthermore, the RUBA strategy could be very difficult to determine and human errors could lead to *wrong* results. The possibility to automate the energy system design and its operation (and to determine optimal solutions using the described methods of artificial intelligence) could be a competitive advantage in the near future (Brynjolfsson & McAfee, 2014; Russell & Norvig, 2012).

However, the ESD method could not identify the exact global optimum. As the sensitivity analysis outlined, on the other hand, in some area around the global optimum, both the design of the system as well as its resulting TOTEX did not change significantly. The ESD method introduced in this Thesis provided near-optimal solutions (strategies DM-Month and DM-Day) that were upper boundaries to the global optimum. The approximation errors inherent in the decomposition method had the following reasons:

- Installation ($\mathbf{I}$) and capacity ($\mathbf{Q}$) variables span over the entire optimization horizon: The introduced CAPEX-OPEX weighting factor improved the result but could not reach the *global* optimum in most cases;
- Energy converters could be turned off at the end of the periods ($p \in PER$) and may need to turn on again in the next period (limited foresight of the method due to the division in subproblems);
- Although the storage operation was described with increasing granularity ($E_{j,k_p,T}, \forall j \in ES, \forall k_p \in TM_p$), the introduction of artificial boundaries between the subproblems resulted in only near-optimal results.

3.7 Further usability: Implementation in a tool with graphical user interface

For enabling other researchers to use the ESD method described in this Thesis, a tool with graphical user interface was developed in MATLAB®. The tool uses object-oriented programming functionality to systematically describe energy converters, energy storages, renewable energy converters and grid connections (as classes). Individual objects can be created from these classes.

The optimal design and energy management of complex multi-modal energy systems was described as four step procedure (see **Figure 3.35**). In a first step, the user of the tool can specify climatic conditions, load profiles and commodity prices. Alternatively, he can generate synthetic load profiles for pre-defined cases and use the comprehensive database look-up for obtaining prices and climatic conditions (compare also **Section 4.1** in the following chapter). The input data is presented graphically by both contour plots and duration curves. In the second step, the user may ignore certain technologies or specify the technologies already installed a priori. Also, model parameters can be customized. Another graphical output helps specifying the parameters. The input parameters are directly checked for consistency. In Step 3, the system is optimized based on the input data defined in the previous steps. The energy system design problem is described directly in MATLAB code. The tool can interact with different open-source and commercial MILP solvers, such as Gurobi (Gurobi Optimization Inc., 2015). Other features include the possibility for sensitivity analysis and automated batch processing of multiple user-defined cases. Finally, in the last step, the technical and

economical results of the system can be analyzed for single as well as multiple cases. Figures can be created in many file formats. Furthermore, the tool also handles the input and output data file management.

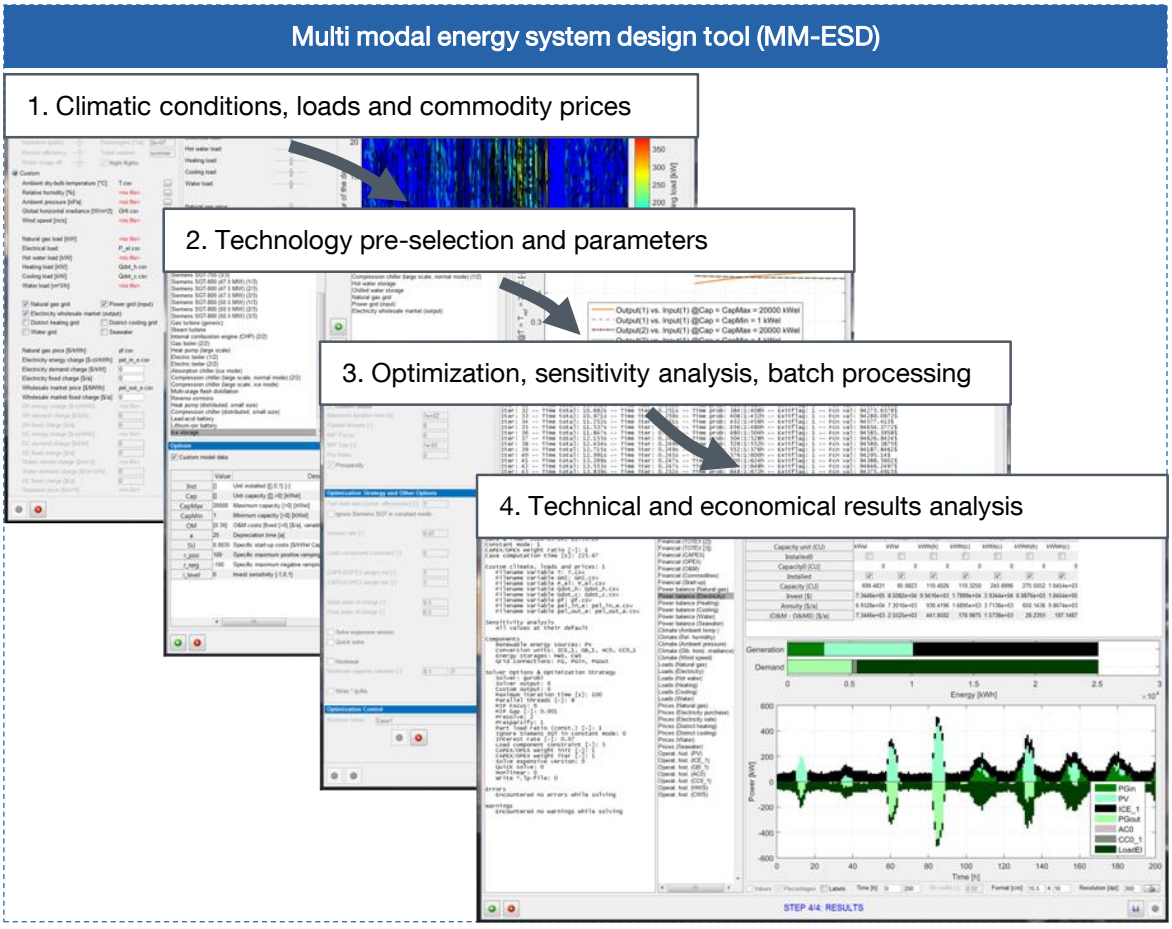

Figure 3.35: Schematic illustration of the multi-modal energy system design tool (MM-ESD) developed in MATLAB® (adapted from Thiem, Danov, et al. (2017)).

4 Use cases: On-site energy systems in cooling-dominated climates

4.1 Description of the use cases

This chapter demonstrates the capabilities of the developed ESD method based on an airport and campus (on-site energy systems) case study. To show the full capability of the method, the study was done for multiple use case locations. The near-optimal designs of the energy systems were investigated, with a particular focus on which energy technologies were installed and with which capacity.

Parts of the airport use case study were previously published in Thiem, Danov, et al. (2017).

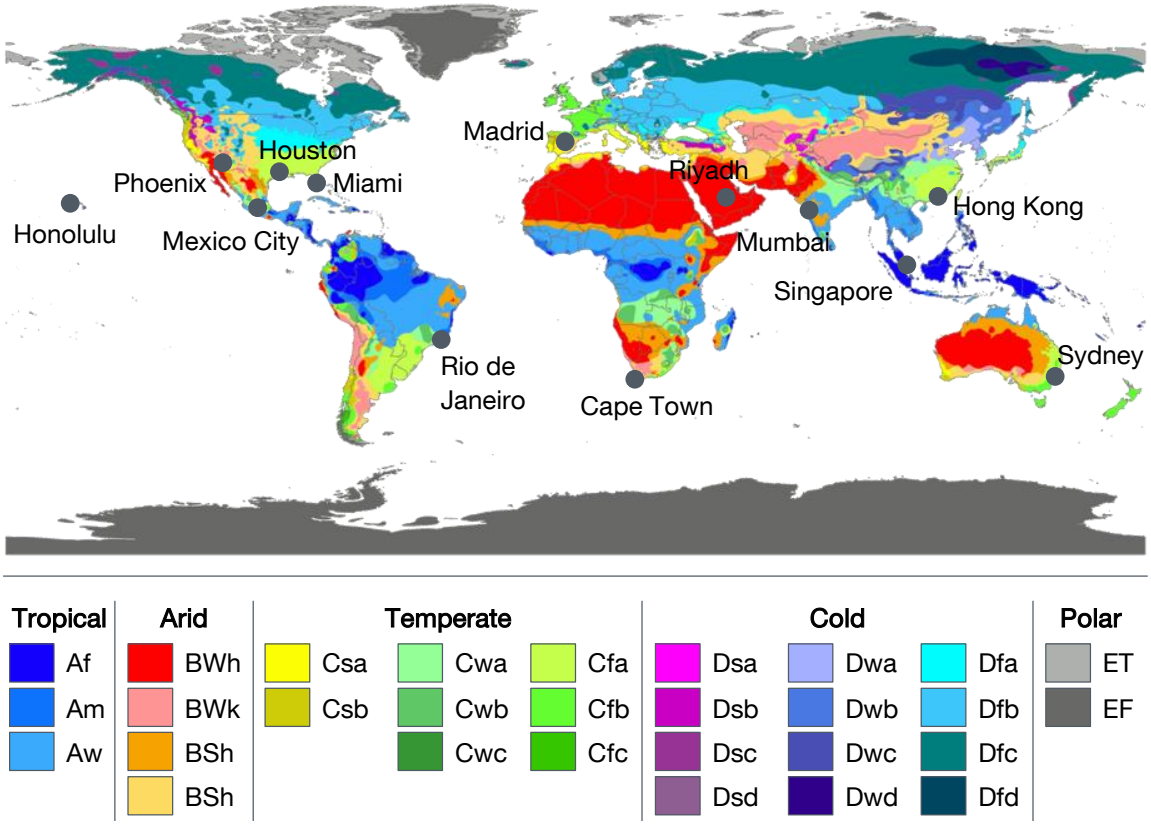

Figure 4.1: The use case locations and their Köppen-Geiger climate classification (modified from Peel, Finlayson, & McMahon (2007)).

4.1.1 Introduction of the use case locations

Different regions in the world do not only experience different climatic conditions, but also have distinct drivers and challenges concerning their energy infrastructure. Whereas the Energy Transition and the required integration of fluctuating renewable energy sources challenges European nations, in North America and Russia the aging infrastructure, in South America non-technical losses, in India distributed generation (i.e., microgrids) and in China and ASEAN countries the electrification of mega cities are main drivers for change of the energy infrastructure (Foosnaes, 2012).

Furthermore, the location, the availability of resources and the national energy policy have an effect on the local commodity prices. Also, prices for energy conversion and storage technologies could be different around the world (International Energy Agency, 2014).

Thirteen locations were chosen to represent different climatic conditions, different challenges and different commodity prices. The selected locations were the metropolitan areas of Cape Town, Hong Kong, Honolulu, Houston, Madrid, Mexico City, Miami, Mumbai, Phoenix, Rio de Janeiro, Riyadh, Singapore and Sydney. The climatic conditions and the prevalent commodity prices are described below.

Climate

The selected cities are located in warm or hot climates that create rather large cooling loads (cooling-dominated climates). The world map in **Figure 4.1** shows these locations and highlights different climates by color-coding according to the Köppen climate classification. The figure shows that the thirteen cities are either located in tropical, arid or temperate climates. The respective climate symbols and their description were tabulated in **Table C.2** in the appendix. See **Table C.1** in the appendix for further information concerning the Köppen climate classification.

The climate of Singapore is a tropical rainforest (very hot and humid). Four other locations (Honolulu, Miami, Mumbai and Rio de Janeiro) have a tropical savannah climate. Hot and dry (arid) climates were investigated for the cities Phoenix and Riyadh. Madrid, on the other hand, has a dry and comparably cold climate. The rest of the cities are located in different temperate climate regions.

Commodity prices

Commodity prices (i.e., specific prices for natural gas, electrical energy, potable water, hot and cold water and carbon dioxide emissions) are essential for analyzing the economics of the site's energy system. In the optimization model, the connection of the site to external grid infrastructure was reduced to a minimum and only the boundary prices (i.e., commodity prices) were considered.

Table D.2 and **Table D.1** (both in the appendix) outline the found (or assumed) commodity prices for all thirteen use case locations and their references, respectively. The assumed exchange rates were listed in **Table E.1** in the appendix. The prices were averaged over a span of up to 10 years, whenever enough data was available (e.g., for natural gas prices at the locations in the United States). Future trends in commodity pricing are very difficult to predict and depend on unforeseeable events such as natural catastrophes and are also subject to speculation. For example, the currently depressed crude oil prices were not foreseen a few years ago. Hence, averaging prices over a span

of years is more reliable than the extrapolation of recent trends (Graham & Dodd, 2008). Whenever available, prices for large industrial consumers were taken. In **Table D.2**, assumptions were indicated with an asterisk (*). These were based on the assumed ratios between different commodity prices shown in **Figure 4.2**.

Table D.2 indicates that the *natural gas prices* differed by an order of magnitude. Gas prices in the Middle East (i.e., Riyadh) were far lower than at other locations, in particular at those far distant from gas fields (e.g., Singapore and Honolulu).

The *electricity prices* were separated into prices for the purchase of electricity from electric utilities and prices for the sale of electricity at the wholesale electricity market. The purchase of electricity is commonly billed per unit of energy (in kWh) and according to the maximum power demand (in kW) each month. The prices for electricity somewhat correlated with the natural gas prices. In addition to energy and demand charges, the site may also be charged a fixed monthly fee (not shown in **Table D.2**). The on- and off-peak prices for time of use tariffs were also indicated in the table. For this study, peak times were assumed from 7 A.M. to 10 A.M. and from 4 P.M. to 9 P.M. (compare, e.g., Florida Power & Light (FPL) (2015)) for *all* use case locations. Wholesale electricity markets were not established at all locations at the time of analyzing the energy system design (e.g., Honolulu). The wholesale market prices fluctuate and depend on many factors (e.g., the season or the hour of the day). Therefore, whenever available, these effects were represented by a time series obtained for a specific historical year.

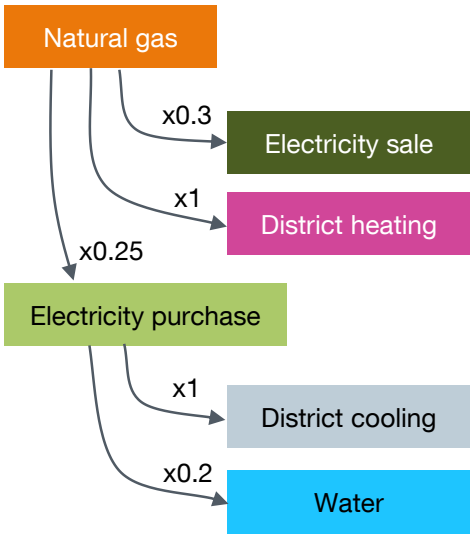

Figure 4.2: Assumed ratios between different commodity prices.[13]

District heating and cooling prices were also listed in **Table D.2**. District heating and cooling grids are *regional* energy systems due to the difficulties (i.e., losses) of transporting hot and cold water over large distances. Not all of the use case locations offer district heating or cooling systems. For example, to the best of the author's knowledge, Rio de Janeiro does not have a district heating or cooling system. This study assumed that the district heating or cooling grid was available at a particular *fictive* site (e.g., an airport), when such a grid was available in the particular city.

The *water prices* indicated in **Table D.2** were computed by adding up both water and wastewater volume charges (compare, e.g., Saving Water Aquarista (2014)). At many locations (e.g., the United States), a larger monthly water consumption was charged at higher rates to encourage water conservation measures (see, e.g., Miami-Dade Water and Sewer Department (2014)). The synthetic load profile generation introduced in

[13] These ratios were assumed, when no published information on commodity prices could be found.

Section 4.1.2 below gave a reasonable order of magnitude for the monthly water consumption based on which water prices were estimated.

Finally, Table D.2 also shows that in 2016 *carbon pricing* was not established at many locations, with the exceptions Cape Town, Hong Kong, Madrid and Mexico City.

A sensitivity analysis was implemented to cope with the uncertainties in the commodity prices compiled from sources with different qualities and to investigate future scenarios of price developments (see Section 4.1.3). The mix of different climatic conditions and prices offered an opportunity for drawing substantive conclusions from the use case results.

4.1.2 Synthetic load profile generation and default sites

Energy system design projects for sites that demand several different forms of energy require profound knowledge of loads to effectively optimize the design. The hot water, heating, cooling and water demand should at least be known in hourly time resolution over the span of an entire year. The electrical energy demand profile should ideally even have a higher time resolution (i.e., minutes or seconds). For the analysis of energy flows, however, and due to the limited availability of minutely data, for this study an hourly resolution of all loads was sufficient. With this assumption, however, dynamic aspects of electric power systems could not be investigated.

Even hourly load profiles were either not available (because it was not measured in this granularity) or confidential (and therefore not published). Thus, a procedure for synthetically generating load profiles (LPG) depending on site-specific parameters (e.g., the ambient temperature) was developed. The LPG model for airport energy systems is exemplarily developed below. For the other two sites, business parks and university campuses, a similar procedure was implemented.

Airports

This study assumed that the energy demand of airports is mainly affected by the following parameters:

- Number of passengers;
- Ambient temperature;
- Building insulation quality;
- Electricity and water usage efficiency;
- Existence of travel seasons;
- Permission of night flights.

The LPG model was designed to output hourly profiles of the electric, hot water, heating, cooling and water demand. The parameters for the airport LPG model were mainly determined based on information published by Cardona et al. in a two-parted paper analyzing the Malpensa airport in Milan, Italy (Köppen climate Cfb) (Cardona, Piacentino, et al., 2006; Cardona, Sannino, et al., 2006).

In a first step, the air-conditioned terminal floor areas were related to their annual number of passengers (see Figure 4.3). Values for both were readily available for many airports around the world. Figure 4.3 shows that airports require a certain minimum floor

area (approximately 10,000 m²) up to approximately 10 million passengers per year. Airport floor areas handling passenger numbers exceeding 10 million per annum could be fitted with a linear fit (note the *semi-log* plot in **Figure 4.3**).

Furthermore, heating degree days (HDD) and cooling degree days (CDD) were defined as follows (ASHRAE, 2013a):

$$HDD = \sum_{i=1}^{N} \max\{T_{\mathrm{h,ref}} - \bar{T}_i, 0\}, \tag{4.1}$$

$$CDD = \sum_{i=1}^{N} \max\{\bar{T}_i - T_{\mathrm{c,ref}}, 0\}. \tag{4.2}$$

The numeric values of the degree days depend on the number of days (N) that are considered (e.g., $N = 365$ for an entire year). Hitchin & Knight (2016) determined daily energy consumption signatures for air-conditioned buildings and showed that the cooling energy demand could be related to the cooling degree days of the respective period. Therefore, the heating energy consumption and the cooling energy consumption were related to their respective degree days. The heating reference temperature ($T_{\mathrm{h,ref}} = 18.3$ °C) and the cooling reference temperature ($T_{\mathrm{c,ref}} = 10$ °C) were chosen to achieve the best fit of thermal energy consumption and degree days (see also ASHRAE (2013a)).

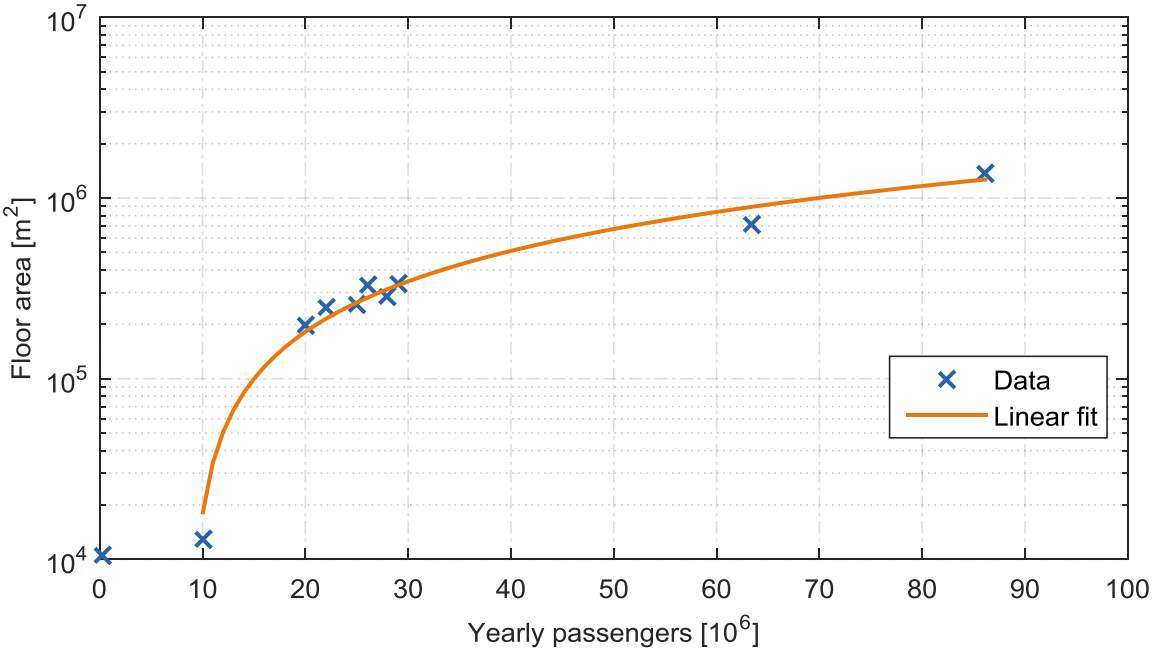

Figure 4.3: Airports' floor areas vs. annual number of passengers (adapted from Thiem, Danov, et al. (2017)).[14]

[14] Data for the following airports was included in this plot: Beijing Capital International Airport (Wikipedia, 2015a), Dibrugarh Airport (Wikipedia, 2015b), Dubai International Airport (Wikipedia, 2015c), Hong Kong International Airport (Airport Authority Hong Kong, 2015a), Kansai International

The specific daily energy consumptions for heating and cooling (per unit floor area and day) were related to the average daily heating and cooling degree days (within a respective month) based on the monthly figures for the Milano-Malpensa airport published in Cardona, Piacentino, et al. (2006) (see **Figure 4.4**). Note that an average building insulation quality for the Malpensa airport was assumed. The specific heating and cooling energy demands, when the terminal buildings are equipped with good or poor insulation qualities, were estimated according to Eicker (2003). The part of the thermal load that was independent of the degree days (at $HDD = 0$ and $CDD = 0$, respectively) was assumed to be also independent of the building insulation quality. Furthermore, it was assumed that the specific heating energy demand at $HDD = 0$ was equal to the hot water demand and the remaining portion of the heating energy demand at $HDD > 0$ was the actual heating load.

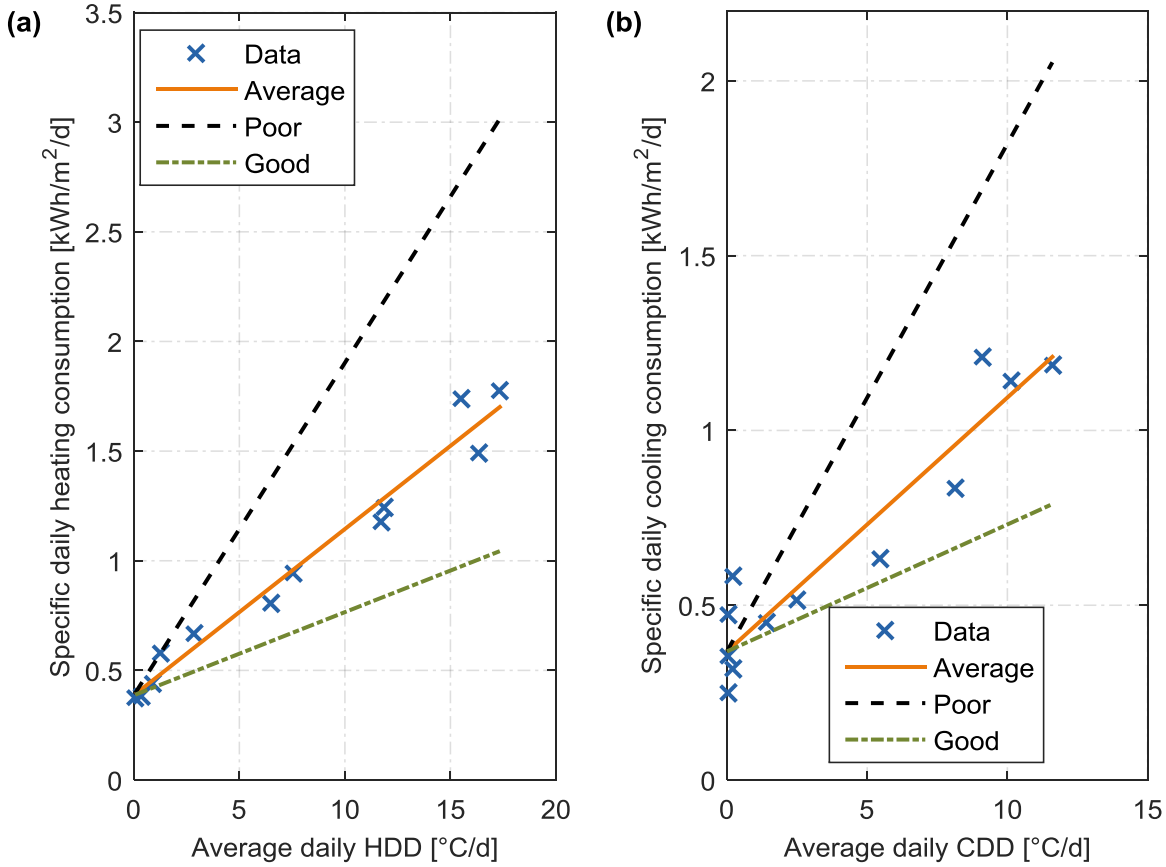

Figure 4.4: Specific daily thermal energy consumption vs. average daily degree days: (a) Heating and hot water, (b) Cooling (with data from Cardona, Piacentino, et al. (2006)) (adapted from Thiem, Danov, et al. (2017)).

Airport (Kansai Airports, 2015), Milan Malpensa Airport, Rome Leonardo da Vinci Fiumicino Airport (Cardona, Piacentino, et al., 2006) and Munich Airport (Flight Hub Reviews, 2015; K + P Architekten und Stadtplaner GmbH, 2015; Munich Airport, 2015).

Cardona, Sannino, et al. (2006) depicted for the Malpensa airport that the electric load did not vary remarkably from day to day. An electric load profile relative to peak load was determined based on the information from this paper. Night flight restrictions were further incorporated into this profile.

Hourly terminal building occupancy profiles were created based on passenger occupancy data that was recorded for the Birmingham Airport with almost 10 million passengers per year (Parker, Cropper, & Shao, 2012). If distinct travel seasons existed for a particular airport, the number of passengers traveling during high travel seasons was approximately twice as much as the number during low seasons (Cardona, Piacentino, et al., 2006; Parker et al., 2012). The recorded passenger occupancy profiles were also adjusted for night flight permissions. The annual water consumption was determined to 15 to 30 L per passenger.[15]

Based on the presented data and fits, electrical and thermal loads could be calculated reversely. The water consumption was directly related to the current occupancy of airport terminal buildings. Both heating and cooling loads were computed based on the fits shown in **Figure 4.4**. Heat gains from the instantaneous passenger occupancy were added to the obtained thermal loads. 40% of the passengers were assumed sitting (100 W), 50% standing at rest or walking slowly (130 W), and 10% walking fast (300 W) (The Engineering Toolbox, 2015). Gaussian-distributed noise (standard deviation corresponding to 5% of the base value) was added to all results. Last but not least, the load profiles were multiplied by a factor so that their annual sums equaled those that were specified before.

Note that this Thesis only considered the airport terminal buildings but did not take the jet fuel demand into consideration. In 2014, the Frankfurt airport in Germany demanded 14.7 million liter jet fuel (kerosene) on average each day for approximately 59.6 million passengers in that year (Fraport AG Frankfurt Airport Services Worldwide, 2015). With the International Air Transportation Association specifications for Jet A Kerosene (min. 42.8 MJ/kg at 775 – 840 kg/m³ density), the average jet fuel demand equals to 5.6 – 6.2 GW, two orders of magnitude more than the energy demand for heating, cooling and electrical equipment of the terminal buildings.

Business parks

The method employed for synthetically generating load profiles for business parks was similar to the one described for airports above. However, different sources of data were used. Two of the DOE commercial reference office buildings (large- and medium-sized) were simulated in EnergyPlus™ for two locations, Miami (Köppen climate Af) and El Paso (BSk) (Deru et al., 2011). The simulation results yielded the required profiles of office building occupancy, as well as the electrical load, the heating and cooling energy demand and the water consumption profiles. By analyzing different combinations of large- and medium-sized office buildings, a correlation between the air-conditioned floor area and the number of employees was derived. With this data, specific thermal energy

[15] The range was determined based on data obtained for the following airports: Copenhagen Airport (Københavns Lufthavne A/S, 2015), Hong Kong International Airport (Airport Authority Hong Kong, 2015b) and Sydney Airport (Sydney Airport, 2009).

demands could be related to their respective degree days (see the airport LPG method for reference). The business park load profiles were then computed based on a similar reverse calculation approach.

University campuses

The floor areas of different universities (with both focus on either teaching or research) were fitted to students and campus staff figures. The hourly occupancy profiles of students and staff on campuses were assumed to be similar to the occupancy figures of business parks. Data from Newcomb, Anderson, & McCormick (2011) was processed for obtaining typical university campus electric load profiles. The specific water consumption range was predicted based on data obtained for three university campuses[16]. The specific heating and cooling loads were related to their respective degree days based on a similar approach as described for the airport LPG model. A university campus located in Hwaseong, Korea (Köppen climate Dwa) was used as the reference (Choi, Lee, Cho, Jeon, & An, 2014).

Concluding remarks

The fit functions and parameters for the three different sites are summarized in Table F.1 in the appendix. The heating and cooling degree days were calculated based on common reference temperatures. However, as indicated in the table, different reference temperatures were used for the three sites. On the one hand, sites exhibit different base loads (degree-days-independent, e.g., for hot water supply), on the other hand thermostat setpoint temperatures might be different. Furthermore, the selected reference temperatures yielded the best fits.

Default sites

A *fictive* default site was constructed for each of the three sites. The assumed parameters were tabulated in Table G.1 in the appendix. This study assumed average building insulation qualities and average electricity and water usage efficiencies. A fictive medium-sized airport with 30 million passengers per year was considered (independent of the actual airport size at each use case location). The default business park could employ 5000 workers. 30,000 students could study at the default university campus, which also could employ 2000 university staff members. The maximum photovoltaic panel (PV) and wind turbine (WT) capacities were constrained due to limited spaces in practice. Figure F.1 in the appendix shows the load profiles determined for a fictive default airport located in Sydney.

4.1.3 Scenarios for sensitivity analysis

A sensitivity analysis was used to cope with the uncertainties of the commodity prices and specific capital costs of energy conversion and storage technologies. Furthermore, the sensitivity analysis enabled the evaluation of future trends and regional differences.

[16] Due to lack of data from universities located in other countries, the three university campuses are all located in the United States: University of California, Berkeley (J. Zhang, 2010), University of California, Santa Cruz (UC Santa Cruz, 2015) and University of Colorado, Boulder (CU Environmental Center, 2006).

The commodity price scenarios were listed in **Error! Reference source not found.** in the appendix. Three groups of scenarios were considered: The *reference* scenario, six *synthetic* scenarios evaluating changes in gas prices, changes in the number of renewable energy converters in the power grid and changes in carbon pricing, as well as four *"real"* scenarios. The table shows the percentage of the assumed price change compared to the reference case. Commodity prices are usually coupled to each other. For example, an increase in the gas price increases the district heating price to some extent (depending on the technology used for generating district heat). The ratios illustrated in **Figure 4.2** were used to estimate unknown prices and to build consistent scenarios.

As illustrated in **Figure 3.8**, different specific capital cost fits for the same technology did not lie exactly on one line but rather spanned an area in the log-log space. Technologies were categorized in groups and their specific capital costs were adjusted concurrently. To evaluate the influences of cost degressions of specific technologies, scenarios based on their minimum capital costs ($i_{\min}$) were defined (see **Error! Reference source not found.** in the appendix and compare also **Figure 3.8**).

4.1.4 Further assumptions

For the energy system design of the introduced use case sites, further assumptions were made:

- Greenfield approach: First of all, this Thesis assumed that the fictive sites were to be constructed entirely from the beginning. Opposed to a Brownfield approach, there were no components of the energy system installed before. The connections to the power and water grid and district heating and cooling grid (if available at a particular location) existed beforehand.
- Superstructure and energy technologies: The superstructure (see **Figure 3.2**) was assumed to include all feasible state-of-the-art technologies (and isiD) that were accurately modeled by the parameters indicated in **Appendix A**. Furthermore, the energy conversion and storage technologies could be arranged in the prescribed way shown in **Figure 3.2**. As outlined before, the energy system was modeled as a one-node system. Therefore, the exact position of technologies at site and the costs for connections between these technologies were neglected.
- Discretization: The optimization horizon of one full year was discretized in hourly time steps, which allowed modeling the system in energy-only terms and achieving adequate computation times. However, the hourly time steps had the disadvantage of introducing *"virtual storages"* (by averaging the actual physics over an entire hour). Especially for the electric side of the system, post-processing will be required before implementation at an actual site. The hourly time step, however, also limited the energy storage use cases (Battke, 2015). Load shifting (e.g., for price arbitrage) and peak shaving (e.g., for reducing the capacities of energy conversion units or for saving demand charges) were the only use cases of energy storages considered in this Thesis. Stability issues of the electric power system were not considered.
- Availability: Additionally, all technologies were considered to be available at 8760 hours throughout the entire year. The optimized scheduling of planned outages is

another optimization problem, which was beyond the scope of this Thesis. Unplanned outages require stochastic optimization techniques and were therefore also not considered. Both planned and unplanned outages, as well as redundancy checks, will be subject of the post-processing. On the upside, each site was connected to an electric grid. The electric grids could always serve as backup electric power supplies. If district heating and cooling grids were available at a particular location, these could also serve as backup heating and cooling power supplies, respectively. Moreover, the thermal inertia of the buildings could help in dealing with short-term outages. Minimum up- and downtimes were not directly modeled. Instead, start-up costs were introduced as outlined in Section 3.4.2.

- Technology capital costs: The compiled technology capital costs (see Appendix B) were taken for all use case locations (independent of the world region, therefore assuming one world market for all energy conversion and storage technologies).
- Commodity prices: The commodity prices were considered to be both deterministic and inelastic. Hence, the sites did not have any influence on the external grids and their prices. This assumption was fairly good because of the limited size and energy demand of the site.
- Load profiles: The synthetic LPG models (see Section 4.1.2 and Appendix F) were used for computing the load profiles for all sites and use case locations using the parameters specified for the fictive default sites (see Appendix G). The fictive default sites along with the scenarios (see Section 4.1.3 and Appendix H) and the Greenfield approach enabled this Thesis to draw substantive *generic* conclusions.
- Salt water and ambient air: Last but not least, both salt water and ambient air were assumed to be available free of charge and in unlimited quantities. Additionally, no constraints for the maximum grid and energy storage capacities were considered.

4.2 Key results of the use case studies

In the following, the key results of the use case studies are depicted and discussed. Figure 4.5 shows an outline of how the results are presented in this Thesis. First, the optimal technologies and capacities for the three sites (i.e., airports, business parks and universities) and the thirteen locations are investigated (Section 4.2.1). The airport case is then elaborated in more detail. With respect to the objectives from Section 1.2, the influence of the prevalent price structure on the optimal generation shares (i.e., generation of electricity, heating and cooling) is analyzed (Section 4.2.2). Comments regarding the economic dispatch of the energy system and the significance of capacity changes are summarized in Section 4.2.3. Furthermore, the design of the energy system (Section 4.2.4) and its sensitivity (Section 4.2.5) are analyzed. The economics of optimized on-site generation are benchmarked against conventional airport energy systems in Section 4.2.6. Finally, the ice-storage-integrated desalination technology and turbine inlet air cooling are investigated (Section 4.2.7).

The different aspects were analyzed for *different locations*, because some effects were more visible (or feasible in the first place) at particular locations.

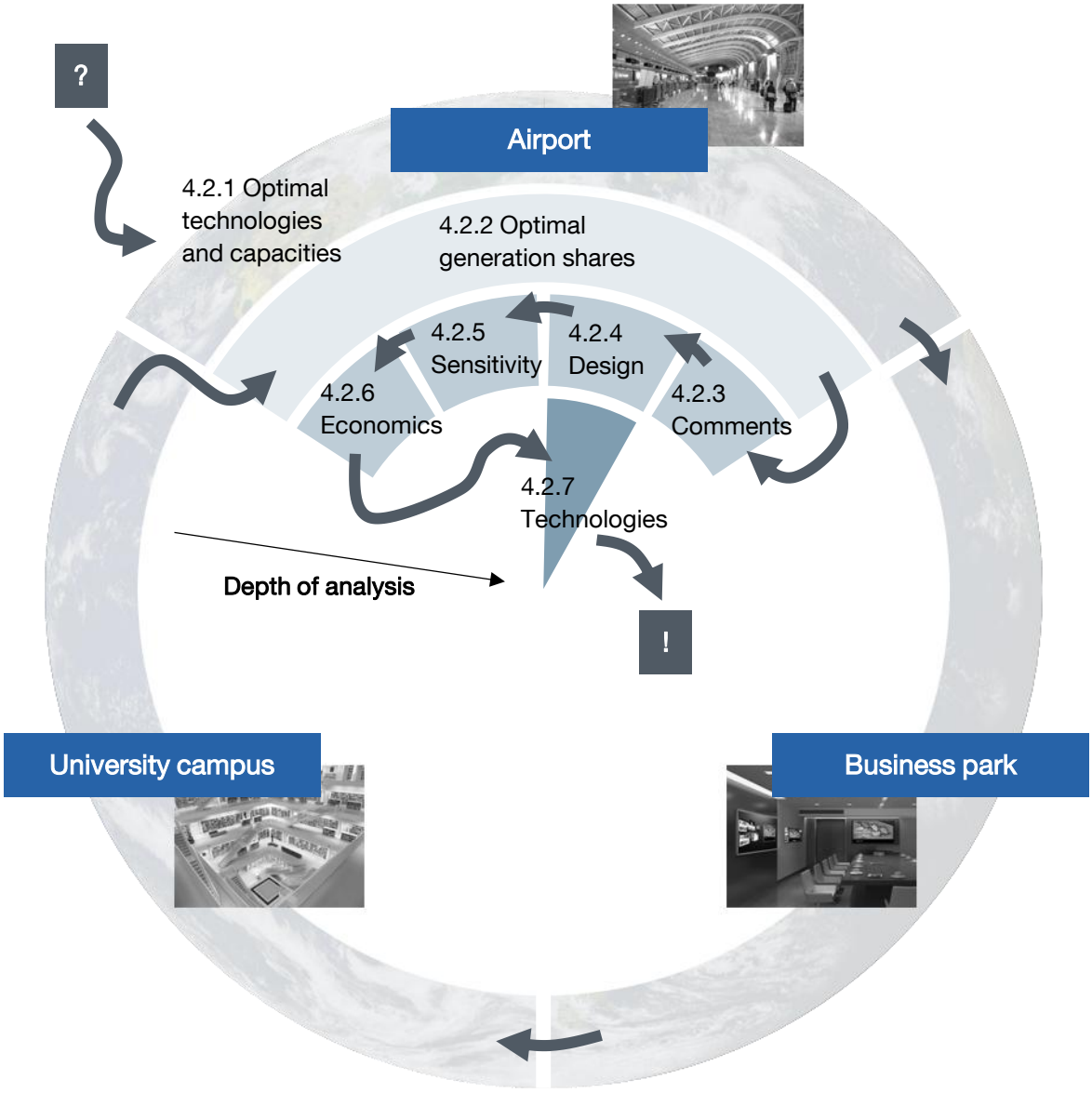

Figure 4.5: Outline of the key results.

4.2.1 What are the optimal technologies and capacities at the three sites?

The optimal technologies and their capacities for the airport energy systems are illustrated in **Figure 4.6**.

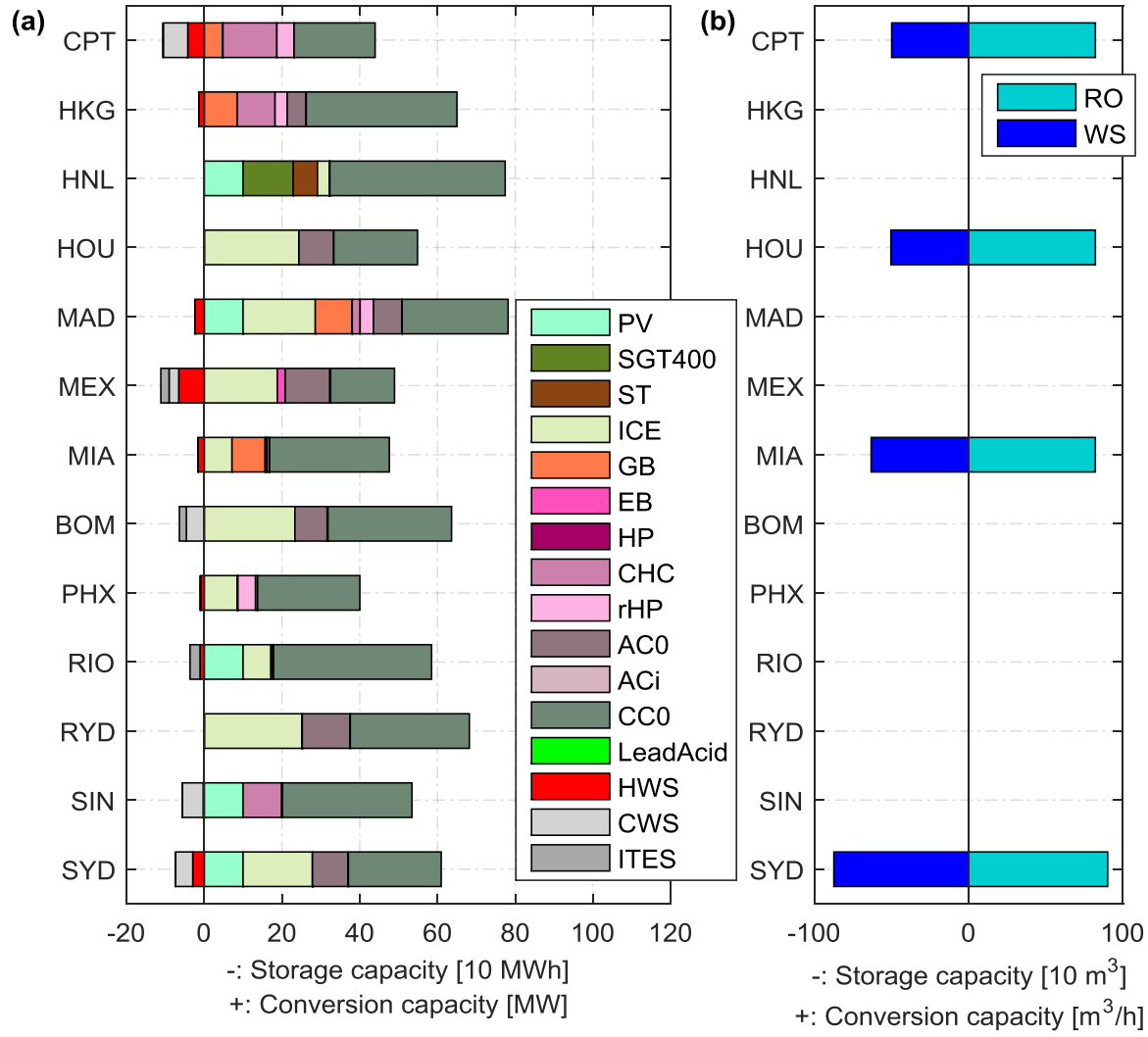

Figure 4.6: Optimal technologies and their capacities for the airport energy systems (adapted from Thiem, Danov, et al. (2017)).

From **Figure 4.6**, the following conclusions could be drawn:

- Power generation from photovoltaic was feasible at five use case locations (HNL, MAD, RIO, SIN and SYD): The LCOE for power generation from PV was lower than the rather high electricity price at these locations;
- Internal combustion engine (ICE) CHP plants were installed at a number of locations showing that the combined generation of power and heating on site was more efficient than drawing electricity from the power grid and individually generating heat;
- CHP based on gas turbine prime movers were only feasible at one location (HNL), here in combination with a steam turbine: According to the data, the models predicted the electrical efficiency of the internal combustion engine higher than the efficiency of a simple cycle gas turbine at similar capital costs (at this load range, < 20 MW_{el}). The SGT-400 with 12.9 MW_{el} was selected (**Figure 3.1: 1.2**) based on the optimal capacity (9.2 MW_{el}) determined in the step before (**Figure**

3.1: 1.1). Note that the SGT-300 only offers 7.9 MW_{el} nominal power output. The turbine inlet air cooling method ISO (compare Section 3.5.3) augmented the power output from the gas turbine.

- Both gas- and electricity-driven heating technologies were installed for the remaining heating demands. Conventional centralized heat pumps were inferior to distributed reversible heat pumps and CHCs;
- Substantive capacities of reversible heat pumps were installed in CPT (Köppen climate Csb), HKG (Cwa), MAD (BSk) and PHX (BWh): In particular in MAD and PHX, summer and winter temperature levels differ significantly. Therefore, reversible heat pumps offer an attractive opportunity to supply heating in winter and cooling in summer using the same devices;
- The combined heating and cooling (CHC) technology (essentially a heat pump that supplies both heating and cooling simultaneously) was found to be an economically attractive option at four locations (CPT, HKG, MAD and SIN);
- The CHP plants were often coupled with absorption chillers for enabling trigeneration (generation of power, heating and cooling);
- Compression chillers were economically attractive at all use case locations: Absorption chillers were only attractive in combination with waste heat from combined heat and power plants; hence, their capacity was limited and compression chillers supplied the rest of the cooling load;
- Thermal energy storages were much more attractive than electrochemical energy storages under the assumptions (e.g., considering 1 h time steps): In particular hot and chilled water storages should be installed at a number of locations. Ice storages were only installed in combination with ammonia-water absorption chillers (ACi) but not in combination with compression chillers (CCi). According to the technologies capital cost survey, ice storages were found to have lower capital costs than chilled water storages (per kWh) at the sizes required for these sites (see Appendix B), however, efficiencies of the chillers are lower at evaporation temperatures suitable for charging ice storages (< 0 °C);
- Reverse osmosis desalination plants coupled with water storages were installed at four locations (CPT, HOU, MIA and SYD): As explained below, the price for the water supply from the grid was higher than the levelized costs of water generation on site. The sufficient availability of salt water at the particular airport location must be checked in the post-processing.

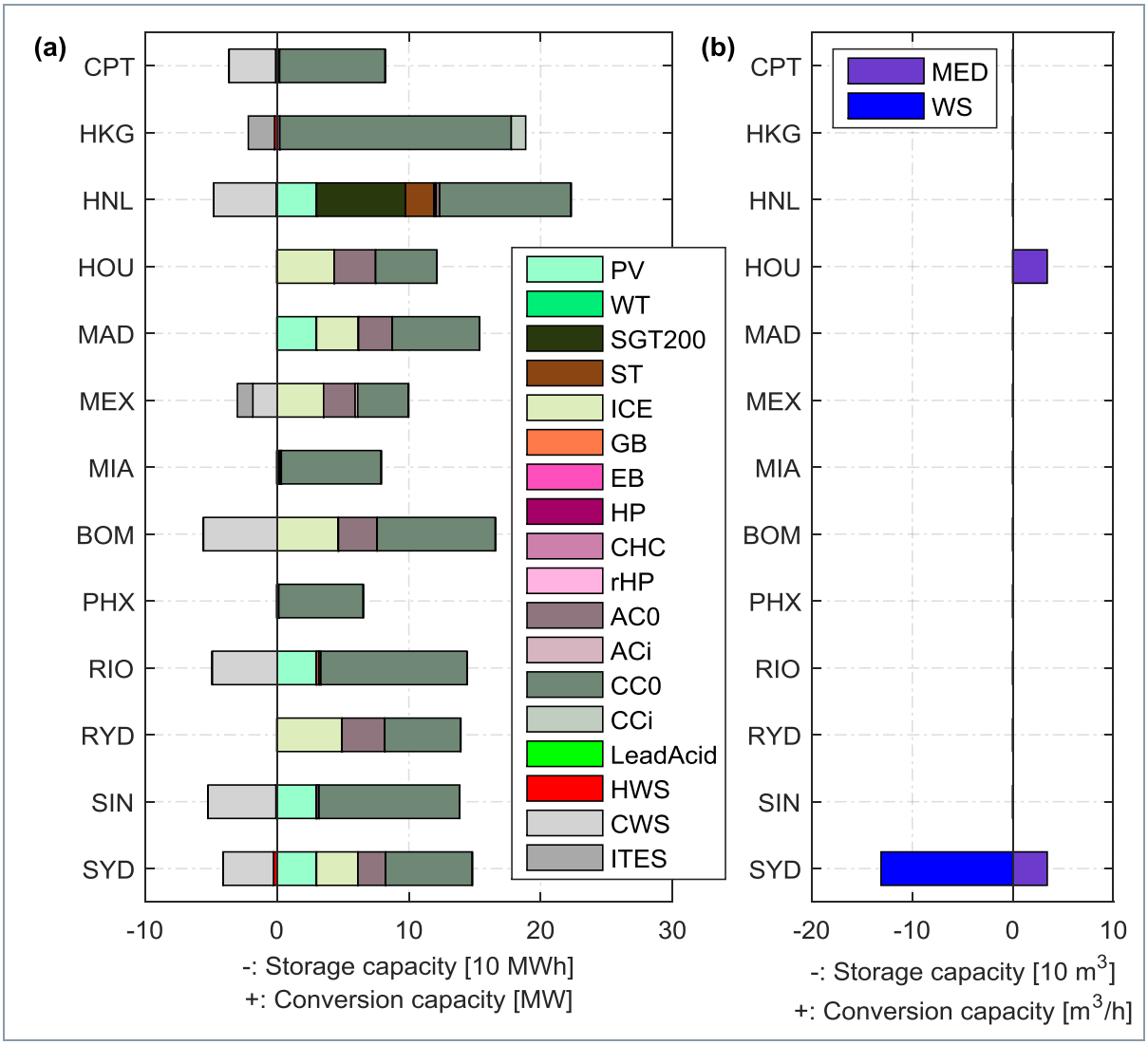

Figure 4.7: Optimal technologies and their capacities for the business park energy systems.

The results for the other two sites, university campuses and business parks (compare **Figure 4.7** and **Figure 4.8**, respectively), show that the on-site generation capacity was reduced at smaller sites with smaller peak loads (e.g., the number of business parks with CHP plants was lower than for the airports). The efficiencies of internal combustion engines and gas turbines at smaller capacities are also smaller. Therefore, at smaller capacities they were not able to compete with grid prices anymore. Other desalination technologies (e.g., MED) could also be economically attractive (see the business park results). The water storage capacity at the university campuses may not be feasible. Further constraints ($Q_{\max} \ll \infty\ \mathrm{kWh}$) should be implemented.

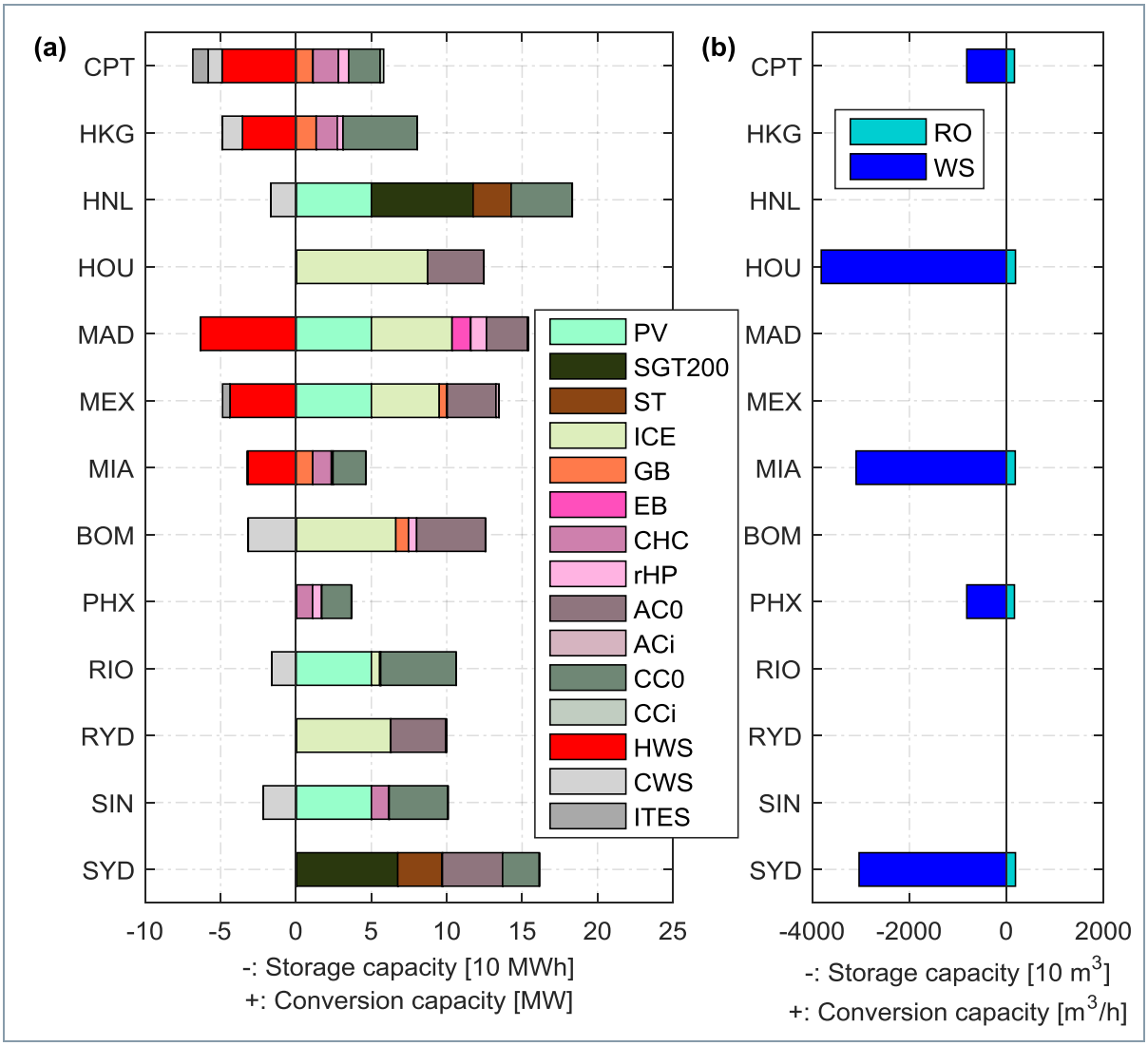

Figure 4.8: Optimal technologies and their capacities for the university campus energy systems.

4.2.2 Can we identify trends between the optimal generation shares of an airport energy system and its prevalent price structure?

Trends between the optimal generation shares of airport energy systems and their underlying commodity prices could help in identifying the optimal generation mix without the need for mathematically optimizing the design of the energy system. This could be used on the one hand for preliminary studies and on the other hand for improving the computation time of the ESD method.

Figure 4.9 (a) depicts the *annual* electricity generation mix for different electricity prices. Note that each vertical line represents the electricity price at one particular location (hence, there are thirteen lines). Other factors, such as different climatic conditions or other prices at the particular locations also influenced the results. However, the plots in **Figure 4.9** may yield certain trends that are valid even though other constraints totally differ.

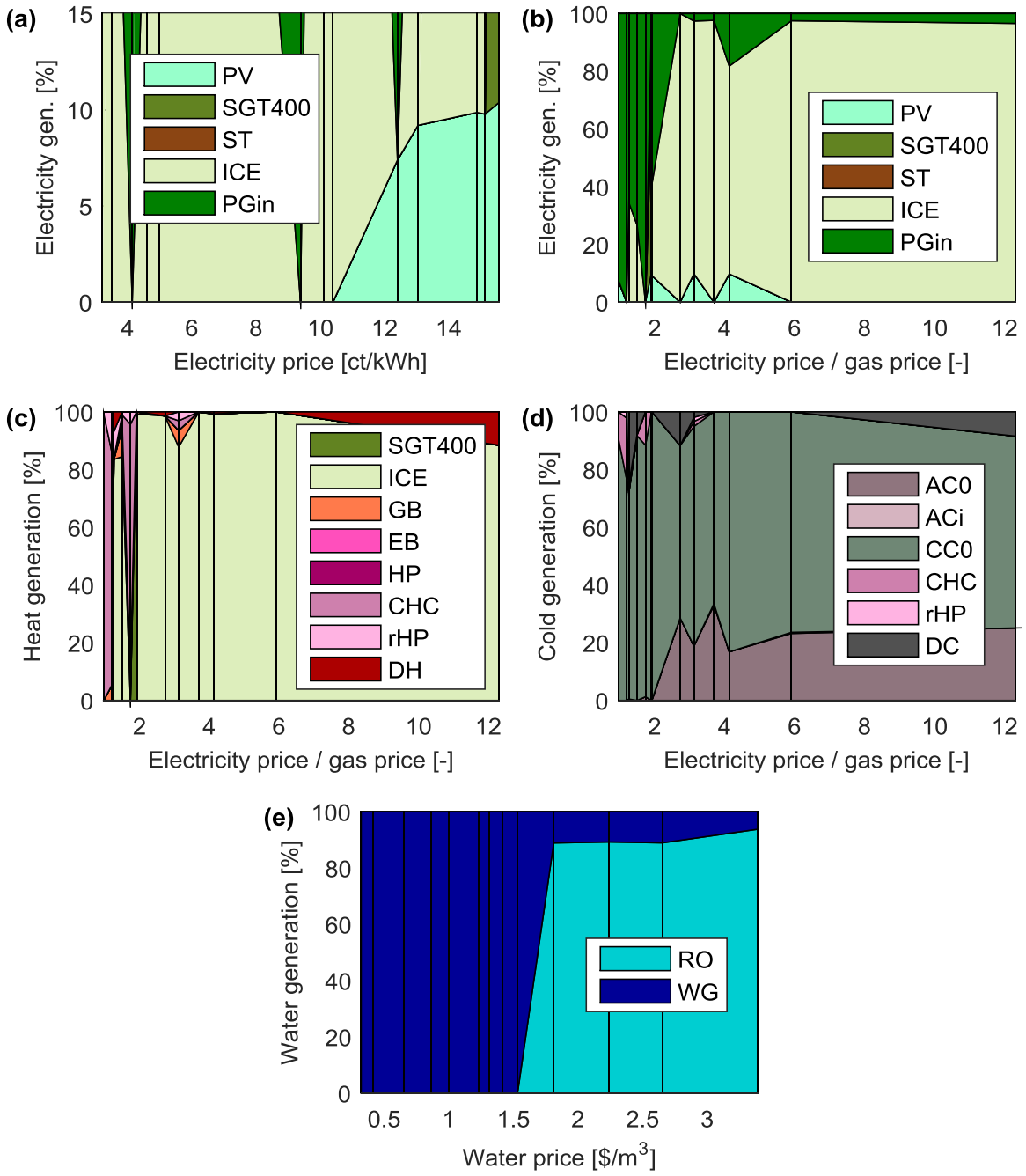

Figure 4.9: Annual optimal generation shares for all thirteen locations (black vertical lines) and different ratios of the annual mean electricity, natural gas and water price (adapted from Thiem, Danov, et al. (2017)).

At electricity prices greater than 10 – 12 ct/kWh, power generation from PV became economically feasible (see **Figure 4.9 (a)**). As **Figure 4.6** showed, the PV capacity was limited to 10 MW due to the assumed limited availability of free space at the airport site. The boundary electricity price for PV to be feasible (10 – 12 ct/kWh) seemed relatively high and was therefore elaborated in more detail. **Figure 4.9 (a)** was derived from the distinct results for airports located in thirteen cities. The three locations, HKG (9.38

ct/kWh electricity price), MEX (10.1 ct/kWh) and BOM (10.39 ct/kWh), are of particular importance (compare also **Table D.2** in the appendix). At all of these three locations, no photovoltaic modules were installed. At the latter two, MEX and BOM, large-size CHP plants supply both electricity and heat. For the same reason as explained in **Section 3.6.3** (i.e., lower efficiencies of the CHP plant at lower part-load ratios), PV was economically unattractive. In HKG, however, no CHP plant was installed. Despite HKG's hot climate (mean annual temperature of 24 °C, see **Table C.2** in the appendix), its global horizontal irradiance is relatively low ($\bar{P}_{\mathrm{PV,HKG}} \approx 148\ \mathrm{W/m^2}$ or $\bar{E}_{\mathrm{PV,HKG}} \approx 1300\ \mathrm{kWh/m^2/a}$ (Meteotest, 2014), see also **Figure 4.10**). With the assumed specific capital costs and operation and maintenance costs for the entire PV system including the inverter ($i_{2,\mathrm{PV}} \approx 1300\ \$/\mathrm{kW\,peak}$ and $o_{2,\mathrm{PV}} \approx 18\ \$/\mathrm{kW\,peak/a}$, see **Table A.1** and **Figure B.5** in the appendix), rated/peak power output at global horizontal irradiance ($GHI_{\mathrm{ref}} = 1000\ \mathrm{W/m^2}$, see **Table A.1** in the appendix) and the annuity factor ($a_{\mathrm{PV}} \approx 0.085$, see **Equation (3.34)**), the levelized costs of electricity from PV in HKG ($LCOE_{\mathrm{PV,HKG}}$) can be derived to

$$LCOE_{\mathrm{PV,HKG}} = \frac{\left(a_{\mathrm{PV}} \cdot i_{2,\mathrm{PV}} + o_{2,\mathrm{PV}}\right) \cdot Q_{\mathrm{PV}}}{\left(\bar{P}_{\mathrm{PV,HKG}}/GHI_{\mathrm{ref}}\right) \cdot Q_{\mathrm{PV}} \cdot 8760\ \mathrm{h}} \approx 9.9\ \frac{\mathrm{ct}}{\mathrm{kWh}} \tag{4.3}$$

Hence, under the assumptions, power generation from PV in HKG is economically unattractive, even at relatively high electricity prices. As **Figure 4.17** in **Section 4.2.5** will show, at other locations, photovoltaic can be economically attractive at lower electricity prices.

Figure 4.9 (a) also shows that gas turbines (SGT-400 in combined cycle) in this load range were only feasible at very high electricity prices (airport located in HNL).

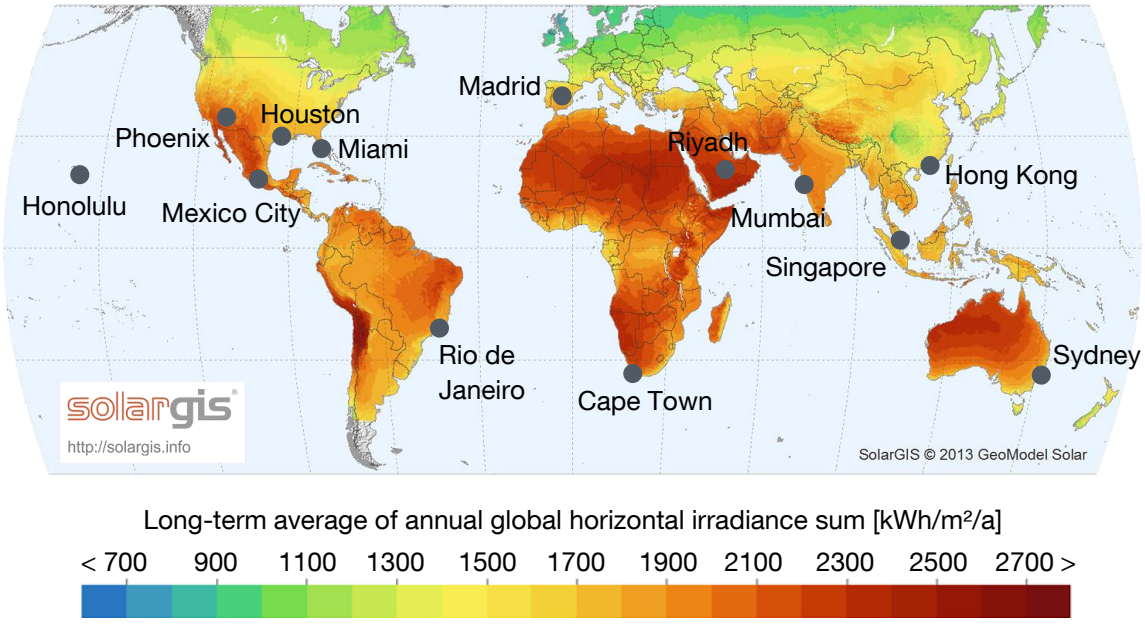

Figure 4.10: Long-term average of annual global horizontal irradiance sum (SolarGIS © 2013 GeoModel Solar).

The annual electricity generation mix was plotted as function of the ratio of the mean electricity price and the gas price in **Figure 4.9 (b)**. The plot shows that internal

combustion engine CHPs were the dominant technology, when the electricity price became greater than two times the gas price. However, the ICEs were not sized to meet 100% of the power demand.

Accordingly, most of the heating energy was supplied by ICEs (see **Figure 4.9 (c)**). At low electricity prices or high gas prices, electricity-driven heaters (mostly heat pumps) were economically more attractive. When the electricity price (at some instances in time) decouples from the gas price by large integration of renewable energy sources, electric heating technologies become more attractive.

Figure 4.9 (d) shows that compression chillers stay the dominant cooling technology, even at higher electricity prices, due to the limited availability of low-cost (waste) heat for absorption chillers. Both district heating and district cooling were used, when prices were competitive, and in particular for peak demands. Interestingly, district cooling tariffs in HKG and SIN were charged both per energy and peak power demand (compare **Table D.2** in the appendix).

Finally, **Figure 4.9 (e)** illustrates that seawater desalination using reverse osmosis plants were interesting for water prices exceeding approximately 2 $/m³.

4.2.3 Some introductory comments regarding the economic dispatch and the significance of capacity changes

The economic dispatch of the Madrid airport energy system was plotted for the months July and December in **Figure 4.11**. **Figure 4.11 (a)** and **Figure 4.11 (b)** show that the electric energy base load could be supplied by the ICE CHP unit. The higher PV power generation in July correlated with the peak power demands and, for example, could be directly used by the compression chillers for cooling (see **Figure 4.11 (e)**). When the hot water and heating load in July was not large enough, “waste” heat from the ICE CHP unit could be used with the absorption chiller for cooling purposes (**Figure 4.11 (c)**). Finally, **Figure 4.11 (d)** and **Figure 4.11 (e)** show that the reversible heat pump could be used for supplying peak heating and cooling loads in winter and summer, respectively.

The energy systems that were investigated for this Thesis were assumed to be Greenfield projects for sites that were to be constructed in the future. Therefore, load profiles could not be known deterministically a priori. The Gaussian distributed noise in the synthetic load profile generation model (see **Section 4.1.2**) was used to create three *similar* cases (C1 to C3) for one site and one location (here, the airport in Madrid).

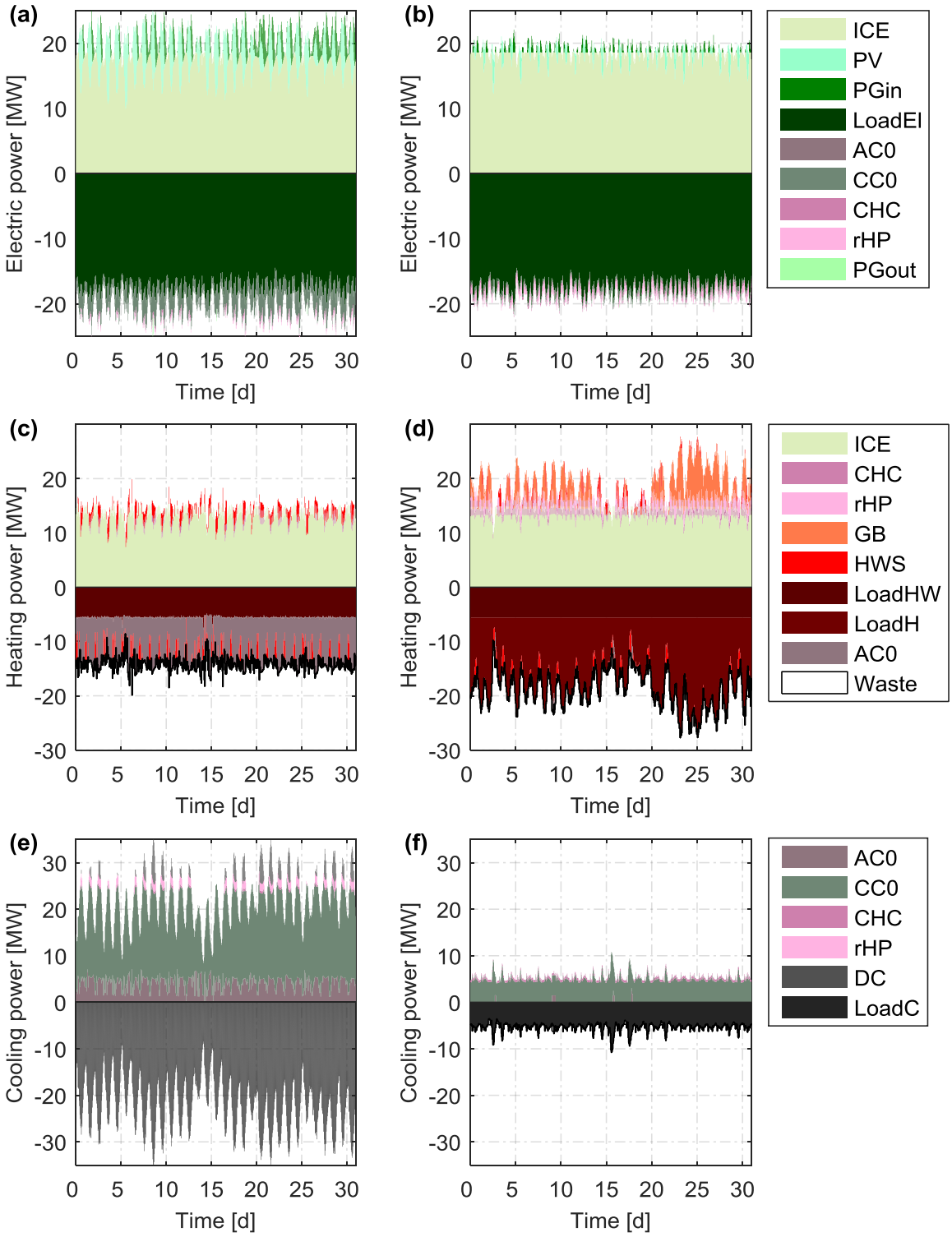

Figure 4.11: Optimal operation of the Madrid airport energy system: Electrical power, heating and cooling power for (a), (c), (e) July; (b), (d), (e) December, respectively.

Figure 4.12 shows the TOTEX and optimal capacities for the three cases. Whereas the TOTEX were approximately the same for all of the three cases, the optimal capacities slightly differed. This further highlighted that in some area around the optimum set of

technologies and their capacities, similar total costs could be achieved (compare also **Section 3.6.4**). Therefore, these slight changes of the capacities could be denoted as *insignificant*. Furthermore, **Figure 4.12** shows that the ESD results were robust, despite the different load profiles (with noise).

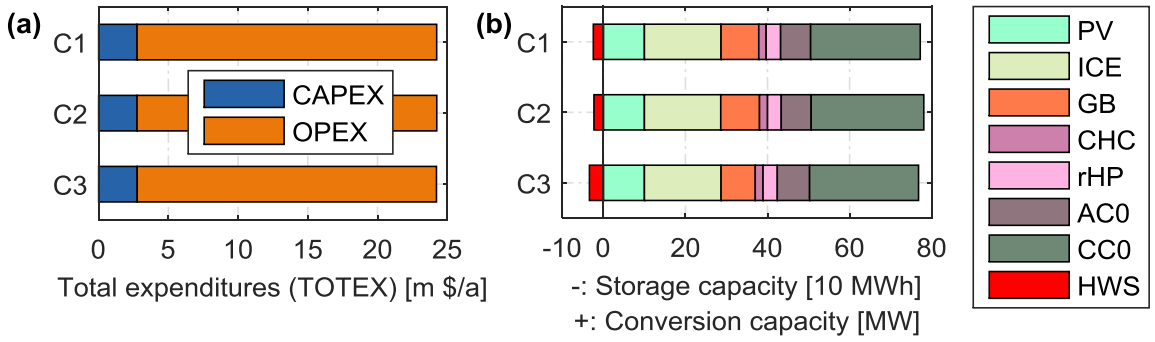

Figure 4.12: The airport in Madrid: (a) Total expenditures and (b) Optimal capacities for three similar cases (C1, C2 and C3).[17]

4.2.4 Final design of the system: Is there one optimal solution for the whole world and how could future trends influence the design?

As **Figure 4.6** already revealed, there was no single optimal energy system applicable for all locations (opposed to a "world car" (Kiley, 2009)). Each energy system differs substantively from the other. Boundary conditions, such as climatic conditions, commodity prices, availability of grids, and many others can be completely different and require an individual analysis for each case. However, as **Section 4.2.1** showed, certain technologies were found to be superior compared to other technologies (e.g., compression chillers and internal combustion engine CHPs). Considering these technologies as modules, ESD could help in combining the right modules for each case.

Figure 4.13 and **Figure 4.14** show two examples of optimal substructures for the two locations Riyadh and Singapore, respectively. The lines indicate relative annual energy flows (normalized for each energy form).[18] The bars on the right side of each input grid, energy converter and storage illustrate the relative capacity share.[19]

---

[17] Gaussian-distributed noise with a standard deviation corresponding to 5% of the base values (see **Section 4.1.2**).

[18] For example, in **Figure 4.13** the annual energy flow of natural gas is greater than the annual energy flow of electricity (both in terms of kWh). Accordingly, the natural gas arrow is thicker than the electricity arrows.

[19] The capacity share was indicated for the following groups: Generating electricity, natural gas, heat, cold, water and storing energy. For example, **Figure 4.13** shows that the absorption chiller (AC) cooling capacity was smaller than the compression chiller (CC) cooling capacity.

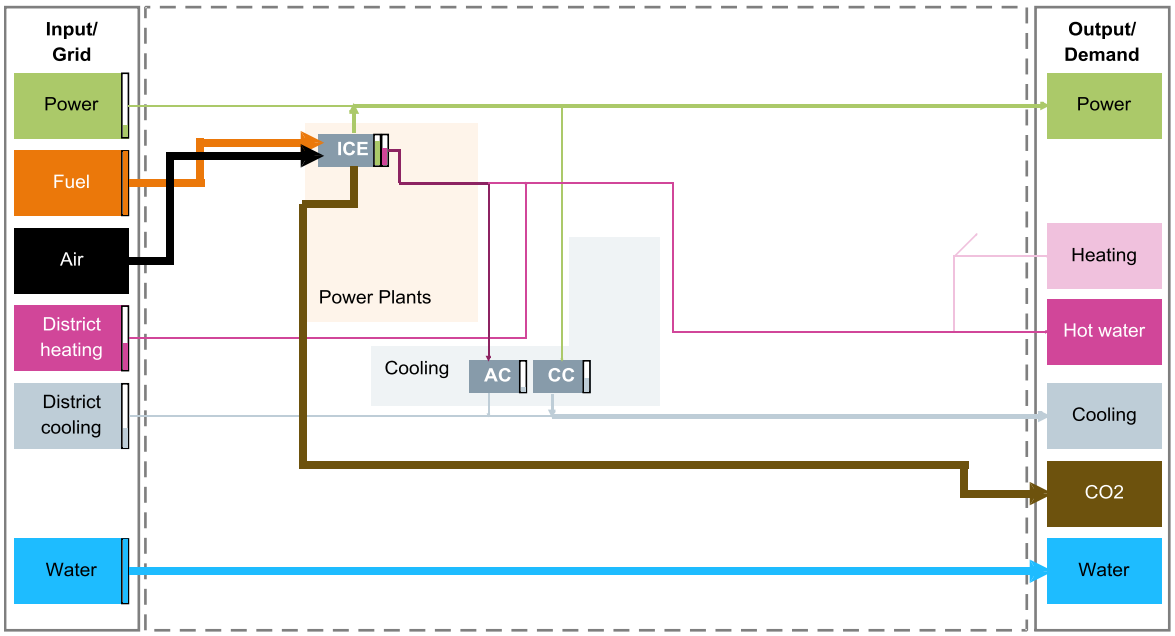

Figure 4.13: Optimal substructure of the Riyadh airport energy system (adapted from Thiem, Danov, et al. (2017)).

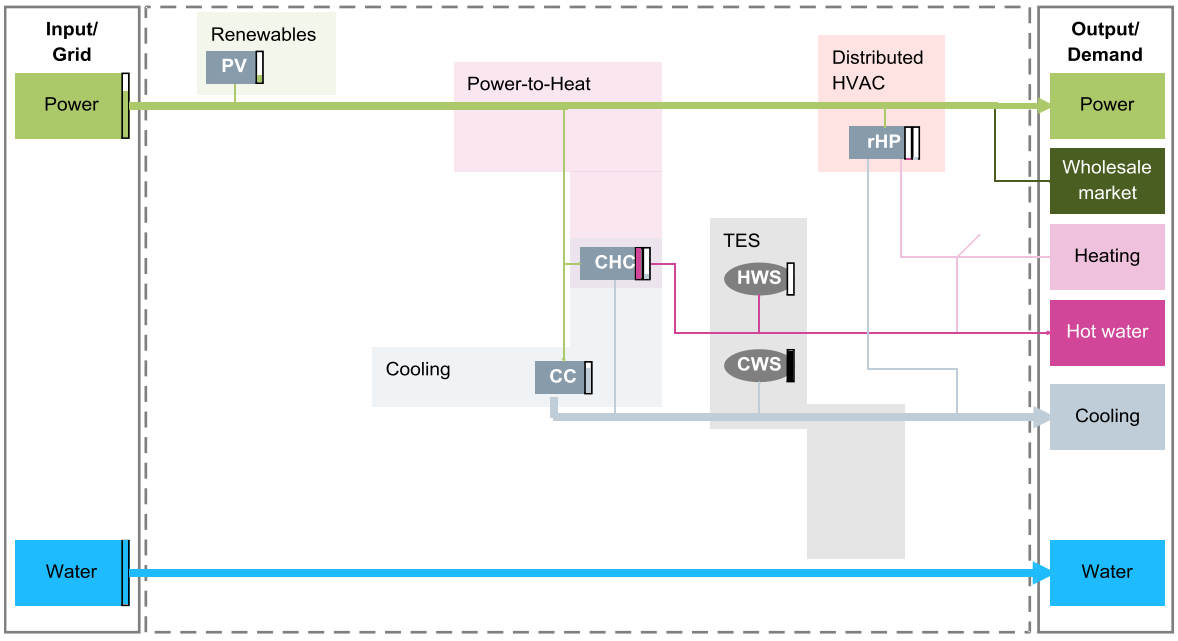

Figure 4.14: Optimal substructure of the Singapore airport energy system (adapted from Thiem, Danov, et al. (2017)).

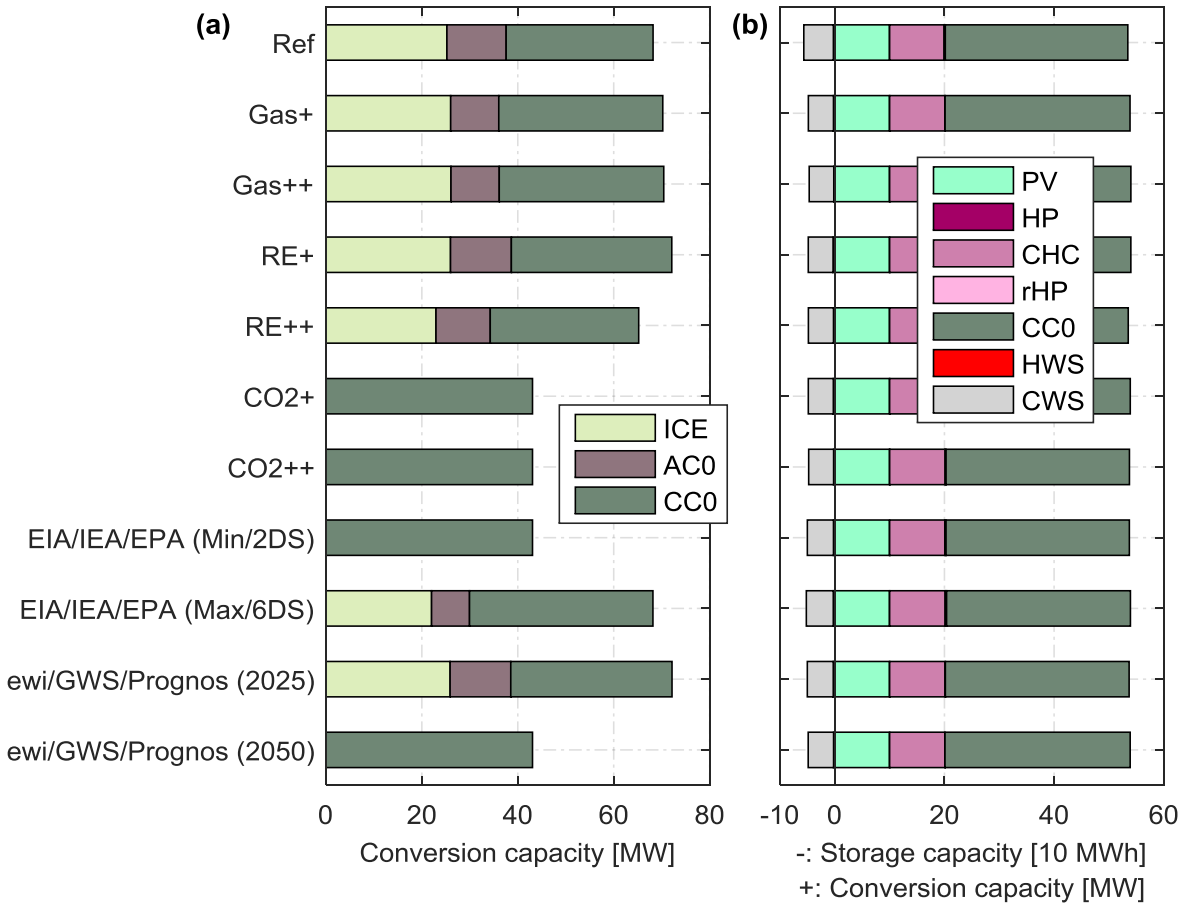

Figure 4.15: Scenario analysis for the (a) Riyadh and (b) Singapore airport energy system (Technology capital costs reference case, iRef).[20]

For the two locations RYD and SIN, the scenarios introduced in **Section 4.1.3** were used to analyze the effect of potential future trends (particularly of commodity prices) on the design of the energy system. **Figure 4.15** shows the optimal technologies and their capacities for the eleven cases (Ref - ewi/GWS/Prognos (2050)) all evaluated for the *technology capital cost reference case* (iRef). Part (b) of the figure clearly shows that the energy system in Singapore was robust to changes. Both electricity and gas were

[20] The following scenarios were plotted in **Figure 4.15** (see **Section 4.1.3** and **Appendix H** for further details): Ref: Reference scenario; Gas+: Gas price increased by 50% compared to Ref; Gas++: Gas price increased by 100% compared to Ref; RE+: Increased share of renewables in the power grid; RE++: Even further increased share of renewables; CO2+: Carbon emission price set to 50 $ per ton CO_2; CO2++: 100 $/t CO_2; EIA/IEA/EPA (Min/2DS and Max/6DS) are scenarios based on predictions for the United States made by the Energy Information Administration (EIA), the International Energy Agency (IEA) and the Environmental Protection Agency (EPA) for two cases (2 degree scenario and 6 degree scenario). Accordingly, ewi/GWS/Prognos (2025 and 2050) are based on predictions for Germany that were made by the Energiewirtschaftliches Institut at the University of Cologne, the Gesellschaft für Wirtschaftliche Strukturforschung (GWS) and the Prognos AG for the years 2025 and 2050.

already expensive in the reference case (Ref). According to the scenario setup, internal combustion engine CHPs could become infeasible in Riyadh, if CO_2 emission prices were increased substantially (see **Figure 4.15 (a)**). However, the CO2+ and CO2++ scenarios did not consider that the electricity prices most likely will also change, when the CO_2 emission prices alter.

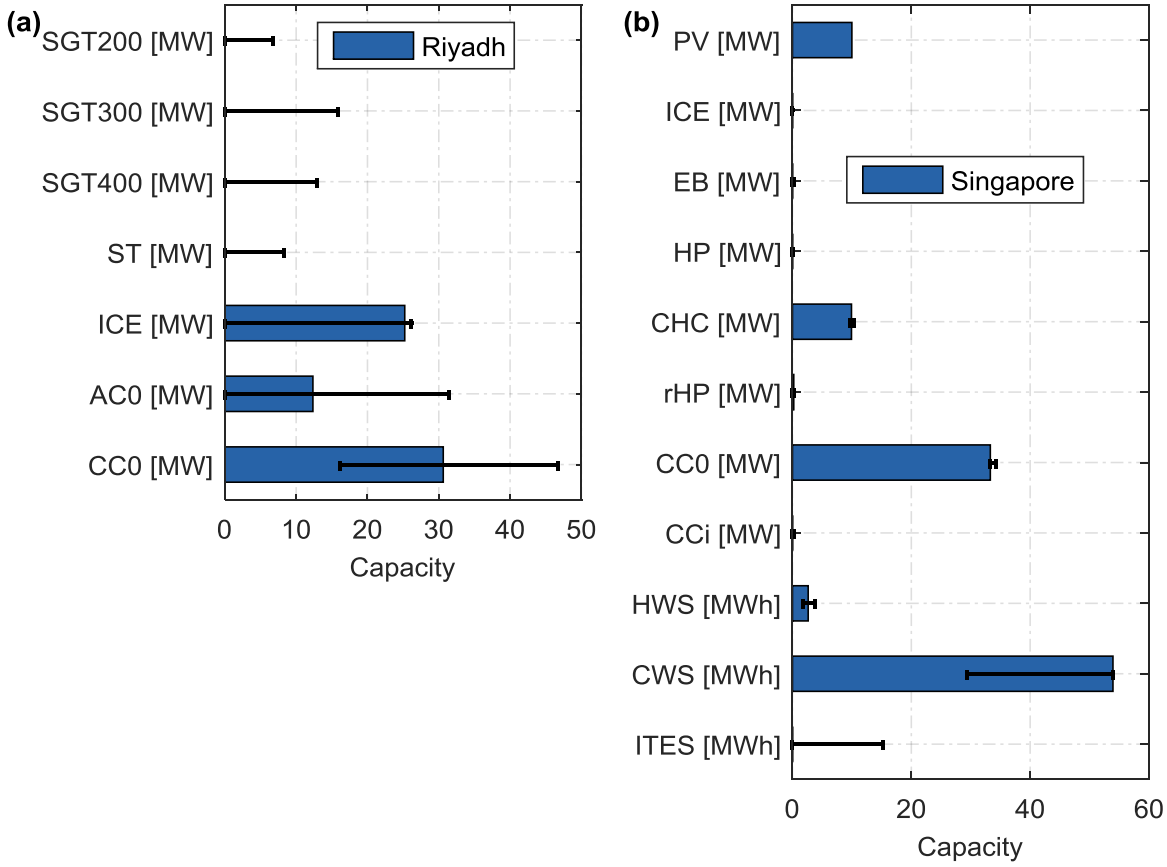

Figure 4.16: Scenario analysis for the (a) Riyadh and (b) Singapore airport energy system: Clustered results for all scenarios (commodity prices and technology capital costs).

In **Figure 4.16**, finally, also changes of the assumed technology capital costs were considered (in a total of 11·7 = 77 scenarios). The results were clustered in the figure in a way that that the optimal capacities of the reference cases were plotted as blue bars and variations in the 77 scenarios were illustrated by error bars indicating the minimum and maximum capacities. **Figure 4.16 (a)** shows that the prime mover of the CHP units could be replaced by gas turbines (instead of combustion engines), when they were offered for reasonably low prices (iGT scenarios). The compression chiller was economically attractive in all scenarios. The Singapore airport energy system was one more time much more robust to changes (compare **Figure 4.16 (b)**). The PV panels, CHC and CC0 were installed in all scenarios with approximately the same capacity. The chilled water storages (CWS) could be partly replaced by ice storages (ITES), in combination with compression chillers (CCi).

The results showed that it depended on the location and its boundary conditions, how the energy system should be designed. In addition to this, it also depended on the location, how sensitive the design was to changes due to potential future trends.

4.2.5 How sensitive is the design to changes of commodity prices and the interest rate? What does a larger PV capacity and cheaper Lithium-ion batteries yield?

For further elaborating the sensitivity of the design of the energy system, parameters were systematically varied. Isolated changes of the natural gas price, the electricity price, the CO2 emission price and the interest rate were analyzed for the CPT airport. **Figure 4.17** shows the resulting optimal capacities (discrete samples indicated by vertical lines).

With increasing natural gas price, internal combustion engine CHPs became economically unattractive (**Figure 4.17 (a)**). Instead, heating was supplied by gas boilers (GB) and heat pumps (both CHC and rHP). Eventually, also gas boilers were replaced by electric boilers. The capacities of the compression chiller and thermal energy storages were fairly constant. The plot in **Figure 4.17 (b)** is almost a mirror image of **Figure 4.17 (a)**. However, at mean annual electricity prices greater than 5.17 ct/kWh (peak prices of 8.15 ct/kWh), PV panels were economically feasible and should be installed. Increasing CO_2 emission prices had the same effects as increasing natural gas prices (**Figure 4.17 (c)**). Finally, **Figure 4.17 (d)** points out that heat pumps (both CHC and rHP) were partly replaced by less capital intense heating technologies (i.e., the gas boiler, GB) with increasing interest rates. Furthermore, ice storages (ITES) tended to have lower capital costs than chilled water storages (CWS) and therefore replaced them at higher interest rates (compare also **Figure B.8** in the appendix). For similar reasons, in some cases in **Figure 4.17 (a) – (c)**, ITES in combination with ammonia-water absorption chillers (ACi) were installed instead of CWS. For example, in **Figure 4.17 (b)**, waste heat from the internal combustion engine could be utilized with ACi and ITES.

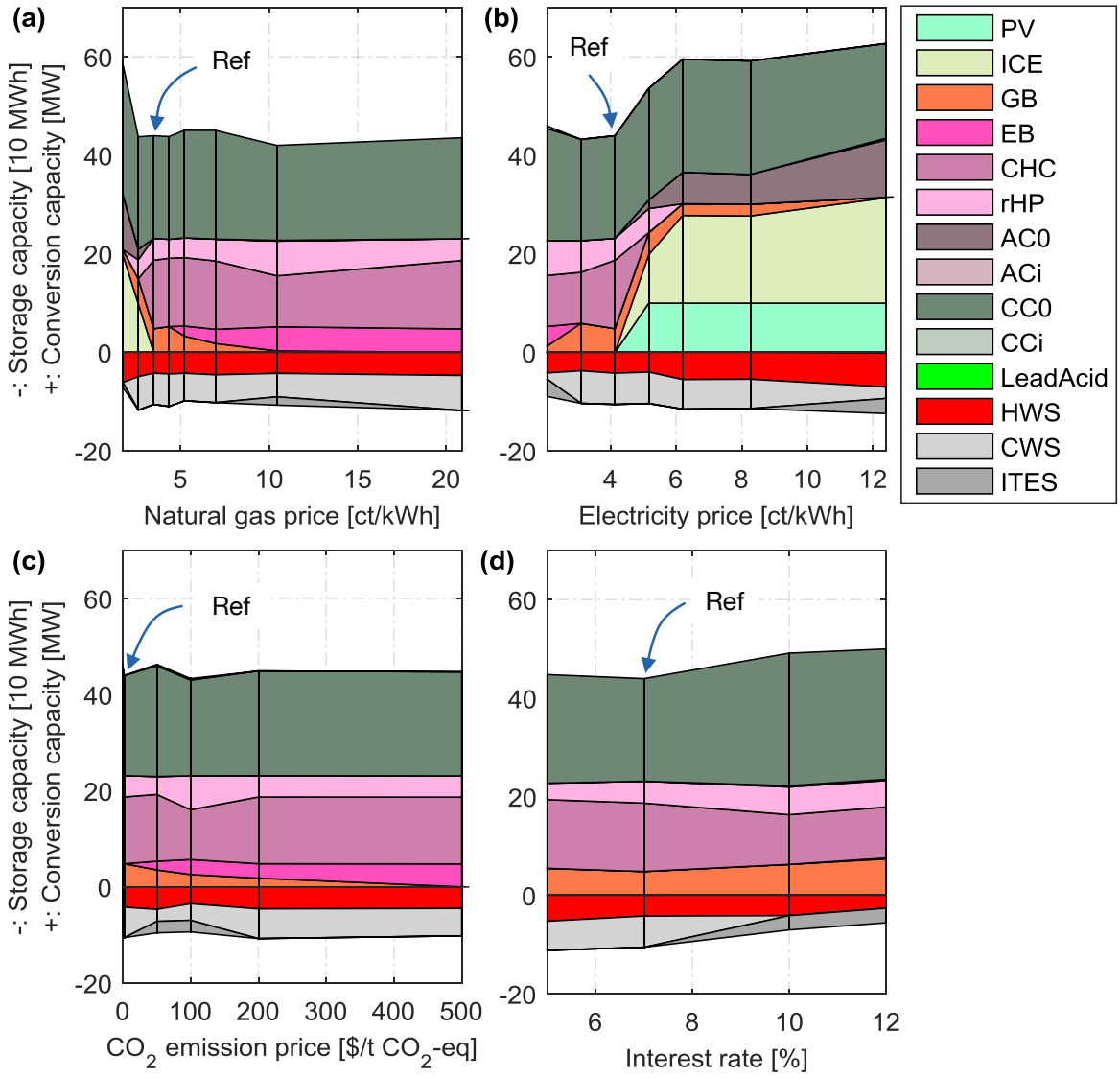

Figure 4.17: Cape Town airport energy system: Sensitivity analysis of the (a) Gas price (Ref = 3.48 ct/kWh), (b) Electricity price (Ref = 4.13 ct/kWh), (c) CO_2 emission price (Ref = 2 $/t) and (d) Interest rate (Ref = 7%).[21]

For evaluating how disruptive technologies such as stationary lithium-ion batteries could change the design of the energy system, a sensitivity study of the lithium-ion batteries specific capital costs was performed. Sauer (2016) forecasted the total hardware costs of stationary lithium-ion batteries from 450 – 520 €/kWh in 2016 to 300 – 380 €/kWh in 2050. Being even more optimistic, this study evaluated specific capital costs from 500 $/kWh down to 100 $/kWh (which is the price only for the cell material according to Sauer (2016)). CPT, MEX and SYD, locations with high TES capacities before, HNL, where a very small (80 kWh) lead-acid battery was installed before and

[21] The electricity price is the mean annual electricity price. Note the time-of-use (TOU) tariff in CPT (see **Table D.2**).

PHX, a location with small storage capacities before, serve as reference locations for this study.

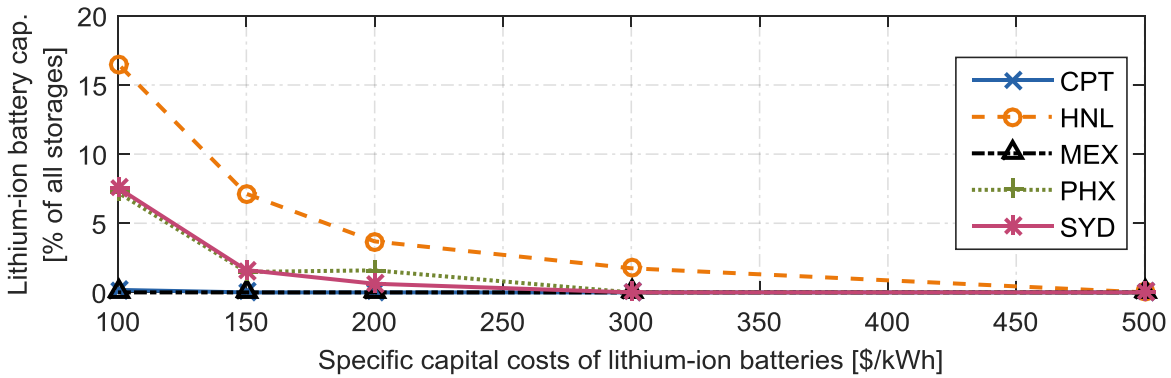

Figure 4.18: Lithium-ion battery capacity as percentage of all storages for different specific capital costs.[22]

Figure 4.18 shows the resulting optimal specific lithium-ion battery capacities (percentage of the overall installed storage capacity) as function of the specific capital costs of lithium-ion batteries. The figure shows that in four out of five cases, lithium-ion batteries were not economically attractive at projected minimum lithium-ion battery prices for 2050 (331 $/kWh) under the assumptions of this Thesis. Considering further use cases for electrochemical energy storages (e.g., operating reserve), stationary lithium-ion batteries might already become economically feasible at capital costs greater than 300 $/kWh. However, **Figure 4.18** also shows that the storage capacity at very optimistic prices of 100 $/kWh would still be lower than 20% of all installed storages, in particular thermal energy storages. Therefore, this study concluded that lithium-ion batteries play a minor role in storage applications that only focus on aspects of *energy* (e.g., peak shaving and load shifting).

Finally, for the Madrid airport energy system, the sensitivity of the maximum PV capacity constraint was investigated. The economic dispatches for the months of July and December were shown in **Figure 4.11** before. The PV capacity was systematically varied from 0 MW to 100 MW (discrete scenarios indicated by vertical lines in **Figure 4.19**). Note that the electric peak load was 21.5 MW (excluding electric loads from the compression chillers or other equipment). **Figure 4.19 (a)** shows that the minimum total expenditures were achieved at a PV capacity of 20 MW; so at approximately peak load capacity. Up to 20 MW, the increase in capital expenditures (CAPEX) were compensated by savings in operating expenditures (OPEX). Exceeding 20 MW, the power generation from PV became so large in some instances in time that they could not be handled economically anymore (e.g., electricity was sold at the wholesale market at rather low prices). With increasing PV capacity, the capacity of the internal combustion engine CHP plant and the gas boiler could only be slightly reduced (see **Figure 4.19 (b)**). Remarkably,

[22] The discrete scenarios are indicated by markers and connected by a line only for better visualization of the individual cases.

for this particular case, the capacity of the hot water storage (HWS) was not increased with increasing PV capacity.

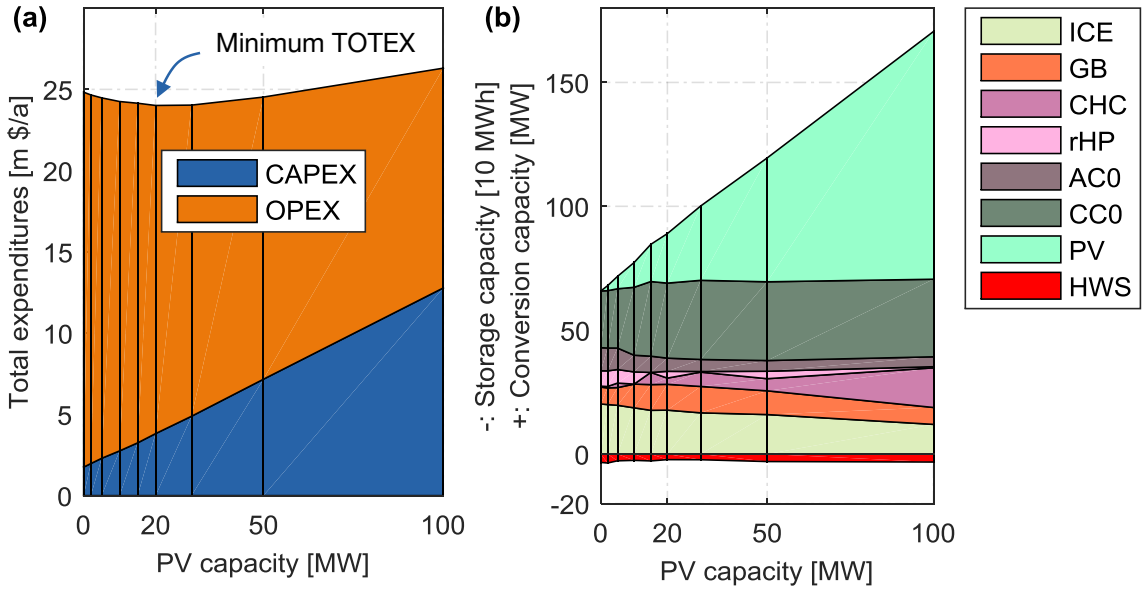

Figure 4.19: Evaluation of the PV capacity for the Madrid airport energy system: (a) Total expenditures, (b) Optimal converter and storage capacities.

The sensitivity analysis in this subsection outlined the influence of commodity price changes on the design of the energy system. Depending on the boundary conditions, the design of the energy system could be optimized in a way to achieve minimum total expenditures. However, in an actual application, the future pricing trends should be carefully investigated to achieve minimum total expenditures over the *entire lifetime* of the energy system. The ESD method could be extended for enabling a multiple year analysis with investment decisions in different years. Unfortunately, this would also increase the computational effort tremendously. A combination of both a simple multiple year analysis (with, e.g., time steps over an entire year) and the detailed ESD method for a single year introduced in this Thesis could fix this problem.

This subsection showed that lithium-ion batteries were not economically feasible for the Madrid airport at capital costs predicted for the year 2050 (300 €/kWh or approximately 331 $/kWh), when not taking any further use cases (such as operating reserve) for lithium-ion batteries into consideration. Finally, this Thesis also showed that a certain maximum PV capacity in terms of economical feasibility existed.

4.2.6 What is the economic advantage of optimized on-site generation and why is it important?

At four locations (HOU, PHX, RYD and SYD) all demands of the airport could be supplied externally from grids (i.e., a natural gas line, a power grid, a district heating and a district cooling grid and a water grid were available). For these four locations, three cases were defined:

- GridOnly: Supply of all energy demands externally from grids;

- GB+CC: GB for hot water and heating energy demands, CC for cooling energy demands. The power and water demand was supplied from the power and water grid, respectively;
- Optim: Optimized on-site generation.

The total expenditures for each of the three cases at each of the four locations were computed. Furthermore, since the commodity prices and the weighted average costs of capital (WACC) had some degree of uncertainty, a sensitivity study of these parameters was also included. **Figure 4.20** summarizes the results for this study. With the exceptions of the scenarios highlighted (A1 and A2), in all cases the simple configuration with GB and CC on site (GB+CC) was cheaper than the supply from grids only (GridOnly). Optimized on-site generation (Optim) was cheaper than GB+CC and GridOnly in all scenarios. Depending on the reference commodity price level at a particular location, the savings for the base case range from 6% to 26% (GB+CC to GridOnly) and 14% to 61% (Optim to GridOnly). Three key conclusions could be drawn from these results:

- First of all, the results show how important the optimization of the multi-modal on-site energy system is;
- Secondly, the highlighted scenarios (A1 and A2) show that simple installations (here GB and CC but potentially also more complex systems that were not optimally sized) could lead to economically inferior results;
- Last but not least, cogeneration and trigeneration on site was an important measure for achieving economical (and also energetically) optimal results. A number of cogeneration system installations at airports in the recent past also exhibit this in reality (decentralized energy, 2007, 2011a, 2011b; Peneva, 2014; Williams, 2012, 2013).

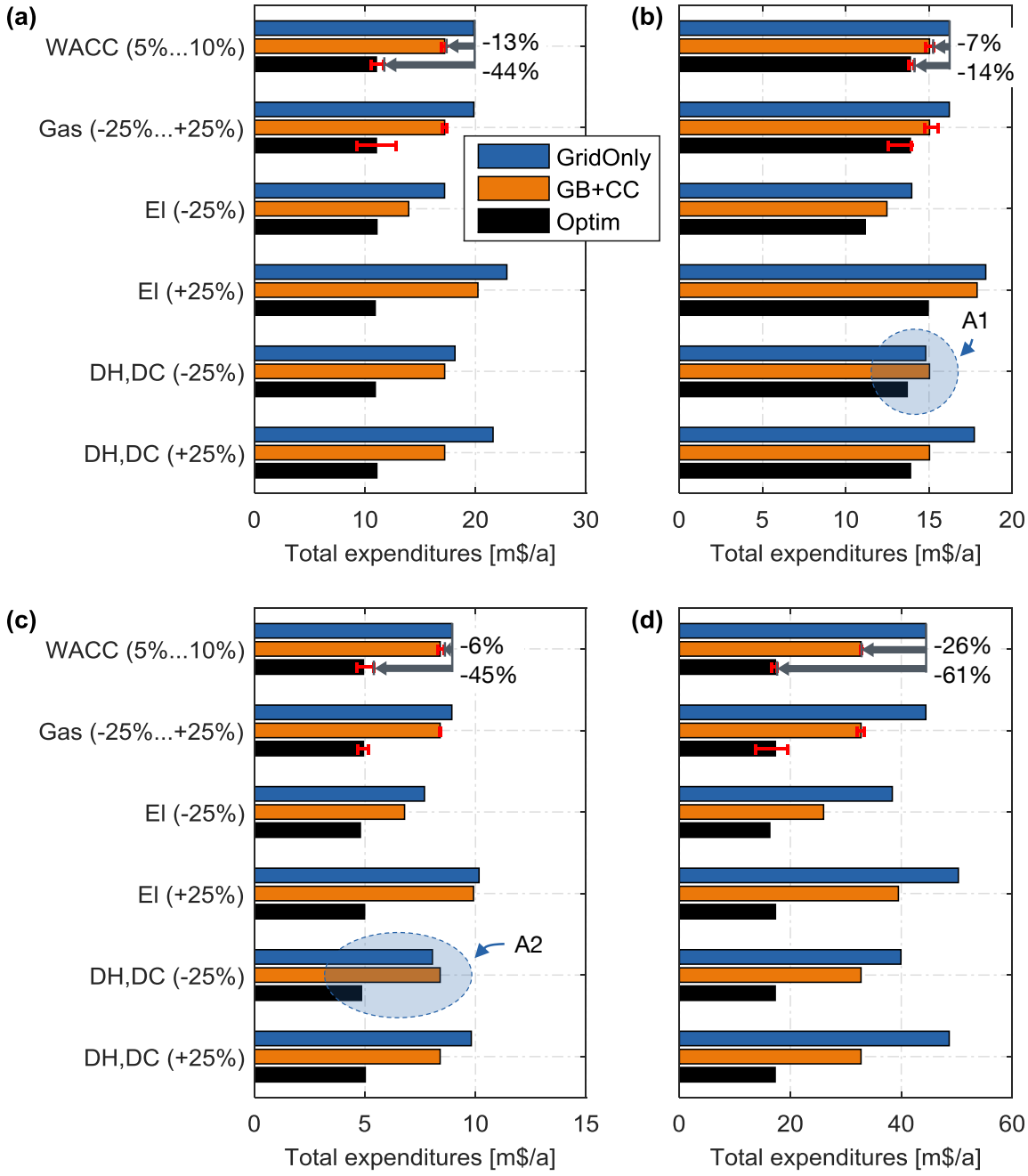

Figure 4.20: Economic evaluation of four airport energy systems: (a) Houston, (b) Phoenix, (c) Riyadh and (d) Sydney. The cases GB+CC (GB for heating, CC for cooling) and Optim (Optimized on-site generation) were compared to case GridOnly (all energy demands drawn from grids): Variation of the weighted average capital costs (WACC), gas price (Gas), electricity price (El) and district heating (DH) and cooling prices (DC) (adapted from Thiem, Danov, et al. (2017)).[23]

[23] Variations of the weighted average capital costs and the gas price are indicated by red-colored error bars.

4.2.7 Can the novel ice-storage-integrated desalination system challenge existing and proven desalination technologies? How important is the climate for turbine inlet air cooling?

We want to continue our deep-dive and answer the following two technology-oriented questions: Could the ice-storage-integrated desalination system become economically feasible and which turbine inlet air cooling methods should be installed in different climates?

Ice-storage-integrated desalination

So far, the isiD system did not appear in any of the optimal technology selections (see, e.g., **Figure 4.6**). Therefore, isiD with four stages as it was experimentally measured (see **Section 3.5.4**) was economically unattractive. However, this study also investigated whether the isiD system would become economically feasible, if it could be improved from four stages to only two stages for desalinating seawater from 35 g salt/kg water to < 1 g/kg (η^+). In an additional case, the specific operation and maintenance costs ($o_{2,\mathrm{isiD}}$) for isiD systems were reduced from 5 $/kWh/a (see **Table A.19**) to 1 $/kWh/a ($o_2^-$).

Three locations were considered for this study. The airport energy systems in Mexico City and Rio de Janeiro were two example systems, where ice storages were installed in the reference case. The isiD capacity was fixed to the ITES capacity determined for the reference case. The Miami airport was selected as another use case location. Note that a reverse osmosis desalination system with water storage was installed in Miami in the reference case. In Miami, the isiD system was sized so that the average yearly cooling load could be handled by the isiD system for one hour (20.8 MWh). The isiD system had a predefined capacity; however, the rest of the energy system technologies were optimized.

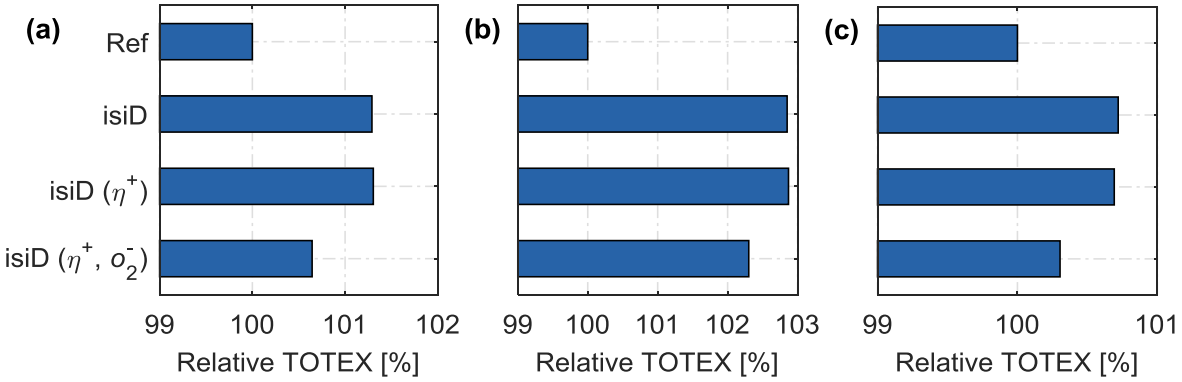

Figure 4.21: Comparison of the total expenditures (relative to the reference case, Ref) for (a) Mexico City, (b) Miami and (c) Rio de Janeiro.

Figure 4.21 shows the economical results for the isiD case study. The total expenditures were plotted as percentages relative to the reference case (see **Figure 4.6**). Total expenditures for all three cases (isiD system with four stages, isiD system with two stages, and isiD system with two stages and reduced O&M costs) were greater than for the reference case at all three locations. Furthermore, the figure shows that improving the efficiency of the isiD system to two stages for desalinating seawater did not improve the

economics of the system considerably. That was because the isiD system was hardly used for storing cooling energy and desalinating water. Note also that decreasing O&M costs significantly improved the economics of the isiD system (but also did not make it economically attractive compared to the reference case).

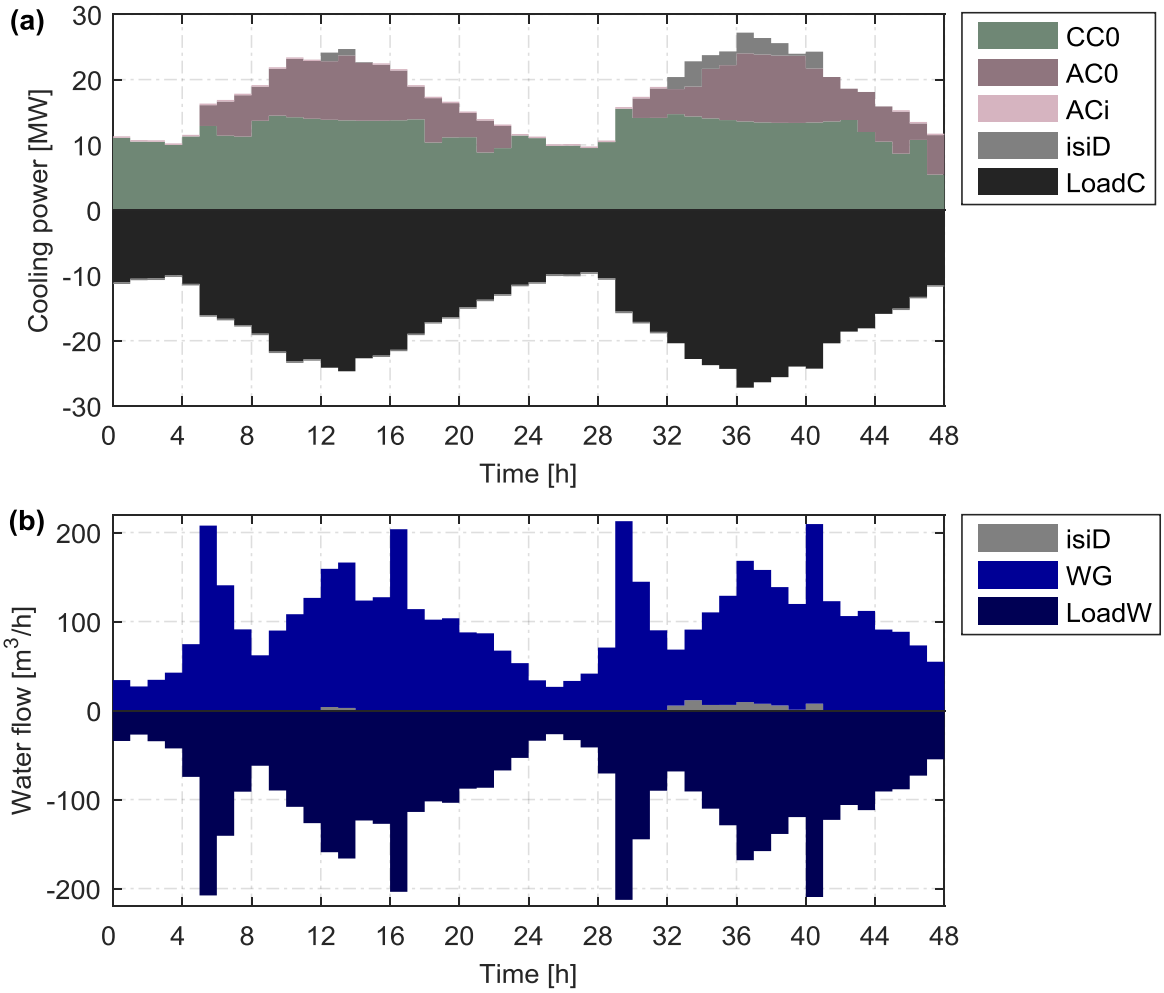

Figure 4.22: Economic dispatch of the isiD system at two example days in summer: (a) Cooling power, (b) Water flow for the isiD system installed at the airport in Mexico City (assuming two stages for desalinating seawater to freshwater quality).

The economic dispatch of the isiD system is further elaborated in **Figure 4.22**. The isiD system was discharged at peak cooling times and always slowly charged at the remaining times (see **Figure 4.22 (a)**). Hence, the isiD system was capable to reduce the peak cooling loads for the remaining chillers (CC0 and AC0). The desalinated water from the isiD system could be used for the water supply (see **Figure 4.22 (b)**). However, since the levelized costs of water generation for the isiD system were much higher (see **Section 3.5.4**) than the price for drawing water from the grid (0.41 $/m³), it was only economically attractive to desalinate water with the isiD system as a by-product, when the system was already attractive as a *cold storage*. However, as **Figure 4.22 (a)** illustrates, the isiD system was only attractive to supply cooling energy at peak cooling

times due to the reduced efficiency of chillers at low evaporation temperatures (< 0 °C, see also **Section 3.5.2**).

isiD systems could become economically attractive, if the following condition was met *and* ice storages were found to be economically attractive beforehand:

$$R_{\mathrm{isiD}} > \Delta_{\mathrm{ITES}\rightarrow\mathrm{isiD}} C_{\mathrm{CAPEX}} + \Delta_{\mathrm{ITES}\rightarrow\mathrm{isiD}} C_{\mathrm{O\&M}}, \tag{4.4}$$

with the revenue (or savings) of using water from the isiD system (R_{isiD}), and changes of CAPEX ($\Delta_{\mathrm{ITES}\rightarrow\mathrm{isiD}} C_{\mathrm{CAPEX}}$) and O&M ($\Delta_{\mathrm{ITES}\rightarrow\mathrm{isiD}} C_{\mathrm{O\&M}}$). The latter two can be computed as follows:

$$\begin{aligned} \Delta_{\mathrm{ITES}\rightarrow\mathrm{isiD}} C_{\mathrm{CAPEX}} &= C_{\mathrm{CAPEX,isiD}} - C_{\mathrm{CAPEX,ITES}} \\ &= a_{\mathrm{isiD}} \cdot \left(i_{1,\mathrm{isiD}} + i_{2,\mathrm{isiD}} Q_{\mathrm{isiD}}\right) - a_{\mathrm{ITES}} \cdot \left(i_{1,\mathrm{ITES}} + i_{2,\mathrm{ITES}} Q_{\mathrm{ITES}}\right), \end{aligned} \tag{4.5}$$

$$\Delta_{\mathrm{ITES}\rightarrow\mathrm{isiD}} C_{\mathrm{O\&M}} = C_{\mathrm{O\&M,isiD}} - C_{\mathrm{O\&M,ITES}} = \left(o_{1,\mathrm{isiD}} + o_{2,\mathrm{isiD}} Q_{\mathrm{isiD}}\right) - \left(o_{1,\mathrm{ITES}} + o_{2,\mathrm{ITES}} Q_{\mathrm{ITES}}\right), \tag{4.6}$$

whereby $Q_{\mathrm{isiD}} = Q_{\mathrm{ITES}}$. The revenue from desalinating water by using the isiD system could be approximately calculated by

$$R_{\mathrm{isiD}} = \alpha \cdot \sum_{k=1}^{8760} \left(\Delta t_k \cdot \dot{Q}_{\mathrm{c},k}\right) \cdot \frac{\beta^{n_{\mathrm{s}}}}{\Delta h_{\mathrm{i}} \cdot \sum_{i=1}^{n_{\mathrm{s}}} (\beta^i)} \cdot p_{\mathrm{w}}, \tag{4.7}$$

with the cooling load ($\dot{\mathbf{Q}}_{\mathrm{c}}$), a factor that describes the amount of cooling supplied by the ice storage (α), the mass ratio of ice to the total storage material ($\beta \approx 0.5 \ldots 0.6$), the number of required stages (n_{s}), the specific enthalpy of freezing water to ice (Δh_{i}) and an annual average water price (p_{w}, i.e., either the price for drawing potable water from the grid or the levelized costs of generating water on site). The capacity constraint of the storage must also be checked.

For the Mexico City airport energy system, the following example elaborates **Equation (4.4)** to **Equation (4.7)** in more detail. The capacity of the ice storage in the reference case was 21.8 MWh. The isiD system was sized accordingly ($Q_{\mathrm{isiD}} = Q_{\mathrm{ITES}} = 21.8\ \mathrm{MWh}$). For case ($\eta^+$, o_2^-), $\Delta_{\mathrm{ITES}\rightarrow\mathrm{isiD}} C_{\mathrm{CAPEX}} = 18{,}318\ \$/\mathrm{a}$ and $\Delta_{\mathrm{ITES}\rightarrow\mathrm{isiD}} C_{\mathrm{O\&M}} = 19{,}005\ \$/\mathrm{a}$. With this, the condition ($R_{\mathrm{isiD}} > 37{,}323\ \$/\mathrm{a}$) could be derived. The term ($\sum_{k=1}^{8760} \left(\Delta t_k \cdot \dot{Q}_{\mathrm{c},k}\right) = 110.3\ \mathrm{GWh/a}$) and the water price ($p_{\mathrm{w}} = 0.41\ \$/\mathrm{m}^3$) were derived from the case study. Assuming $\Delta h_{\mathrm{i}} = 92.53\ \mathrm{kWh/m^3}$, $\beta = 0.5$ and $n_{\mathrm{s}} = 2$, $\beta^{n_{\mathrm{s}}} / \left[\Delta h_{\mathrm{i}} \cdot \sum_{i=1}^{n_{\mathrm{s}}} (\beta^i)\right]$ could be derived to 0.0036 m³/kWh. With this, a condition for α could be derived to

$$\alpha > \frac{37{,}323\ \$/\mathrm{a}}{162{,}912\ \$/\mathrm{a}} = 0.23. \tag{4.8}$$

Equation (4.8) means that more than 23% of the annual cooling energy demand should be supplied by the ice storage to make the isiD system economically attractive. Note that α was assumed to be the same for the isiD system and the ice storage. However, in the Mexico City case, the ice storage supplies only approximately 0.6% of the cooling energy demand. Therefore, the system was economically not attractive and only 2070 m³/a of the annual water demand (720,000 m³/a) were supplied by the isiD system (in both η^+ cases).

To summarize, neglecting all technological difficulties and requirements for research and development, the results show that the ice-storage-integrated desalination system was not found feasible at a variety of favorable conditions.

Turbine inlet air cooling

The only airport location, where a gas turbine was economically feasible, was Honolulu (see **Figure 4.6**). Honolulu has a tropical savannah climate (Köppen climate Aw) with high humidity. To assess the influence of the *climate* on turbine inlet air cooling, Riyadh was selected as second use case location for this study. Riyadh has a hot arid desert climate (BWh).

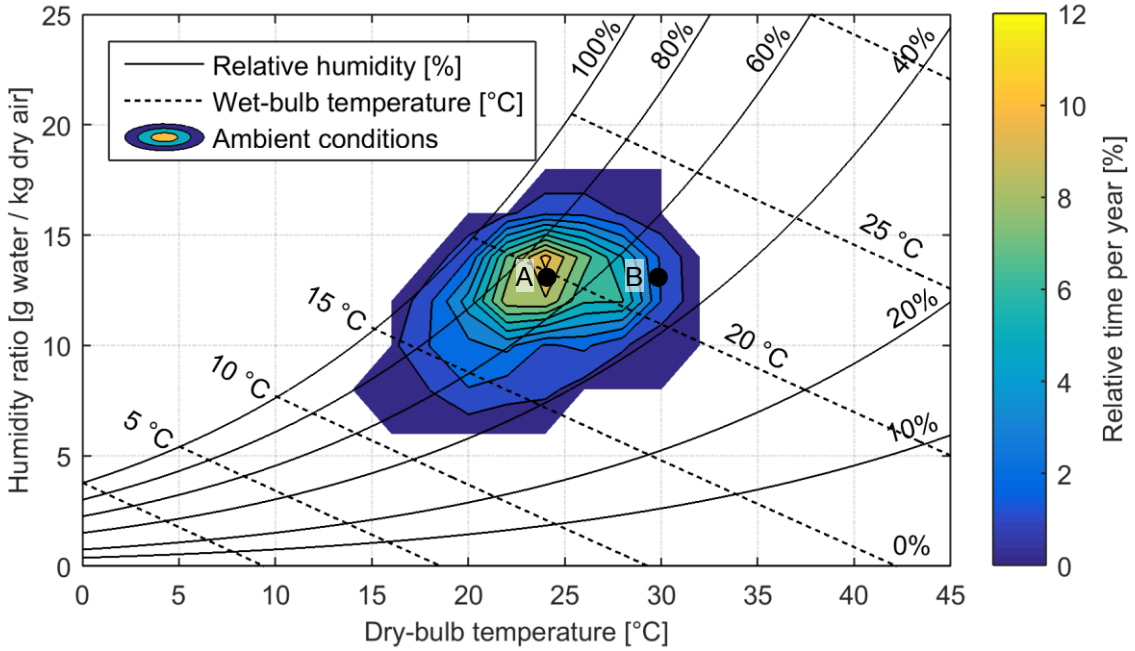

Figure 4.23: Honolulu yearly ambient conditions (based on data from Meteotest (2014)).

Figure 4.23 shows the yearly ambient conditions in Honolulu in a psychometric chart (compare also **Figure 3.18**).[24] For this figure, the humidity ratio (X) – dry-bulb temperature (T) plotting area was scattered by ΔX = 2 g/kg and ΔT = 2 K. The contour plot in **Figure 4.23** illustrates the relative time of a certain ambient condition (combination of temperature and humidity) within a typical year in HNL. The plot outlines the hot and humid climate in HNL. For explanation, two points (A and B) were plotted in the figure. Approximately 10% of the representative year (10% of 8760 h), the dry-bulb temperature in HNL was 24 °C at 70% relative humidity (A). Approximately 2-3% per year, the dry-bulb temperature was 30 °C at 50% relative humidity (B). **Figure 4.24** illustrates the yearly ambient conditions in Riyadh. This diagram outlines the hot and arid climate in RYD. Most of the hours of the representative year, the ambient conditions were at rather low

[24] The psychometric chart was plotted for the mean annual ambient pressure in Honolulu.

humidity ratios and hence low relative humidities (10 – 25%) between points (C and D). Note that the two psychometric charts slightly differ due to different ambient pressures.[25]

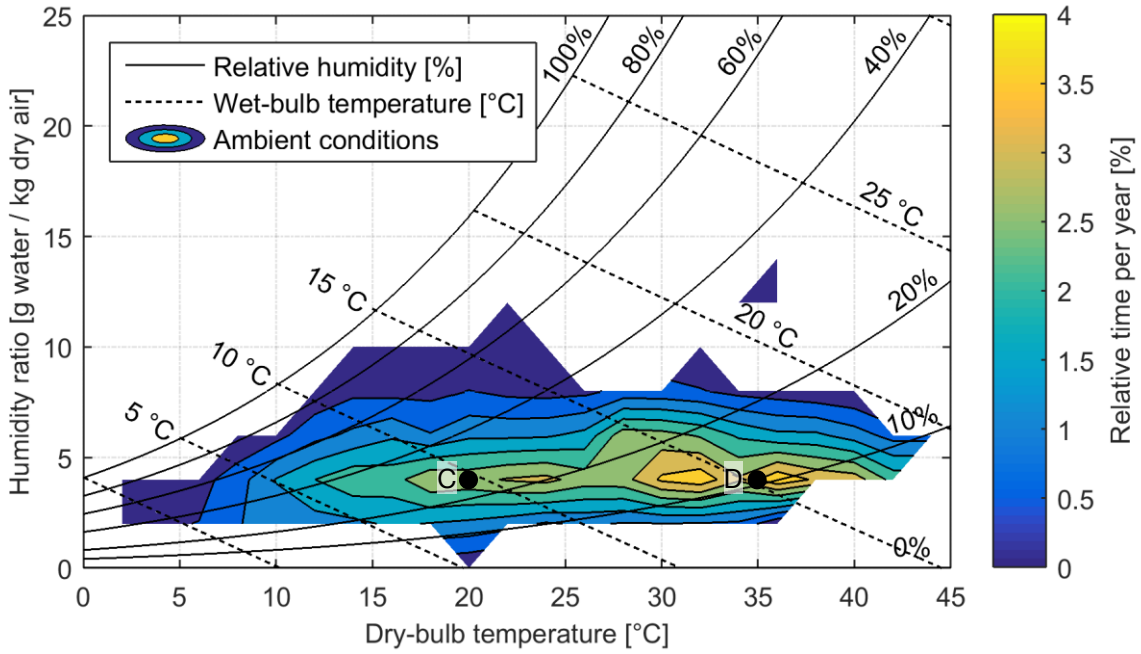

Figure 4.24: Riyadh yearly ambient conditions (based on data from Meteotest (2014)).

For this study, at each of the two locations, a Siemens gas turbine SGT-400 with 12.9 MW nominal electric power output was installed (compare also the performance map of the SGT-400 in **Figure 3.5**). Furthermore, for each location, different TIAC installations were investigated (a total of four cases). For Case NoTIAC, no TIAC methods were installed; Case Evap uses evaporative cooling; and Cases DewPoint and ISO use active cooling (compare also **Figure 3.18**). The energy system design method was allowed to optimize the entire system, design and operation, around the fixed SGT-400 installations.

Figure 4.25 shows the resulting total expenditures of the entire airport energy system relative to the NoTIAC case and the optimal technologies and their *nominal* capacities. Note that the *actual* capacities at high ambient temperatures were lower with NoTIAC (compare the performance map of the SGT-400 in **Figure 3.5**). **Figure 4.25 (a)** shows that TIAC method ISO was slightly more cost-efficient in Honolulu than NoTIAC. In the following, TIAC method ISO is investigated in more detail for Honolulu. However, the cost savings were not significant to justify an installation of any additional TIAC equipment in Honolulu (compare also **Figure 4.12**). The SGT-400 in Honolulu was installed as combined cycle power plant (see **Figure 4.25 (b)**).

The SGT-400 in Riyadh, on the other hand, was installed as simple cycle unit. The hot exhaust gases were used for powering an absorption chiller, which could generate chilled

[25] The mean annual ambient pressure was 101.57 kPa in Honolulu and 93.81 kPa in Riyadh (Meteotest, 2014).

water in combination with a compression chiller (see **Figure 4.25 (d)**). **Figure 4.25 (c)** outlines that cost savings were significant by using TIAC in Riyadh (about 4% of the total expenditures of the entire energy system could be saved due to TIAC). Particularly evaporative cooling (TIAC method Evap) achieved the lowest total expenditures. This could be easily explained by the dry climate in Riyadh. Furthermore, **Figure 4.25 (d)** shows that the capacity of the internal combustion engine CHP as additional power plant could be reduced by improving (i.e., augmenting) the power output from the gas turbine at high ambient temperatures. In addition to this, the capacity of the compression chiller did not have to be increased for TIAC method Evap. This TIAC method was also the method selected for further investigation of the Riyadh airport TIAC installation.

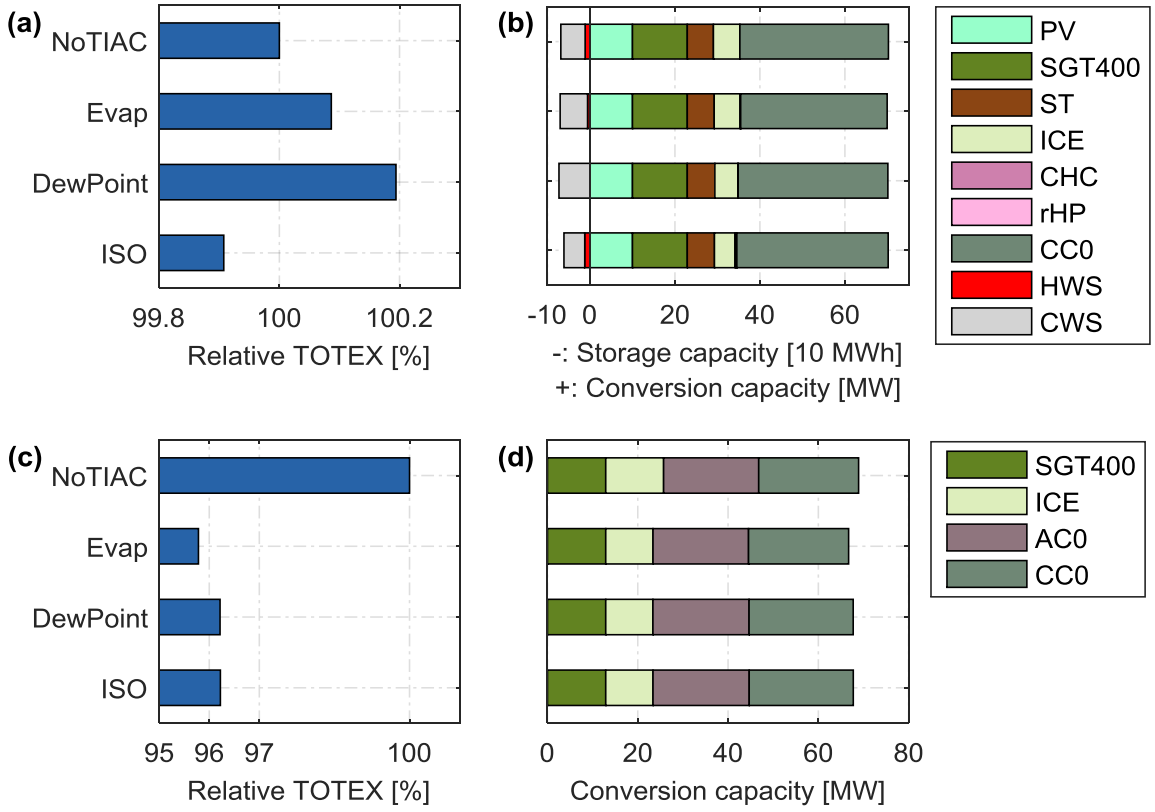

Figure 4.25: Comparison of relative total expenditures of the entire airport energy system (relative to NoTIAC) and optimal capacities for different turbine inlet air cooling methods at the locations (a), (b) Honolulu and (c), (d) Riyadh.

In Riyadh, both of the TIAC methods, DewPoint and ISO, lead to similar total expenditures. Indeed, the technical performance of the two TIAC systems is almost the same, due to the dry ambient conditions in RYD (**Figure 4.24**, compare also **Figure 3.18**). By active cooling of the inlet air, both systems can achieve 15 °C (ISO temperature) most of the time. Note that the reference system in RYD (see **Figure 4.6**) with internal combustion engine CHP was still cheaper than the SGT-400 with TIAC method Evap introduced here. **Figure 4.25** clearly reveals that the climatic conditions were very important for choosing the right TIAC technology.

In order to further elaborate the cost savings achieved by the installation of TIAC systems, the levelized costs of electricity (LCOE) for the different SGT-400 systems were

compared. For the two reference cases without any TIAC installations (NoTIAC), the LCOE ($LCOE_{\text{SGT-400,NoTIAC}}$) was defined as

$$LCOE_{\text{SGT-400,NoTIAC}} = \frac{\sum_{j\in\{\text{SGT-400,ST}\}}\left(C_{\text{CAPEX},j} + C_{\text{O\&M},j}\right) + C_{\text{Comm,f,SGT-400}}}{\sum_{j\in\{\text{SGT-400,ST}\}}\left(E_{\text{el},j}\right)}, \tag{4.9}$$

where $C_{\text{Comm,f,SGT-400}}$ denotes the costs for the gas supplied to the gas turbine and $\sum_{j\in\{\text{SGT-400,ST}\}}\left(E_{\text{el},j}\right)$ is the annual electric energy generated by both SGT-400 and steam turbine. The LCOE ($LCOE^{*}_{\text{SGT-400},i}$) for the SGT-400 installations with turbine inlet air cooling (method i) were defined as

$$LCOE^{*}_{\text{SGT-400},i} = \frac{\begin{array}{c}\sum_{j\in\{\text{SGT-400,ST}\}}\left(C_{\text{CAPEX},j} + C_{\text{O\&M},j}\right) + \sum_{j\in U}\left(\Delta C_{\text{CAPEX},j} + \Delta C_{\text{O\&M},j}\right)\\ +C_{\text{CAPEX,TIAC}} + C_{\text{O\&M,TIAC}} + C_{\text{Comm,f,SGT-400}} + C_{\text{Comm,w,TIAC}}\end{array}}{\sum_{j\in\{\text{SGT-400,ST}\}}\left(E_{\text{el},j}\right)}, \tag{4.10}$$

with $U \in$ {ICE,AC0,CHC,CC0,HWS,CWS}, the water charges (or reduced charges) due to TIAC ($C_{\text{Comm,w,TIAC}}$) and the difference of the capital expenditures ($\Delta C_{\text{CAPEX},j}$) and operation and maintenance costs ($\Delta C_{\text{O\&M},j}$) compared to the NoTIAC case. Note that **Equations (4.9) and (4.10)** do not account for the heat extraction from the hot exhaust gases. **Equation (4.10)** is a generalization of **Equation (4.9).**

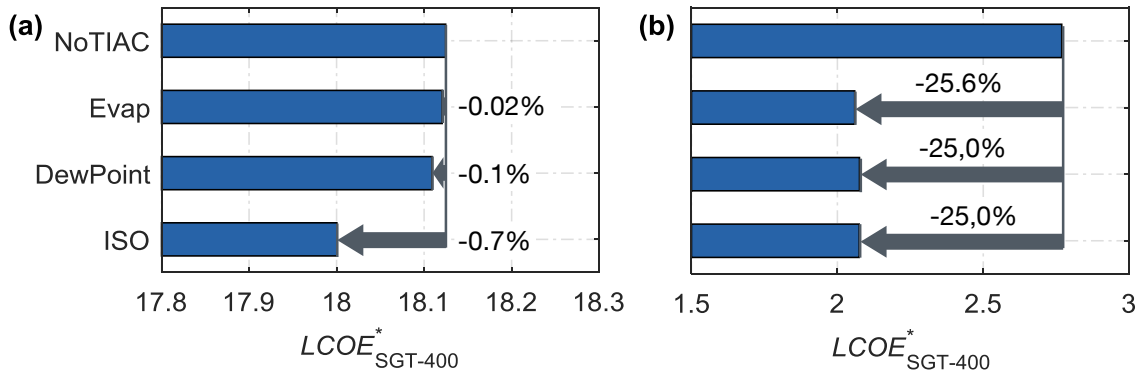

Figure 4.26: Levelized costs of electricity generation by the SGT-400 gas turbine for different TIAC systems: (a) Honolulu, (b) Riyadh.

Figure 4.26 shows the resulting LCOE for the SGT-400 installations. The numeric values between HNL and RYD clearly differ due to different gas prices (see **Table D.2** in the appendix). The LCOEs in HNL were higher than the electricity energy charge in HNL. However, the electricity tariff in HNL had also an unneglectable demand charge. Furthermore, the utilization of heat was not included in the calculation of the LCOE. The specific cost savings for power generation by the SGT-400 system were less than 1% in HNL but significantly higher in RYD (approximately 25%). The latter emphasizes the importance of turbine inlet air cooling in hot and arid climates.

Figure 4.27 and **Figure 4.28** show, at which conditions it is attractive to cool the turbine inlet air in Honolulu and Riyadh, respectively. The TIAC usage parameter for a certain area with size ($\Delta X, \Delta T$) (see contour plots in **Figure 4.27** and **Figure 4.28**) was defined as the number of hours the turbine inlet air was cooled per year at these ambient

conditions divided by the total number of hours per year at these ambient conditions. **Figure 4.27** and **Figure 4.28** also show the compressor inlet conditions, when the turbine inlet air was cooled.

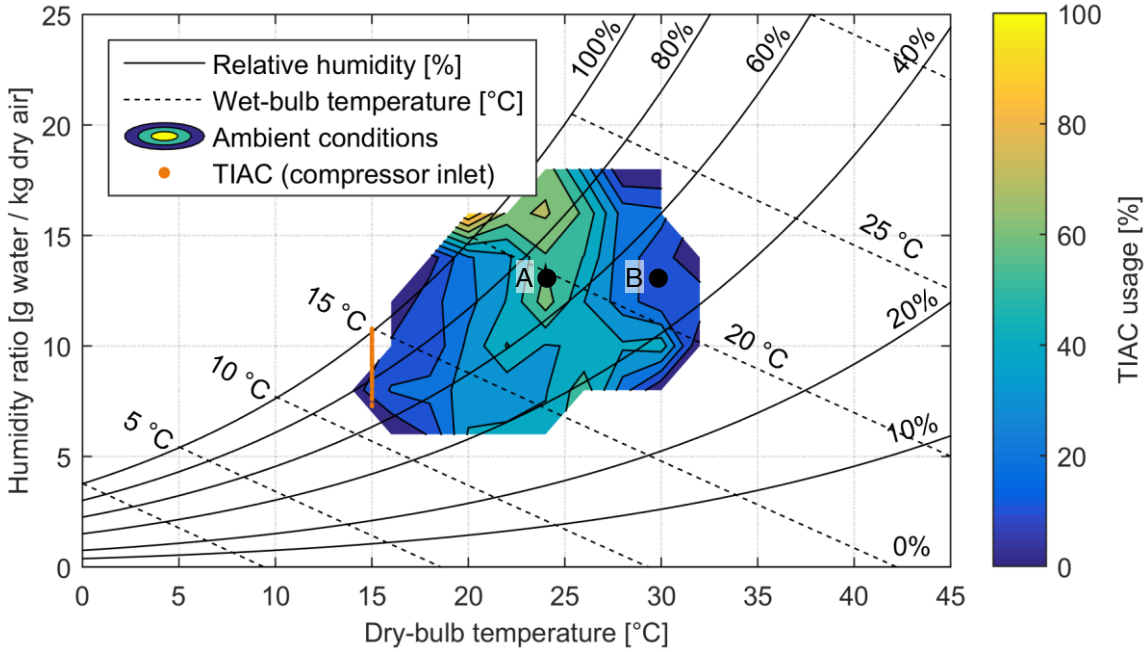

Figure 4.27: Turbine inlet air cooling (TIAC method ISO) usage in Honolulu for an entire year.

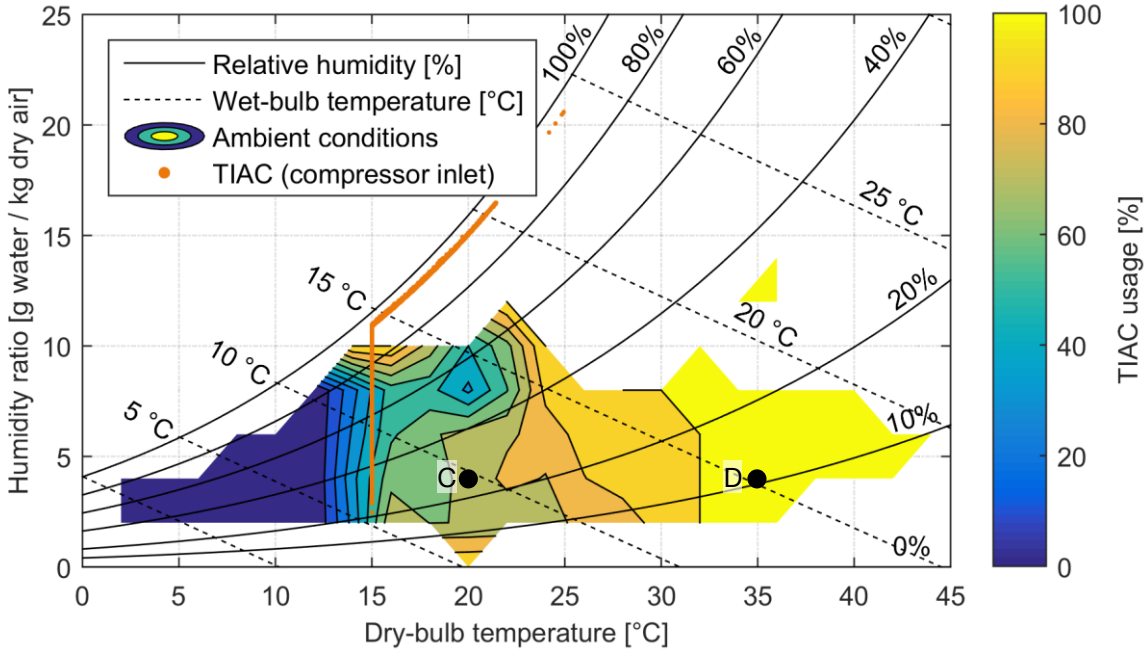

Figure 4.28: Turbine inlet air cooling (TIAC method Evap) usage in Riyadh for an entire year.

Figure 4.27 depicts that TIAC method ISO was mostly used at a narrow band of around 22 – 26 °C dry-bulb temperature (see, e.g., Point A), which were also the ambient conditions with the greatest occurrences throughout the year (see Point A in **Figure 4.23**). This indicates that active cooling was not economically efficient anymore at high dry-bulb temperatures (> 26 °C, Point B) due to the larger required cooling demands.[26] Furthermore, it was not necessary to cool the turbine inlet air at ambient dry-bulb temperatures below 22 °C.

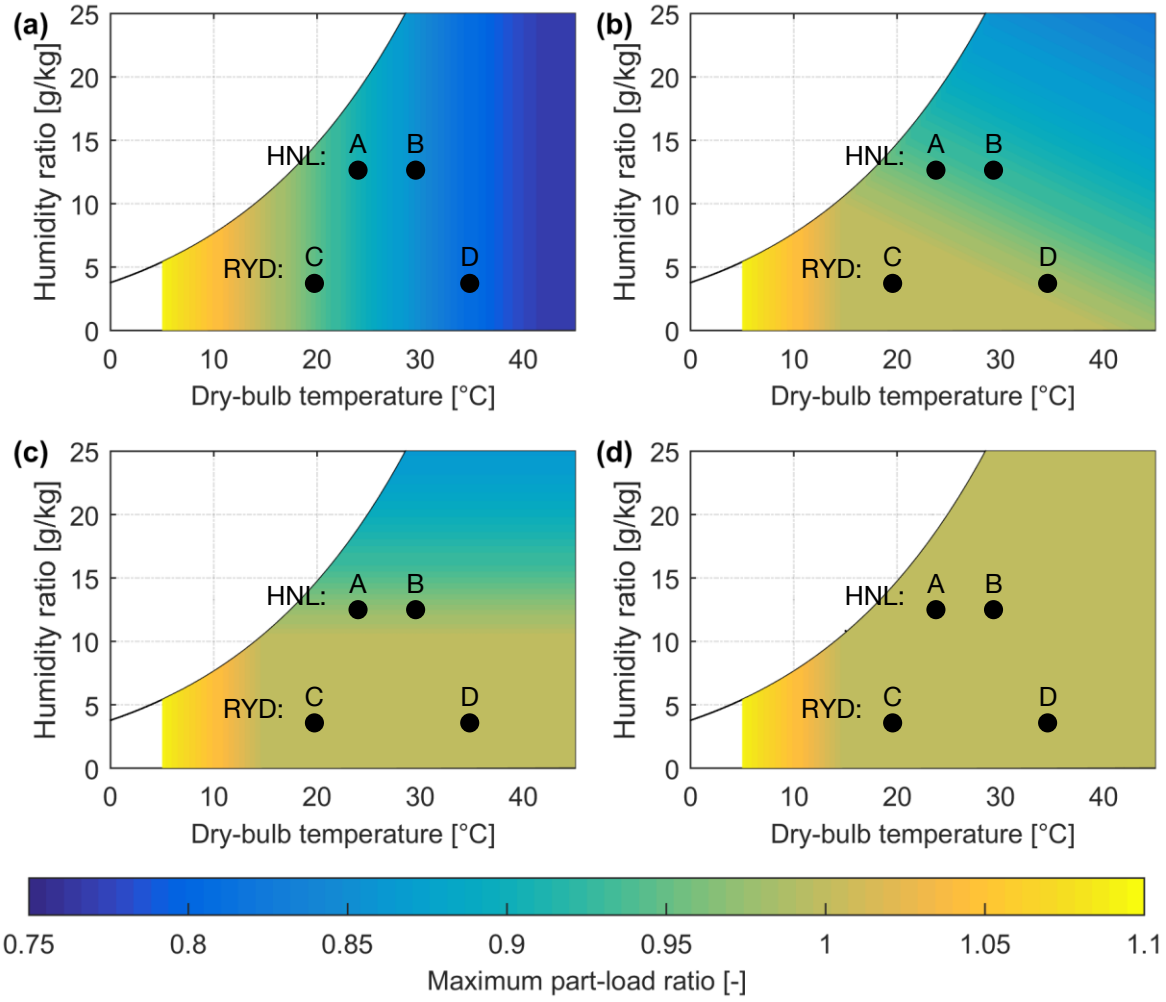

Figure 4.29: Turbine inlet air cooling potential (maximum part-load ratio) for the Siemens gas turbine SGT-400 as function of the ambient conditions: (a) No turbine inlet air cooling (NoTIAC), (b) Evaporative cooling (Evap), (c) Active cooling to dew-point temperature (DewPoint), and (d) Active cooling to ISO temperature (ISO).

[26] Since the overall electric demands at the HNL airport increased with higher ambient dry-bulb temperatures (not shown here), the electric demand could not have been the cause for reduced TIAC usage at higher ambient temperatures. However, ambient conditions in Point B were less likely to occur during the year (compare **Figure 4.23**). Hence, the TIAC usage results in Point B are less representative.

Figure 4.28 illustrates that the TIAC usage in Riyadh was almost monotonically increased with higher ambient dry-bulb temperatures. For example, in Point C, the turbine inlet air was cooled at 60% of the time. In Point D, on the other hand, TIAC was used in every hour Riyadh had these ambient conditions (100%).

With the turbine inlet air cooling model and the SGT-400 model, the contour plots in **Figure 4.29** were derived. The figure shows four psychometric charts; the maximum part-load ratios ($u_{\max}$) at particular ambient conditions were indicated by color coding. **Figure 4.29 (a)** shows $u_{\max}$ for the NoTIAC case. With higher ambient dry-bulb temperatures, the maximum power output from the SGT-400 is reduced. By evaporating water droplets in the inlet air (Evap), the turbine inlet air could be cooled and the available power output could be augmented (**Figure 4.29 (b)**). When water is available at a low price, evaporative cooling of the inlet air is a cost-efficient TIAC technology to augment the power output (compare the Points D in **Figure 4.29 (a)** and **Figure 4.29 (b)**). **Figure 4.29 (c)** and **Figure 4.29 (d)** show $u_{\max}$ for the two active turbine inlet air cooling methods (DewPoint and ISO). In Point B, active cooling increased the available power output. However, active cooling requires additional equipment, such as a compression chiller or an absorption chiller and a heat exchanger. Furthermore, the cooling loads may be so large that active cooling is not feasible anymore (compare Point B in **Figure 4.27**).

The results highlight that the ESD method presented in this Thesis is capable of accurately choosing the most attractive turbine inlet air cooling method. Furthermore, TIAC could be optimally controlled. The results also show that TIAC is able to significantly reduce total expenditures at sites located in desert climates, in particular by the use of evaporative cooling technologies.

5 Conclusion and outlook

5.1 Conclusions

5.1.1 The method: Features and feasibility

The novel superstructure-based energy system design (ESD) method was formulated as mixed-integer linear programming problem. Although the optimization model was *linear*, the model was formulated in a way that *nonlinear* part-load efficiencies could be considered. The basic functionality of the ESD method was successfully benchmarked against a state-of-the-art ESD tool. However, the ESD method developed in this Thesis incorporated further features, such as the modeling framework for integrating part-load efficiencies. This study showed that the consideration of part-load efficiencies could significantly change the design of energy systems compared to cases, where part-load characteristics were not considered. For reducing the computational effort of the ESD optimization problem, a decomposition method based on a time-scale separation idea was developed. Furthermore, a physical model for moist air was derived. Based on this model, the ESD method was modified for integrating turbine inlet air cooling.

Advantages

Using the introduced method for the design of multi-modal on-site energy systems has several advantages: First of all, the described method enables the integration of considerably detailed energy converter models including part-load efficiencies. Due to more accurate models, future business models could also include performance guarantees. This Thesis showed that significant cost savings could be achieved by optimizing the on-site generation. Opposed to engineering rules of thumps, *proofed* optimal designs can be achieved (according to the given input data). Furthermore, the method can be automated and human errors can be reduced to a minimum. Because of that, a tool derived from this method could be used not only exclusively by technical experts and significant cost savings in designing energy systems could be achieved.

Limitations

The ESD method could also be used with 15 min time steps instead of the hourly time steps used in the case study in this Thesis. However, computation time would increase manifold. In this Thesis, the restriction to 1 h time steps introduced virtual storages. Although the decomposition method reduced the computational effort required for ESD significantly, its results are to some extend only near-optimal. In addition to this, the analysis in this study was limited to one representative year. For improvements, a longer planning horizon over multiple years should be considered.

5.1.2 Conclusions from the use cases

Based on synthetic load profile generation models for airports, business parks and university campuses, use cases for thirteen locations around the world were defined. The

results affirm the importance of cogeneration and trigeneration systems on site. These systems have the ancillary effect of reducing the primary energy usage. Furthermore, the airport case study showed that renewable energy converters, such as photovoltaic, are economically attractive today at a multitude of locations even without designated feed-in tariffs. Thermal energy storages, in particular hot water storages and chilled water storages, offer an opportunity for demand-side management of heating and cooling loads (peak shaving and load shifting). With the former, the capacity of energy converters or demand charges can be reduced. The latter enables shifting peak loads to off-peak times. Because with the presented ESD method multi-modal energy systems are considered already in the design stage, the demand-side management savings potential can be fully recognized early in the planning phase. Electrochemical energy storages (here, lithium-ion batteries) were not economically attractive under the given assumptions, even at substantially lower specific capital costs for the system (300 $/kWh). Including other use cases, such as operating reserve markets, may make stationary lithium-ion batteries feasible at higher capital costs. Furthermore, short-term power surges were flattened out by the use of one-hour time steps. Batteries may be necessary for the reliable operation of the on-site electric system, in particular when in island-mode operation.

Given that gas turbines were economically attractive at a particular location, turbine inlet air cooling (TIAC) could augment the power output at peak times and therefore allow the installation of smaller gas turbines or reduce the required additional power supply from other on-site power plants or the power grid. The climatic conditions at a particular location determine the selection of the TIAC method. This Thesis demonstrated that evaporative cooling methods are economically more attractive in arid climates and active cooling methods are rather more attractive in maritime climates.

Last but not least, due to optimized on-site generation, significant cost savings could be achieved at all investigated locations. The cost savings were achieved at the expense of earnings of the utility companies. If everyone was to optimize his own-generation, even at smaller scale (e.g., building level), the assumption of deterministic prices of today cannot hold any longer. Furthermore, if the amount of energy drawn from grids was reduced significantly, the grids could not be financed in the same way as today. However, this also shows that (power) utility companies may have to adjust their business models to stay profitable (e.g., increase the fixed annual fees).

5.2 Outlook

5.2.1 Future development possibilities for the ESD method

In order to determine adequate future boundary conditions, e.g., commodity prices, the detailed project-level ESD method presented in this Thesis could be coupled with national or international grid studies described by rather simplified models. Additionally, further important research questions arise. For example: What are the implications on the design of the national energy system, if several decentralized sites rely heavily on multi-modal on-site generation? How could feasible new business models for utility companies look like?

By increasing the temporal resolution of the energy system design (e.g., seconds instead of one hour), operating reserve markets or other future flexible markets could be modeled and energy storages have further use cases. Hence, they may become economically more attractive. Because of that, the design of the energy system could be changed.

When the ESD method shall be used for city- or district-level applications, the one-node model could be changed to a multi-node model. This requires research in the development of a network model.

For the use cases in this Thesis, redundancy or outage issues of components were not considered and were subject of the post-processing. Ideally, these could be integrated directly in the ESD method; for example, by implementing availability factors and optimally planning scheduled outage times. Unplanned outages could be compensated by checking first for backup grids (e.g., a district heating grid), and if these are not available installing those technologies with the lowest capital costs and capacities sufficient to meet peak demands.

Bringing this all together, the ESD method should be used for a field test to experimentally validate the optimal design results.

Bibliography

2G Energy AG. (2012). *Lastflexible Blockheizkraftwerke*. Heek.

Aboumahboub, T., Schaber, K., Tzscheutschler, P., & Hamacher, T. (2010a). Optimal Configuration of a Renewable-based Electricity Supply Sector. *WSEAS Transactions on Power Systems*, *5*(2), 120–129.

Aboumahboub, T., Schaber, K., Tzscheutschler, P., & Hamacher, T. (2010b). Optimization of the Utilization of Renewable Energy Sources in the Electricity Sector. In *Proceedings of the 5th IASME/WSEAS International Conference on Energy & Environment* (pp. 196–204).

Aboumahboub, T., Schaber, K., Wagner, U., & Hamacher, T. (2012). On the CO2 emissions of the global electricity supply sector and the influence of renewable power-modeling and optimization. *Energy Policy*, *42*, 297–314. http://doi.org/10.1016/j.enpol.2011.11.088

Adamek, F., Arnold, M., & Andersson, G. (2014). On Decisive Storage Parameters for Minimizing Energy Supply Costs in Multicarrier Energy Systems. *IEEE Transactions on Sustainable Energy*, *5*(1), 102–109. http://doi.org/TSTE.2013.2267235a

Advanced Manufacturing Office at U.S. Department of Energy. (2012). *Upgrade Boilers with Energy-Efficient Burners*. Washington, DC, USA. Retrieved from https://www1.eere.energy.gov/manufacturing/tech_assistance/pdfs/steam24_burners.pdf

Aichele, C. (2012). *Smart Energy*. Wiesbaden: Vieweg+Teubner Verlag. http://doi.org/10.1007/978-3-8348-1981-9

Airport Authority Hong Kong. (2015a). Fact Sheets. Retrieved October 9, 2015, from http://www.hongkongairport.com/eng/media/facts-figures/facts-sheets.html

Airport Authority Hong Kong. (2015b). Water Management. Retrieved October 9, 2015, from https://www.hongkongairport.com/eng/sustainability/environmental-management/water-management.html

Al-Ibrahim, A. M., & Varnham, A. (2010). A review of inlet air-cooling technologies for enhancing the performance of combustion turbines in Saudi Arabia. *Applied Thermal Engineering*, *30*(14–15), 1879–1888. http://doi.org/10.1016/j.applthermaleng.2010.04.025

Al-Karaghouli, A., & Kazmerski, L. L. (2012). Comparisons of Technical and Economic Performance of the Main Desalination Processes With and Without Renewable Energy Coupling. In *Proceedings of the World Renewable Energy Forum*. Denver, Colorado.

Alhazmy, M. M., & Najjar, Y. S. H. (2004). Augmentation of gas turbine performance using air coolers. *Applied Thermal Engineering*, *24*(2–3), 415–429. http://doi.org/10.1016/j.applthermaleng.2003.09.006

Ameri, M., & Hejazi, S. H. (2004). The study of capacity enhancement of the Chabahar gas turbine installation using an absorption chiller. *Applied Thermal Engineering*, *24*(1), 59–68. http://doi.org/10.1016/S1359-4311(03)00239-4

Ameri, M., Hejazi, S. H., & Montaser, K. (2005). Performance and economic of the thermal energy storage systems to enhance the peaking capacity of the gas turbines. *Applied Thermal Engineering*, *25*(2–3), 241–251. http://doi.org/10.1016/j.applthermaleng.2004.05.012

American Water. (2009). *Tampa Bay Seawater Desalination Plant*. Retrieved from http://www.amwater.com/files/tampabayseawaterdesalinationplantcasestudy6.16.09.pdf

Anderson, O. E. (1953). *Refrigeration in America: A History of a New Technology and Its Impact*. Princeton: Princeton University Press.

Arizona Public Service Company. (2012a). *Rate Schedule E-34 - Extra Large General Service*. Phoenix, Arizona. Retrieved from https://www.aps.com/library/rates/e-34.pdf

Arizona Public Service Company. (2012b). *Rate Schedule E-35 - Extra Large General Service Time of Use*. Phoenix, Arizona. Retrieved from https://www.aps.com/library/rates/e-35.pdf

Aschmann, V., Effenberger, M., & Gronauer, A. (2011). *BHKW in der Praxis*. *DLR Betreiberseminar Themenbereich Technik*.

ASHRAE. (2009). Climatic Design Information. In *2009 ASHRAE® Handbook - Fundamentals* (p. 14.1-14.46). Atlanta, GA, USA: ASHRAE.

ASHRAE. (2013a). *2013 ASHRAE® Handbook - Fundamentals* (SI Edition). Atlanta, GA, USA: ASHRAE.

ASHRAE. (2013b). ASHRAE Equipment Life Expectancy chart. Retrieved from http://www.culluminc.com/wp-content/uploads/2013/02/ASHRAE_Chart_HVAC_Life_Expectancy 1.pdf

Association for the Advancement of Sustainability in Higher Education. (2012). Top Ten Solar Photovoltaic Installations Lists. Retrieved April 8, 2016, from http://www.aashe.org/resources/campus-solar-photovoltaic-installations/top10/

ASUE. (2014). *BHKW-Kenndaten 2014/2015*. Berlin.

Austin Energy. (2014). *Commercial and Industrial Rates*. Austin, TX, USA.

Australian Energy Market Operator. (2016). Aggregated Price & Demand: 2011 - 2016. Retrieved June 7, 2016, from http://www.aemo.com.au/Electricity/Data/Price-and-Demand/Aggregated-Price-and-Demand-Data-Files/Aggregated-Price-and-Demand-2011-to-2016

Aviso, K. B., Sy, C. L., Ubando, A. T., & Tan, R. R. (2015). Target-oriented robust optimization of polygeneration systems. *Chemical Engineering Transactions*, *45*, 199–204. http://doi.org/10.3303/CET1545034

Baehr, H. D., & Kabelac, S. (2009). *Thermodynamik* (14th ed.). Berlin, Heidelberg: Springer Berlin Heidelberg. http://doi.org/10.1007/978-3-642-00556-5

Balijepalli, V. S. K. M., Pradhan, V., Khaparde, S. A., & Shereef, R. M. (2011). Review of

demand response under smart grid paradigm. *2011 IEEE PES International Conference on Innovative Smart Grid Technologies-India, ISGT India 2011*, 236–243. http://doi.org/10.1109/ISET-India.2011.6145388

Ballester, C., & Furió, D. (2015). Effects of renewables on the stylized facts of electricity prices. *Renewable and Sustainable Energy Reviews*, *52*, 1596–1609. http://doi.org/10.1016/j.rser.2015.07.168

Balmorel. (2014). Balmorel. Retrieved November 24, 2014, from http://www.eabalmorel.dk/

Banat, F. (2007). Economic and technical assessment of desalination technologies. In *From Red Sea to Dead Sea - Water and Energy*. Geneva. Retrieved from http://www.desline.com/Geneva/Banat.pdf

Barigozzi, G., Perdichizzi, A., Gritti, C., & Guaiatelli, I. (2015). Techno-economic analysis of Gas Turbine inlet air cooling for Combined Cycle power plant for different climatic conditions. *Applied Thermal Engineering*, *82*, 57–67. http://doi.org/10.1016/j.applthermaleng.2015.02.049

Basrawi, F., Yamada, T., & Obara, S. (2014). Economic and environmental based operation strategies of a hybrid photovoltaic–microgas turbine trigeneration system. *Applied Energy*, *121*, 174–183. http://doi.org/10.1016/j.apenergy.2014.02.011

Battery University. (n.d.). Can the lead-acid battery compete in modern times? Retrieved April 8, 2016, from http://batteryuniversity.com/learn/article/can_the_lead_acid_battery_compete_in_modern_times

Battery University. (2016a). BU-403: Charging Lead Acid. Retrieved April 3, 2016, from http://batteryuniversity.com/learn/article/charging_the_lead_acid_battery

Battery University. (2016b). BU-409: Charging Lithium-ion. Retrieved April 3, 2016, from http://batteryuniversity.com/learn/article/charging_lithium_ion_batteries

Battke, B. (2015). Enabling investment in energy storage technologies - An assessment of business models. In *Proceedings of the 9th International Renewable Energy Storage Conference*. Duesseldorf, Germany.

Bhattacharyya, S. C., & Timilsina, G. R. (2010). A review of energy system models. *International Journal of Energy Sector Management*, *4*(4), 494–518. http://doi.org/10.1108/17506221011092742

Biegler, L. T., & Grossmann, I. E. (2004). Retrospective on optimization. *Computers and Chemical Engineering*, *28*(8), 1169–1192. http://doi.org/10.1016/j.compchemeng.2003.11.003

Bitzer Kühlmaschinenbau GmbH. (2015a). *Semi-Hermetic Compact Screw Compressors*. Sindelfingen.

Bitzer Kühlmaschinenbau GmbH. (2015b). *Semi-Hermetic Reciprocating Compressors*. Sindelfingen.

Black & Veatch Holding Company. (2012). *Cost and Performance data for Power Generation Technologies*. Retrieved from http://bv.com/docs/reports-studies/nrel-cost-report.pdf

Blain, B. B. (2006). Melting Markets: The Rise and Decline Of the Anglo-Norwegian Ice

Trade, 1850-1920. *Global Economic History Network*, *20*(6).

Blanke, M., Kinnaert, M., Lunze, J., & Staroswiecki, M. (2006). *Diagnosis and Fault-Tolerant Control*. Springer Berlin Heidelberg. http://doi.org/10.1007/978-3-540-35653-0

Board of Water Supply at City & County of Honolulu. (2015). Rates and Charges. Retrieved August 18, 2015, from http://www.hbws.org/cssweb/display.cfm?sid=1175

Bonfiglio, A., Barillari, L., Brignone, M., Delfino, F., Pampararo, F., Procopio, R., … Robba, M. (2013). An optimization algorithm for the operation planning of the University of Genoa smart polygeneration microgrid. In *2013 IREP Symposium Bulk Power System Dynamics and Control - IX Optimization, Security and Control of the Emerging Power Grid* (pp. 1–8). Rethymnon, Greece: IEEE. http://doi.org/10.1109/IREP.2013.6629397

Boyce, M. P. (2012). *Gas Turbine Engineering Handbook* (4th ed.). Waltham, MA, USA: Elsevier Inc.

Bracco, S., Delfino, F., Pampararo, F., Robba, M., & Rossi, M. (2012). A system of systems model for the control of the university of Genoa Smart Polygeneration Microgrid. In *2012 7th International Conference on System of Systems Engineering (SoSE)* (pp. 7–12). IEEE. http://doi.org/10.1109/SYSoSE.2012.6384186

Bracco, S., Delfino, F., Pampararo, F., Robba, M., & Rossi, M. (2013a). Planning and management of sustainable microgrids: The test-bed facilities at the University of Genoa. In *2013 Africon*. Pointe-Aux-Piments: IEEE. http://doi.org/10.1109/AFRCON.2013.6757862

Bracco, S., Delfino, F., Pampararo, F., Robba, M., & Rossi, M. (2013b). The University of Genoa smart polygeneration microgrid test-bed facility: The overall system, the technologies and the research challenges. *Renewable and Sustainable Energy Reviews*, *18*, 442–459. http://doi.org/10.1016/j.rser.2012.10.009

Bracco, S., Dentici, G., & Siri, S. (2013). Economic and environmental optimization model for the design and the operation of a combined heat and power distributed generation system in an urban area. *Energy*, *55*, 1014–1024. http://doi.org/10.1016/j.energy.2013.04.004

Bracco, S., Dentici, G., & Siri, S. (2016). DESOD : A mathematical programming tool to optimally design a distributed energy system. *Energy*, *100*, 298–309. http://doi.org/10.1016/j.energy.2016.01.050

Braunagel, J. (2010). *Entwicklung eines innovativen Kälteversorgungskonzeptes für den Großmarkt Hamburg mit einer für ein Smart Grid optimierten Auslegung und Betriebsweise*. Hamburg University of Applied Sciences. Retrieved from https://www.haw-hamburg.de/fileadmin/user_upload/Forschung/CC4E/Projekte/weitere_Energiethemen/Intelligente_Netze/Diplomarbeit_Johannes_Braunagel.pdf

Bruckner, T., Groscurth, H.-M., & Kümmel, R. (1997). Competition and synergy between energy technologies in municipal energy systems. *Energy*, *22*(10), 1005–1014. http://doi.org/10.1016/S0360-5442(97)00037-6

Brynjolfsson, E., & McAfee, A. (2014). *Second Machine Age: Work, Progress, and*

Prosperity in a Time of Brillant Technologies. Norton & Company.

Business Standard. (2015, April 1). Natural gas price slashed by 7.7% to $4.66 per unit. New Dehli. Retrieved from http://www.business-standard.com/article/economy-policy/natural-gas-price-slashed-by-7-7-to-4-66-per-unit-115033100907_1.html

Câmara de Comercialização de Energia Elétrica. (2016). *Preço Médio da CCEE (R$/MWh)*. Retrieved from https://www.ccee.org.br/portal/faces/pages_publico/o-que-fazemos/como_ccee_atua/precos/precos_medios?_afrLoop=1147292570755651#@?_afrLoop=1147292570755651&_adf.ctrl-state=m3img3nz0_4

Capuder, T., & Mancarella, P. (2014). Techno-economic and environmental modelling and optimization of flexible distributed multi-generation options. *Energy*, *71*, 516–533. http://doi.org/10.1016/j.energy.2014.04.097

Cardona, E., Piacentino, A., & Cardona, F. (2006). Energy saving in airports by trigeneration. Part I: Assessing economic and technical potential. *Applied Thermal Engineering*, *26*(14–15), 1427–1436. http://doi.org/10.1016/j.applthermaleng.2006.01.019

Cardona, E., Sannino, P., Piacentino, A., & Cardona, F. (2006). Energy saving in airports by trigeneration. Part II: Short and long term planning for the Malpensa 2000 CHCP plant. *Applied Thermal Engineering*, *26*(14–15), 1437–1447. http://doi.org/10.1016/j.applthermaleng.2006.01.020

Carrier. (2008). *Kaltwasser-Systeme - Preisliste 2008/2009*.

Carvalho, M., Lozano, M. A., Ramos, J., & Serra, L. M. (2013). Synthesis of trigeneration systems: Sensitivity analyses and resilience. *The Scientific World Journal*, *2013*. http://doi.org/10.1155/2013/604852

Carvalho, M., Serra, L. M., & Lozano, M. A. (2011). Optimal synthesis of trigeneration systems subject to environmental constraints. *Energy*, *36*(6), 3779–3790. http://doi.org/10.1016/j.energy.2010.09.023

Cengiz, M. S., & Mamiş, M. S. (2015). Price-Efficiency Relationship for Photovoltaic Systems on a Global Basis. *International Journal of Photoenergy*, *2015*, 1–12. http://doi.org/10.1155/2015/256101

Center for Energy Economics at University of Texas at Austin, & Instituto Tecnológico y de Estudios Superiores de Monterrey. (2013). *Guide to Electric Power in Mexico*. Retrieved from http://www.beg.utexas.edu/energyecon/2013 E.pdf

Chaplin, M. (2016). Ice phases. Retrieved August 31, 2016, from http://www1.lsbu.ac.uk/water/ice_phases.html

China Energy Group at Lawrence Berkeley National Laboratory. (2014). *Key China Energy Statistics 2014*. Retrieved from http://eetd.lbl.gov/sites/all/files/key_china_energy_stattistics_2014_online.final_.pdf

Choi, D., Lee, M., Cho, K., Jeon, H., & An, J. (2014). Energy Consumption Pattern Analysis by University Building Characteristics for the Composition of Green Campus in Korea. *International Journal of Applied Engineering Research*, *9*(24), 24847–24855.

Chung, D., Davidson, C., Fu, R., Ardani, K., & Margolis, R. (2015). *U.S. Photovoltaic*

Prices and Cost Breakdowns: Q1 2015 Benchmarks for Residential , Commercial, and Utility-Scale Systems. Retrieved from http://www.nrel.gov/docs/fy15osti/64746.pdf

City Gas Pte Ltd. (2015). *Historical town gas tariffs (piped gas) - 2007 to 2015*. Singapore.

City of Cape Town. (2014). *Utility Services - Electricity Services (Consumptive)*. Cape Town, South Africa. Retrieved from https://www.capetown.gov.za/en/electricity/Elec tariffs 201415/Schedule of Consumptive Tariffs.pdf

City of Houston. (2014). *2014 Water & Sewer Rates*. Retrieved from https://edocs.publicworks.houstontx.gov/documents/divisions/resource/ucs/2014_ water_rates.pdf

City of Phoenix. (2014). *Water and Wastewater Utility Bill Comparisons*. Phoenix, Arizona. Retrieved from https://www.phoenix.gov/financesite/Documents/Water and WW Bill Compare April 2014.pdf

Claessen, F. N., & Poutré, H. La. (2014). *Towards a European Smart Energy System - ICT innovation goals and considerations*. Brussels, Belgium.

Clark, J. (2014). Solid-liquid phase diagrams: Salt solution. Retrieved May 11, 2015, from http://www.chemguide.co.uk/physical/phaseeqia/saltsoln.html?_sm_byp=iVVsnvwV kkMvrWMQ

CleaverBrooks. (2010). *Boiler efficiency guide*. Thomasville. Retrieved from http://www.cleaver-brooks.com/reference-center/insights/boiler-efficiency-guide.aspx

Connolly, D., Lund, H., Finn, P., Mathiesen, B. V., & Leahy, M. (2011). Practical operation strategies for pumped hydroelectric energy storage (PHES) utilising electricity price arbitrage. *Energy Policy*, *39*(7), 4189–4196. http://doi.org/10.1016/j.enpol.2011.04.032

Connolly, D., Lund, H., Mathiesen, B. V., & Leahy, M. (2011). The first step towards a 100% renewable energy-system for Ireland. *Applied Energy*, *88*(2), 502–507. http://doi.org/10.1016/j.apenergy.2010.03.006

Connolly, D., Lund, H., Mathiesen, B. V., Pican, E., & Leahy, M. (2012). The technical and economic implications of integrating fluctuating renewable energy using energy storage. *Renewable Energy*, *43*, 47–60. http://doi.org/10.1016/j.renene.2011.11.003

Connolly, D., Lund, H., Mathiesen, B. V., Werner, S., Möller, B., Persson, U., … Nielsen, S. (2014). Heat Roadmap Europe: Combining district heating with heat savings to decarbonise the EU energy system. *Energy Policy*, *65*, 475–489. http://doi.org/10.1016/j.enpol.2013.10.035

Connolly, D., Lund, H., Mathiesen, B. V., & Leahy, M. (2010). A review of computer tools for analysing the integration of renewable energy into various energy systems. *Applied Energy*, *87*(4), 1059–1082. http://doi.org/10.1016/j.apenergy.2009.09.026

Coronas, A., & Bruno, J. C. (2007). Polycity - Cerdanyola / Spain: Integration of Renewables into the DHC Network - Optimisation and Energy Assessment. *1st European Conference on Polygeneration*, 77–92.

Crastan, V. (2010). *Weltweite Energiewirtschaft und Klimaschutz 2009*. Berlin, Heidelberg:

Springer Berlin Heidelberg. http://doi.org/10.1007/978-3-642-10787-0

CU Environmental Center. (2006). *Campus Water Use*. Retrieved from http://www.colorado.edu/ecenter/sites/default/files/attached-files/campus_water_use.pdf

Cummings, R. O. (1949). *The American Ice Harvests: A Historical Study in Technology, 1800 - 1918*. Berkeley and Los Angeles: California University Press.

Daikin. (2014). *Applied Systems - Preisliste*. Brunn am Gebirge, Germany. Retrieved from http://www.daikin.pt/docs/Applied systems catalogue_ECPEN14-400.pdf

Danov, V., Schäfer, J., & Thiem, S. (2016). Desalination of saltwater. Germany. Retrieved from https://www.google.com/patents/WO2016071199A1?cl=en

Dawoud, B., Zurigat, Y. H., & Bortmany, J. (2005). Thermodynamic assessment of power requirements and impact of different gas-turbine inlet air cooling techniques at two different locations in Oman. *Applied Thermal Engineering*, *25*(11–12), 1579–1598. http://doi.org/10.1016/j.applthermaleng.2004.11.007

decentralized energy. (2007, December 18). Two Italian airports use cogen for energy self-sufficiency. *Decentralized Energy*. Retrieved from http://www.decentralized-energy.com/articles/2007/12/two-italian-airports-use-cogen-for-energy-self-sufficiency.html

decentralized energy. (2011a, January 18). Thousandth LM6000 gas turbine shipped. *Decentralized Energy*. Retrieved from http://www.decentralized-energy.com/articles/2011/01/thousandth-lm6000.html

decentralized energy. (2011b, November 1). European airports lead the way to on-site energy supplies. *Decentralized Energy*. Retrieved from http://www.decentralized-energy.com/articles/print/volume-12/issue-6/features/european-airports-lead-the-way-to-on-site-energy-supplies.html

Department of Development and Planning at Aalborg University. (2014). EnergyPLAN - Advanced Energy Systems Analysis Computer Model. Retrieved November 24, 2014, from http://www.energyplan.eu/

Deru, M., Field, K., Studer, D., Benne, K., Griffith, B., Torcellini, P., … Crawley, D. (2011). *U.S. Department of Energy Commercial Reference Building Models of the National Building Stock*. Golden, Colorado. Retrieved from http://www.nrel.gov/docs/fy11osti/46861.pdf

Destro, N., Benato, A., Stoppato, A., & Mirandola, A. (2016). Components design and daily operation optimization of a hybrid system with energy storages. *Energy*, 1–9. http://doi.org/10.1016/j.energy.2016.05.097

Dinçer, İ., & Rosen, M. A. (2011). *Thermal Energy Storage*. Chichester, UK: John Wiley & Sons, Ltd. http://doi.org/10.1002/9780470970751

Dinçer, İ., & Zamfirescu, C. (2012). *Sustainable Energy Systems and Applications*. Boston, MA: Springer US. http://doi.org/10.1007/978-0-387-95861-3

do Nascimento, M. A. R., de Oliveira Rodrigues, L., dos Santos, E. C., Batista Gomes, E. E., Goulart Dias, F. L., Gutirrez Velasques, E. I., & Alexis Miranda Carrillo, R. (2013). Micro Gas Turbine Engine: A Review. In B. Ernesto (Ed.), *Progress in Gas Turbine Performance* (pp. 107–141). InTech. http://doi.org/10.5772/54444

domotec. (2015). *Preisliste 2015*. Retrieved from http://domotec.ch/wp-content/uploads/2014/07/pl-allgemein-d.pdf

Dorfner, J. (2015). Optimal Planning of Urban Infrastructure Networks for Multiple Energy Carriers. In *5th MSE Colloquium*. Munich.

Dorfner, J. (2016). Energy transmission networks at different scales - Method results and limits. In *3rd Science and Energy Seminar*.

Dorfner, J., & Hamacher, T. (2014). Large-scale district heating network optimization. *IEEE Transactions on Smart Grid*, *5*(4), 1884–1891. http://doi.org/10.1109/TSG.2013.2295856

dynamic Energy & Water Solutions. (n.d.). *Kingdom of Saudi Arabia Electricity Tariffs*. Retrieved from http://www.dynamic-ews.com/Tariffs/Electricity Tariffs/KSA.pdf

Economic Consulting Associates. (2009). *The Potential of Regional Power Sector Integration: South African Power Pool Transmission and Trading Case Study*. London, UK. Retrieved from http://www.esmap.org/sites/esmap.org/files/BN004-10_REISP-CD_South African Power Pool-Transmission & Trading.pdf

Education Design Showcase. (2015). East Los Angeles College - 1 Megawatt Photovoltaic Power Facility. Retrieved April 8, 2016, from http://www.educationdesignshowcase.com/view.esiml?pid=209

Ehyaei, M. a., Tahani, M., Ahmadi, P., & Esfandiari, M. (2015). Optimization of fog inlet air cooling system for combined cycle power plants using genetic algorithm. *Applied Thermal Engineering*, *76*, 449–461. http://doi.org/10.1016/j.applthermaleng.2014.11.032

Eicker, U. (2003). *Solar Technologies for Buildings* (1st ed.). West Sussex, England: John Wiley & Sons, Ltd.

Electrical and Mechanical Services Department at The Government of the Hong Kong Special Administrative Region. (2013). Water-cooled Air Conditioning Systems (WACS). Retrieved August 19, 2015, from http://www.emsd.gov.hk/emsd/eng/pee/wacs.shtml

Elimelech, M. (2012). Seawater Desalination. In *2012 NWRI Clarke Prize Conference*. Newport Beach, California. Retrieved from http://www.nwri-usa.org/documents/Elimelech_000.pdf

EMD International A/S. (2013). *How to Guide - Making automatic calculation of the operation strategy in energyPRO*. Aalborg, Denmark. Retrieved from http://www.emd.dk/files/energypro/HowToGuides/Making automatic calculation of the operation strategy in energyPRO.pdf

EMD International A/S. (2014). energyPro. Retrieved November 24, 2014, from http://www.emd.dk/energypro/

ENERCON GmbH. (2015). *ENERCON Product Overview*. Retrieved from http://www.enercon.de/p/downloads/ENERCON_Produkt_en_web_072013.pdf

Energinet.dk, & Energistyrelsen. (2012). *Technology data for energy plants*.

Energy Market Company. (2016). Price Information. Retrieved August 20, 2015, from https://www.emcsg.com/marketdata/priceinformation#priceDataView

Energy Technology Systems Analysis Program. (2014). Overview of TIMES Modelling Tool. Retrieved November 24, 2014, from http://iea-etsap.org/index.php/etsap-tools/model-generators/times

Euroheat & Power. (2013). *Statistics Overview*. Retrieved from http://www.euroheat.org/wp-content/uploads/2016/03/2013-Country-by-country-Statistics-Overview.pdf

EXAIR Corporation. (2016). Price List. Retrieved March 2, 2016, from http://www.exair.com/content/pricelist/exairpricelist.pdf?nwk=1

FannieMae. (2014). *Instructions for Performing a Multifamily Property Condition Assessment - Appendix F: Estimated Useful Life Tables*. Retrieved from https://www.fanniemae.com/content/guide_form/4099f.pdf

Fath, H. E. S., & Ismail, M. A. (2009). Enhancing the Part Load Operational Performance of MSF Desalination Plants. In *Proceedings of the Thirteenth International Water Technology Conference (IWTC 13)* (pp. 1479–1488). Hurghada, Egypt.

Fawcett, A. A. (2010). *EPA Analysis of the American Power Act in the 111th Congress*. Retrieved from http://www.epa.gov/climatechange/economics/economicanalyses.html

Fazlollahi, S., Becker, G., & Maréchal, F. (2014a). Multi-objectives, multi-period optimization of district energy systems: II—Daily thermal storage. *Computers & Chemical Engineering*, *71*, 648–662. http://doi.org/10.1016/j.compchemeng.2013.10.016

Fazlollahi, S., Becker, G., & Maréchal, F. (2014b). Multi-objectives, multi-period optimization of district energy systems: III. Distribution networks. *Computer and Chemical Engineering*, *66*, 82–97. http://doi.org/http://dx.doi.org/10.1016/j.compchemeng.2014.02.018

Fazlollahi, S., Bungener, S. L., Mandel, P., Becker, G., & Maréchal, F. (2014). Multi-objectives, multi-period optimization of district energy systems: I. Selection of typical operating periods. *Computers and Chemical Engineering*, *65*, 54–66. http://doi.org/http://dx.doi.org/10.1016/j.compchemeng.2014.03.005

Fazlollahi, S., Mandel, P., Becker, G., & Maréchal, F. (2012). Methods for multi-objective investment and operating optimization of complex energy systems. *Energy*, *45*(1), 12–22. http://doi.org/10.1016/j.energy.2012.02.046

Federal Energy Regulatory Commission. (2013a). *Southeast Electric Market: Overview and Focal Points*. Retrieved from http://www.ferc.gov/market-oversight/mkt-electric/southeast/2013/10-2013-elec-se-archive.pdf

Federal Energy Regulatory Commission. (2013b). *Southwest Electric Market: Overview and Focal Points*. Retrieved from https://www.ferc.gov/market-oversight/mkt-electric/southwest/2013/10-2013-elec-sw-archive.pdf

Feldman, D., Barbose, G., Margolis, R., James, T., Weaver, S., Darghouth, N., … Wiser, R. (2014). *Photovoltaic System Pricing Trends - Historical, Recent, and Near-Term Projections - 2014 Edition*. Retrieved from http://www.nrel.gov/docs/fy14osti/62558.pdf

Fields, A. (2016). Combined Heat and Power (CHP). Retrieved April 7, 2016, from https://www.wbdg.org/resources/chp.php

Flight Hub Reviews. (2015). Munich International Flight Hub. Retrieved October 9, 2015, from http://flight-hub-reviews.com/munich-international-flight-hub/

Florida Power & Light (FPL). (2015). Business rates, clauses and storm factors - Effective June 2015. Retrieved June 1, 2015, from https://www.fpl.com/rates/pdf/June2015_Business.pdf

Foosnaes, A. H. (2012). *Smart Grid – the Industry Perspective*. Oslo.

Fraport AG Frankfurt Airport Services Worldwide. (2015). *Zahlen, Daten, Fakten 2015 zum Flughafen Frankfurt*. Frankfurt am Main. Retrieved from http://www.fraport.de/content/fraport/de/misc/binaer/presse/publikationen/2015/zahlen--daten--fakten-2015/jcr:content.file/zahlen-daten-fakten-2015.pdf

Fritsch, P., Knaus, W., Merkl, G., Preininger, E., Rautenberg, J., Weiß, M., & Wricke, B. (2010). *Mutschmann/Stimmelmayr Taschenbuch der Wasserversorgung* (15th ed.). Vieweg+Teubner Verlag.

Fuentes-Cortés, L. F., Dowling, A. W., Rubio-Maya, C., Zavala, V. M., & Ponce-Ortega, J. M. (2016). Integrated design and control of multigeneration systems for building complexes. *Energy*, 1–14. http://doi.org/10.1016/j.energy.2016.05.093

Gamou, S., Ito, K., Yokoyama, R., & Yoshida, S. (2004). Structural Optimization of Energy Supply System from Economic Viewpoint. *JSME International Journal*, *47*(2), 173–179.

Gebhardt, M., Kohl, H., & Steinrötter, T. (2002). *Preisatlas - Ableitung von Kostenfunktionen für Komponenten der rationellen Energienutzung*. Duisburg-Rheinhausen.

Geidl, M. (2007). *Integrated Modeling and Optimization of Multi-Carrier Energy Systems*. ETH Zurich. Retrieved from http://e-collection.library.ethz.ch/eserv/eth:29506/eth-29506-02.pdf

Geidl, M., & Andersson, G. (2005). A modeling and optimization approach for multiple energy carrier power flow. In *2005 IEEE Russia Power Tech* (pp. 1–7). IEEE. http://doi.org/10.1109/PTC.2005.4524640

Geidl, M., Koeppel, G., Favre-Perrod, P., Klöckl, B., Andersson, G., & Fröhlich, K. (2007). Energy hubs for the future. *IEEE Power & Energy Magazine*, *5*(1), 24–30.

gfai tech GmbH. (2014). Toolkit for Optimization of Energy Systems. Retrieved November 24, 2014, from http://www.top-energy.de/

Global Water Intel. (2005). *The 2005 GWI Water Tariff Survey*.

Glover, F. (1975). Improved Linear Integer Programming Formulations of Nonlinear Integer Problems. *Management Science*, *22*(4), 455–460.

Gomes, I. (2014). *Brazil: Country of the future or has its time come for natural gas?* Oxford Institute for Energy Studies.

Gordon, J. M., & Ng, K. C. (1995). A general thermodynamic model for Absorption Chillers: Theory and Experiment. *Heat Recovery Systems & CHP*, *15*(1), 73–83.

Graham, B., & Dodd, D. L. (2008). *Security Analysis*. (6th, Ed.). McGraw-Hill Education Ltd.

Green Turbine. (n.d.). GREEN TURBINE™ 1.5 kW. Retrieved April 6, 2016, from

http://www.greenturbine.eu/GT1.html

Guinot, B. (2016). Energy Analysis at the Territory Scale. In *CEA-TUM Summer School 2016*. Frauenchiemsee.

Gurobi Optimization Inc. (2015). Gurobi Optimizer Reference Manual. Retrieved from http://www.gurobi.com

Hamacher, T. (2015). Future of the power system: how can we keep it simple? In *MSE Winter School 2015*. Ohlstadt, Germany.

Hamacher, T., Huber, M., Dorfner, J., Schaber, K., & Bradshaw, A. M. (2013). Nuclear fusion and renewable energy forms: Are they compatible? *Fusion Engineering and Design*, *88*(6–8), 657–660. http://doi.org/10.1016/j.fusengdes.2013.01.074

Hawaiian Electric Company Inc. (2012a). *Schedule P - Large Power Service*. Retrieved from https://www.hawaiianelectric.com/Documents/my_account/rates/hawaiian_electric_rates/heco_rates_sch_p.pdf

Hawaiian Electric Company Inc. (2012b). *Schedule U - Time-of-Use Service*. Retrieved from https://www.hawaiianelectric.com/Documents/my_account/rates/hawaiian_electric_rates/heco_rates_sch_u.pdf

Henning, H.-M., & Palzer, A. (2013). *Energiesystem Deutschland 2050*. Freiburg. Retrieved from http://www.ise.fraunhofer.de/de/veroeffentlichungen/veroeffentlichungen-pdf-dateien/studien-und-konzeptpapiere/studie-energiesystem-deutschland-2050.pdf

Higashi, N. (2009). *Natural Gas in China: Market evolution and strategy*. *Energy markets and security*. Retrieved from https://www.iea.org/publications/freepublications/publication/nat_gas_china.pdf

Hitchin, R., & Knight, I. (2016). Daily energy consumption signatures and control charts for air-conditioned buildings. *Energy and Buildings*, *112*, 101–109. http://doi.org/10.1016/j.enbuild.2015.11.059

HOMER Energy. (2014). HOMER Pro. Retrieved November 24, 2014, from http://www.homerenergy.com/HOMER_pro.html

Hundt, M., Barth, R., Sun, N., Wissel, S., & Voß, A. (2009). *Verträglichkeit von erneuerbaren Energien und Kernenergie im Erzeugungsportfolio - Technische und ökonomische Aspekte*. Retrieved from http://www.ier.uni-stuttgart.de/publikationen/pb_pdf/Hundt_EEKE_Langfassung.pdf

Hurst, T. B. (2008). Top Five Micro Wind Turbines. Retrieved April 6, 2016, from http://cleantechnica.com/2008/03/21/the-five-best-micro-wind-turbines/

Ibrahim, T. K., Rahman, M. M., & Abdalla, A. N. (2011). Improvement of gas turbine performance based on inlet air cooling systems: A technical review, *6*(4), 620–627. http://doi.org/10.5897/IJPS10.563

Indian Energy Exchange. (2016). Area Prices. Retrieved April 5, 2016, from http://www.iexindia.com/marketdata/areaprice.aspx

Ingels, M. (1991). *Willis Haviland Carrier: Father of Air Conditioning* (1st ed.). Carrier Corporation.

International Carbon Action Partnership. (2016). *ETS Detailed Information - Brazil*. Retrieved from https://icapcarbonaction.com/en/?option=com_etsmap&task=export&format=pdf&layout=list&systems[]=79

International Energy Agency. (2012). *Electricity Information*. Luxemburg. Retrieved from http://www.iea.org/media/training/presentations/statisticsmarch/electricityinformation.pdf

International Energy Agency. (2014). *WEIO 2014-Power Generation Investment Assumptions*. Retrieved from http://www.worldenergyoutlook.org/media/weowebsite/2014/weio/WEIO2014PGAssumptions.xlsx

International Energy Agency. (2015). Energy Technology Perspectives (ETP) - Framework Assumptions. Retrieved January 1, 2016, from https://www.iea.org/etp/etpmodel/assumptions/

K + P Architekten und Stadtplaner GmbH. (2015). Flughafen München Terminal 2. Retrieved October 9, 2015, from http://www.kochundpartner.de/cms/projekte/terminal2/kochpartner-terminal2.pdf

Kallrath, J. (2013). *Gemischt-ganzzahlige Optimierung: Modellierung in der Praxis* (2nd ed.). Wiesbaden: Springer Fachmedien Wiesbaden. http://doi.org/10.1007/978-3-658-00690-7

Kallrath, J., Rebennack, S., Pardalos, P. M., & Scheidt, M. (2009). *Optimization in the Energy Industry*. (J. Kallrath, S. Rebennack, P. M. Pardalos, & M. Scheidt, Eds.). Berlin, Heidelberg: Springer Berlin Heidelberg.

Kansai Airports. (2015). Airport Facilities Information. Retrieved October 9, 2015, from http://www.kansai-airport.or.jp/en/map/guidance/

Keirstead, J., Jennings, M., & Sivakumar, A. (2012). A review of urban energy system models: Approaches, challenges and opportunities. *Renewable and Sustainable Energy Reviews*, *16*(6), 3847–3866. http://doi.org/10.1016/j.rser.2012.02.047

Kiley, D. (2009, June 4). Can Ford's "World Car" Bet Pay Off? *BloombergBusinessweek*. Retrieved from http://www.bloomberg.com/news/articles/2009-06-04/can-fords-world-car-bet-pay-off

Kim, J. S., Chen, J., & Garcia, H. E. (2016). Modeling, control, and dynamic performance analysis of a reverse osmosis desalination plant integrated within hybrid energy systems. *Energy*, *112*, 52–66. http://doi.org/10.1016/j.energy.2016.05.050

Københavns Lufthavne A/S. (2015). Water consumption. Retrieved October 9, 2015, from https://www.cph.dk/en/about-cph/csr/Environment-and-energy/water-and-soil/water-consumption/

Konstantin, P. (2013). *Praxisbuch Energiewirtschaft* (3rd ed.). Berlin, Heidelberg: Springer Berlin Heidelberg. http://doi.org/10.1007/978-3-642-37265-0

Krause, T., Andersson, G., Fröhlich, K., & Vaccaro, A. (2011). Multiple-Energy Carriers: Modeling of Production, Delivery, and Consumption. *Proceedings of the IEEE*, *99*(1), 15–27. http://doi.org/10.1109/JPROC.2010.2083610

Kumar, N., Besuner, P. M., Lefton, S. A., Agan, D. D., & Hilleman, D. D. (2012). *Power*

Plant Cycling Costs. Retrieved from http://wind.nrel.gov/public/wwis/aptechfinalv2.pdf

Kummert, M. (2007). *Using GenOpt With TRNSYS 16 and Type 56*. Strathclyde. Retrieved from http://sel.me.wisc.edu/trnsys/demos/genopt-type56.pdf

Lako, P. (2010). *Combined Heat and Power*. Retrieved from http://www.iea-etsap.org/web/e-techds/pdf/e04-chp-gs-gct_adfinal.pdf

Lam, H. L., Klemeš, J. J., Kravanja, Z., & Varbanov, P. S. (2011). Software tools overview: process integration, modelling and optimisation for energy saving and pollution reduction. *Asia-Pacific Journal of Chemical Engineering*, *6*(5), 696–712. http://doi.org/10.1002/apj.469

Lambert, T., Gilman, P., & Lilienthal, P. (2006). Micropower System Modeling with Homer. *Integration of Alternative Sources of Energy*, 379–418. http://doi.org/10.1002/0471755621.ch15

Lancaster University. (2015). Wind Turbine. Retrieved April 8, 2016, from http://www.lancaster.ac.uk/sustainability/low-carbon-technologies/wind-turbine/

Lechler. (2016). Series 166.2. Retrieved March 3, 2016, from http://www.lechler.de/is-bin/intershop.static/WFS/LechlerUS-Shop-Site/LechlerUS-Shop/en_US/PDF/02_produkte/industrie/02_Pneumatic/Series_166.2.pdf

Lechner, C., & Seume, J. (2010). *Stationäre Gasturbinen*. Berlin Heidelberg: Springer-Verlag. http://doi.org/10.1007/978-3-540-92788-4

Lee, T.-S., & Lu, W.-C. (2010). An evaluation of empirically-based models for predicting energy performance of vapor-compression water chillers. *Applied Energy*, *87*(11), 3486–3493. http://doi.org/10.1016/j.apenergy.2010.05.005

Liu, P. (2009). *Modelling and Optimization of Polygeneration Energy Systems*. Imperial College London.

Liu, P., Georgiadis, M. C., & Pistikopoulos, E. N. (2011). Advances in Energy Systems Engineering. *Industrial & Engineering Chemistry Research*, *50*(9), 4915–4926. http://doi.org/10.1021/ie101383h

Liu, P., Gerogiorgis, D. I., & Pistikopoulos, E. N. (2007). Modeling and optimization of polygeneration energy systems. *Catalysis Today*, *127*(1–4), 347–359. http://doi.org/10.1016/j.cattod.2007.05.024

Liu, P., & Pistikopoulos, E. N. (2010). A Multi-Objective Optimization Approach to Polygeneration Energy Systems Design. *AIChE Journal*, *56*(5), 1218–1234. http://doi.org/10.1002/aic

Liu, P., Pistikopoulos, E. N., & Li, Z. (2010). Decomposition Based Stochastic Programming Approach for Polygeneration Energy Systems Design under Uncertainty. *Industrial & Engineering Chemistry Research*, *49*(7), 3295–3305. http://doi.org/10.1021/ie901490g

Liu, W., Lund, H., & Mathiesen, B. V. (2011). Large-scale integration of wind power into the existing Chinese energy system. *Energy*, *36*(8), 4753–4760. http://doi.org/10.1016/j.energy.2011.05.007

López, J. (2012). Combustion Engine vs Gas Turbine: Ramp rate. Retrieved April 6, 2016, from http://www.wartsila.com/energy/learning-center/technical-

comparisons/combustion-engine-vs-gas-turbine-ramp-rate

Lozano, M. a., Carvalho, M., & Serra, L. M. (2011). Allocation of economic costs in trigeneration systems at variable load conditions. *Energy and Buildings*, *43*(10), 2869–2881. http://doi.org/10.1016/j.enbuild.2011.07.002

Lozano, M. A., Ramos, J. C., Carvalho, M., & Serra, L. M. (2009). Structure optimization of energy supply systems in tertiary sector buildings. *Energy and Buildings*, *41*(10), 1063–1075. http://doi.org/10.1016/j.enbuild.2009.05.008

Lozano, M. A., Ramos, J. C., & Serra, L. M. (2010). Cost optimization of the design of CHCP (combined heat, cooling and power) systems under legal constraints. *Energy*, *35*(2), 794–805. http://doi.org/10.1016/j.energy.2009.08.022

Lozano Serrano, M. A., & Saravia, J. R. (2010). Optimal Cogeneration Technology Selection for Residential and Commercial Buildings. *Cogeneration & Distributed Generation Journal*, *25*(4), 8–19. http://doi.org/10.1080/15453669.2010.10132361

Lund, H. (1997). Does Environmental Impact Assessment really support technological change? Analyzing Alternatives to Coal-Fired Power Stations in Denmark. *Environ Impact Assess Rev 1997*, *17*, 357–370.

Lund, H. (2014). *Renewable Energy Systems: A Smart Energy Systems Approach to the Choice and Modeling of 100% Renewable Solutions* (2nd ed.). Elsevier Science.

Lund, H., Andersen, A. N., Østergaard, P. A., Mathiesen, B. V., & Connolly, D. (2012). From electricity smart grids to smart energy systems – A market operation based approach and understanding. *Energy*, *42*(1), 96–102. http://doi.org/10.1016/j.energy.2012.04.003

Lund, H., & Münster, E. (2006). Integrated energy systems and local energy markets. *Energy Policy*, *34*(10), 1152–1160. http://doi.org/10.1016/j.enpol.2004.10.004

Lund, H., & Salgi, G. (2009). The role of compressed air energy storage (CAES) in future sustainable energy systems. *Energy Conversion and Management*, *50*(5), 1172–1179. http://doi.org/10.1016/j.enconman.2009.01.032

Lund, H., Werner, S., Wiltshire, R., Svendsen, S., Thorsen, J. E., Hvelplund, F., & Mathiesen, B. V. (2014). 4th Generation District Heating (4GDH). *Energy*, *68*, 1–11. http://doi.org/10.1016/j.energy.2014.02.089

Lydia, M., Kumar, S. S., Selvakumar, A. I., & Prem Kumar, G. E. (2014). A comprehensive review on wind turbine power curve modeling techniques. *Renewable and Sustainable Energy Reviews*, *30*, 452–460. http://doi.org/10.1016/j.rser.2013.10.030

Mancarella, P. (2014). MES (multi-energy systems): An overview of concepts and evaluation models. *Energy*, *65*, 1–17. http://doi.org/10.1016/j.energy.2013.10.041

Mandri, Y., Rich, A., Mangin, D., Abderafi, S., Bebon, C., Semlali, N., … Bouhaouss, A. (2011). Parametric study of the sweating step in the seawater desalination process by indirect freezing. *Desalination*, *269*(1–3), 142–147. http://doi.org/10.1016/j.desal.2010.10.053

Matar, W., Murphy, F., Pierru, A., & Rioux, B. (2014). *Lowering Saudi Arabia's fuel consumption and energy system costs without increasing end consumer prices*. Retrieved from www.kapsarc.org/research/publications/lowering-saudi-arabias-fuel-consumption-and-energy-system-costs-without-increasing-end-consumer-

prices/ks1403dp02c_optimizing_saudi_energy_system_discussion_paper

Mathiesen, B. V., Lund, H., Connolly, D., Wenzel, H., Østergaard, P. a., Möller, B., … Hvelplund, F. K. (2015). Smart Energy Systems for coherent 100% renewable energy and transport solutions. *Applied Energy*, *145*, 139–154. http://doi.org/10.1016/j.apenergy.2015.01.075

Mathiesen, B. V., Lund, H., & Nørgaard, P. (2008). Integrated transport and renewable energy systems. *Utilities Policy*, *16*(2), 107–116. http://doi.org/10.1016/j.jup.2007.11.007

Mehling, H., & Cabeza, L. F. (2008). *Heat and cold storage with PCM*. Berlin/Heidelberg: Springer-Verlag. http://doi.org/10.1007/978-3-540-68557-9

Mendes, G., Ioakimidis, C., & Ferrão, P. (2011). On the planning and analysis of Integrated Community Energy Systems: A review and survey of available tools. *Renewable and Sustainable Energy Reviews*, *15*(9), 4836–4854. http://doi.org/10.1016/j.rser.2011.07.067

Menon, R. P., Paolone, M., & Maréchal, F. (2013). Study of optimal design of polygeneration systems in optimal control strategies. *Energy*, *55*, 134–141. http://doi.org/10.1016/j.energy.2013.03.070

Meteotest. (2014). *meteonorm - Global Meteorological Database*. Bern, Switzerland. Retrieved from http://www.meteonorm.com/images/uploads/downloads/flyer_meteonorm_7.pdf

Mezher, T., Fath, H., Abbas, Z., & Khaled, A. (2011). Techno-economic assessment and environmental impacts of desalination technologies. *Desalination*, *266*(1–3), 263–273. http://doi.org/10.1016/j.desal.2010.08.035

Miami-Dade Water and Sewer Department. (2014). *Schedule of Rates*. Miami, Florida, USA.

Microgrids at Berkeley Lab. (2016). Distributed Energy Resources Customer Adoption Model. Retrieved May 21, 2016, from https://building-microgrid.lbl.gov/projects/der-cam

Moghaddam, I. G., Saniei, M., & Mashour, E. (2016). A Comprehensive Model for self-scheduling an Energy Hub to Supply Cooling , Heating and Electrical Demands of a building. *Energy*, *94*, 157–170. http://doi.org/10.1016/j.energy.2015.10.137

Möller, B., & Lund, H. (2010). Conversion of individual natural gas to district heating: Geographical studies of supply costs and consequences for the Danish energy system. *Applied Energy*, *87*(6), 1846–1857. http://doi.org/10.1016/j.apenergy.2009.12.001

Moné, C., Smith, A., Maples, B., & Hand, M. (2015). *2013 Cost of Wind Energy Review*. Golden, Colorado. Retrieved from http://www.nrel.gov/docs/fy15osti/63267.pdf

Munich Airport. (2015). General information. Retrieved October 9, 2015, from http://www.munich-airport.de/en/company/facts/allg1/index.jsp

Münster, M., & Lund, H. (2009). Use of waste for heat, electricity and transport—Challenges when performing energy system analysis. *Energy*, *34*(5), 636–644. http://doi.org/10.1016/j.energy.2008.09.001

Mussati, S. F., Barttfeld, M., Aguirre, P. A., & Scenna, N. J. (2008). A disjunctive

programming model for superstructure optimization of power and desalting plants. *Desalination*, *222*(1–3), 457–465. http://doi.org/10.1016/j.desal.2007.01.162

Natural Resources Canada. (2014). RETScreen. Retrieved November 24, 2014, from http://www.nrcan.gc.ca/energy/software-tools/7465

Newcomb, Anderson, & McCormick. (2011). *Strategic Energy Plan - University of Hawai'i at Manoa*.

Ng, K. C., Chua, H. T., Ong, W., Lee, S. S., & Gordon, J. M. (1997). Diagnostics and Optimization of Reciprocating Chillers: Theory and Experiment. *Applied Thermal Engineering*, *17*(3), 263–276.

Niemi, R., Mikkola, J., & Lund, P. D. (2012). Urban energy systems with smart multi-carrier energy networks and renewable energy generation. *Renewable Energy*, *48*, 524–536. http://doi.org/10.1016/j.renene.2012.05.017

NUS Consulting Group. (2014). *2013 - 2014 International Electricity & Natural Gas Report & Price Survey*. Retrieved from http://www.bizcommunity.com/f/1411/NUS_Energy_Market_Survey_-_Report_2014_(Final).pdf

Office of Energy Efficiency & Renewable Energy at Department of Energy. (n.d.). Furnaces and Boilers. Retrieved April 3, 2016, from http://energy.gov/energysaver/furnaces-and-boilers

OMI-Polo Español S.A. (2015). Evolución del Mercado de Energía Eléctrica. Retrieved March 4, 2016, from http://www.omie.es/inicio

Ong, S., Campbell, C., Denholm, P., Margolis, R., & Heath, G. (2013). *Land-Use Requirements for Solar Power Plants in the United States*. Golden, Colorado. Retrieved from http://www.nrel.gov/docs/fy13osti/56290.pdf

Orecchini, F., & Santiangeli, A. (2011). Beyond smart grids – The need of intelligent energy networks for a higher global efficiency through energy vectors integration. *International Journal of Hydrogen Energy*, *36*(13), 8126–8133. http://doi.org/10.1016/j.ijhydene.2011.01.160

Ortiga, J. (2010). *Modelling Environment for the Design and Optimisation of Energy Polygeneration Systems*. Universitat Rovira i Virgili.

Ortiga, J., Bruno, J. C., & Coronas, A. (2008). Multi-objective optimization of polygeneration systems integrated in district heating and cooling networks. In B. Braunschweig & X. Joulia (Eds.), *18th European Symposium on Computer Aided Process Engineering - ESCAPE 18*.

Ortiga, J., Bruno, J. C., & Coronas, A. (2011). Selection of typical days for the characterisation of energy demand in cogeneration and trigeneration optimisation models for buildings. *Energy Conversion and Management*, *52*(4), 1934–1942. http://doi.org/10.1016/j.enconman.2010.11.022

Ortiga, J., Bruno, J. C., & Coronas, A. (2012). Operational Experience of the Polygeneration Plant in Parc de l'Alba (Spain): Start-up and First Results. In *Utility Exhibition on Power and Energy Systems: Issues & Prospects for Asia (ICUE), 2011 International Conference* (pp. 1–5). IEEE.

Ortiga, J., Bruno, J. C., & Coronas, A. (2013). Operational optimisation of a complex

trigeneration system connected to a district heating and cooling network. *Applied Thermal Engineering*, *50*(2), 1536–1542. http://doi.org/10.1016/j.applthermaleng.2011.10.041

Ortiga, J., Bruno, J. C., Coronas, A., & Grossman, I. E. (2007). Review of optimization models for the design of polygeneration systems in district heating and cooling networks. In *17th European Symposium on Computer Aided Process Engineering*.

Østergaard, P. A., & Lund, H. (2011). A renewable energy system in Frederikshavn using low-temperature geothermal energy for district heating. *Applied Energy*, *88*(2), 479–487. http://doi.org/10.1016/j.apenergy.2010.03.018

Ouda, O. K. M. (2013). Review of Saudi Arabia Municipal Water Tariff. *World Environment*, *3*(2), 66–70. http://doi.org/10.5923/j.env.20130302.05

Papageorgiou, M., Leibold, M., & Buss, M. (2012). *Optimierung* (3rd ed.). Berlin, Heidelberg: Springer Berlin Heidelberg. http://doi.org/10.1007/978-3-540-34013-3

Parisio, A., Del Vecchio, C., & Vaccaro, A. (2012). A robust optimization approach to energy hub management. *International Journal of Electrical Power & Energy Systems*, *42*(1), 98–104. http://doi.org/10.1016/j.ijepes.2012.03.015

Parker, J., Cropper, P., & Shao, L. (2012). A Calibrated Whole Building Simulation Approach to Assessing Retrofit Options for Birmingham Airport. In *First Building Simulation and Optimization Conference* (pp. 49–56). Loughborough, UK: IBPSA-England.

Peel, M. C., Finlayson, B. L., & McMahon, T. A. (2007). Updated world map of the Köppen-Geiger climate classification. *Hydrol. Earth Syst. Sci.*, *11*, 1633–1644. Retrieved from www.hydrol-earth-syst-sci.net/11/1633/2007/

Peneva, A. (2014, September 23). Milan airport' s tri-generation profits soar. *Decentralized Energy*. Retrieved from http://www.decentralized-energy.com/articles/print/volume-15/issue-5/features/milan-airport-s-tri-generation-profits-soar.html

Piacentino, A., & Barbaro, C. (2013). A comprehensive tool for efficient design and operation of polygeneration-based energy µgrids serving a cluster of buildings. Part II: Analysis of the applicative potential. *Applied Energy*, *111*, 1222–1238. http://doi.org/10.1016/j.apenergy.2012.11.079

Piacentino, A., Barbaro, C., Cardona, F., Gallea, R., & Cardona, E. (2013). A comprehensive tool for efficient design and operation of polygeneration-based energy µgrids serving a cluster of buildings. Part I: Description of the method. *Applied Energy*, *111*, 1204–1221. http://doi.org/10.1016/j.apenergy.2012.11.078

Piacentino, A., & Cardona, F. (2008). An original multi-objective criterion for the design of small-scale polygeneration systems based on realistic operating conditions. *Applied Thermal Engineering*, *28*(17–18), 2391–2404. http://doi.org/10.1016/j.applthermaleng.2008.01.017

Plank, R. (1959). Sorptionskältemaschinen. In *Handbuch der Kältetechnik*.

Plura, S. (2008). *Entwicklung einer zweistufigen Absorptionskältemaschine zur effizienten Kraft-Wärme-Kälte-Kopplung*. TU München. Retrieved from http://deposit.ddb.de/cgi-bin/dokserv?idn=99198384x

Powell, K. M., Kim, J. S., Cole, W. J., Kapoor, K., Mojica, J. L., Hedengren, J. D., & Edgar, T. F. (2016). Thermal energy storage to minimize cost and improve efficiency of a polygeneration district energy system in a real-time electricity market. *Energy*, *113*, 52–63. http://doi.org/10.1016/j.energy.2016.07.009

Prenzel, M. (2015). *Experimentelle Untersuchung einer Eisspeicher-integrierten Meerwasserentsalzung an einer selbst konzipierten Versuchsanlage*. Technische Hochschule Nürnberg Georg Simon Ohm.

problogic. (2013). America's largest commercial airports by acreage. Retrieved June 8, 2016, from https://panethos.wordpress.com/2013/01/15/americas-largest-commercial-airports-by-acreage/

Rahman, M. S., Ahmed, M., & Chen, X. D. (2006). Freezing-Melting Process and Desalination: I. Review of the State of the Art. *Separation & Purification Reviews*, *35*(2), 59–96. http://doi.org/10.1080/15422110600671734

Raindrops Water Technologies. (n.d.). Industrial RO Plant. Retrieved April 8, 2016, from http://www.roplant.net/industrial-ro-plant.html

Raths, S., Koopmann, S., Müller, C., Meinerzhagen, A., Falke, T., Cramer, M., … Schnettler, A. (2015). The Energy System Development Plan (ESDP). In *ETG Kongress*. Bonn. Retrieved from http://floriansteinke.net/papers/VDE_ESDP_Poster.pdf

Razak, A. M. Y. (2007). *Industrial gas turbines: Performance and operability*. Cambridge, UK: Woodhead Publishing Limited.

Recknagel, H., Sprenger, E., & Albers, K.-J. (2014). *Taschenbuch für Heizung + Klima Technik Band 1* (77th ed.). Deutscher Industrieverlag.

Red Energy. (2015a). *Living Energy Saver - Business - Energy Made Easy Reference RED21871MS*.

Red Energy. (2015b). *Standing Offer - Business - Energy Made Easy Reference RED79307SS*.

Rehfeldt, K., Wallasch, A.-K., & Lüers, S. (2013). *Kostensituation der Windenergie an Land in Deutschland*. Varel. Retrieved from https://www.wind-energie.de/sites/default/files/download/publication/kostensituation-der-windenergie-land-deutschland/20140730_kostensituation_windenergie_land.pdf

Rekioua, D. (2014). *Wind Power Electric Systems*. London: Springer London. http://doi.org/10.1007/978-1-4471-6425-8

Rich, A., Mandri, Y., Mangin, D., Rivoire, A., Abderafi, S., Bebon, C., … Veesler, S. (2012). Sea water desalination by dynamic layer melt crystallization: Parametric study of the freezing and sweating steps. *Journal of Crystal Growth*, *342*(1), 110–116. http://doi.org/10.1016/j.jcrysgro.2011.03.061

Rizzuti, L., Ettouney, H. M., & Cipollina, A. (2007). *Solar Desalination for the 21st Century*. (L. Rizzuti, H. M. Ettouney, & A. Cipollina, Eds.). Dordrecht: Springer Netherlands. http://doi.org/10.1007/978-1-4020-5508-9

Rubio-Maya, C., Uche-Marcuello, J., Martínez-Gracia, A., & Bayod-Rújula, A. A. (2011). Design optimization of a polygeneration plant fuelled by natural gas and renewable energy sources. *Applied Energy*, *88*(2), 449–457.

http://doi.org/10.1016/j.apenergy.2010.07.009

Rubio-Maya, C., Uche, J., & Martínez, A. (2011). Sequential optimization of a polygeneration plant. *Energy Conversion and Management*, *52*(8–9), 2861–2869. http://doi.org/10.1016/j.enconman.2011.01.023

Ruf, H., Funk, D., Stakic, D., Ditz, K., Neuchel, E., Heilscher, G., & Meier, F. (2014). *OPtimising Hybrid Energy grids for smart citieS - WP3 Monitoring and System Analysis*. Retrieved from http://www.orpheus-project.eu/images/pdf/D3_2_revised.pdf

Russell, S., & Norvig, P. (2012). *Künstliche Intelligenz - Ein moderner Ansatz* (3rd ed.). Pearson Studium.

Sachan, A. K. (2012). *Study of the Integration of District Heating and Cooling with an Electro-Thermal Energy Storage System*. École Polytechnique Fédérale de Lausanne.

Saif, Y., & Almansoori, A. (2016). A capacity expansion planning model for integrated water desalination and power supply chain problem. *Energy Conversion & Management*, *122*, 462–476. http://doi.org/10.1016/j.enconman.2016.06.011

San Diego Gas & Electric Company. (2013). *San Diego Community College District*. San Diego, CA. Retrieved from https://www.sdge.com/sites/default/files/documents/223488684/2013 Energy Showcase Case Study - SDCCD FINAL FOR WEB 050313.pdf?nid=5156

Sanaye, S., Fardad, A., & Mostakhdemi, M. (2011). Thermoeconomic optimization of an ice thermal storage system for gas turbine inlet cooling. *Energy*, *36*(2), 1057–1067. http://doi.org/10.1016/j.energy.2010.12.002

Sasakura Engineering Co. Ltd. (n.d.). Seawater Desalination Technology. Retrieved April 8, 2016, from http://www.sasakura.co.jp/e/products/water/103.html#p105

Sauer, D. U. (2016). Lithium-ion batteries become the benchmark for stationary applications – Markets, players, prices, technology. In *10th International Renewable Energy Storage Conference*. Dusseldorf: EUROSOLAR.

Saving Water Aquarista. (2014). Cape Town water and sanitation tariff 2014 to 2015. Retrieved August 18, 2015, from http://www.savingwater.co.za/2014/05/03/13/cape-town-water-and-sanitation-tariff-2014-to-2015/

Schaber, K. (2013). *Integration of Variable Renewable Energies in the European power system: a model-based analysis of transmission grid extensions and energy sector coupling*. Technische Universität München.

Schaber, K., Steinke, F., & Hamacher, T. (2012). Transmission grid extensions for the integration of variable renewable energies in Europe: Who benefits where? *Energy Policy*, *43*, 123–135. http://doi.org/10.1016/j.enpol.2011.12.040

Schaber, K., Steinke, F., Mühlich, P., & Hamacher, T. (2012). Parametric study of variable renewable energy integration in Europe: Advantages and costs of transmission grid extensions. *Energy Policy*, *42*, 498–508. http://doi.org/10.1016/j.enpol.2011.12.016

Schlesinger, M., Lindenberger, D., & Lutz, C. (2014). *Entwicklung der Energiemärkte – Energiereferenzprognose*. Retrieved from

http://www.bmwi.de/BMWi/Redaktion/PDF/Publikationen/entwicklung-der-energiemaerkte-energiereferenzprognose-endbericht,property=pdf,bereich=bmwi2012,sprache=de,rwb=true.pdf

Schmid, W. (2014, June 17). Speicher beleben KWK-Markt. *Elektro.net*. Retrieved from http://www.elektro.net/36709/speicher-beleben-kwk-markt/

Schneider, G. F. (2014). *Optimization of Distributed Energy Supply Systems by Branch-and-Price*. RWTH Aachen.

Schröder, A., Kunz, F., Meiss, J., Mendelevitch, R., & von Hirschhausen, C. (2013). *Current and Prospective Costs of Electricity Generation until 2050*. Berlin. Retrieved from https://www.diw.de/documents/publikationen/73/diw_01.c.424566.de/diw_datadoc_2013-068.pdf

Siemens AG. (2005). *SGT-200 Industrial Gas Turbine*. New Jersey, USA.

Siemens AG. (2009a). *SGT-300 Industrial Gas Turbine*. Erlangen, Germany.

Siemens AG. (2009b). *SGT-400 Industrial Gas Turbine*. Erlangen, Germany. Retrieved from http://www.energy.siemens.com/mx/pool/hq/power-generation/gas-turbines/SGT-400/Brochure Gas Turbine SGT-400 for Power Generation.pdf

Siemens AG. (2014). *SGT-800 Gas Turbine*. Erlangen, Germany.

Siemens AG. (2015). *SGT-750 Gas Turbine - Proven technology. Verified results.* Erlangen, Germany.

Siemens AG. (2016). *SGT-8000H gas turbine series – proven in commercial operations*. Erlangen, Germany. Retrieved from http://www.energy.siemens.com/hq/pool/hq/SGT-8000H_Gas_Turbine_series_EN.pdf

Singapore District Cooling Pte Ltd. (2015). *Tariffs for District Cooling Service with Effect from 1 May 2015*. Singapore. Retrieved from http://www.singaporepower.com.sg/irj/go/km/docs//wpccontent/Sites/Singapore District Cooling/Site Content/Overview/documents/SDC change of tariff wef 1 May 15.pdf

Singapore Government. (2015). Water Pricing in Singapore. Retrieved August 18, 2015, from http://www.pub.gov.sg/general/Pages/WaterTariff.aspx

Singapore Power. (2016). *Electricity Tariff (2010-2016)*. Singapore. Retrieved from http://www.singaporepower.com.sg/irj/go/km/docs/wpccontent/Sites/SP Services/Site Content/Tariffs/documents/Historical Electricity Tariff.pdf

Skoplaki, E., & Palyvos, J. A. (2009). On the temperature dependence of photovoltaic module electrical performance: A review of efficiency/power correlations. *Solar Energy*, *83*(5), 614–624. http://doi.org/10.1016/j.solener.2008.10.008

Söderman, J., & Pettersson, F. (2006). Structural and operational optimisation of distributed energy systems. *Applied Thermal Engineering*, *26*(13), 1400–1408. http://doi.org/10.1016/j.applthermaleng.2005.05.034

SOLAIR. (n.d.). Absorption Chillers. Retrieved April 7, 2016, from http://www.solair-project.eu/143.0.html

Solaranlagen-Portal. (2015). Modulpreise für Photovoltaik Anlagen. Retrieved March 4, 2016, from http://www.solaranlagen-portal.com/solar/solaranlage/preise/modulpreise

Stadler, M. (2016). *DER-CAM - Decision support tool for decentralized energy systems*.

Stadler, P., Ashouri, A., & Maréchal, F. (2016). Model-based Optimization of Distributed and Renewable Energy Systems in Buildings. *Energy and Buildings*, *120*, 103–113. http://doi.org/10.1016/j.enbuild.2016.03.051

Steinke, F., Wolfrum, P., & Hoffmann, C. (2013). Grid vs. storage in a 100% renewable Europe. *Renewable Energy*, *50*, 826–832. http://doi.org/10.1016/j.renene.2012.07.044

Sterner, M., & Stadler, I. (2014). *Energiespeicher- Bedarf, Technologien, Integration*. Berlin Heidelberg: Springer Vieweg. http://doi.org/10.1007/978-3-642-37380-0

Stovall, T. K., & Tomlinson, J. J. (1990). *Commercial Cool Storage Laboratory Test Procedure*. Oak Ridge, TN, USA.

Sydney Airport. (2009). Water Management at Sydney Airport. Retrieved October 9, 2015, from http://www.sydneyairport.com.au/corporate/~/media/files/corporate/about us/fact sheets/water management.pdf

the carbon report. (2016). How will the draft carbon tax bill affect your business? Retrieved April 12, 2016, from http://www.thecarbonreport.co.za/the-proposed-south-african-carbon-tax/

The Engineering Toolbox. (2015). Metabolic Heat Gain from Persons. Retrieved October 9, 2015, from http://www.engineeringtoolbox.com/metabolic-heat-persons-d_706.html

The National Renewable Energy Laboratory. (2004). *How much land will PV need to supply our electricity?* Washington, DC, USA. Retrieved from http://www.nrel.gov/docs/fy04osti/35097.pdf

The National Renewable Energy Laboratory. (2016). Distributed Generation Renewable Energy Estimate of Costs. Retrieved April 6, 2016, from http://www.nrel.gov/analysis/tech_lcoe_re_cost_est.html

The Wall Street Journal. (2015). U.S.-dollar foreign-exchange rates in late New York trading (08/18/2015). Retrieved August 19, 2015, from http://online.wsj.com/mdc/public/page/2_3021-forex.html

The World Bank. (2005). *Mexico Infrastructure Public Expenditure Review (IPER)*. Retrieved from https://openknowledge.worldbank.org/bitstream/handle/10986/8309/3348310MX.pdf

The World Bank. (2015). *Request for expression of interest for selection # 1189177 - World Bank Urban and Energy Departments Terms of Reference Resource (Energy & Water) Efficiency & Rooftop Solar PV for Schools in Rio de Janeiro*.

The World Bank. (2016). Air transport, passengers carried. Retrieved January 1, 2016, from http://data.worldbank.org/indicator/IS.AIR.PSGR

Thiem, S., Born, A., Danov, V., Schäfer, J., & Hamacher, T. (2016). Optimized Cold

Storage Energy Management - Miami and Los Angeles Case Study. In *Proceedings of the 5th International Conference on Smart Cities and Green ICT Systems* (pp. 271–278). Rome, Italy: SCITEPRESS - Science and and Technology Publications. http://doi.org/10.5220/0005759602710278

Thiem, S., Born, A., Danov, V., Schäfer, J., Hamacher, T., & Vandersickel, A. (2016). Physical and Empirical Modeling of Ice storages for Partial Charge and Discharge. In *Proceedings of the 10th International Renewable Energy Storage Conference*. Duesseldorf, Germany.

Thiem, S., Born, A., Danov, V., Vandersickel, A., Schaefer, J., & Hamacher, T. (2016). Modeling of Ice Storages for Integration in Smart Combined Heat, Cold and Power (CHCP) Plants. In *Proceedings of the Integration of Sustainable Energy Conference*. Nuremberg: convivus.

Thiem, S., Born, A., Danov, V., Vandersickel, A., Schäfer, J., & Hamacher, T. (2017). Automated identification of a complex storage model and hardware implementation of a model-predictive controller for a cooling system with ice storage. *Applied Thermal Engineering*, *121*, 922–940. http://doi.org/10.1016/j.applthermaleng.2017.04.149

Thiem, S., Danov, V., Metzger, M., Schäfer, J., & Hamacher, T. (2017). Project-level multi-modal energy system design - Novel approach for considering detailed component models and example case study for airports. *Energy*, *133*, 691–709. http://doi.org/10.1016/j.energy.2017.05.159

Thiem, S., Danov, V., Schaefer, J., & Hamacher, T. (2015). Ice thermal energy storage (ITES) – Experimental investigation and modeling for integration into multi modal energy system (MMES). In *Proceedings of the 9th International Renewable Energy Storage Conference*. Duesseldorf, Germany.

Thiem, S., Danov, V., Schäfer, J., & Hamacher, T. (2015). Kältemaschinen mit Eisspeicher in Smart Grids - Modellbasierte Betriebsführung zur Kostenoptimierung. In *Deutsche Kälte-Klimatagung 2015*.

Thomson, M. (2005). Energy Efficiency in Reverse Osmosis Systems. In *ADU-RES Seminar*. Hammamet, Tunesia. Retrieved from http://www.adu-res.org/pdf/Loughborough.pdf

Tiwari, A. (2015). Industrial Electricity Tariff Slabs and Rates for all states in India in 2015. Retrieved August 18, 2015, from https://www.bijlibachao.com/news/industrial-electricity-tariff-slabs-and-rates-for-all-states-in-india-in-2015.html

TRNSYS. (2014). Transient System Simulation Tool. Retrieved November 24, 2014, from http://www.trnsys.com/

TUM ENS. (2014). tum-ens/urbs - A linear optimisation model for distributed energy systems. Retrieved November 24, 2014, from https://github.com/tum-ens/urbs

Turbinesinfo. (2016). Steam Turbine Efficiency. Retrieved April 7, 2016, from http://www.turbinesinfo.com/steam-turbine-efficiency/

Tzen, E. (n.d.). *Desalination Technologies (I)*. Retrieved from http://www.cres.gr/kape/publications/pdf/PRODES/DESALINATION_GENERAL_1.pdf

U.S. Energy Information Administration. (2015a). *Annual Energy Outlook 2015 with*

projections to 2040. Washington, DC, USA. Retrieved from http://www.eia.gov/forecasts/aeo/pdf/0383(2015).pdf

U.S. Energy Information Administration. (2015b). *Natural Gas Industrial Price*. Retrieved from http://www.eia.gov/dnav/ng/ng_pri_sum_a_epg0_pin_dmcf_m.htm

U.S. Energy Information Administration. (2015c). U.S. Natural Gas Exports and Re-Exports by Point of Exit. Retrieved August 18, 2015, from http://www.eia.gov/dnav/ng/ng_move_poe2_dcu_nus-nmx_a.htm

U.S. Energy Information Administration. (2016). Wholesale Electricity and Natural Gas Market Data. Retrieved April 5, 2016, from http://www.eia.gov/electricity/wholesale/index.cfm

UC Santa Cruz. (2015). How the campus has managed water. Retrieved August 12, 2015, from http://www.ucsc.edu/conserving-water/ucsc-conservation-history.html

Ünal, A. N., Ercan, S., & Kayakutlu, G. (2015). Optimisation studies on tri-generation: a review. *International Journal of Energy Research*, *39*(10), 1311–1334. http://doi.org/10.1002/er.3342

United Nations General Assembly. (2005). *Resolution adopted by the General Assembly - 60/1. 2005 World Summit Outcome*. Retrieved from http://data.unaids.org/Topics/UniversalAccess/worldsummitoutcome_resolution_24oct2005_en.pdf

Urbaneck, T., Schirmer, U., Platzer, B., Uhlig, U., Göschel, T., & Zimmermann, D. (2005). *Kältespeicher – Überblick zum Stand der Technik*. Chemnitz.

v. Cube, H. L. (1981). *Lehrbuch der Kältetechnik Band 1* (3rd ed.). Karlsruhe: Müller.

van der Geest, P. J. (2009). *Wind Turbines near Airports - Problems and solutions for wind turbine siting in the vicinity of airports*.

VDI-Gesellschaft Verfahrenstechnik und Chemieingenieurwesen. (2010). *VDI Heat Atlas* (2nd ed.). Berlin, Heidelberg: Springer Berlin Heidelberg. http://doi.org/10.1007/978-3-540-77877-6

Viessmann. (2015). *Heating with Gas*. Allendorf, Germany. Retrieved from http://www.nrcan.gc.ca/sites/www.nrcan.gc.ca/files/energy/pdf/energystar/Heating_With_Gas.pdf

Voll, P. (2013). *Automated optimization-based synthesis of distributed energy supply systems*. RWTH Aachen. Retrieved from http://darwin.bth.rwth-aachen.de/opus3/volltexte/2014/4913/

Voll, P., Jennings, M., Hennen, M., Shah, N., & Bardow, A. (2015). The optimum is not enough: A near-optimal solution paradigm for energy systems synthesis. *Energy*, *82*, 446–456. http://doi.org/10.1016/j.energy.2015.01.055

Voll, P., Klaffke, C., Hennen, M., & Bardow, A. (2013). Automated superstructure-based synthesis and optimization of distributed energy supply systems. *Energy*, *50*, 374–388. http://doi.org/10.1016/j.energy.2012.10.045

Voll, P., Lampe, M., Wrobel, G., & Bardow, A. (2012). Superstructure-free synthesis and optimization of distributed industrial energy supply systems. *Energy*, *45*(1), 424–435. http://doi.org/10.1016/j.energy.2012.01.041

Wakui, T., Kawayoshi, H., & Yokoyama, R. (2016). Optimal structural design of residential power and heat supply devices in consideration of operational and capital recovery constraints. *Applied Energy*, *163*, 118–133. http://doi.org/10.1016/j.apenergy.2015.10.154

Wakui, T., Kinoshita, T., & Yokoyama, R. (2014). A mixed-integer linear programming approach for cogeneration-based residential energy supply networks with power and heat interchanges. *Energy*, *68*, 29–46. http://doi.org/10.1016/j.energy.2014.01.110

Wakui, T., & Yokoyama, R. (2011). Optimal sizing of residential gas engine cogeneration system for power interchange operation from energy-saving viewpoint. *Energy*, *36*(6), 3816–3824. http://doi.org/10.1016/j.energy.2010.09.025

Wakui, T., & Yokoyama, R. (2014). Optimal structural design of residential cogeneration systems in consideration of their operating restrictions. *Energy*, *64*, 719–733. http://doi.org/10.1016/j.energy.2013.10.002

Wakui, T., & Yokoyama, R. (2015). Optimal structural design of residential cogeneration systems with battery based on improved solution method for mixed-integer linear programming. *Energy*, *84*, 106–120. http://doi.org/10.1016/j.energy.2015.02.056

Wang, H., & Chen, Q. (2014). Impact of climate change heating and cooling energy use in buildings in the United States. *Energy and Buildings*, *82*, 428–436. http://doi.org/10.1016/j.enbuild.2014.07.034

Water Supplies Department at the Government of the Hong Kong Special Administrative Region. (2015). WSD - Water and Sewage Tariff. Retrieved August 18, 2015, from http://www.wsd.gov.hk/en/customer_services_and_water_bills/water_and_sewage_tariff/water_and_sewage_tariff/

WaterWorld. (2013). Global desalination capacity growing substantially, finds study. Retrieved November 5, 2015, from http://www.waterworld.com/articles/2013/10/global-desalination-capacity-tops-80-million-cubic-meters-per-day.html

Weber, C. I. (2008). *Multi-Objective Design and Optimization of District Energy Systems including Polygeneration Energy Conversion Technologies*. École Polytechnique Fédérale de Lausanne.

Weber, C., & Shah, N. (2011). Optimisation based design of a district energy system for an eco-town in the United Kingdom. *Energy*, *36*(2), 1292–1308. http://doi.org/10.1016/j.energy.2010.11.014

West, J. D., & Braun, J. E. (1999). Performance of a Volumetric Method for Measuring State of Charge for Ice Storage Systems. *ASHRAE Transactions: Research*, 318–324.

Wikipedia. (2015a). Beijing Capital International Airport. Retrieved October 9, 2015, from https://en.wikipedia.org/wiki/Beijing_Capital_International_Airport

Wikipedia. (2015b). Dibrugarh Airport. Retrieved October 9, 2015, from https://en.wikipedia.org/wiki/Dibrugarh_Airport

Wikipedia. (2015c). Dubai International Airport. Retrieved October 9, 2015, from https://en.wikipedia.org/wiki/Dubai_International_Airport

Williams, D. (2012, June 11). Dusseldorf Airport powered by CHP. *Decentralized Energy*. Retrieved from http://www.decentralized-energy.com/articles/2012/06/dusseldorf-airport-powered-by-chp.html

Williams, D. (2013, August 8). Significant contribution from CHP to thriving Munich airport. *Decentralized Energy*. Retrieved from http://www.decentralized-energy.com/articles/2013/08/significant-contribution-from-chp-to-thriving-munich-airport.html

Wirth, H. (2015). *Aktuelle Fakten zur Photovoltaik in Deutschland*. Retrieved from https://www.ise.fraunhofer.de/de/veroeffentlichungen/veroeffentlichungen-pdf-dateien/studien-und-konzeptpapiere/aktuelle-fakten-zur-photovoltaik-in-deutschland.pdf

World Bank Group Climate Change, & Ecofys. (2015a). *Carbon Pricing Watch 2015*. Washington, DC, USA. Retrieved from http://www-wds.worldbank.org/external/default/WDSContentServer/WDSP/IB/2015/08/26/090224b08309a09a/4_0/Rendered/PDF/Carbon0pricing0e0released0late02015.pdf

World Bank Group Climate Change, & Ecofys. (2015b). *State and Trends of Carbon Pricing*. Washington, DC, USA. Retrieved from http://www.worldbank.org/content/dam/Worldbank/document/Climate/State-and-Trend-Report-2015.pdf

Wraneschitz, H. (2014, May 16). Neuer Wärmespeicher macht Kraftwerksbetrieb flexibler. *VDI-Nachrichten.com*. Retrieved from http://www.vdi-nachrichten.com/Technik-Wirtschaft/Neuer-Waermespeicher-Kraftwerksbetrieb-flexibler

Wu, J., Yan, J., Jia, H., Hatziargyriou, N., Djilali, N., & Sun, H. (2016). Integrated Energy Systems. *Applied Energy*, *167*, 155–157. http://doi.org/10.1016/j.apenergy.2016.02.075

Yang, C., Yang, Z., & Cai, R. (2009). Analytical method for evaluation of gas turbine inlet air cooling in combined cycle power plant. *Applied Energy*, *86*(6), 848–856. http://doi.org/10.1016/j.apenergy.2008.08.019

Yang, Y., Zhang, S., & Xiao, Y. (2015a). An MILP (mixed integer linear programming) model for optimal design of district-scale distributed energy resource systems. *Energy*, *90*(0), 1901–1915. http://doi.org/10.1016/j.energy.2015.07.013

Yang, Y., Zhang, S., & Xiao, Y. (2015b). Optimal design of distributed energy resource systems coupled with energy distribution networks. *Energy*, *85*(0), 433–448. http://doi.org/http://dx.doi.org/10.1016/j.energy.2015.03.101

Yeomans, H., & Grossmann, I. E. (1999). A systematic modeling framework of superstructure optimization in process synthesis. *Computers & Chemical Engineering*, *23*(6), 709–731. http://doi.org/10.1016/S0098-1354(99)00003-4

Yokoyama, R. (2007). Optimal Configuration Design of Gas Turbine Cogeneration Plants by a MILP Decomposition Approach. In *Proceedings of ASME Turbo Expo 2007: Power for Land, Sea and Air* (pp. 691–700). Montreal, Canada: ASME.

Yokoyama, R., Fujiwara, K., Ohkura, M., & Wakui, T. (2014). A revised method for robust optimal design of energy supply systems based on minimax regret criterion. *Energy Conversion and Management*, *84*, 196–208. http://doi.org/10.1016/j.enconman.2014.03.045

Yokoyama, R., Hasegawa, Y., & Ito, K. (2002). A MILP decomposition approach to large scale optimization in structural design of energy supply systems. *Energy Conversion and Management*, *43*(6), 771–790. http://doi.org/10.1016/S0196-8904(01)00075-9

Yokoyama, R., & Ito, K. (2004). Effect of Inlet Air Cooling by Ice Storage on Unit Sizing of a Gas Turbine Cogeneration Plant. *Journal of Engineering for Gas Turbines and Power*, *126*(2), 351. http://doi.org/10.1115/1.1692011

Yokoyama, R., & Ito, K. (2006). Performance Evaluation of Gas Turbine Cogeneration Plants Using a Design Optimization Tool: OPS-Design. In *Proceedings of ASME Turbo Expo 2006: Power for Land, Sea and Air* (pp. 713–722). Barcelona, Spain: ASME.

Yokoyama, R., Shinano, Y., Taniguchi, S., Ohkura, M., & Wakui, T. (2014). *Optimization of energy supply systems by MILP branch and bound method in consideration of hierarchical relationship between design and operation*. Berlin-Dahlem.

Younos, T., & Grady, C. A. (2014). *Potable Water - Emerging Global Problems and Solutions*. (T. Younos & C. A. Grady, Eds.). Springer International Publishing. http://doi.org/10.1007/978-3-319-06563-2

Zetzsche, M. (2012). *Experimentelle Untersuchungen und regelungstechnische Optimierung einer Ammoniak / Wasser-Absorptionskältemaschine in Kombination mit einem solar angetriebenen Kühlsystem mit Eisspeicher*. University Stuttgart.

Zhang, J. (2010). *UC Berkeley water usage & conservation study report*. Retrieved from http://sustainability.berkeley.edu/sites/default/files/UC_BERKELEY_WATER_CONSERVATION_REPORT_CACS_2010.pdf

Zhang, Y., & Lu, N. (2013). Demand-side management of air conditioning cooling loads for intra-hour load balancing. In *2013 IEEE PES Innovative Smart Grid Technologies Conference (ISGT)* (pp. 1–6). IEEE. http://doi.org/10.1109/ISGT.2013.6497905

Zhou, Z., Liu, P., Li, Z., & Ni, W. (2013). An engineering approach to the optimal design of distributed energy systems in China. *Applied Thermal Engineering*, *53*(2), 387–396. http://doi.org/10.1016/j.applthermaleng.2012.01.067

Zurigat, Y. H., Dawoud, B., & Bortmany, J. (2006). On the technical feasibility of gas turbine inlet air cooling utilizing thermal energy storage. *International Journal of Energy Research*, *30*(5), 291–305. http://doi.org/10.1002/er.1148

Appendix

A Technology model parameters

Notation of sources

Sources are referenced wherever applicable. When a parameter was validated by an *experiment*, it is indicated accordingly. *Physical models* were developed in MATLAB® and also based on the Reference Fluid Thermodynamic and Transport Properties Database (REFPROP). For some parameters, no references were available. *Assumptions* (probability > 90%) and *guesses* (probability ca. 50%) were made for these parameters.

Renewable energy technologies

Table A.1: Photovoltaic (PV) model parameters.

Variable	Function of	Value / Model	Source
$Q_{\min}$, $Q_{\max}$	-	0 – site-specific kW	Assumption
o_1, o_2	-	18 $/kW/a (13 – 45 $/kW/a)	(Henning & Palzer, 2013; International Energy Agency, 2014; The National Renewable Energy Laboratory, 2016)
n	-	25 a	(Henning & Palzer, 2013; The National Renewable Energy Laboratory, 2016)
u	$\mathbf{T}_{\text{amb}}$, **GHI**	• Temperature coefficient: 0.0045 1/K • Rated power capacity at 1000 W/m² global horizontal irradiance	(Skoplaki & Palyvos, 2009)

Table A.2: Wind turbine (WT) model parameters.

Variable	Function of	Value / Model	Source
$Q_{\min}$, $Q_{\max}$	-	2.6 – site-specific kW	(Hurst, 2008)

Variable	Function of	Value / Model	Source
o_1, o_2	-	33 $/kW/a (31 – 50 $/kW/a)	(Henning & Palzer, 2013; International Energy Agency, 2014; Moné, Smith, Maples, & Hand, 2015; The National Renewable Energy Laboratory, 2016)
n	-	20 a	(The National Renewable Energy Laboratory, 2016)
u	$\mathbf{v}_w$	• Cut-in wind speed: 2 m/s • Rated wind speed: 11.94 m/s • Furling wind speed: 25 m/s • Fitted for Enercon E-82 2 MW onshore wind turbine • Parameters in **Equation (3.50)**: $c_1 = -0.000821\ \mathrm{s}^3/\mathrm{m}^3$, $c_2 = 0.2102\ \mathrm{s/m}$, $c_3 = -43.961\ m/\mathrm{s}$	(ENERCON GmbH, 2015; Lydia et al., 2014)

Energy converters

Table A.3: Gas turbine (GT) model parameters.

Variable	Function of	Value / Model	Source
$Q_{\min}$, $Q_{\max}$	-	15 - ∞ kW	(do Nascimento et al., 2013)
o_1, o_2	-	30 $/kW/a (18 – 40 $/kW/a)	(Henning & Palzer, 2013; International Energy Agency, 2014; Lako, 2010)
n	-	25 a	(Henning & Palzer, 2013; Lako, 2010)
s	-	medium	(Kumar et al., 2012; Schröder et al., 2013)
r^+	-	100 %/h	(Black & Veatch Holding Company, 2012; Lechner &

Variable	Function of	Value / Model	Source
			Seume, 2010)
r^-	-	-100 %/h	(Black & Veatch Holding Company, 2012; Lechner & Seume, 2010)
$\mathbf{u}_{\min}$	Q	• Siemens SGT datasheet models • Physical model for inlet air cooling • Minimum exhaust temperature assumed to 100 °C (for computing thermal efficiency) • TIAC equipment was sized beforehand according to the ambient conditions of the particular location; and costs for the different TIAC methods were determined	(Baehr & Kabelac, 2009; Siemens AG, 2005, 2009a, 2009b, 2014, 2015)
$\mathbf{u}_{\max}$	$\mathbf{T}_{\text{amb}}$, $\mathbf{p}_{\text{amb}}$, $\boldsymbol{\varphi}_{\text{amb}}$, Q		
$\boldsymbol{\eta}$	$\mathbf{T}_{\text{amb}}$, $\mathbf{p}_{\text{amb}}$, $\boldsymbol{\varphi}_{\text{amb}}$, Q, $\mathbf{u}$		

Table A.4: Steam turbine including heat recovery steam generator, condenser and feedwater pump (ST; entire steam cycle) model parameters.

Variable	Function of	Value / Model	Source
$Q_{\min}$, $Q_{\max}$	-	1.5 - ∞ kW	(Green Turbine, n.d.)
o_1, o_2	-	30 $/kW/a (18 – 50 $/kW/a)	(International Energy Agency, 2014; Lako, 2010)
n	-	25 a	(Henning & Palzer, 2013; International Energy Agency, 2014; Lako, 2010)
s	-	high	(Kumar et al., 2012; Schröder et al., 2013)
r^+	-	100 %/h	(Black & Veatch Holding Company, 2012)

Variable	Function of	Value / Model	Source
r^-	-	-100 %/h	(Black & Veatch Holding Company, 2012)
$\mathbf{u}_{\min}$	-	0.38	(Hundt, Barth, Sun, Wissel, & Voß, 2009)
$\mathbf{u}_{\max}$	-	1	Assumption
$\boldsymbol{\eta}$	$\mathbf{u}$	Steam cycle without heat extraction	(Siemens AG, 2016; Turbinesinfo, 2016)

Table A.5: Internal combustion engine (ICE) model parameters.

Variable	Function of	Value / Model	Source
$Q_{\min}$, $Q_{\max}$	-	1 - ∞ kW	(ASUE, 2014)
o_1, o_2	-	30 $/kW/a (21 – 300 $/kW/a)	(Henning & Palzer, 2013; Lako, 2010)
n	-	25 a	(Henning & Palzer, 2013; Lako, 2010)
s	-	low	(Fields, 2016; Kumar et al., 2012; Schröder et al., 2013)
r^+	-	100 %/h	(López, 2012)
r^-	-	-100 %/h	(López, 2012)
$\mathbf{u}_{\min}$	-	0.5	(ASUE, 2014)
$\mathbf{u}_{\max}$	$\mathbf{T}_{\text{amb}}$	Model based on published data (e.g., fits of performance curves provided by literature)	(2G Energy AG, 2012)
$\boldsymbol{\eta}$	$\mathbf{T}_{\text{amb}}$, Q, $\mathbf{u}$		(2G Energy AG, 2012; Aschmann, Effenberger, & Gronauer, 2011; ASUE, 2014)

Table A.6: Gas boiler (GB) model parameters.

Variable	Function of	Value / Model	Source
$Q_{\min}$,	-	1.8 - ∞ kW	(Viessmann, 2015)

Variable	Function of	Value / Model	Source
$Q_{\max}$			
o_1, o_2	-	5.65 $/kW/a (4 – 7.3 $/kW/a)	(Energinet.dk & Energistyrelsen, 2012; Henning & Palzer, 2013)
n	-	20 a	(ASHRAE, 2013b; FannieMae, 2014; Henning & Palzer, 2013)
s	-	low	Guess
r^+	-	100 %/h	Assumption
r^-	-	-100 %/h	Assumption
$\mathbf{u}_{\min}$	-	0.1	(Advanced Manufacturing Office at U.S. Department of Energy, 2012)
$\mathbf{u}_{\max}$	-	1	(Advanced Manufacturing Office at U.S. Department of Energy, 2012)
$\boldsymbol{\eta}$	$\mathbf{u}$	0.974 (100% load); 0.97 (50% load)	(CleaverBrooks, 2010; Office of Energy Efficiency & Renewable Energy at Department of Energy, n.d.; Ruf et al., 2014)

Table A.7: Heat pump (HP) model parameters.

Variable	Function of	Value / Model	Source
$Q_{\min}$, $Q_{\max}$	-	2 - ∞ kW	(Daikin, 2014)
o_1, o_2	-	4 $/kW/a (rHP, 2.1 – 6 $/kW/a); 15 $/kW/a (HP, CHC, 6 – 24.5 $/kW/a)	(Energinet.dk & Energistyrelsen, 2012; Henning & Palzer, 2013)
n	-	15 a (rHP); 20 a (HP, CHC)	(ASHRAE, 2013b; Henning & Palzer, 2013)
s	-	very low	Experiment

Variable	Function of	Value / Model	Source
r^+	-	100 %/h	Experiment
r^-	-	-100 %/h	Experiment
$\mathbf{u}_{\min}$	$\mathbf{T}_{\text{amb}}$	0.25 (decreasing with decreasing $\mathbf{T}_{\text{amb}}$)	(Recknagel, Sprenger, & Albers, 2014)
$\mathbf{u}_{\max}$	$\mathbf{T}_{\text{amb}}$	1 (decreasing with decreasing $\mathbf{T}_{\text{amb}}$)	(Recknagel et al., 2014)
$\boldsymbol{\eta}$	$\mathbf{T}_{\text{amb}}$	• $(\mathbf{T}_{\text{h,supply}} - \mathbf{T}_{\text{amb}})$ fit • Heat supply temperature: 50 °C (rHP); 80 °C (HP, CHC) • Reference COP (@ 40 °C lift): 2.5 (rHP); 4 (HP, CHC)	(Henning & Palzer, 2013; Recknagel et al., 2014)

Table A.8: Electric boiler (EB) model parameters.

Variable	Function of	Value / Model	Source
$Q_{\min}$, $Q_{\max}$	-	1 - ∞ kW	(domotec, 2015)
o_1, o_2	-	1.5 $/kW/a	(Energinet.dk & Energistyrelsen, 2012)
n	-	15 a	(ASHRAE, 2013b)
s	-	none	Assumption
r^+	-	100 %/h	Assumption
r^-	-	-100 %/h	Assumption
$\mathbf{u}_{\min}$	-	0	Assumption
$\mathbf{u}_{\max}$	-	1	Assumption
$\boldsymbol{\eta}$	-	0.99	(Office of Energy Efficiency & Renewable Energy at Department of Energy, n.d.)

Table A.9: Absorption chiller (AC) model parameters.

Variable	Function of	Value / Model	Source
$Q_{\min}$, $Q_{\max}$	-	35 - ∞ kW	(SOLAIR, n.d.)
o_1, o_2	-	2.5 $/kW/a	(Gebhardt, Kohl, & Steinrötter, 2002)
n	-	20 a	(ASHRAE, 2013b; Dinçer & Zamfirescu, 2012)
s	-	low	Guess
r^+	-	100 %/h	Assumption
r^-	-	-100 %/h	Assumption
$\mathbf{u}_{\min}$	-	0.2	(Plura, 2008)
$\mathbf{u}_{\max}$	-	1	(Plura, 2008)
$\boldsymbol{\eta}$	$\mathbf{T}_{amb}$, $\mathbf{u}$	Gordon-Ng absorption chiller model derived from physical model	Physical model; (Gordon & Ng, 1995; Plank, 1959; Plura, 2008; v. Cube, 1981; Voll, 2013)

Table A.10: Compression chiller (CC) model parameters.

Variable	Function of	Value / Model	Source
$Q_{\min}$, $Q_{\max}$	-	1 (cc) / 20 (CC) - ∞ kW	(Carrier, 2008; Daikin, 2014)
o_1, o_2	-	4.4 $/kW/a (rHP); 8.8 $/kW/a (CC)	(Gebhardt et al., 2002)
n	-	15 a (cc); 20 a (CC)	(ASHRAE, 2013b)
s	-	very low	Experiment
r^+	-	100 %/h	Experiment
r^-	-	-100 %/h	Experiment
$\mathbf{u}_{\min}$	$\mathbf{T}_{amb}$	Model derived from	(Bitzer Kühlmaschinenbau

Variable	Function of	Value / Model	Source
$\mathbf{u}_{max}$	$\mathbf{T}_{amb}$	datasheets • CCi, rHP: Reciprocating compressor (Bitzer 4PE-12.F3Y, 134a) • CC0, CHC: Screw compressor (Bitzer CSVH38-290Y, 134a) • Cooling supply temperature: 12 °C (rHP); 8 °C (CC0, CHC); -5 °C (CCi) • Condenser temperature difference: 10 °C (rHP); 3 °C (CC0, CCi)	GmbH, 2015a, 2015b)
$\boldsymbol{\eta}$	$\mathbf{T}_{amb}$, $\mathbf{u}$		

Table A.11: Multi-stage flash distillation (MSFD) model parameters.

Variable	Function of	Value / Model	Source
Q_{min}, Q_{max}	-	4 - ∞ m³/h	(Sasakura Engineering Co. Ltd., n.d.)
o_1, o_2	-	3994.56 $/(m³/h)/a	(Younos & Grady, 2014)
n	-	25 a	Assumption
s	-	medium	Guess
r^+	-	50 %/h	Guess
r^-	-	-50%/h	Guess
$\mathbf{u}_{min}$	-	0.6	(Fath & Ismail, 2009)
$\mathbf{u}_{max}$	-	1	Assumption
$\boldsymbol{\eta}$	$\mathbf{u}$	76.4 kWh_{th}/m^3; 4.25 kWh_{el}/m^3; 3.1 m^3_{sw}/m^3	(Al-Karaghouli & Kazmerski, 2012; Banat, 2007; Mezher, Fath, Abbas, & Khaled, 2011; Rizzuti, Ettouney, & Cipollina, 2007; Thomson, 2005; Tzen, n.d.)

Table A.12: Multiple effect distillation (MED) model parameters.

Variable	Function of	Value / Model	Source
$Q_{\min}$, $Q_{\max}$	-	1.5 - ∞ m³/h	(Sasakura Engineering Co. Ltd., n.d.)
o_1, o_2	-	3994.56 $/(m³/h)/a	(Younos & Grady, 2014)
n	-	25 a	Assumption
s	-	medium	Guess
r^+	-	50 %/h	Guess
r^-	-	-50%/h	Guess
$\mathbf{u}_{\min}$	-	0.6	Assumption
$\mathbf{u}_{\max}$	-	1	Assumption
$\boldsymbol{\eta}$	$\mathbf{u}$	51.4 kWh_{th}/m^3; 2 kWh_{el}/m^3; 3.1 m^3_{sw}/m^3	(Al-Karaghouli & Kazmerski, 2012; Banat, 2007; Mezher et al., 2011; Rizzuti et al., 2007; Thomson, 2005; Tzen, n.d.)

Table A.13: Reverse osmosis (RO) model parameters.

Variable	Function of	Value / Model	Source
$Q_{\min}$, $Q_{\max}$	-	0.1 - ∞ m³/h	(Raindrops Water Technologies, n.d.)
o_1, o_2	-	3293.76 $/(m³/h)/a	(Younos & Grady, 2014)
n	-	30 a	(American Water, 2009)
s	-	low	Guess
r^+	-	100 %/h	Guess
r^-	-	-100 %/h	Guess

Variable	Function of	Value / Model	Source
$\mathbf{u}_{\min}$	-	0.1	Guess
$\mathbf{u}_{\max}$	-	1	Assumption
$\boldsymbol{\eta}$	$\mathbf{u}$	6 kWh_{el}/m^3; 2.5 m^3_{sw}/m^3	(Al-Karaghouli & Kazmerski, 2012; Banat, 2007; Elimelech, 2012; Mezher et al., 2011; Rizzuti et al., 2007; Thomson, 2005; Tzen, n.d.)

Energy storages

Table A.14: Lead-acid battery (LeadAcid) model parameters.

Variable	Function of	Value / Model	Source
$Q_{\min}$, $Q_{\max}$	-	0 - ∞ kWh	Assumption
o_1, o_2	-	0.51 $/kWh/a	(Sterner & Stadler, 2014)
n	-	10 a	(Sterner & Stadler, 2014)
r^+	-	8.34 %/h	(Battery University, n.d., 2016a; Sterner & Stadler, 2014)
r^-	-	-100 %/h	(Battery University, n.d., 2016a; Sterner & Stadler, 2014)
η_{ch}	-	0.815	(Sterner & Stadler, 2014)
η_{dch}	-	0.815	(Sterner & Stadler, 2014)
l	-	0.00708 %/h	(Sterner & Stadler, 2014)

Table A.15: Lithium-ion battery (LiIon) model parameters.

Variable	Function of	Value / Model	Source
$Q_{\min}$, $Q_{\max}$	-	0 - ∞ kWh	Assumption

Variable	Function of	Value / Model	Source
o_1, o_2	-	0.49 $/kWh/a	(Sterner & Stadler, 2014)
n	-	15 a	(Sterner & Stadler, 2014)
r^+	-	100 %/h	(Battery University, 2016b; Sterner & Stadler, 2014)
r^-	-	-100 %/h	(Battery University, 2016b; Sterner & Stadler, 2014)
η_{ch}	-	0.935	(Sterner & Stadler, 2014)
η_{dch}	-	0.935	(Sterner & Stadler, 2014)
l	-	0.00102 %/h	(Sterner & Stadler, 2014)

Table A.16: Hot water storage (HWS) model parameters.

Variable	Function of	Value / Model	Source
Q_{min}, Q_{max}	-	0 - ∞ kWh	Assumption
o_1, o_2	-	0.1025 $/kWh/a	(Sterner & Stadler, 2014)
n	-	40 a	(Henning & Palzer, 2013)
r^+	-	20 %/h	Experiment; (Wraneschitz, 2014)
r^-	-	-20 %/h	Experiment; (Wraneschitz, 2014)
η_{ch}	-	0.98	Experiment
η_{dch}	-	0.98	Experiment
l	-	0.5 %/h	Experiment; (Schmid, 2014)

Table A.17: Chilled water storage (CWS) model parameters.

Variable	Function of	Value / Model	Source
$Q_{\min}$, $Q_{\max}$	-	0 - ∞ kWh	Assumption
o_1, o_2	-	0.1025 $/kWh/a	(Sterner & Stadler, 2014)
n	-	40 a	(Henning & Palzer, 2013)
r^+	-	15 %/h	Assumption; (Wraneschitz, 2014)
r^-	-	-15 %/h	Assumption; (Wraneschitz, 2014)
η_{ch}	-	0.98	Assumption
η_{dch}	-	0.98	Assumption
l	-	0.334 %/h	Assumption; (Schmid, 2014)

Table A.18: Ice thermal energy storage (ITES) model parameters.

Variable	Function of	Value / Model	Source
$Q_{\min}$, $Q_{\max}$	-	0 - ∞ kWh	Assumption
o_1, o_2	-	0.1025 $/kWh/a	(Sterner & Stadler, 2014)
n	-	25 a	Experiment
r^+	-	20 %/h	Experiment
r^-	-	-20 %/h	Experiment
η_{ch}	-	0.98	Experiment
η_{dch}	-	0.98	Experiment
l	-	0.134 %/h	Experiment

Table A.19: Ice-storage-integrated desalination (isiD) model parameters.

Variable	Function of	Value / Model	Source
$Q_{\min}$, $Q_{\max}$	-	0 - ∞ kWh	Assumption
o_1, o_2	-	5 $/kWh/a	Guess
n	-	15 a	Guess
r^+	-	20 %/h	Experiment
r^-	-	-20 %/h	Experiment
η_{ch}	-	0.98	Experiment
η_{dch}	-	0.98 (1666.67 kWh_{th}/m^3; 16 m^3_{sw}/m^3)	Experiment
l	-	0.134 %/h	Experiment

Table A.20: Water storage (WS) model parameters.

Variable	Function of	Value / Model	Source
$Q_{\min}$, $Q_{\max}$	-	0 - ∞ m^3	Assumption
o_1, o_2	-	2.5 $/$m^3$/a	Assumption; (Sterner & Stadler, 2014)
n	-	40 a	(Henning & Palzer, 2013)
r^+	-	100 %/h	Assumption
r^-	-	-100 %/h	Assumption
η_{ch}	-	0.995	Assumption
η_{dch}	-	0.995	Assumption
l	-	0	Assumption

B Specific capital cost functions

Table B.1: Technologies capital costs: References.

Reference	Source
[C01]	(ASUE, 2014)
[C02]	(Braunagel, 2010)
[C03]	(Chung, Davidson, Fu, Ardani, & Margolis, 2015)
[C04]	(Eicker, 2003)
[C05]	(Energinet.dk & Energistyrelsen, 2012)
[C06]	(Feldman et al., 2014)
[C07]	(Gebhardt et al., 2002)
[C08]	(Henning & Palzer, 2013)
[C09]	(International Energy Agency, 2014)
[C10]	(Lako, 2010)
[C11]	(Prenzel, 2015)
[C12]	(Rehfeldt, Wallasch, & Lüers, 2013)
[C13]	(Solaranlagen-Portal, 2015)
[C14]	(Sterner & Stadler, 2014)
[C15]	(Wirth, 2015)
[C16]	(Younos & Grady, 2014)
[C17]	Own fits based on personal communications with and price lists from several manufacturers (e.g., Carrier, Daikin, Calmac, Colibri, Mattes Engineering) (2016)

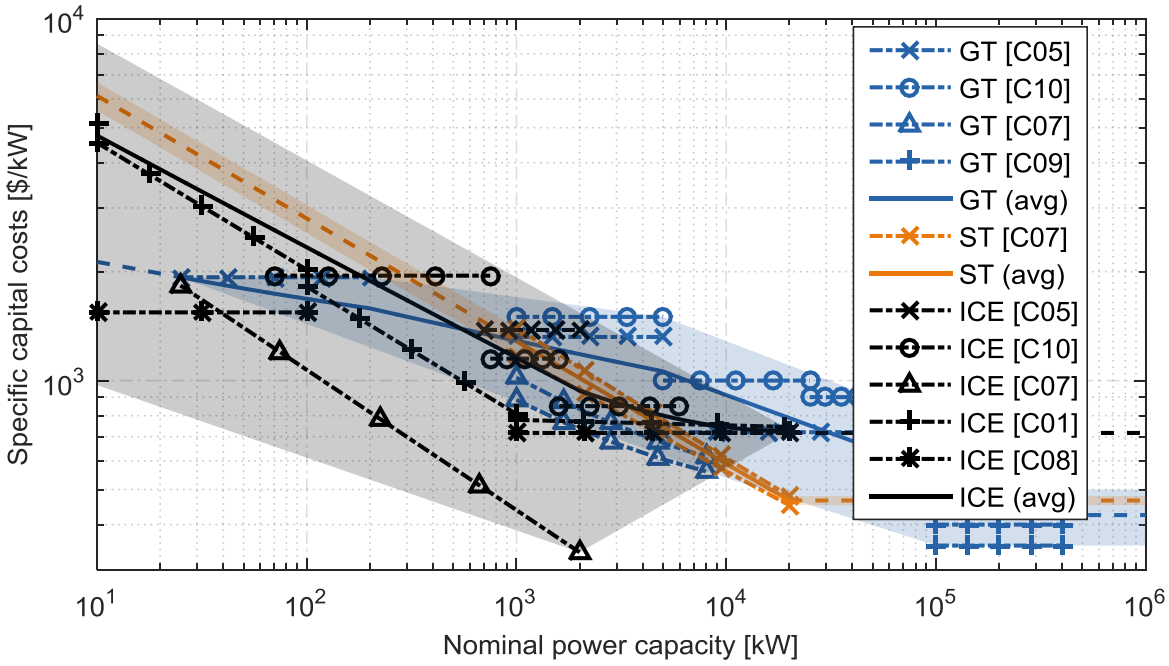

Figure B.1: Specific capital costs for power plants.

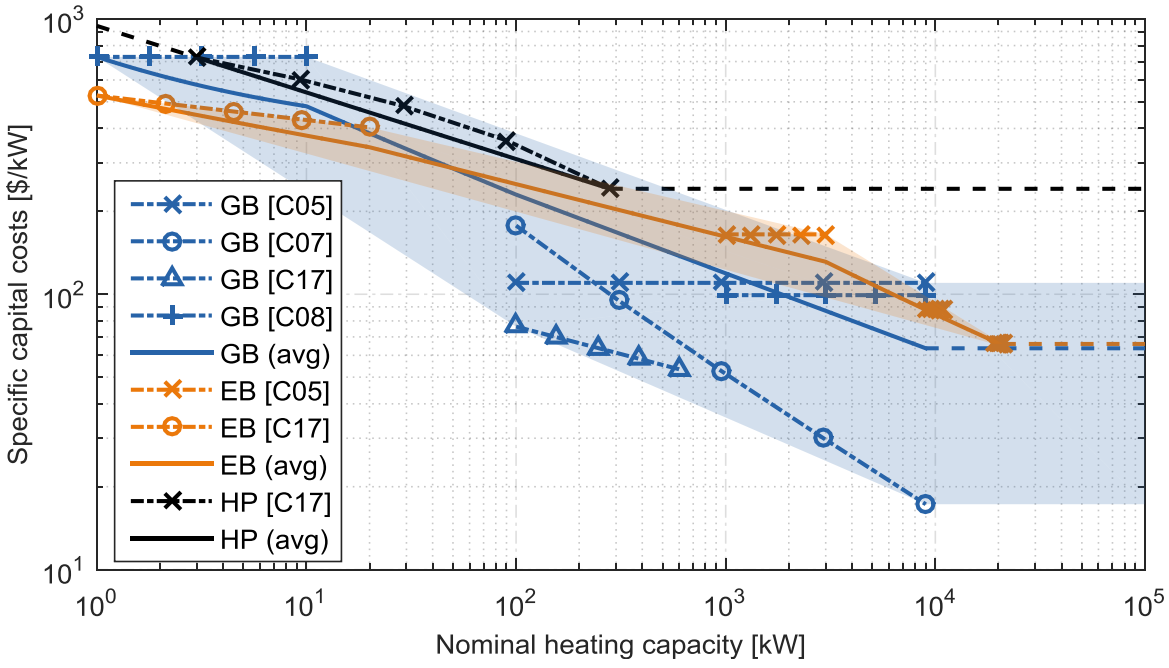

Figure B.2: Specific capital costs for heating technologies.

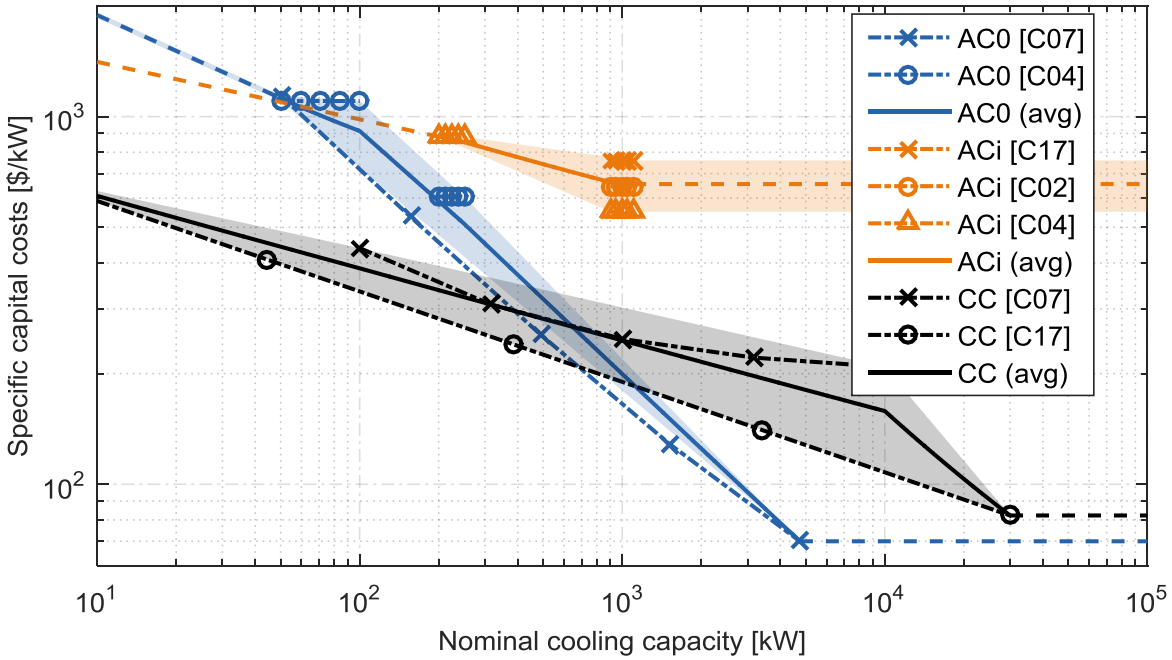

Figure B.3: Specific capital costs for chillers.

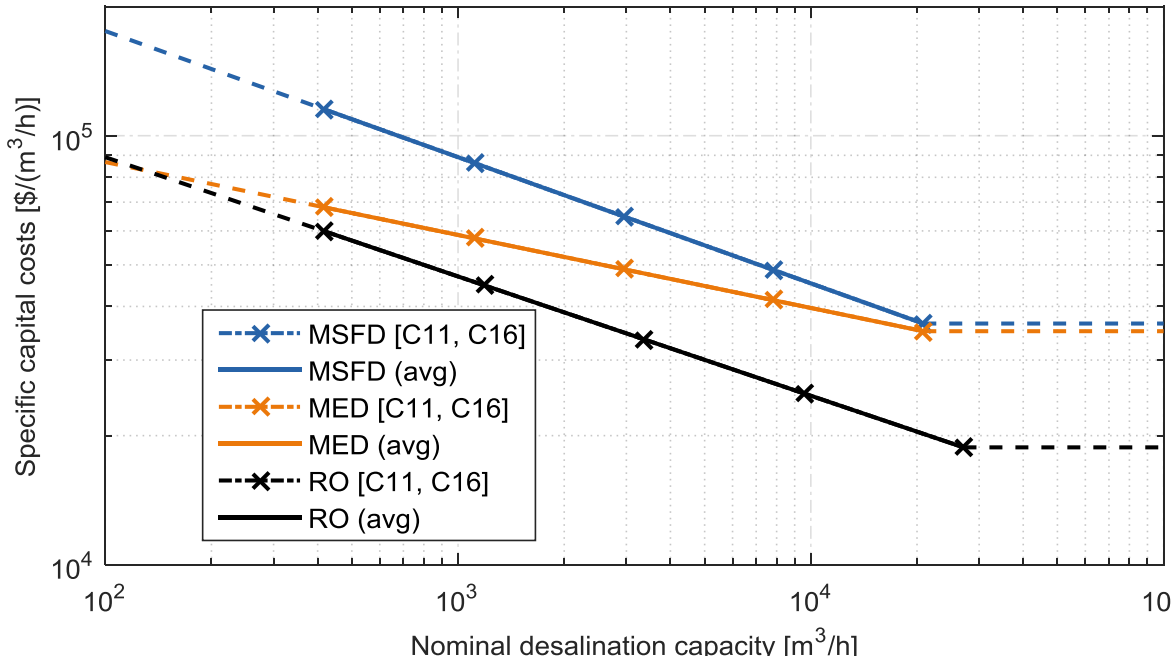

Figure B.4: Specific capital costs for desalination technologies.

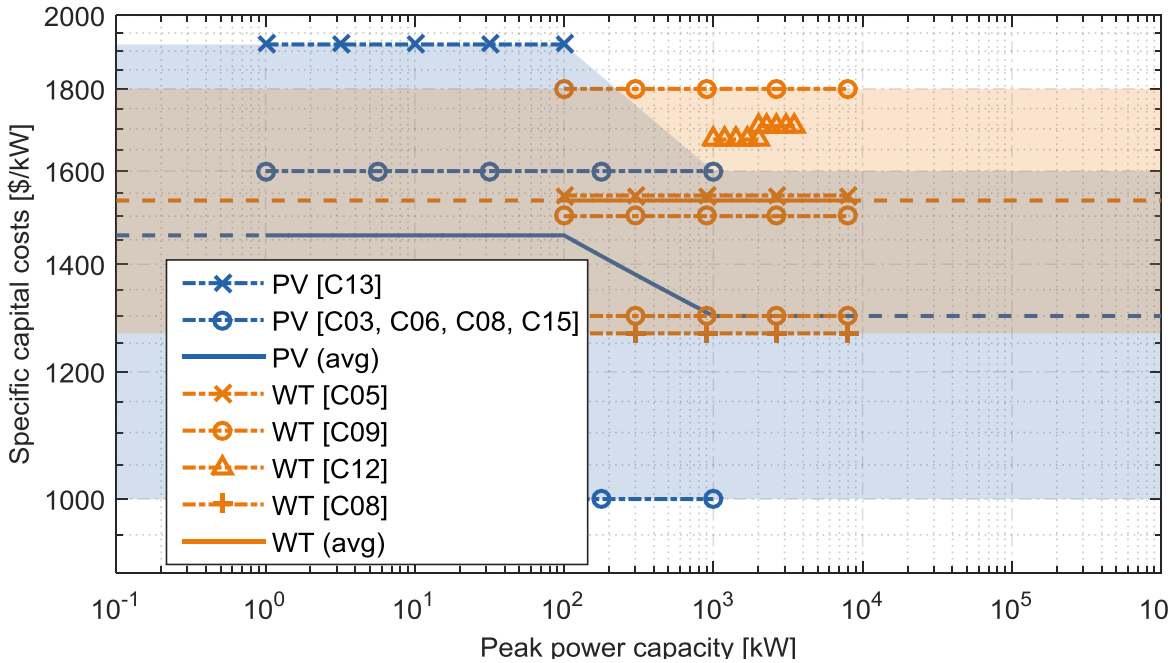

Figure B.5: Specific capital costs for renewable energy technologies.

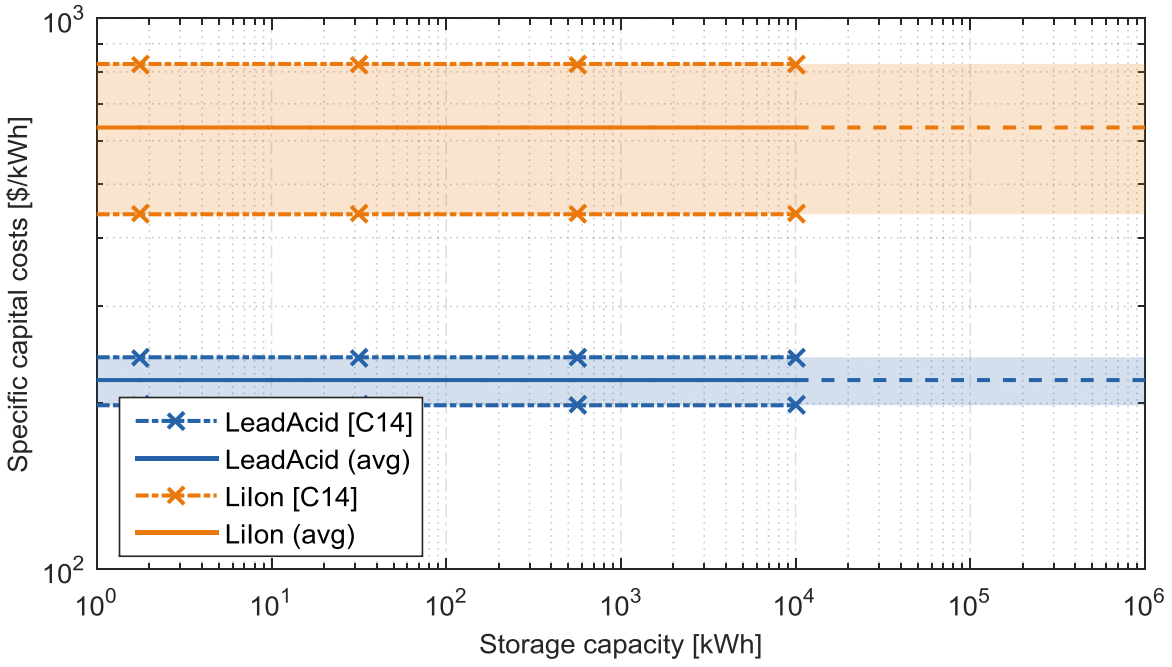

Figure B.6: Specific capital costs for electrochemical energy storages.

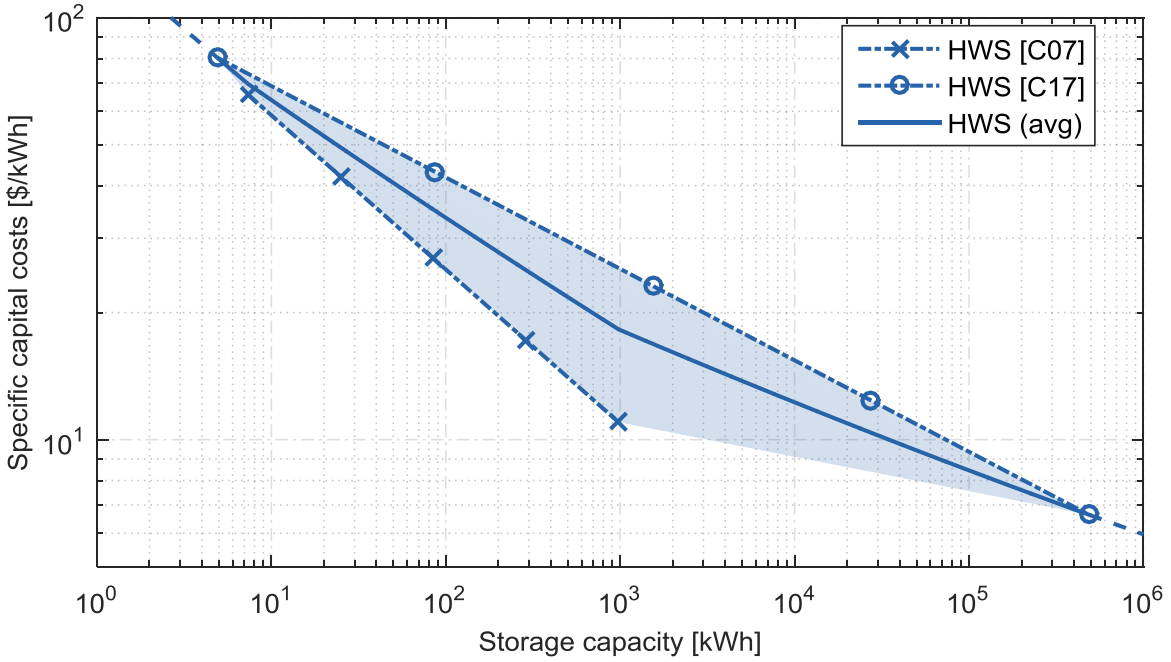

Figure B.7: Specific capital costs for ‘heat’ storages.

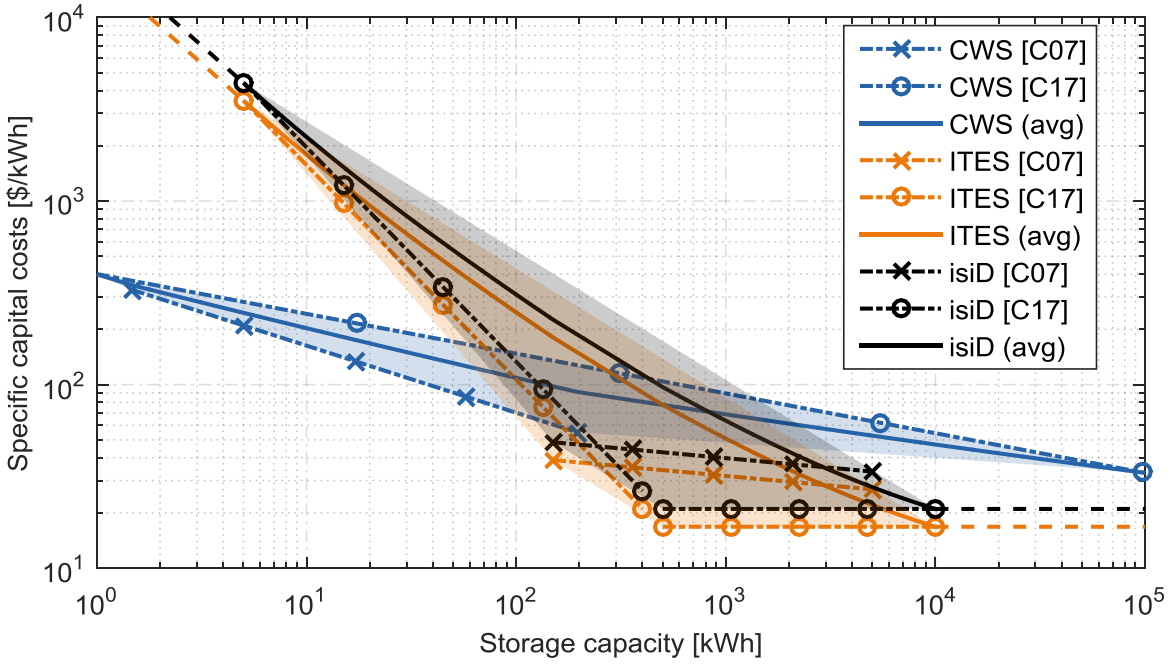

Figure B.8: Specific capital costs for ‘cold’ storages.

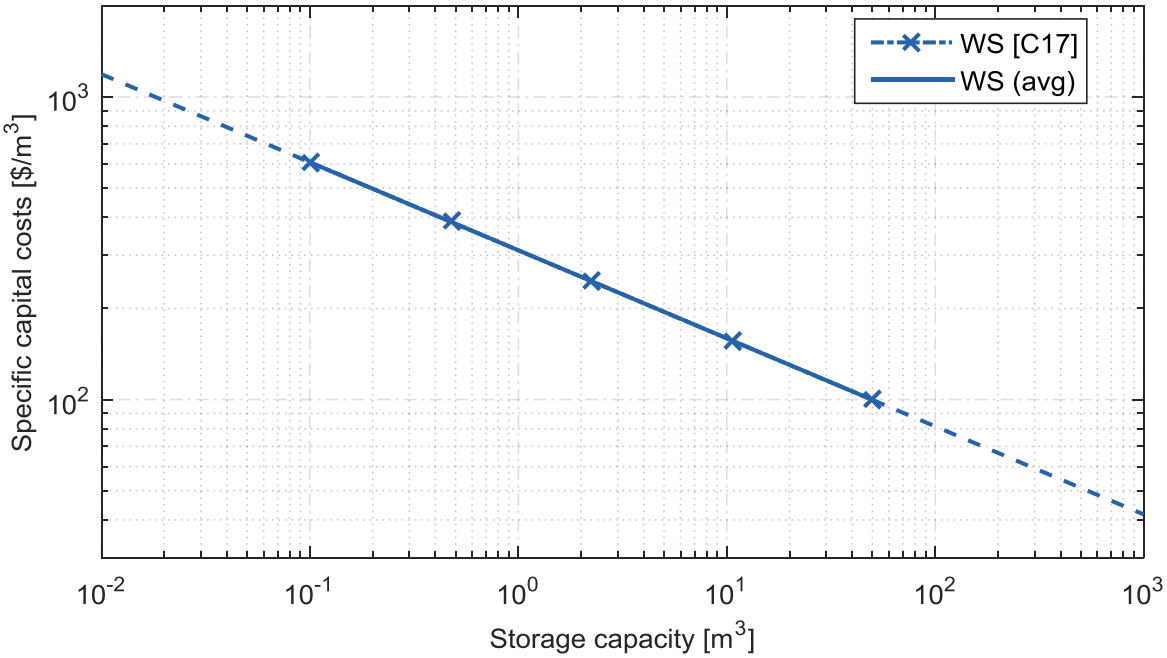

Figure B.9: Specific capital costs for water storages.

C Köppen climate symbols

Table C.1: (Relevant) Köppen climate symbols and their defining criteria (Peel et al., 2007).

1st	2nd	3rd	Description	Criteria[27]
A			Tropical	$T_{cold} \geq 18$ °C
	f		Rainforest	$P_{dry} \geq 60$ mm
	m		Monsoon	~Af $\cap$ $P_{dry} \geq 100 - MAP/25$
	w		Savannah	~Af $\cap$ $P_{dry} < 100 - MAP/25$
B			Arid	$MAP < 10 \cdot P_{threshold}$
	W		Desert	$MAP < 5 \cdot P_{threshold}$
	S		Steppe	$MAP \geq 5 \cdot P_{threshold}$
		h	Hot	$MAT \geq 18$ °C
		k	Cold	$MAT < 18$ °C
C			Temperate	$T_{hot} > 10$ °C $\cap$ $0 < T_{cold} < 18$ °C
	s		Dry summer	$P_{s,dry} < 40$ mm $\cap$ $P_{s,dry} < P_{w,wet}/3$
	w		Dry winter	$P_{w,dry} < P_{s,wet}/10$
	f		Without dry season	~Cs $\cap$ ~Cw
		a	Hot summer	$T_{hot} \geq 22$ °C
		b	Warm summer	~a $\cap$ $T_{mon,10} \geq 4$
		c	Cold summer	~a $\cap$ ~b $\cap$ $1 \leq T_{mon,10} < 4$

[27] Criteria defined with the mean annual precipitation (MAP) [mm], mean annual temperature (MAT) [°C], temperature of the hottest month (T_{hot}), temperature of the coldest month (T_{cold}), number of months where the temperature was above 10 °C ($T_{mon,10}$), precipitation of the driest month (P_{dry}), precipitation of the driest month in summer ($P_{s,dry}$), precipitation of the driest month in winter ($P_{w,dry}$), precipitation of the wettest month in summer ($P_{s,wet}$), precipitation of the wettest month in winter ($P_{w,wet}$), and threshold ($P_{threshold}$) that was calculated as $P_{threshold} = 2 \cdot MAT$ mm/°C (if 70% of MAP in winter), $P_{threshold} = 2 \cdot MAT$ mm/°C + 28 mm (if 70% of MAP in summer), and $P_{threshold} = 2 \cdot MAT$ mm/°C + 14 mm (otherwise). Summer (winter) was the warmer (colder) six month period of October – March and April – September (Peel et al., 2007).

Table C.2: Abbreviation, mean annual temperature (MAT), mean annual precipitation (MAP), Köppen climate classification and verbal description for all use case locations (based on data from Meteotest (2014)).

Location	Abbr.	MAT [°C]	MAP [mm]	Köppen climate symbol	Description
Cape Town	CPT	16.8	477.0	Csb	Temperate, dry and warm summer
Hong Kong	HKG	24.0	1918.6	Cwa	Temperate, dry winter, hot summer
Honolulu	HNL	24.9	415.5	Aw	Tropical savannah
Houston	HOU	20.7	1358.8	Cfa	Temperate, without dry season, hot summer
Madrid	MAD	15.3	384.0	BSk	Arid steppe, cold
Mexico City	MEX	16.7	1094.9	Cwb	Temperate, dry winter, warm summer
Miami	MIA	24.7	1605.2	Aw	Tropical savannah
Mumbai	BOM	27.6	2316.0	Aw	Tropical savannah
Phoenix	PHX	24.2	159.1	BWh	Arid desert, hot
Rio de Janeiro	RIO	24.0	968.2	Aw	Tropical savannah
Riyadh	RYD	26.8	41.9	BWh	Arid desert, hot
Singapore	SIN	27.6	2253.3	Af	Tropical rainforest
Sydney	SYD	18.2	1018.9	Cfa	Temperate, without dry season, hot summer

D Commodity prices

Table D.1: Commodity prices: References.

Reference	Source
[P01]	(NUS Consulting Group, 2014)
[P02]	(City of Cape Town, 2014)
[P03]	(Economic Consulting Associates, 2009)
[P04]	(Saving Water Aquarista, 2014)
[P05]	(the carbon report, 2016)
[P06]	(World Bank Group Climate Change & Ecofys, 2015b)
[P07]	(World Bank Group Climate Change & Ecofys, 2015a)
[P08]	(Higashi, 2009)
[P09]	(China Energy Group at Lawrence Berkeley National Laboratory, 2014)
[P10]	(Electrical and Mechanical Services Department at The Government of the Hong Kong Special Administrative Region, 2013)
[P11]	(Water Supplies Department at the Government of the Hong Kong Special Administrative Region, 2015)
[P12]	(U.S. Energy Information Administration, 2015b)
[P13]	(Hawaiian Electric Company Inc., 2012a)
[P14]	(Hawaiian Electric Company Inc., 2012b)
[P15]	(Board of Water Supply at City & County of Honolulu, 2015)
[P16]	(Austin Energy, 2014)
[P17]	(U.S. Energy Information Administration, 2016)
[P18]	(Euroheat & Power, 2013)
[P19]	(City of Houston, 2014)
[P20]	(International Energy Agency, 2012)
[P21]	(OMI-Polo Español S.A., 2015)

Reference	Source
[P22]	(Sachan, 2012)
[P23]	(Global Water Intel, 2005)
[P24]	(U.S. Energy Information Administration, 2015c)
[P25]	(Center for Energy Economics at University of Texas at Austin & Instituto Tecnológico y de Estudios Superiores de Monterrey, 2013)
[P26]	(The World Bank, 2005)
[P27]	(Florida Power & Light (FPL), 2015)
[P28]	(Federal Energy Regulatory Commission, 2013a)
[P29]	(Miami-Dade Water and Sewer Department, 2014)
[P30]	(Business Standard, 2015)
[P31]	(Tiwari, 2015)
[P32]	(Indian Energy Exchange, 2016)
[P33]	(Arizona Public Service Company, 2012a)
[P34]	(Arizona Public Service Company, 2012b)
[P35]	(Federal Energy Regulatory Commission, 2013b)
[P36]	(City of Phoenix, 2014)
[P37]	(Gomes, 2014)
[P38]	(The World Bank, 2015)
[P39]	(Câmara de Comercialização de Energia Elétrica, 2016)
[P40]	(International Carbon Action Partnership, 2016)
[P41]	(Matar, Murphy, Pierru, & Rioux, 2014)
[P42]	(dynamic Energy & Water Solutions, n.d.)
[P43]	(Ouda, 2013)
[P44]	(City Gas Pte Ltd., 2015)
[P45]	(Singapore Power, 2016)

Reference	Source
[P46]	(Energy Market Company, 2016)
[P47]	(Singapore District Cooling Pte Ltd, 2015)
[P48]	(Singapore Government, 2015)
[P49]	(Red Energy, 2015b)
[P50]	(Red Energy, 2015a)
[P51]	(Australian Energy Market Operator, 2016)

Table D.2: Commodity prices.[28]

Location	Natural gas	Electricity purchase		Electr. sale	Distr. heat.	District cooling		Water	CO_2
	[ct/kWh]	[ct/kWh][29]	[$/kW]	[$/MWh][30]	[ct/kWh]	[ct/kWh]	[$/kW]	[$/m³]	[$/t]
CPT	3.48 [P01]	2.94 / 6.52 [P02]	7.18 [P02]	22.7 [P03]	-	-	-	1.81 [P04]	2 [P05-P07]
HKG	5.43 [P08]	9.38 [P09]	0*	-	-	2.53 [P10]	14.97 [P10]	1.23 [P11]	3.5 [P06-P07]
HNL	8.19 [P12]	14.9 / 16.9 [P13-P14]	24.34 [P13-P14]	-	-	3.63*	17.42*	1.31 [P15]	0 [P06-P07]
HOU	1.83 [P12]	4.81 / 5.31 [P16]	14.65 [P16]	33.81 (D) [P17]	4.46 [P18]	2.55*	0*	2.65 [P19]	0 [P06-P07]
MAD	4.78 [P01]	14.88 [P20]	0*	55.15 (M) [P21]	-	8.87 [P22]	0*	1.41 [P23]	9 [P06-

[28] Assumptions are denoted with asterisk (*).

[29] On-peak and off-peak rates are indicated by two values.

[30] Time series are denoted with H (hourly), D (daily) or M (monthly).

Location	Natural gas	Electricity purchase		Electr. sale	Distr. heat.	District cooling		Water	CO_2
	[ct/kWh]	[ct/kWh][29]	[$/kW]	[$/MWh][30]	[ct/kWh]	[ct/kWh]	[$/kW]	[$/m³]	[$/t]
									P07]
MEX	2.74* [P24]	10.1 [P25]	0*	-	-	-	-	0.41 [P26]	1 [P06-P07]
MIA	3.09 [P12]	3.86 / 6.09 [P27]	12.45 [P27]	34.39 [P28]	-	2.5*	0*	2.24 [P29]	0 [P06-P07]
BOM	1.76 [P30]	10.39 [P31]	0*	41.8 (H) [P32]	-	2.8*	16.58*	0.32 [P23]	0 [P06-P07]
PHX	2.8 [P12]	3.22 / 4.08 [P33-P34]	15.79 [P33-P34]	29.41 [P35]	4.46 [P18]	1.84*	0*	1.53 [P36]	0 [P06-P07]
RIO	6.82 [P37]	13.04 [P38]	0*	81.64 (M) [P39]	-	-	-	1 [P23]	0 [P06-P07, P40]
RYD	0.26 [P41]	3.2 [P42]	0*	-*	0.45*	1.61 [P22]	0*	0.65 [P43]	0 [P06-P07]
SIN	12.92 [P44]	10.3 / 16.71 [P45]	5.34 [P45]	124.26 (H) [P46]	-	3.08 [P47]	14.77 [P47]	0.86 [P48]	0 [P06-P07]
SYD	3.67 [P01]	7 / 31.40 [P49-P50]	0*	28.74 (H) [P51]	6.36*	5.18*	30.64*	3.39 [P23]	0 [P06-P07]

E Exchange rates

Table E.1: U.S.-dollar foreign-exchange rates in late New York trading from August 18, 2015 (The Wall Street Journal, 2015).

Country/currency	In US$	Per US$
Americas		
Brazil real	0.2884	3.4699
Mexico peso	0.061	16.4037
Asia-Pacific		
Australian dollar	0.734	1.3624
China yuan	0.1564	6.3938
Hong Kong dollar	0.129	7.7547
India rupee	0.01526	65.524
Singapore dollar	0.7124	1.4037
Europe		
Euro area euro	1.1025	0.9071
Switzerland franc	1.0233	0.9772
Middle East/Africa		
Qatar rial	0.2746	3.6419
Saudi Arabia riyal	0.2666	3.7512
South Africa rand	0.0775	12.9039

F Synthetic load profile generation

Table F.1: Fits and parameters for the load profile generation models.[31,32]

Parameter	Airports	Business parks	University campuses	
(Air-conditioned) floor area [m²]	max {10^4, -1.46·10^5 + 0.0164 · *pax*}	max {2·10^3, -2.76 ·10^4 + 58.58 · *empl*}	max {5·10^4, -5.94 ·10^4 + 7.86 · *stud* + 83.78 · *staff*}	
Specific heating (and hot water) energy demand per unit area and day [kWh/m²/d]	0.3866 + 0.0758 · *ins* · $HDD_{18.3}$	$c_1 + c_2 \cdot ins \cdot HDD_{10}$ Weekdays: c_1 = 0.008, c_2 = 0.0076 Saturdays: c_1 = 0.006, c_2 = 0.0044 Sundays: c_1 = 0.0012, c_2 = 0.0002	0.0422 + 0.0309 · *ins* · $HDD_{15.5}$	
Specific cooling energy demand per unit area and day [kWh/m²/d]	0.368 + 0.0726 · *ins* · $CDD_{18.3}$	$c_1 + c_2 \cdot ins \cdot CDD_{10}$ Weekdays: c_1 = 0.0342, c_2 = 0.0326 Saturdays: c_1 = 0.0441, c_2 = 0.022 Sundays: c_1 = 0.0324, c_2 = 0.0176	0.0246 + 0.0123 · *ins* · $CDD_{15.5}$	
Specific electric energy demand per unit population [kWh/1]	Good: 4.5 Average: 5.15 Poor: 5.8	Good: 4·10^3 Average: 6·10^3 Poor: 8·10^3	Good: 1·10^3 Average: 1.5·10^3 Poor: 2·10^3	
Water consumption per unit population [L/1]	Good: 16.7 Average: 24 Poor: 31.3	Good: 2·10^3 Average: 6·10^3 Poor: 10·10^3	Good: 3·10^4 Average: 4.5·10^4 Poor: 6·10^4	
Population activity			Students	Staff
Sitting	40%	-	60%	50%

[31] The fits were defined based on the following parameters: The annual number of passengers (pax), the number of employees working in the business park area ($empl$), the number of students ($stud$) and the number of staff on campus ($staff$), the daily heating degree days ($HDD_{T_{ref}}$) and the daily cooling degree days ($CDD_{T_{ref}}$) with reference temperature (T_{ref} in °C) subscripted. The building insulation quality factor (ins) is 0.5 for well insulated, 1 for average and 2 for poorly insulated buildings.

[32] See **Section 4.1.2** for references.

Standing, walking	50%	-	30%	40%
Fast walking	10%	-	10%	10%

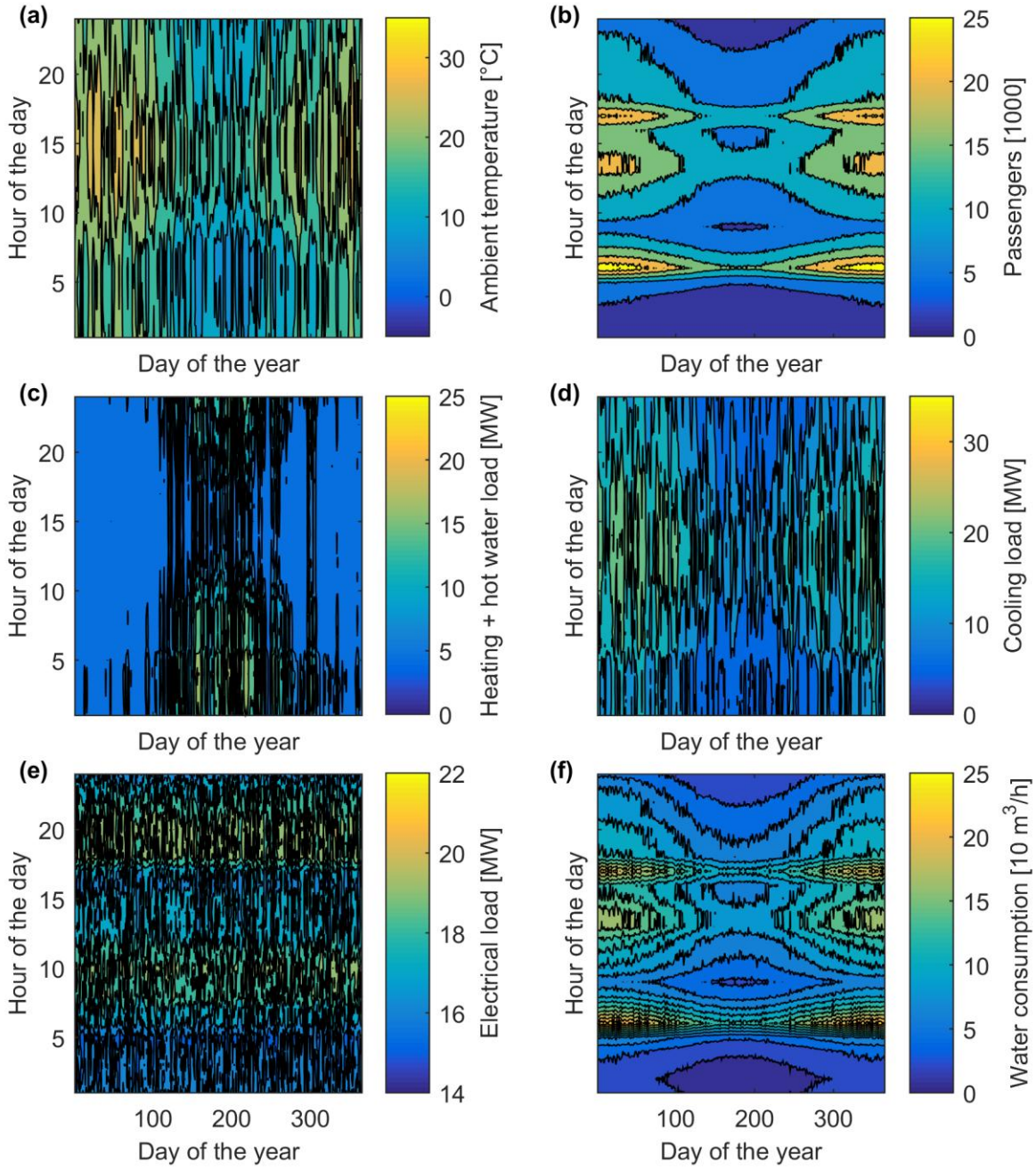

Figure F.1: Example load profiles for a default (fictive) airport located in Sydney.

G Default sites

Table G.1: Parameters of the three default (fictive) sites.

Parameter	Airport	Business park	University campus
Building insulation quality	Average	Average	Average
Electricity usage efficiency	Average	Average	Average
Water usage efficiency	Average	Average	Average
	Number of annual passengers [1/a]	Number of employees [-]	Number of students [-]
	30 m	5 k	30 k
	Travel season [-]	-	Number of staff [-]
	Location-specific (summer)	-	2 k
	Night flights [-]	-	-
	Yes	-	-
Max. PV capacity [MW]	10 (Ong, Campbell, Denholm, Margolis, & Heath, 2013; problogic, 2013)	3 (Association for the Advancement of Sustainability in Higher Education, 2012; Education Design Showcase, 2015; Ong et al., 2013; San Diego Gas & Electric Company, 2013)	5 (Association for the Advancement of Sustainability in Higher Education, 2012; Education Design Showcase, 2015; Ong et al., 2013; San Diego Gas & Electric Company, 2013)
Max. WT capacity [MW]	0 (van der Geest, 2009)	9 (Lancaster University, 2015; The National Renewable Energy Laboratory, 2004)	15 (Lancaster University, 2015; The National Renewable Energy Laboratory, 2004)

H Scenario analysis

Table H.1: Commodity price scenarios.[33]

Name		Natural gas	Electricity purchase	Electricity sale	District heating	District cooling	Water	CO2 [$/t]
Reference								
Ref		-	-	-	-	-	-	-
Synthetic								
Gas+		+50%	+12%	+15%	+50%	+12%	+2%	-
Gas++		+100%	+25%	+30%	+100%	+25%	+5%	-
RE+		-	+25%	-12%	-	+25%	+5%	-
RE++		-	-12%	-25%	-	-12%	-2%	-
CO2+		-	-	-	-	-	-	50
CO2++		-	-	-	-	-	-	150
Real								
EIA/ IEA/ EPA[34]	Min/ 2DS	+80%	+20%	+25%*	+80%*	+20%*	+4%*	150
	Max/ 6DS	+140%	+35%	+40%*	+140%*	+35%*	+7%*	50
ewi/ GWS/ Prognos[35]	2025	+40%	+48%	-18%	+40%*	+48%*	-*	20
	2050	+80%	+24%	+70%	+80%*	+24%*	-*	85

[33] Assumptions are denoted with asterisk (*).

[34] The two scenarios (Min/2DS and Max/6DS) were compiled based on future scenarios published for the United States (Fawcett, 2010; International Energy Agency, 2015; U.S. Energy Information Administration, 2015a).

[35] The two scenarios (2025 and 2050) were compiled based on future scenarios published for Germany (Schlesinger, Lindenberger, & Lutz, 2014).

Table H.2: Technology capital cost scenarios.[36]

Name	Description	RE	GT, ST	ICE	GB	HP[37], EB	AC	CC	MSFD, MED	RO	ECES	TES
iRef	Reference case	-	-	-	-	-	-	-	-	-	-	-
iRE	Cheap renewable energy converters	m	-	-	-	-	-	-	-	-	-	-
iGT	Cheap gas turbines	-	m	-	-	-	m	-	m	-	-	-
iICE	Cheap internal comb. engines	-	-	m	-	-	m		m	-	-	-
iP2X	Cheap power-to-X converters	m	-	-	-	m	-	m	-	m	-	-
iECES	Cheap ECES	m	-	-	-	-	-	-	-	-	m	-
iTES	Cheap TES	m	-	-	-	-	-	-	-	-	-	m

[36] An "m" indicates that minimum specific capital costs ($i_{\min,j}$ instead of $i_{\text{avg},j}$) were used for a particular technology (j) (compare also **Figure 3.8**).

[37] HP includes all heat pump technologies (HP, CHC and rHP).

I Picture sources

Table I.1: List of figures and their (external) picture sources.

Figure	Picture sources
Figure 1.1	https://pixabay.com/en/airport-interior-travel-terminal-144331/ https://pixabay.com/en/interior-design-tv-multi-screen-828545/ https://pixabay.com/en/stuttgart-library-white-books-980526/
Figure 1.2	https://pixabay.com/en/earth-blue-planet-globe-planet-11015/ https://pixabay.com/en/stack-of-books-vintage-books-book-1001655/ https://pixabay.com/en/mathematics-formula-physics-school-1453828/ https://pixabay.com/en/gears-cogs-machine-machinery-1236578/
Figure 2.1	https://pixabay.com/en/clouds-sunny-warm-patches-weather-37009/ https://pixabay.com/en/village-icon-icon-village-1001598/ https://pixabay.com/en/dollar-money-us-dollar-seem-funds-1294424/ https://pixabay.com/en/cogwheel-gear-gearwheel-cog-145804/ https://pixabay.com/en/bag-money-wealth-revenue-finance-147782/ https://pixabay.com/en/calculator-calculate-numbers-1464008/ https://pixabay.com/en/helmet-safety-safety-helmet-work-158268/ https://pixabay.com/en/energy-efficiency-energy-154006/
Figure 2.5	https://pixabay.com/en/power-poles-upper-lines-power-lines-503935/ https://pixabay.com/en/oil-pump-jack-sunset-clouds-1407715/ https://pixabay.com/en/fire-embers-heat-flame-hot-3314/ https://pixabay.com/en/ice-frost-winter-1092875/ https://pixabay.com/en/water-drop-rain-falling-pouring-164046/
Figure 4.1	https://commons.wikimedia.org/wiki/File:World_Koppen_Classification_(with_authors).svg
Figure 4.5	https://pixabay.com/en/airport-interior-travel-terminal-144331/ https://pixabay.com/en/interior-design-tv-multi-screen-828545/ https://pixabay.com/en/stuttgart-library-white-books-980526/
Figure 4.10	https://commons.wikimedia.org/wiki/File:SolarGIS-Solar-map-World-map-en.png

Index

U

V